LATERAL-TORSIONAL BUCKLING BEHAVIOUR OF MONOSYMMETRIC STEEL SECTIONS FORMED WITH FLANGE UPSTANDS

Kenny Mudenda

A dissertation submitted in partial fulfilment of requirements for the Doctor of Philosophy degree

in the

Department of Civil Engineering

Faculty of Engineering and the Built Environment

UNIVERSITY OF CAPE TOWN

August 2023

Plagiarism Declaration

I, Kenny Mudenda, hereby declare that the work on which this thesis is based is my original work (except where acknowledgments indicate otherwise) and that neither the whole work nor any part of it has been, is being, or is to be submitted for another degree in this or any other university. I authorise the University to reproduce for the purpose of research either the whole or any portion of the contents in any manner whatsoever. The Harvard reference style in EndNote X7 has been employed for citations.

Signature: Date: 14.08.2023

Abstract

The study of the lateral-torsional buckling behaviour of steel beams has been largely focused on doubly symmetric beams and less so on monosymmetric sections. Monosymmetric sections, however, do offer some advantages over doubly symmetric beams if the monosymmetry is applied in a way that it can be exploited. This is because the effects of monosymmetry can work to increase or decrease the moment capacity. Identifying these cases is therefore essential. In the current study the behaviour of a monosymmetric section produced by introducing flange upstands as stiffeners is explored. The upstands convert a standard doubly symmetric section into a monosymmetric section. The change in member properties is first explored with the movement of shear center relative to the geometric centroid being of particular interest. It is observed that the shear center initially moves away from the centroid towards the stiffened flange, reaches a stationery point and then starts to move away from this flange. This leads to the shear center then intersecting the centroid so that for a monosymmetric section, at a certain upstand height, the shear center and centroid are coincident. This results in a monosymmetric section taking on a property typically associated with a doubly symmetric section. A study of the change in the monosymmetry constant of the section also reveals that at a given upstand height the monosymmetric section also takes on another property associated with doubly symmetric sections, that of the monosymmetry constant having a value of zero.

Further study of the critical elastic moment change with change in upstand height reveals that the section initially has a significant increase in the value of the critical elastic moment with upstand height followed by a trend of diminishing increase rate. In some cases, this trend then reverses so that with an increase in upstand height the critical elastic moment starts to decrease. The region where the monosymmetry acts beneficially to increase section capacity represents a target domain before the monosymmetry then starts working to diminish the member capacity. This second region represents an undesirable domain for the use of these upstands. This observed behaviour, therefore, leads to identification of a domain of upstand heights in which the positive effect of monosymmetry can be exploited. The junction between the two regions, given by a critical upstand height, can be reasonably approximated based on the upstand height at which the shear center and centroid coincide. Engineers who may want to make use of flange stiffeners need to be aware of these trends to better manage the strengthening of doubly symmetric members so that material is used economically and not wasted in regions were the returns are minimal or diminishing.

The application of this domain has been demonstrated for linear elastic buckling cases as well as for inelastic buckling cases so that real member behaviour is also simulated. Although applied for strengthening cases in the current study the principle can be used for section optimization at member selection stage should members with upstands be an option. Equations obtained using the Rayleigh-Ritz energy method were employed for the elastic critical buckling study for two transverse load cases. Finite element models were

then employed for the nonlinear analysis for the inelastic buckling cases. Residual stresses have not been included in the finite element models. Geometric imperfections as well as material constitutive behaviour were incorporated in the models. This gives a realistic picture of 'real' member behaviour despite not including residual stresses. The results from the nonlinear study support those from the linear elastic study in demonstrating how the beneficial domain can be exploited.

Dedication

This work is dedicated to those who have stood with, cared for and supported me through this remarkable journey of searching and discovery.

A special dedication goes to my family who have sacrificed so much to allow me to travel this journey.

Acknowledgement

I would like to acknowledge my supervisor Prof. Alphose Zingoni who has been a source of inspiration and encouragement throughout the period I undertook my research. His contribution has been pivotal in assisting me to find my way through the maze of inquiry. My gratitude goes to the Structural Engineering and Mechanics (SEM) research group for providing access to the software that I used for my study. The students of this research group have in various ways and through many conversations helped me to deal with aspects of my work and, to receive valuable feedback and encouragement.

Table of Contents

List of Figures

List of Tables

Abbreviations

AISC	American Institute of Steel Construction
C	Centroid
CSA	Canadian Standards Association
DE	Differential equation
EC3	Eurocode 3
ECCS	European convention for constructional steelwork
Eq.DS	Equivalent doubly symmetric section
FEA	Finite element analysis
FEM	Finite element model
GMNA	Geometrical and material nonlinear analysis
GMNIA	Geometrical and material nonlinear with imperfection analysis
LPF	Load proportionality factor
MS	Monosymmetric section
ODE	Ordinary differential equation
NCCI	Non-contradictory complementary information
NF	Narrow flange
SAISC	Southern African Institute of Steel Construction
SASCH	Southern African Steel Construction Handbook
SC	Shear center
UDL	Uniformly distributed load
WF	Wide flange
1D, 2D, 3D	One dimension, two-dimension, three dimension
PRFELB	Plane rigid frame elastic lateral buckling (software)

List of selected symbols

α	Upstand height
α_c	Upstand height at coincidence of shear center and centroid
C_b, ω_2	Moment gradient factor
E	Elastic modulus
G	Shear modulus
η	Ratio of upstand height to unstiffened member height ($\alpha/_H$)
λ	Load Factor
M	Applied moment
M_r	Resistance moment
M_{cr}	Critical elastic moment
$M_{cr,0}$	Critical elastic moment of unstiffened member
$M_{cr,1}$	Critical elastic moment of stiffened member
$M_{cr,2}$	Critical elastic moment of larger (replacement) doubly symmetric member
u	Lateral deflection along the horizontal axis
v	Vertical deflection
$\bar{y}$	Centroid position measured from base
y_{sc}	Shear center position measured from base
r_y	radius of gyration about minor axis

CHAPTER 1 INTRODUCTION

1.1 PROBLEM STATEMENT

The study of buckling instability either in the form of flexural, torsional or other coupled modes is indispensable for structural steel members used either in flexure, direct compression or a combination of both. This is particularly true for members that do not have lateral support over some portion of the length in the longitudinal direction and subject to compressive stresses either from major axis bending or direct compression forces. The critical form of instability for flexural members subjected to major axis bending is that of lateral-torsional buckling. For compression members the types of instability of concern are flexural buckling about the most slender axis, torsional buckling about a point axis as well as coupled modes such as torsional-flexural buckling.

A lot of research has been devoted to studying the behaviour, both elastic and inelastic, of doubly symmetric sections. Much less effort has been dedicated to monosymmetric sections. Existing research on monosymmetric sections has focused mainly on standard I-shaped sections, channels, and tees. These sections are shown in Fig. 1-1. In order to make use of monosymmetric sections of non-standard geometries their behaviour under load must be fully understood. Moreover, by understanding the mechanics involved in the behaviour of these sections, wide use of them can be made in addition to generating knowledge that could be extended to other applications.

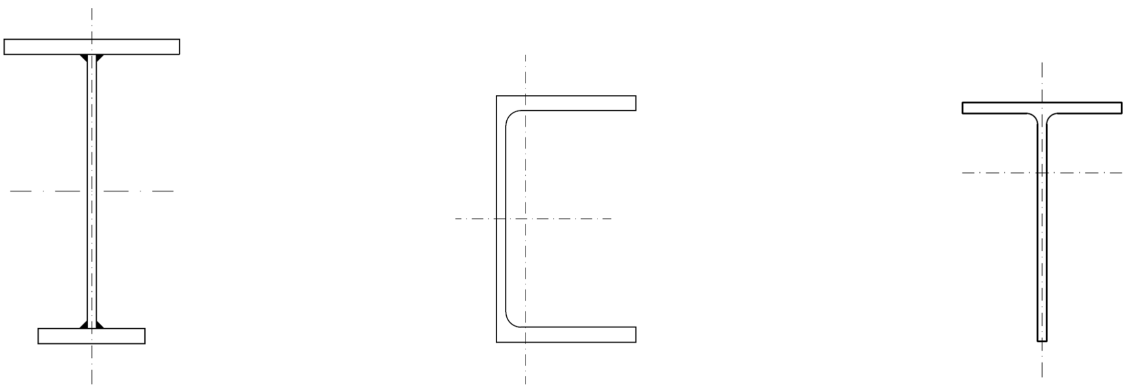

(a) I-Shaped section (b) Channel Section (c) Tee - Section

Fig. 1-1 Common monosymmetric sections

The load carrying capacities of some monosymmetric sections such as standard channel and tee sections are relatively limited, compared to doubly symmetric I-shaped sections of similar depths. These sections would not typically find use in heavily loaded members. It may be desirable in some instances to enhance the capacity of these sections, whether beams or columns, and this may be done by employing flange upstands or flange stiffeners. Similar enhancement may be applied to standard doubly symmetric sections. These sections with flange upstands are shown in Fig. 1-2.

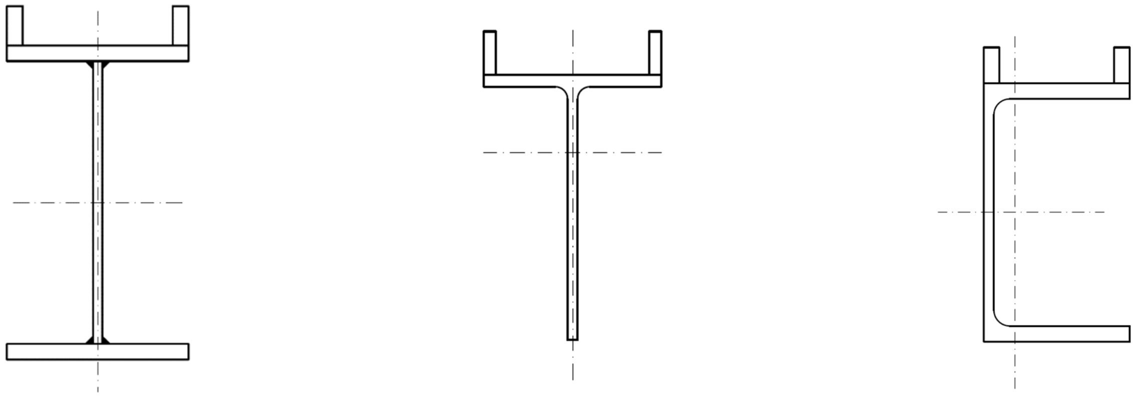

Fig. 1-2 Sections with flange upstands

These section geometries, with flange upstands, have the potential for increased strength, including improved buckling characteristics compared to sections without upstands. To make use of such sections, the lateral-torsional and torsional-flexural behaviour must be well understood, as well as the effect of compression stress on the stiffeners or upstands when these are subjected to flexural compression stress. In addition, any unusual behaviour due to the unique geometry needs to be understood thoroughly. Not much information exists in the current literature on sections with flange end stiffeners for beams or columns. The existing literature covers only a few forms of rolled sections with lips. One form is an I-shaped section beam with flange downstand lips as shown in Fig. 1-3.

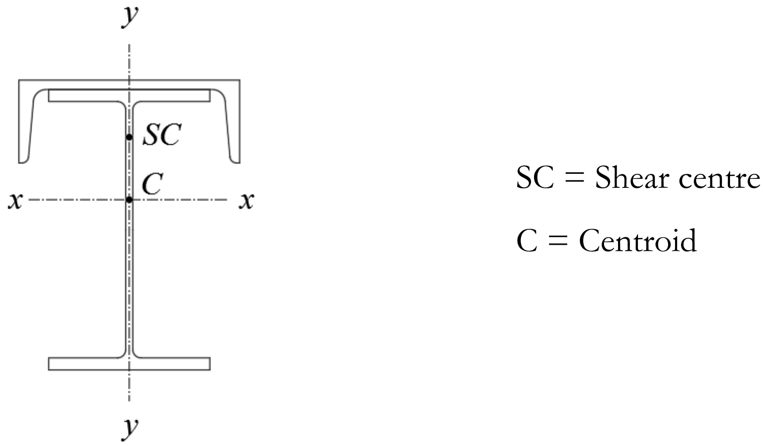

Fig. 1-3 Section with flange downstands

The others are rolled sections with downstand lips on the top flange Kitipornchai and Trahair (1980) and rolled sections with angles welded onto the top flange (Bijak et al., 2019) and (Movaghati, 2019). These sections are used predominantly as crane beams for light to medium duty industrial cranes. The downstand lips provide enhancement of capacity about the minor axis, akin to a channel bending about its strong axis, to accommodate the effect of horizontal loads from the travelling crane. Strength enhancement of the entire section for bending about the major axis may be a secondary benefit even for these sections.

1.2 RATIONALE

When design engineers have to employ the use of structural steel members in particular structures, they have to consider the nature and magnitude of applied loads the members will be subjected to during their lifespan. In addition to this, they have to determine the resistance of the member to the possible failure modes when subjected to these loads or their effects. If engineers lack an adequate understanding of the behaviour of these members when subjected to loads, as well as the mechanisms through which they can resist failure due to the action of the loads, then they cannot fully exploit the use of these members. Monosymmetric beams with flange stiffeners in the form of upstands include such members. These could be standard sections with plates welded on as stiffeners or could be hot-rolled members with flange end lips. The word stiffeners will be used to denote any of the two forms.

Although they could potentially find use in some engineering applications, there is little or no information on how such geometries behave with regards to lateral-torsional buckling instability; one of the most likely failure modes for laterally unrestrained members. This study therefore aims to make such information available. Potential uses for these members include:

(i). Stiffening of existing members (stiffeners welded onto flanges of sections)
(ii). Applications where lips may be required as guides
(iii). Optimised cross sections for specific applications

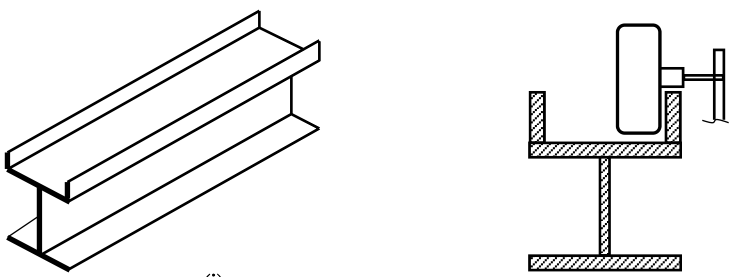

(i) (ii)

Fig. 1-4 Potential application of upstands

In addition, the knowledge generated could find use in other applications such as in mechanical and aeronautical components, where monosymmetric section components may be employed. Monosymmetric sections tend to exhibit peculiar behaviour and hence a study of their buckling behaviour for any unique geometry is warranted. The peculiar behaviour is usually as a result of the complexities arising from having a non-coincident shear centre and geometric centroid.

1.3 RESEARCH QUESTIONS

(i). What is the lateral-torsional buckling behaviour of monosymmetric section geometries having the monosymmetry introduced by virtue of flange stiffeners?

(ii). Is it possible to prove the existence of monosymmetric geometries, particularly those with flange stiffeners, which possess properties of doubly symmetric sections, in particular a coincident shear centre and centroid, or a monosymmetry constant of value zero? How would this peculiarity affect the member behaviour?

(iii). Are the existing elastic critical buckling load formulas for monosymmetric sections particularly those used for I-shaped and tee-shaped monosymmetric sections applicable, after suitable modification, to monosymmetric sections with flange stiffeners used in flexure?

(iv). What is the inelastic behaviour of the monosymmetric sections with flange stiffeners?

(v). Do flange stiffeners significantly increase the critical buckling load as well as ultimate strength of steel members compared to that of similar geometry without the stiffeners?

(vi). Can members incorporating flange stiffeners meet aspects of 'lean design' where lighter doubly symmetric members when stiffened with flange upstands can obviate removal and replacement with heavier 'off the shelf' sections that may entail higher cost.

1.4 SCOPE OF STUDY

The scope of the study is limited to specific non-standard geometry sections. The sections considered are derivatives of standard doubly symmetric I-shaped (narrow flange) and H-shaped (wide flange I-shape) sections which are converted to monosymmetric cross sections through the introduction of flange end upstands or stiffeners. This is shown in Fig. 1-5.

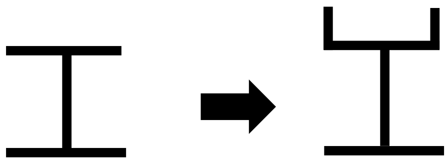

Fig. 1-5 Standard section and its derivative with upstands for the current study

In the current study the ultimate strength will be based on a geometrical and material nonlinear analysis, with the effects of residual stress not included. Experimental testing is required to characterise the nature and distribution of residual stresses and this falls outside the scope.

1.5 THESIS LAYOUT

The thesis is divided into eight (8) chapters. Chapter 1 introduces the topic and presents the rationale for the study. A literature review is presented in chapter 2 where previous research in the broad area of lateral-torsional buckling, as well as specifically on monosymmetric sections is presented. This provides a background to the area of research being undertaken as well as an overview of the current state of knowledge around the topic. Chapter 3 presents the derivation of mathematical expressions for some key geometrical parameters that are required for determining the critical load of beams. The chapter also presents a study on the effects of the shear centre position movement with the change in the height of the upstands on the beam. The unique movement of the shear centre is highlighted and the effects of this forms an important part of the studies in the chapters that follow. Chapter 4 outlines and reviews methods employed for solving the buckling problem in beams. A mathematical equation for predicting the critical buckling load for a monosymmetric section is developed for the sections used in the current study based on an energy method. A point load at midspan and a UDL, both applied on the flange, are selected as load cases to explore. A finite element model is developed and used to verify the applicability of the equations derived in Chapter 4 to the proposed section. Chapter 5 presents results of a parametric study on how the shear centre behaviour from Chapter 3 influences the critical buckling moment of the section considered. The equations developed in Chapter 4 are used for this parametric study. Results on trends obtained from the parametric study are presented. Chapter 6 looks at practical applications stemming from the behaviour observed in Chapter 5. Chapter 7 presents a study using a calibrated finite element model of the section under consideration to extend the demonstration of practical application from Chapters 5 and 6 into the nonlinear behaviour range. This is aimed at predicting member strength as would be observed in a physical test or real-life application. Chapter 8 presents a summary of the work carried out in the study and offers a conclusion. Recommendations for future work are also presented.

CHAPTER 2 LITERATURE REVIEW

2.1 INTRODUCTION

Lateral-torsional buckling occurs in beams due to the nature of stresses arising from flexure about the strong (major) axis. Members in flexure will typically have both compressive and tensile stresses with a point of no stress, the neutral axis, where the stresses change from tensile to compressive. Flexure happens about the centroid of the cross section which would coincide with the sections' neutral axis. In flexural members it is the part in compression that is particularly susceptible to buckling. In the case of lateral-torsional buckling the compressive side of the member buckles at a critical load and starts to deflect sideways in a plane perpendicular to the bending plane of the beam. However, because the beam has a stable part under tensile stress this part resists the sideways movement of the compression part which invariably leads to a twist of the member. The sideways (lateral) movement accompanied by a twist (torsion) of the member leads to the description of this failure mode as lateral-torsional buckling (LTB). An example of this is shown in Fig.2-1 for uniform moment loading with the axis of the beam aligned with the Z-axis in cartesian coordinates. In this illustration '*L*' is the length of the beam, '*u*' the lateral displacement, 'ϕ' the twist angle of the beam and 'v' an accompanying vertical displacement.

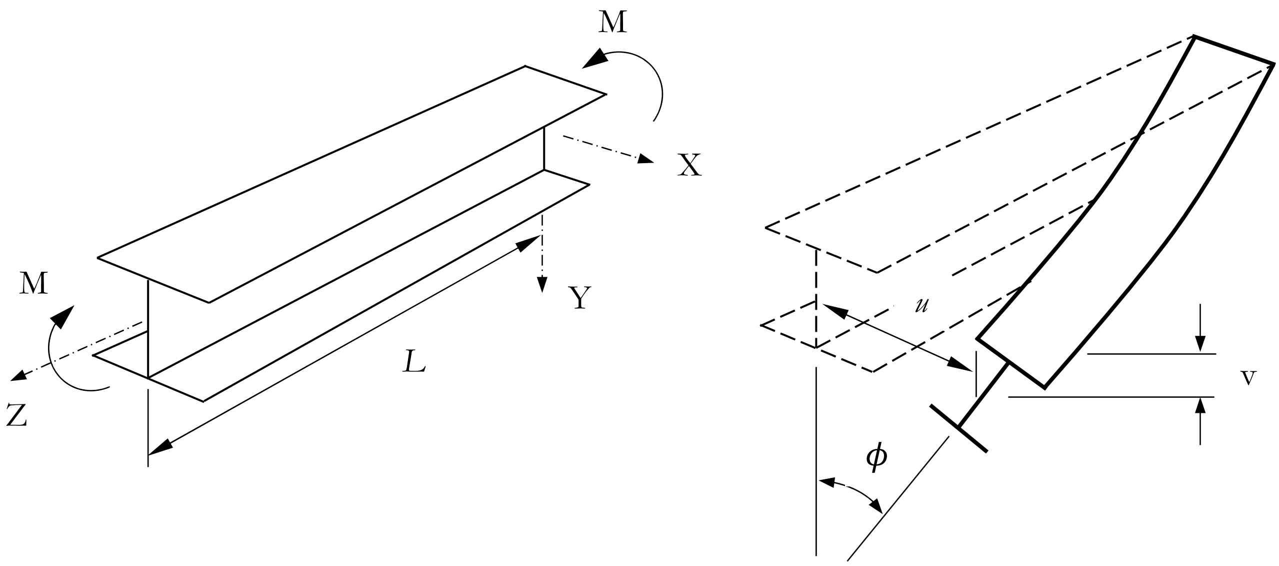

Fig.2-1 Lateral-torsional buckling of a simply supported I-beam in pure bending

The lateral-torsional buckling behaviour of monosymmetric beams has an added complexity because whereas bending happens about the centroidal axis, twist occurs for a prismatic member about a longitudinal axis which runs through the member shear centre. If the two do not coincided, as is the case with doubly and point symmetric members, then this complexity introduced by non-coincidence of the two axes leads to secondary effects that have a bearing on torsional rigidity and hence on the critical buckling load. The implication of non-coincidence for monosymmetric sections is that there is an increase or decrease in the critical moment or critical load depending on the position of the shear centre relative to the geometric centroid.

Lateral-torsional buckling continues to provide unique challenges to designers who need to make use of members in situations where there is a constraint to placing lateral restraints to the compression flange. Applications such as industrial structures where components, plant and machinery are supported on beams with little or no flooring as well as crane runway beams are typical examples. Although a lot of knowledge now exists on the topic some scope still remains for further exploration. One of those areas is the application of non-standard geometries that are monosymmetric in nature. Lateral-torsion buckling (also referred to as flexural-torsional buckling by some authors) arises when a beam carrying a transverse load, and bending about its major axis, suddenly loses the ability to carry this load at a value of applied load referred to as the critical elastic load. The current study focuses on monosymmetric beams. The challenge with monosymmetric beams has been apparent from the early years of research on the topic. This is demonstrated, in no small way, by the controversy over the 'Wagner hypothesis' that was raised by Ojalvo (1981). The concept was proposed by Wagner (1936) to explain, in part, why angle sections under axial compression can fail by a torsional failure mode. The concept was then extended to explain certain types of monosymmetric beam bucking problems by other researchers. Although widely considered resolved and expressed as such by researchers such as Kitipornchai et al. (1987), Goto and Chen (1989), Kang et al. (1992), Trahair (1993), Alwis and Wang (1996) and Falgoust (2004), some researchers still consider the controversy not fully resolved (Ziemian, 2010). The controversy was not fundamentally on nullifying the fact that the hypothesis leads to correct prediction of member behavior, but rather on the basis of its formulation (Falgoust, 2004). The Wagner hypothesis, still today, remains the basis upon which much of the research on monosymmetric members is grounded. The movement of the shear center away from the centroid, a condition not observed with bi-symmetric sections, is the source of complexity with monosymmetric sections. This, therefore, becomes an important consideration whenever one deals with monosymmetric sections.

Rockey and Nethercot (1971) outlined five main factors that affect lateral-torsional buckling behavior. Thirty-nine (39) years later a list of factors affecting lateral-torsional buckling was also given by (Ziemian 2010). A comparison of the two lists is given in Table 2-1. Evidence of research progress over the years on the topic of lateral-torsional buckling can be seen from a comparison of the list of factors influencing lateral-torsional buckling provided by Rockey and Nethercot (1971) and that by Ziemian (2010). Early research focused on single span beams with end conditions idealized as pinned or fixed which greatly reduced the complexity of studying beam behaviour. Later research has been extended to continuous beams, elastic restraints at ends and intermediate points as well as many other member conditions far different from the simple form and configuration of the beams in early work. The exhaustive list provided by Ziemian (2010) indicates the extent to which research carried out in the intervening years was able to shed more light on our understanding of lateral-torsional buckling behaviour. From the factors listed in Table 2-1 it is easy to locate from past studies in the literature which of the factors have been addressed in the study under review. This also then provides a sufficient basis from which to formulate the purpose for the current study and identify where it makes a unique contribution to the literature. The scope for increasing the lateral-torsional buckling capacity of a member will always be dependent upon the constraints placed in the use of the member. The use or application determines which factors are unalterable and which ones present scope for change or alteration.

Table 2-1 List of factors affecting lateral-torsional buckling behavior according to Rockey and Nethercot (1971) and Ziemian (2010)

S/N	Factors according to Rockey and Nethercot (1971)*	S/N	Factors according to Ziemian (2010)
1	Material properties	1	Material properties
2	Geometry	2	Type of cross-section
3	Span	3	Distance between lateral and/or torsional braces
4	Loading type member is subjected to	4	Type and position of loads
5	Conditions of lateral support provided	5	Restraints at the ends and at intermediate positions along the beam axis
**Imperfections implied in study*		6	Continuity at supports
		7	Presence or absence of stiffening devices that restrain warping at critical locations
		8	Cross-section distortion and interaction between local and overall buckling
		9	Changes in cross-section e.g. steps, taper, copes, holes etc.
		10	Prestressing
		11	Imperfections in the form of residual stresses, initial imperfections of geometry and loading

Rockey and Nethercot (1971) identified the conditions of lateral restraint as the factor offering greatest possibility for increasing the beams stability against lateral buckling. In the current study it is recognized that introducing lateral restraints along the beam is not always a possibility. An example is light or medium duty crane beams in industrial buildings where the compression flange is not restrained along its entire length. Fabrication costs may prohibit the type of structural form that would provide restraints to the compression flange along the length of the beam either continuously or at discrete points. Therefor for these cases altering the section geometry presents the best opportunity for increasing the beams stability against lateral buckling. This is the approach that is taken in the current study. The introduction of stiffeners on the flange of the section and how these influence member behavior is studied. Examples of similar approaches are those proposed by Bijak et al. (2019) and Movaghati (2019) who suggested welding angle sections to the top flange to create flange end downstands. Previous studies have also reported the possibility of influencing member behavior without altering the other applicable factors. These have largely focused on restricting the warping of the flanges to increase the warping rigidity of the member. Szewczak et al. (1983) considered various configurations of plate stiffeners welded to the web and flanges of beams to achieve this. The different configurations were shown to have varying success. The current study looks at a simple approach of adding stiffeners to the flanges and observing how varying the stiffener height affects the shear center position relative to the centroid and how this influences member behavior. The introduction of these flange stiffeners makes the cross-section monosymmetric. Research on monosymmetric sections cannot be dissociated from research on doubly symmetric (or bi-symmetric) beam sections from which its research is in effect an extension. The research on doubly symmetric sections predates that on monosymmetric sections and is presented first. The research on monosymmetric sections is then explored and finally studies on general aspects of beam buckling are presented.

2.2 DOUBLY SYMMETRIC SECTIONS

Studies into the lateral-torsional buckling behaviour of steel beams first began with that for doubly symmetric beams. Early reported work by Michell (1899), for instance, was based on rectangular cross sections. Earlier studies have been reported in Flint (1948) and attributed to the time when hot rolled steel sections started to become available. Over the years it has come to be acknowledged that extensive research in lateral-torsional buckling has been largely devoted to doubly symmetric sections. In many countries doubly symmetric sections form a large part of available stock items of steel hot rolled members. These members find widespread use in buildings and other structures. It is therefore no surprise that an extensive amount of research has been devoted to these members. Some of the theoretical predictions are also easier to formulate with doubly symmetric sections for which the shear center and geometric centroid coincide.

Early research primarily made use of two broad approaches to determine the elastic critical buckling load; firstly, an approach based on finding governing differential equations formulated from a slightly displaced configuration of the member just as buckling is initiated. Secondly, an approach based on energy methods such as minimization of potential energy and conservation of energy (Bradford, 1992). Solving the differential equations from the former approach varied in complexity depending on the case considered. Because closed form solutions exist only for a few cases, for most practical cases approximate methods had to be employed to arrive at solutions for the critical buckling load. Similarly, for the energy methods in many cases an assumption of the deformed shape needs to be made and may affect the accuracy of the outcome. Commonly used Since the 1970s a third method emerged as a new versatile approach for buckling analysis and this was facilitated by the emergence of the digital computer. This method is the finite element method (FEM). The method is, in part, an extension of the matrix method and has the power of being able to analyze complex three-dimensional problems. Experimental studies are rare due to the high cost associated with these particularly if statistically significant results are to be obtained. However, some experimental studies have been carried out to validate theoretical models as well as to calibrate finite element models.

2.2.1 Analytical Studies – doubly symmetric beams

2.2.1.1 *Elastic buckling*

Theoretical or Analytical prediction of the elastic critical buckling load was initially carried out on rectangular sections based on classical methods as presented by Michell (1899). Similar work has been reported to have been carried out by Prandtl (1907) [reported in Timoshenko and Gere (1961)]. In the study by Michell (1899) governing differential equations were generated for both cantilever and simply supported beams with either point loads, end moments or a uniformly distributed load as the applied load. Bessel's functions were used to solve the governing differential equations to obtain the critical load. Experimental work was also carried out to validate results from the analytical equations derived and solved. Good correlation was observed in this study. This early work was easy to solve analytically as it involved the assumption of Euler-Bernoulli beam behaviour. Under this assumption plain sections remain plain and the effects of transverse shear are ignored. In addition, rectangular beams do not suffer from effects of warping and the shear center is coincident with the geometric centroid. End conditions were largely based on simply supported beams as well as cantilevers. It is interesting to note that theoretical treatment of open sections has been reported in Flint (1948) as having being carried out in the mid to late twentieth century however, this did not consider the full section but treated the compression flange as a column that could buckle. The next evolution of research was carried out by researchers such as Stephen Timoshenko who extended the derivation of the theoretical critical buckling load to thin-walled open cross-sections that were susceptible to warping effects when undergoing buckling (Timoshenko and Gere, 1961). In these cross-sections plain sections do not remain plane and therefore the warping effects potentially play a significant role in the member behaviour. The analytical approaches used consciously considered the entire cross section in formulating the solutions for the critical loads.

Early research was based on very specific loading and boundary conditions for which closed-form solutions to the governing differential equations existed. These are simply supported beams with twist prevented at the supports, warping allowed to occur freely and loaded by equal end moments. This type of end condition is obtained when using a 'fork type' support as illustrated in Fig.2-2.

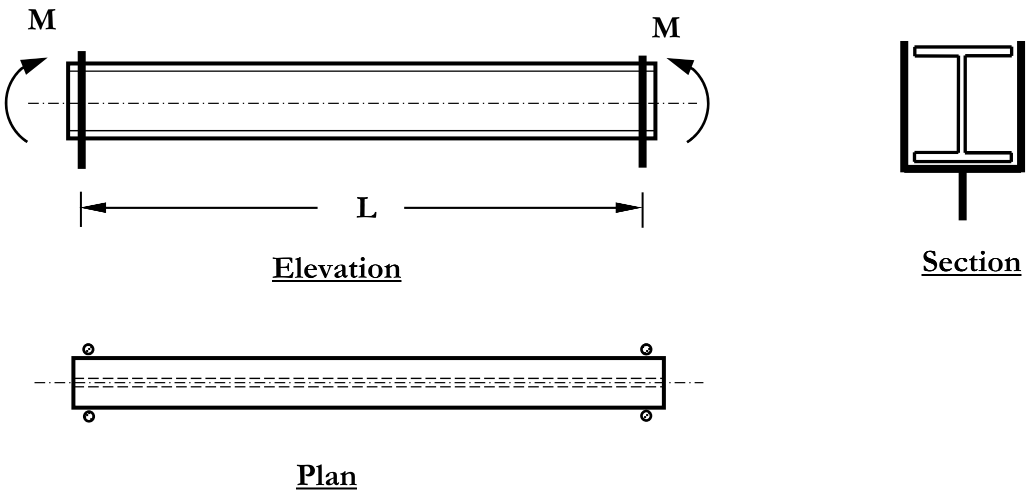

Fig.2-2 Simply supported beam with 'fork' type simple supports

For changes in any of the boundary conditions, warping restraint condition or loading form, the governing differential equations generally no longer have a closed form solution and must be solved using a numerical or approximate method. Other considerations such as load height application with respect to the shear center or centroid also lead to nonlinear governing differential equations for which closed form solutions do not exist or are at best tedious to obtain. Therefore, a lot of the early research then focused on incorporating these conditions and presenting the results in a format that could be easily used by design engineers in routine design. It is also worth noting that, generally, elastic buckling problems, based on the bifurcation phenomenon, lend themselves well to be evaluated as eigenvalue problems for which non-zero solutions for the dependent variable exist only for certain discrete values of some parameter. The values of the parameter, for which nonzero solutions exist, are known as the eigenvalues (Chajes, 1974). The buckled geometry is then captured using the resulting eigenvectors. Of interest is the lowest eigenvalue which corresponds to the desired critical load. The eigenvector accompanying this eigenvalue is the corresponding buckling mode shape.

It was always desired to keep a single simple format of the critical buckling equation and simply account for different load positions relative to the shear center, different bending moment profiles and different boundary conditions using appropriate factors. In the early stages of the development of the Eurocode this was done by way of a three-factor formula.

In North America various other factors were used. For the different bending moment diagrams the idea was to come up with an equivalent uniform moment factor which could relate the actual critical buckling load to that obtained from the case of equal and opposite end moments creating a uniform moment. The critical moment equation for the case of equal and opposite end moments is thus the benchmark equation with appropriate factors being developed to account for the deviations mentioned above. An example is shown in equation 2.1 of the critical buckling equation for a simply supported singly symmetric I-shaped section for the benchmark case as given by Galambos (1968). Equation 2.2 then shows the equation from the SAISC (2016) handbook now with a factor for end boundary condition and load height (K) as well as for nature of bending moment also known as the moment gradient factor (ω_2) included.

$$M_{ocr} = \frac{\pi^2 E I_y}{L^2} \left\{ \frac{\beta_x}{2} + \sqrt{\left(\frac{\beta_x}{2}\right)^2 + \left[\frac{C_w}{I_y} + \frac{GJ\,(L)^2}{E I_y \pi^2}\right]} \right\} \tag{2.1}$$

$$M_{ocr} = \frac{\omega_2 \pi^2 E I_y\, \beta_x}{2\,(KL)^2} \left\{ 1 + \sqrt{1 + \frac{4}{{\beta_x}^2}\left[\frac{C_w}{I_y} + \frac{GJ\,(KL)^2}{E I_y \pi^2}\right]} \right\} \tag{2.2}$$

This demonstrates how researchers have strived to develop a benchmark equation with factors being used for conditions deviating from the benchmark case. This discounts the need for having multiple design equations and simplifies the design process. The benchmark case is attractive because it has a closed form solution and gives a neat equation, however, it reflects conditions unlikely to be encountered in real structures hence the need for the applied factors.

Research work carried out by Bleich and Timoshenko in the early twentieth century on doubly symmetric beams was presented in their respective book publications (Bleich, 1952 and Timoshenko, 1936). The work of Bleich (1952) was novel and intended to bridge the gap between highly theoretical research outputs and knowledge required in a format suitable for design. The author indicated that Timoshenko had derived the fundamental equations of torsion of doubly symmetric I-beams and solved these. These solutions are also presented in Timoshenko (1936). It must be mentioned that a lot of the early research on doubly symmetric beams as reported in (Bleich, 1952) was not available in English. Presenting the outcomes of these, and other studies in the books by Bleich and Timoshenko presented above gave a lot of insight into the state of knowledge at that time. The work by Timoshenko was particularly important as it provided solutions to specific problems for beams of rectangular geometries as well as for I-shaped open cross-sections.

Various loading configurations were considered including the common ones of end moments, uniformly distributed loads and point loads (Timoshenko & Gere, 1961). One major importance with the work done by Timoshenko was the determination of solutions for beams of open sections subjected to transverse loads. Before this work, previous research on open sections had focused on the loading cases of end moments and, combinations of end moments and thrust in the beam members, or the case of a point load at the tip for cantilevers.

As indicated, some of the early studies on lateral buckling considered the case of combinations of thrust and end moments in order to cater for the likely loading cases found in structural frames. Research on lateral buckling of beams subjected to thrust and end moments was presented by Timoshenko (1936), DiMaggio et al. (1952) and Salvadori (1955). Interaction curves for the case of thrust and equal end moments were presented by Timoshenko (1936) and Johnston (1941), for rectangular beams and I-beams respectively, and these took the form:

$$\frac{P}{P_{cr}} + \left(\frac{M}{M_{cr}}\right)^2 = 1 \qquad (2.3)$$

in which P_{cr} is the Euler buckling load and M_{cr} is the critical value of the end moment without thrust.

The work by Salvadori (1955) sought to extend these to the case of I-beams under thrust and unequal end moments by making use of an energy method; the Rayleigh-Ritz method. The drawback with these approaches was the limitation of not considering the applied loading along the length of the beam. After this period a lot of the research on beams reverted to the case of beams loaded laterally or with end moments and having no thrust. Members having thrust and flexure were re-classified as beam-columns, and not beams, with separate design approaches used for these. Once the focus for beams was established as that of flexure only, studies could focus on understanding and controlling lateral buckling using relevant and applicable loading cases and boundary conditions. In order to simplify the application of lateral-torsional buckling design many codes adopted an approach of retaining the critical buckling equation associated with the closed form solution case of simply supported beam with equal end moments as the basic equation. Other load cases were simply accommodated by employing an equivalent uniform moment factor. Other factors could also be incorporated into the basic equation to account for any other considerations such as different end conditions or load height application.

Ways of controlling LTB have been the focus for many studies on members susceptible to this failure mode. One of the ways lateral buckling could be controlled was the introduction of lateral restraints along the member. The effect of discrete and continuous semi-rigid bracing in stabilizing beams against lateral-torsional buckling was studied by Rockey and

Nethercot (1971). Theoretical relationships established were compared with results from an experimental study carried out as part of the research. Good correlation was obtained. The effect of using torsional restraints at mid-span or off-center was investigated by Valentino and Trahair (1998). Effects of moment distribution and load height on the elastic flexural-torsional buckling of beams with these torsional restraints were studied. Design approximations and procedures were developed. A comprehensive review on the subject of beam stability bracing has been given by Yura (2001). An optimal design of steel beams by considering elastic nature of restrains at supports has been presented by Piotrowski and Szychowski (2019). An analytical model incorporating elastic restraints against warping and torsion at supports, that could be used to calibrate numerical models, was developed by the authors. A stiffness index factor for elastic supports, ranging from '0' for completely free to '1' for completely fixed, was developed and implemented.

The possibility of a buckling mode in which the cross section of the member distorts and displaces was investigated by Hancock (1978). This buckling mode came to be known as a distortional buckling mode. It is the third possible mode of buckling for a steel member in addition to those of local buckling and lateral-torsional buckling. Although observed in some previous studies no specific study on this buckling mode had been undertaken. The finite strip method was employed to identify the distortional buckling modes and corresponding critical loads. Distortional buckling was found not to have significant effect on flexural-torsional buckling unless thin webs are used or for very short beam lengths. A study of similar effect observed in beams supported on seats and restrained only on the tension flange was carried out by Bradford and Trahair (1983). Web distortions were anticipated to have more pronounced effect in deep, short-span beams. A simple design rule was developed for these I-beams in uniform bending with unrestrained top flanges. The relevance of lateral-distortional buckling to design situations was discussed by Bradford (1992). Previous research on the topic carried out in Australia was summarized by the author. It has been reported by Pi and Trahair (2000) that beams with slender webs and stocky flanges are more likely to buckle in a lateral-distortional mode. Reduction in member resistance due to web distortion was thus studied by the authors. The effect of elastic end warping stiffness when coupled with web distortion was also of particular interest. One of the finite element models used in the study, based on Pi and Trahair (1997), assumes an I-section to be composed of two rigid flanges connected by a flexible web. The Vlasov (1961) theory of torsion and Euler-Bernoulli theory of bending are used for the flanges, and Kirchhoff theory of plate bending used for the web plate. New equations for the lateral-distortional buckling moment were proposed and are similar to those for flexural-torsional buckling with torsional and warping rigidity replaced by 'effective' properties. End warping restraints were also considered. Distortional buckling was clarified as occurring in two distinct forms; un unrestrained mode and a restrained mode (Zirakian and Boyajian, 2018). A review of recent studies on the subject was presented, with potential avenues for future research highlighted.

Several investigations touching on various pertinent aspects of lateral-torsional buckling are presented here. The relation to properties identified in Table 2-1 can easily be established. An optimization technique to maximize the elastic flexural-torsional buckling capacity has been reported by Wang et al. (1990). This is seen as a critical exercise not only for economy but also increasingly for sustainability considerations. A better understanding of behaviour also generally leads to less conservatism on one hand and safer practices on another and is in itself an optimization process. A more accurate approach for the determination of elastic lateral-torsional buckling load which incorporates accurately the effects of moment gradient , lateral end restraint and beam slenderness was presented by Pandey and Sherbourne (1990). A superposition approach was used with warping and torsion modes treated separately and then combined. Derivation of the classical energy equation for lateral buckling of doubly symmetric thin-walled beams is presented by Pi et al. (1992). This was done to verify the correctness of an alternative energy equations presented by Gellin and Lee (1988), Pandey and Sherbourne (1990) and De Jong (1990). While the alternative equation gave similar results as the classical equation for uniform bending it was feared that incorrect results would be obtained for nonuniform bending cases. The alternative equation was found to be incorrect for some cases which were outlined.

The continuing need to find the elastic buckling load for beams was highlighted by Wang et al. (1994) who indicated the need to identify this as the upper limit to member buckling strength. It also was commonly used in design codes as the first step when determining ultimate capacity. The authors also presented an automated Rayleigh-Ritz method for the elastic buckling analysis of doubly symmetric I-beams subjected to arbitrary loading. Various end support conditions, discrete rigid bracing and internal supports were considered. Simplified lateral-torsional buckling equations were proposed by White and Jung (2003) for I-beams and channel sections. These were proposed to overcome shortcomings identified in the equations used in several North American design standards at that time. The equations were said to be exact for doubly symmetric sections and to improve the approximation accuracy for singly symmetric I-shaped sections compared to existing approaches. Authors Lopez et al. (2006) reviewed the equivalent uniform moment factor used in design codes. A new general closed form expression to compute the moment factor for any moment distribution and support condition was presented. New knowledge presented on lateral-torsional buckling can also be challenged as indicated with the work of Pi et al. (1992) in the preceding paragraph. A governing differential equation derived by Lamb and Eamon (2015) for doubly symmetric wide flange beams was similarly challenged. Trahair (2016) highlighted the inclusion of an unexpected term and the omission of an expected term in the equation. It was shown, in this case, that the proposed equation was in error with the correct formulation demonstrated using various approaches including calculus of variations, equilibrium of twisted beam, finite integral, finite element analysis and energy methods.

Research in the field of lateral-torsional buckling, as indeed in other related areas, finds its way into design standards for use by design engineers. As new knowledge is discovered the design standard approaches are refined or updated. A study on provisions in the Canadian standard CAN/CSA-S16 to account for load height effect was presented by Wong et al. (2015). The authors proposed an effective length method to account for loads applied away from the shear center. It was stated that the proposed approach would reduce conservatism while maintaining simplicity appropriate for use in design. Lateral-torsional buckling of European wide flange I-section beams was studied by Yilmaz et al. (2017). An analytical model based on the Ritz method was established with a closed form analytical equation developed. Combinations of loads were considered, and the equation results were compared to numerical results based on 1D finite element analysis. Good agreement was obtained. The lateral-torsional buckling behaviour and failure modes of cantilever and two-span steel beams was studied by Winkler et al. (2017). These models were compared to corresponding simple beams which are considered often as the basis for developing simplified models for design purpose. An understanding on the accuracy and consistency of using simplified models was sought.

A simplified first order torsion theory based on the Vlasov theory was developed by Wang et al. (2012) for restrained torsion of open thin-walled sections with shear deformation effects included. Shear deformation effects are considered important in short beams. Theories that ignore these are considered appropriate for long or slender beams.

Although much of the reported research has been devoted to simply supported beams and extensions to beams in frames, a considerable amount of research has also been carried out on cantilever beams. A study of critical buckling moment of an overhang cantilever with influence of back-span considered has been presented by Venter et al. (2019). A simplified design calculation procedure, which includes an appropriate buckling parameter, was developed from the results of the study. Even the reported work of Michell (1899) included studies on cantilever beams. More recently Trahair (2008) studied the lateral buckling of steel I-section beams used as crane monorails. These types of beams are often not well restrained against twisting. They have supports at intervals along the top flange with a free bottom flange. The influence of restraints on the elastic lateral buckling was investigated.

2.2.1.2 Inelastic buckling

It became apparent to researchers early on that elastic critical buckling load predictions often gave critical load values that were observed to be higher than actual failure loads in real specimens. This is partly because the critical elastic load is based on assumptions of an ideal member with no imperfections and also, in some cases, the critical buckling load value is much larger than the load that would cause material yield in the member or in parts of the member. Once parts of the member start to reach the yield stress, the effective modulus of the cross section is altered and therefore this affects the critical buckling load

(Chajes, 1974). Real beams of intermediate length experience inelastic buckling. Several studies have been reported on the inelastic lateral-torsional buckling behaviour of steel beams including by Galambos (1963), Galambos (1968), Trahair and Kitipornchai (1972), Kitipornchai and Trahair (1975a) and Kitipornchai and Trahair (1975b). A method of solution of the inelastic buckling of hot rolled wide flange beams subjected to equal end moments was presented by Galambos (1960). Stiffness reduction due to yielding as well as effect of residual stress were considered. An exact approach was first presented and then a simplified equation was suggested. Nethercot (1974) carried out a study on the inelastic buckling of doubly symmetric I-section beams containing welding type residual stresses. Based on results obtained a method of approximating the beam buckling curve was suggested. It was observed to compare favorably with available experimental results. Treatment of inelastic buckling using a transfer matrix formulation as well as using a finite element method approach was presented by Yoshida et al. (1977). Behaviour of two span continuous beams was investigated in the study. Predictions of the two methods were compared with results of tests on both single span and continuous beams. A study on the lateral instability of I-beams with imperfections was presented by Yoshida and Maegawa (1984). The study distinguished between the lateral-torsional buckling load and the ultimate load carrying capacity of a beam. The former being a bifurcation problem and the latter being the strength of a real beam with geometrical and material imperfections. Effect of residual stress type, loading conditions and geometrical imperfection on the ultimate load was examined.

In order for residual stress effects to be accounted for in inelastic buckling studies their nature and distribution needs to be known. Although models of residual stress patterns exist for many stock sections, Szalai and Papp (2005) indicate that some existing models may have a drawback of not satisfying equilibrium equations connected with torsion and warping of the profile due to residual stresses present in the member. A new stress pattern was proposed by the authors which satisfies all equilibrium equations.

A method for determining ultimate strength of beams using inelastic buckling has been presented by Trahair and Hancock (2004) based on reduced elastic moduli. Results were checked against strength curves in the Australian standard AS4100 (1998). A methodology for the resistance evaluation of beams subject to lateral-torsion instability has also been presented by Rebelo et al. (2009). Finite element modelling, with imperfections accounted for, was then carried out for the same elements. The target failure probability of Eurocode 0 (CEN, 2002) was used to define partial safety factors. Trahair (2010) indicated that methods used for design of steel beams supported at both ends were not suitable for the design of cantilevers. In this regard the author pointed out the danger of simply modifying methods for supported beams and applying them to cantilevers. Design methods for cantilevers based on elastic buckling (design by buckling) and inelastic buckling were proposed with a worked example provided. A stiffness reduction approach is presented by Kucukler et al. (2014) for lateral-torsional buckling assessment of steel beams. The method considers the influence of imperfections through the reduction of the elastic and shear modulus values. The proposed method was verified with results from nonlinear finite element modelling. The novelty of the approach is that linear buckling approaches can be used as long as the modulus values are adjusted to suit the inelastic state. A resolution of discrepancies between design curves used in North American codes and the conservative ultimate strengths obtained from nonlinear finite element models was undertaken by Subramanian and White (2017). Imperfection levels used in finite element models were reported to be conservative when an inverse solution approach was applied to test data. Inelastic lateral buckling of continuous beams has been investigated by Trahair (2019) with comparisons made between predictions and ultimate strength values in the AISC code.

2.2.1.3 Pre-buckling deformations

In the formulation of the elastic critical load values discussed earlier authors developed analytical models for predicting the elastic critical load without considering that there is some prior deflection of the member in the direction of the applied loads before reaching the critical load when displacements at failure are in a direction perpendicular to that of load application. These prior displacements are known as 'pre-buckling' displacements. The effects of these pre-buckling displacements were initially not investigated, and it appears this was partly due to the observation that shallow arches bent in the concave orientation exhibited stable configuration as opposed to those in a convex shape. Thus, it appears that it was assumed ignoring the pre-buckling displacements, for simply supported beams at least, was a conservative approach.

The influence of pre-buckling displacements on the elastic critical loads of thin bars of open sections have been presented by Roberts and Azizian (1983). An energy method approach was employed in this study to generate the governing differential equations. Both closed form and numerical solutions to the differential equations are presented. Other studies by Erkmen and Attard (2011) and Mohri et al (2012) reported utilizing approaches based on nonlinear large displacement theory as well as those on linear buckling. These studies were able to demonstrate that sections with large flanges and hence large ratio of minor axis to major axis second moment of area are more sensitive to pre buckling displacement than those with a lower ratio. This implies that H-beams would be more sensitive than I-beams. The study by Mohri et al (2012) shows that the sensitivity is greater for bottom flange loading than it is for top flange loading. Trahair (1993) presents an equation for adjustment of the critical elastic moment of a simply supported beam subject to uniform moment with consideration of pre-buckling displacements and it is presented here in equation (2.4). The equation can be re-written in the form of the elastic critical buckling load without consideration of pre-buckling displacement divided by a factor that depends on the ratio of second moment of area of minor axis over that of the major axis i.e., (EI_y/EI_x). This can be re-written as a factor (k_1).

$$M = \frac{M_{cr}}{\sqrt{\left[\left(1 - EI_y/EI_x\right) \cdot \{1 - (GJ/2EI_x)(1 + \pi^2 EC_w/GJL^2)\}\right]}} \qquad 2.4$$

in which

$$M_{cr} = \sqrt{\left(\pi^2 EI_y/L^2\right) \cdot (GJ + \pi^2 EC_w/L^2)} \qquad 2.5$$

Equation (2.4) can be written as (2.6) with $\left(k_1 = 1 - EI_y/EI_x\right)$ and $k_2 = \{1 - (GJ/2EI_x)(1 + \pi^2 EC_w/GJL^2)\}$. So that as the second moment of area ratio approaches ‘1’, there is a corresponding increase in the critical elastic moment of the section. This illustrates why wide flange sections have a higher sensitivity to pre-buckling displacements as they have a higher ratio than do narrow flange I-sections. However, it must be noted that prebuckling displacements for simply supported beams are likely to lead to amplification of the critical elastic moment, due to the concave ‘reverse arch’ shape, and are therefore a conservative effect. Neglecting the effect from prebuckling displacements is therefore a conservative approach for the case of a beam which is sagging due to the ‘inverted arch’ effect which tends to provide stiffness to the beam. This, from a design standpoint, would be desirable and provides a preferred redundancy. Trends for the flexural stiffness ratio in k_1 are presented, for the section considered in the current study, in Appendix A. These give an indication of the effect that pre-buckling displacements would have on the critical elastic moment.

$$\frac{M}{M_{cr}} = \left(\frac{1}{k_1}\right)^{0.5} \cdot \left(\frac{1}{k_2}\right)^{0.5} \qquad 2.6$$

It has been suggested by Pi and Trahair (2000) that for the failure mode of lateral-distortional buckling, ignoring pre-buckling deformations is valid only for cases where there are small ratios of minor axis torsional and flexural stiffness to major axis flexural stiffness. When the ratios are not small then effects of prebuckling displacements need to be considered. So, it is a similar case to that of critical elastic global buckling.

2.2.2 Experimental Studies – doubly symmetric beams

Experimental studies, though useful in providing empirical data, have been limited in magnitude and scope when compared to reported analytical and numerical studies. One of the reasons that can be attributed to this is the cost and time factors of carrying out experiments (Rebelo et al., 2009). Experiments take time to set up and great care must be taken to set up the experiments so that desired parameters can be accurately measured and read. Some practical difficulties with testing beams and challenges in interpreting results have been highlighted by Kitipornchai and Trahair (1975b). The authors indicated that not many full-scale tests had been carried out previously. It was realized early on in the study of steel beams that the behaviour of real beams generally does not match theoretical predictions based on elastic theory except for long slender beams. This is because beams in the intermediate range can experience inelastic behaviour either due to parts of the member starting to fail before others based on the nature of the stress distribution, or due to imperfections. Imperfections can either be geometric, as a consequence of manufacturing tolerances, or material due to residual stresses locked into the member at the cooling stage of manufacture, if hot rolled. This meant that experimental data could only be compared to theoretical predictions if these had considered inelastic behaviour. The influence of the inelastic behaviour is only diminished for long slender beams.

Experimental data has been very useful in informing researchers on how real members behave and have formed the basis for semi-empirical design equations in many design standards. Experiments not only help to validate analytical equations or theoretical concepts, but they also help to calibrate numerical models from which parametric analyses can be conveniently carried out. Some of the early experimental work has been reported by Michell (1899) who validated results from analytical equations with experiments on long span cantilever rectangular beams. Results obtained were in close agreement. The post-buckling behaviour of wide flange beams was investigated experimentally by Lee and Galambos (1962). The study yielded a number of observations including a cut off length of $45r_y$ beyond which observed failure mode was that of lateral-torsional buckling. The study was further extended to continuous beams, with the critical span having fully yielded adjacent segments, by Prasad and Galambos (1963). A similar cut off length, this time of $40r_y$, was observed and reported. Beams of this length or more failed by lateral-torsional buckling while shorter beams experienced failure by local buckling. No distinction was given between inelastic and elastic LTB. Inelastic buckling tests on simply supported I-beams were carried out by Kitipornchai and Trahair (1975b). In these tests as-rolled beams as well as annealed beams (i.e. beams with the residual stresses largely removed) were used subjected to a central point load. The boundary conditions were consistent with 'fork type' supports which allow warping to take place freely but prevent member rotation at the supports. The experimental results showed that for the beams tested geometrical imperfections had a greater influence on behaviour than residual stresses. The experimental results compared well with theoretical predictions. The experiment outcome was also used to confirm that the Australian Code rules at the time had consistent load factors in the elastic and inelastic ranges. While highlighting challenges encountered with previous full-scale beam experiments the authors had sought to minimize or eliminate the identified uncertainties. Tests to study the inelastic buckling of simply supported continuous I-beams was carried out by Dux and Kitipornchai (1983). Various moment gradients were employed with the applied loading. Measurement of geometrical and material imperfections was included. Comparisons of results obtained to theoretical predictions were made.

The study of laterally unsupported beams from a statistical consideration was presented by Fukumoto et al. (1980). This was undertaken in order to have reliable statistical data on imperfections such as residual stresses and initial out of straightness in beams. The study was also undertaken to provide statistical data for lateral buckling strength of beams under nominally identical conditions of loading, supports and member sizes. Test specimens from three series of lengths were considered and the loading employed was that of a midspan point load. Residual stress measurements, out of straightness and tensile coupon tests of flange and web were also carried out. Results on degree of correspondence between various beam parameters and the scattered ultimate strength were reported. The actual full plastic moment of the specimen was observed to have a high influence on the variation in the ultimate strength. Having observed that there are three buckling modes of failure possible for open thin-walled sections; (a) local buckling of plate elements, (b) lateral-torsional buckling and (c) combined local and lateral-torsional buckling (interaction buckling), Kubo and Fukumoto (1988) carried out experimental tests on beams susceptible to the mode (c) of interaction buckling. A particular range of flange width-thickness ratio and web width-thickness ratio was employed so that sections were not necessarily compact. It was reported that intermediate length beams failed by in an interaction buckling mode, while long span beams failed by a lateral-torsional buckling mode. Experimental ultimate strength was compared to nominal design strength specifications of North America. It was found that design approaches based on the effective width concept gave reasonable estimates. This study is deemed to be more applicable to cold-formed sections or plate girders with thin webs or flanges were the thin members are non-compact.

In the last decade there has been a steady shift towards the use of high performance and high strength steel in some countries. These steels offer, among other things, the advantage of increased strength with Bradford and Liu (2016) reporting grades of up to 690 MPa. The downside is that with increased strength there is a tendency to use the member in a configuration that makes them slender and thus susceptible to buckling. Tests on GJ steel, a high-performance steel produced in China, were carried out by Yang et al. (2016). In this study flexural tests were carried out on welded H-section beams. The results obtained were used to calibrate a numerical model. The numerical model was used to carry out a parametric study whose results were used to verify whether current design standards in China, Europe and North America predict the flexural strength of GJ steel beams correctly. Results indicated that the Chinese codes predicted the strength appropriately, The Eurocode gave conservative predictions and the American code predicted strengths that were too high. The test setup used is illustrated in Figures 2-3 and 2-4.

Another high-performance steel designated as WGJ steel which has been developed in China was tested for lateral-torsional buckling behaviour by Xu et al. (2018). The study was similar to that carried out by Yang et al (2016) on GJ steel, the difference being that results were compared with design provisions of only two design standards. It was found in this study that the design equations in the Chinese code gave less safe margins for overall stability design of welded I-section beams fabricated from WGJ steel. It was found that the Eurocode on the other hand appeared to give conservative results in all conditions.

Fig.2-3 Test setup employed by Yang et al (2016)

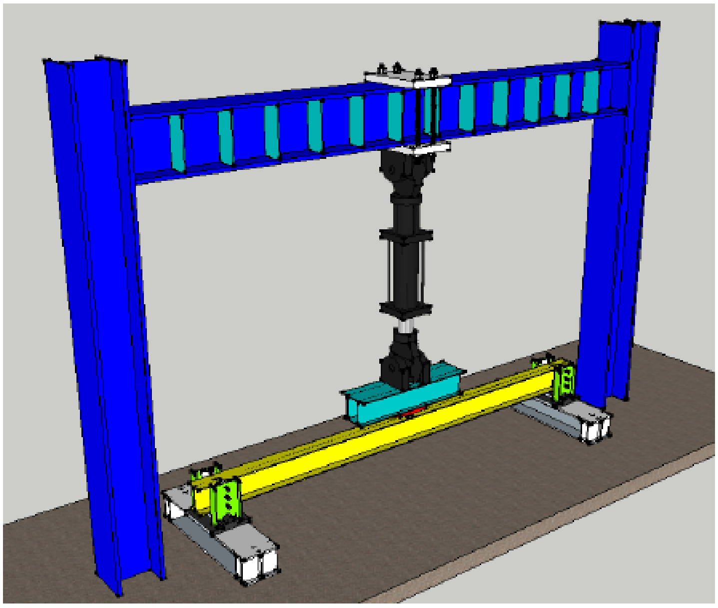

Fig.2-4 Test set up 3D model (from Yang at al., 2016)

In order for material imperfections to be incorporated in numerical models the nature and distribution of residual stresses in members need to be known. Therefore, over the years several tests have been carried out to characterize these. Experimental results on the determination of residual stresses and their distribution in various shapes were given by Tebedge and Tall (1973). These covered various hot-rolled as well as welded sections including wide-flange, angle and tee-sections. Young (1975) surveyed a large number of previous measurements and established typical patterns for inelastic buckling strength calculations. Measured patterns in commonly used British beam and column sections agreed with the established typical patterns. American residual stress assumptions were noted to be unrealistic in distribution and magnitude. Confidence was expressed that the selected typical patterns were consistent with British hot rolled sections. Due to the sometimes widely varying models of residual stress patterns it continues to be common for those carrying out experimental test such as Yang et al. (2016), and a few others presented before, to carry out their own tests on the residual stress pattern of members investigated. An experimental, numerical and statistical analysis of residual stresses in tapered I-beams has been presented by Tankova et al. (2019). Systemized information on residual stress distribution and magnitude was generated with guidelines for statistical characterization of residual stress in welded members proposed. One novel approach used in this study is that of numerically predicting the residual stress distribution for welded beams using a simulation of the welding process.

It is clear that despite the challenges in carrying out full-scale beam tests for lateral-torsional buckling behaviour information that is obtained from correctly calibrated tests is invaluable. It helps to not only develop the semi-empirical design equations but also to calibrate numerical models which can be economically used to perform parametric analyses.

2.2.3 Numerical Studies – doubly symmetric beams

Numerical methods for solving buckling problems arose due to the limited nature of cases that yielded closed form solutions based on classical solution methods. Typically, closed form solutions were possible when the governing differential equations for the buckling problem were linear. Methods for solving ordinary differential equations (ODEs) were employed in determining the non-trivial solutions yielding the critical loads. However, many of the loading cases and boundary conditions lead to governing differential equations that are nonlinear differential equations. Classical closed form solutions to many of these equations do not exist and therefore researchers have to turn to approximate methods of solutions; numerical methods. Several numerical methods have been developed over the years based on both approaches of static-kinematic formulations as well as energy methods. For many years the methods of finite differences as well as finite integrals were predominantly employed for the numerical solution of buckling problems. Approximate methods have been presented by Timoshenko and Gere (1961) while the method of finite integrals, with elaboration on its merits, has been presented by Brown and Trahair (1968). Many texts have presented the use of the finite difference method including Chajes (1974) as well as Ozbasaran (2013). An approach that has gained a lot of popularity since the 1970s is the finite element method (FEM) due to its power and versatility. Its development saw rapid growth largely due to two important advances; the development of the digital computer and, the improvements in application of matrix methods in structural analysis and mechanics. This numerical approach is amenable to use with digital computers. Over the years the finite element method has developed as an indispensable tool in many forms of buckling analysis and the capabilities of software to model, analyze and display results have grown in complexity. Numerical analysis also holds the advantage over experimental testing in that once the model is calibrated lots of parametric analyses can be carried out generating lots of useful data that would otherwise be too expensive and time consuming with experimental testing. However, because numerical methods are based on approximate approaches they have to be used judiciously with thorough knowledge of inherent errors and limitations, and how these can be managed in realistic models.

A finite element procedure for analyzing inelastic beam and beam-columns of arbitrary cross sections has been presented by Rajasekaran and Murray (1973). The authors made use of the tangent modulus approach to inelastic buckling where strain reversal is assumed not to occur. The formulation presented includes expressions for programming section properties and element matrices. The technique presented was illustrated by some problems for which known results were available. A finite element procedure for obtaining the critical buckling load for three-dimensional structures idealized by planar two-dimensional elements was presented by Johnson and Will (1974). The accuracy of the procedure was verified by comparing results with those obtained for problems whose classical solutions are available. Comparisons with results from an experimental test were also presented. Because, as indicated, the numerical methods are based on approximate methods various authors studied different formulations in an attempt to find element formulations that could capture and model desired behaviour the most realistically. In this vein Attard (1986) presented two new finite element formulations for calculation of the lateral buckling load for elastic straight prismatic beams. The criterion used was based on the positive definiteness of the second variation of total potential energy. Both formulations were tested with problems having classical solutions or against experimentally determined results and were shown to be accurate. A numerical method, based on the energy methods, to predict the lateral-torsional buckling loads of transversely loaded slender doubly symmetric beams containing unreinforced web openings was presented by Thevendran and Shanmugam (1991). Cantilevered and simply supported beams with openings along the web centerline were considered. Critical loads obtained were compared with experimental results. Good agreement was obtained between numerical and experimental results. Effects of lateral bracing to the compression flange as well as torsional bracing in controlling lateral-torsional buckling were studied by Yura and Phillips (1992). Cross section distortion at bracing points was observed to significantly affect efficiency of torsional bracing. Analytical solutions led to development of two bracing equations; one for lateral bracing and one for torsional bracing. Bracing equations' results and the results from the computer software analysis were found to compare well with results from seventy-six (76) lateral buckling tests carried out under the study.

Developments in the digital computer not only saw widespread application of numerical methods but also saw the emergence of general purpose and commercial software based on numerical approaches. One such software is PRFELB. The merits of using this software for flexural-torsional buckling considerations of beams, beam-columns and plane frames were presented by Papangelis et al. (1998). The software would also enable implementation of the method of 'design by buckling' which was at the time permitted in several steel design standards. Moment gradient or 'equivalent moment factors' used by design codes of practice were investigated for different load cases using a numerical model based on the finite element technique by Sayed-Ahmed (2004). Effects of load applied at a height away from the shear center were considered. New moment gradient equations with consideration of load height were introduced.

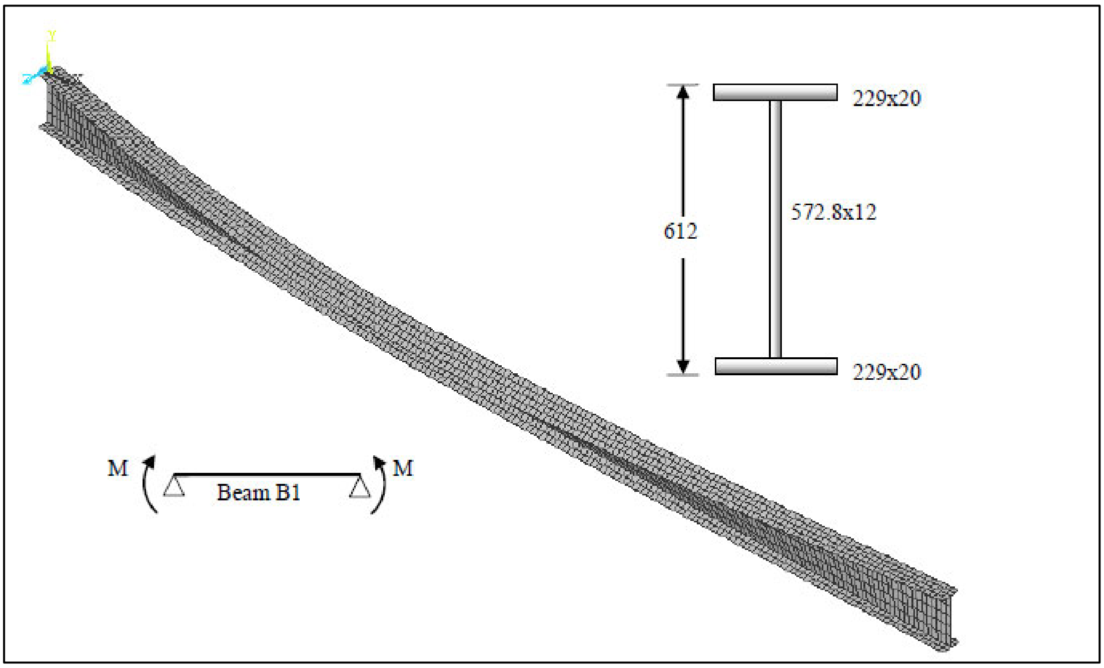

Fig.2-5 Buckling mode from finite element model by Sayed-Ahmed (2004)

Optimization of members used in structures where moments vary over the span has over the years led to considerations of using tapered members. In order to understand the buckling behavior of web-tapered I-beams Raftoyiannis and Adamankos (2010) presented a numerical approach for determining the critical lateral-torsional buckling load. Various taper ratios were investigated. Modification factors for the elastic critical moment with reference to mean cross-section were given. Further studies on lateral-torsional buckling of web-tapered I-beams was carried out by Kovac (2012). This study used both one dimensional (1D) and three-dimensional (3D) finite element analysis software to validate analytical equations developed as well as their solutions.

As with analytical equations for ultimate strength it became imperative to develop numerical models that would not only predict elastic critical buckling loads but also be able to capture the real behaviour of beams that have imperfections. The capability and application of numerical modelling therefore developed into consideration of inelastic behaviour and ultimate strength predictions. In this vein a study carried out by Kala (2013) dealt with the problem of lateral-torsional buckling of simply supported I-beams undergoing major axis bending. Numerical modelling was used to study the statistical characteristics of imperfections by way of a sensitivity analysis. Principal imperfections affecting lateral beam buckling strength were discussed. A further study on random effects of initial imperfections on the ultimate load-carrying capacity was carried out using non-linear finite element analysis by Kala and Vales (2017b). The authors also present a global sensitivity analysis of stochastic effects of initial imperfections and residual stress on the resistance of steel I-beams Kala and vales (2017a). A study on the buckling strength of hybrid steel I-beams was presented by Shokouhian and Shi (2015). Hybrid steel beams used in this study made use of two different high-strength steels; one for the web and a higher strength for the flanges. Numerical models were calibrated with experimental data and then used to carry out parametric analyses. Material nonlinearity as well as geometric imperfections were accounted for. The stress-strain relationship was obtained from coupon tests and applied in the models. An equation for design of hybrid high strength steel sections was presented. This was compared to provisions in Eurocode and the American Institute of Steel Construction (AISC) standard. Close agreement with the proposed method in the Eurocode was observed. The authors also proposed a method of establishing flexural strength independent from section classification. With the use of high strength steel (HSS) gaining widespread use understanding its flexural-torsional buckling strength has attracted particular focus. A study by Bradford and Liu (2016) on the flexural-torsional buckling strength of HSS beams has been presented. The focus was on HSS beams with yield stress in excess of 690 MPa. A commercially available numerical analysis software was used for the study. Stress-strain curves and residual stresses were incorporated in the models. A strength design formulation was proposed based on the outcomes of the study. A numerical study on the lateral-torsional buckling behaviour of steel beams subjected to huge-mass impact loads was carried out by Zhang et al. (2018). Impact kinetic energy was found to have a greater effect on lateral-torsional buckling than momentum. The study was reported as being carried out to understand load effects that can be brought about by extreme events or shock that can result from explosions, impact or falling objects associated with fire. Numerical simulations were compared with experimental results from tests on narrow rectangular beams.

The choice of model is critical in obtaining accurate results with numerical analysis. For finite element analysis this is best aided by understanding the capabilities and limitations of each approach and element type. For 3D buckling analysis the choice is typically between a shell element model or a model with solid elements. The finite element modelling of lateral-torsional buckling using shell and solid elements has been presented by Vales and Stan (2017). Initial imperfections are incorporated in both models for analysis of resistance.

The difference and correlation between results was discussed as were the advantages and disadvantages of both methods.

The use of slender, class 4, I-beam hot-rolled members is rare and generally avoided in practice due to susceptibility to local buckling effects. The only exception being plate girders where slender webs are commonly employed albeit stiffened. Design aids for sections with slender members are required to assist designers in case a situation arises where their use is merited. Design formulae for estimating the design strength of these beams were proposed by Couto and Real (2019). Finite element models were used in the study to carry out an extensive parametric study based on nonlinear analysis. The models were calibrated against experimental tests available in the literature. Both material and geometrical imperfections were considered. A novel concept, the effective section factor (E.S.F.) was developed to account for the observed coupled local and lateral-torsional buckling interactive modes. An experimental and numerical evaluation of the inelastic lateral-torsional buckling behaviour of I-section cantilevers was undertaken by Demirhan et al. (2020). Numerical models were used in a two-step procedure to obtain nonlinear load-deflection behaviour based on the RIKS method. The results from the numerical analysis were compared to results from experiments carried out in the study. It was shown that the numerical approach used was able to predict buckling loads, vertical displacements and torsional rotations to an acceptable level in the design stage.

The evolution of numerical models that evaluate elastic critical buckling to those that are able to consider inelastic behaviour has been shown in the studies presented. Numerical models have thus become indispensable in determining real behaviour of structural members and evaluating their ultimate strength provided that the magnitude and nature of imperfections are known.

2.3 MONOSYMMETRIC SECTIONS

The study into the behaviour of monosymmetric cross-section evolved from that of doubly symmetric beams. Early monosymmetric beams were largely in the form of an I-shaped section with unequal width flanges. The geometries later included compound sections of I-sections with channel caps and in the case of Australia, an I-shaped section with top flange downstand lips. It appears other cross-section types with transverse loading along the plane of symmetry are not prevalent or not significantly reported on. The current study evaluates a type of monosymmetric cross-section but with stiffener plates introduces as upstands on the flange. Much of the research on monosymmetric sections is grounded on the work of Wagner and Pretschner (1934) as well as Wagner (1936). In studying the torsional buckling of members in compression Wagner (1936) theorized that in the slightly deformed configuration, the torsional stiffness was affected by stresses setting up moments about the shear center arising from a transverse component of force in the inclined longitudinal fibers. Thus the St. Venant torsion now had an accompanying factor in the governing differential equation. Compressive longitudinal stress tends to reduce torsional strength while tensile stress increases it. For doubly symmetric sections, where the geometric centroid and shear center coincide, these torques cancel each other out and have no effect resulting in a measure of simplicity. For monosymmetric sections the torques do not balance if the shear center and centroid do not coincide and hence this contributes either to an increase or a decrease in the torsional stiffness depending on the location of the shear center. This has come to be commonly referred to as the 'Wagner effect' (Anderson and Trahair, 1972), (Wang and Kitipornchai, 1986a).

The research into monosymmetric sections is presented in the sections that follow under the categories of studies based on theoretical predictions, that based on experimental work and that based on numerical work.

2.3.1 Analytical studies – monosymmetric beams

2.3.1.1 General

Early work on the study of monosymmetric sections has been presented by Hill (1942) who studied the elastic critical buckling moment of an I-shaped beam with unequal width flanges. Equations for the case of equal end moment loading were obtained analytically for the support conditions of a simply supported beam as well as for fixed end supports. Hill accounted for the twist resistance of the flanges using an approximate expression but did not elaborate on how this was derived. For the simply supported case a governing differential equation based on the slightly deformed shape was formulated and evaluated for the critical elastic moment. For the fixed supports an energy method was employed to generate the equation for the critical elastic moment. Experiments were carried out on Aluminium beams to validate the theoretical results. Although test results gave slightly lower moments than obtained from the equations they were largely in agreement. One beam that had a markedly lower failure load was rationalized to have failed by inelastic buckling as the yield load was lower than the theoretical buckling load. Although work done by Goodier (1942) looked at theoretical buckling load equations for an arbitrary cross section subjected to end moments and centric thrust, the relevant equation for a monosymmetric section subjected to end moments could be obtained by retaining only those parameters or variables that apply to monosymmetric cross sections. The work by O'Connor (1964) sought to further earlier work presented by Bleich (1952) by including refinements that considered orders of magnitude so that small terms were not indiscriminately discarded. The work presented by Anderson and Trahair (1972) was a seminal study with regards stability of monosymmetric beams and cantilevers. The study included the practical case of transverse loading. Also, in this study the correct form of the monosymmetry parameter, the parameter that captures the *Wagner effect*, was determined to be the one presented by Goodier (1942). The form proposed by O'Connor (1964) and an approach proposed by Bleich (1952) were shown to be in error. The confirmed form has been in use in studies on the buckling behaviour of monosymmetric beams over the years and remains largely the form used to date. The authors also presented information on the effects of monosymmetry and position of applied load relative to the shear center on the elastic buckling of I-shaped simply supported beams and cantilevers. Experiments on high strength Aluminium beams were also carried out to confirm the obtained information.

It was recognized by Kitipornchai and Trahair (1980) that calculation for monosymmetric sections members such as the warping constant and monosymmetry constant can be cumbersome for routine design. The authors presented simplified approximate equations for these properties and gave the validity range that applied. Roberts and Azizian (1984) presented critical buckling load equations for monosymmetric simply supported and cantilever beams with different loading conditions. The authors included the influence of prebuckling displacements. Closed form solutions were presented. Where these could not be obtained, numerical solutions were given. For cases where the buckled shape could not be approximated as a single half sine wave, finite element solutions, neglecting prebuckling displacements, were obtained. A similar study was also reported (Roberts and Burt, 1985). Critical buckling loads for simply supported monosymmetric sections were also presented by Wang and Kitipornchai (1986a). Results were based on finite integral solutions as well as energy methods. Particular study was dedicated to the moment modification factors used to adjust for loading conditions not being that of equal end moments. It was found that moment modification factors should not be based on those used with doubly symmetric beams. The authors proposed simple approximate formulas. Guidelines for achieving the optimum I-shaped section monosymmetric beam were given. The study was then extended to cantilever beams (Wang and Kitipornchai, 1986b) subjected to an end moment as well as for transverse loads. Solutions from a numerical method were compared to those obtained from an energy method; the Rayleigh-Ritz approach. Simple approximate formulas were presented. Further study on the elastic lateral buckling of simply supported monosymmetric beams under moment gradient was reported by Kitipornchai et al. (1986). Approximate buckling formulas considering more accurate moment modification factors were presented. Pekoz (1992) also presented a study on general solutions for the lateral buckling moment of singly symmetric sections. Effect of load location relative to shear center as well as moment gradient were studied. Design provisions for the case of moment gradient were outlined. The effect of load height on the lateral-torsional buckling behaviour of simply supported monosymmetric steel beams has been presented by Morkhade and Gupta (2013). The effect of including shear deformation as well as prebuckling deformations in some specific cases of the lateral-torsional buckling problem has been presented by Erkmen and Attard (2011).

A critical review of Vlasov's theory of stability when considering in-plane bending of thin-walled elastic beams has been presented by Saucha and Rados (2001). The authors highlighted an inconsistency in the derivation of differential equations for the case of transverse bending with a centric axial load. A consistent derivation was presented. Existing theories used to develop buckling equations for simply supported monosymmetric sections were reviewed by Tong and Zhang (2003) with a new approach being proposed. Approaches presented by Bleich (1952), Lu et al. (1983) and Trahair (1993) formed part of the review. The authors developed a new approach similar to that proposed by Trahair (1993) and also showed that the theory by Lu et al (1983) was in greater error when compared with experimental test results. The version of the monosymmetric elastic critical buckling equation reviewed uses three factors: C_1, C_2 and C_3 in the formula. This format is commonly referred to as the '3-factor formula' and is slightly different in presentation to that given by Anderson and Trahair (1972). It has been reported by Baláž and Koleková (1999) that Djubek and Mrazik (1958) were the first to show the convenience of expressing the critical elastic buckling equation for monosymmetric sections in terms of three coefficients accounting for different loading and boundary conditions. This led to the expression that came to be known as the 3-factor formula. The study by Tong and Zhang (2003) was extended to include the case of lateral-torsional buckling of cantilever beams in Zhang and Gengshu (2008). A surprising result was observed by Camotim et al. (2012) where it was reported that for the I-section monosymmetric beams investigated the case of uniform moment was not the one that gave the lowest critical buckling moment. This is counterintuitive as that is the case for doubly symmetric beams. The behaviour was demonstrated and, an explanation based on mechanics and mathematics explaining the surprising behaviour provided. It is worth noting that even though the authors could not locate in the literature anywhere where such a discrepancy was observed or explained, an observation on some unusual behaviour with monosymmetric sections had been made by Bradford et al. (2002). This was observed while the authors were investigating the critical load position of two applied point loads, representing the traveling crane bridge, applied on a monosymmetric crane runway beam. The different established methods for obtaining the critical buckling moment; the differential equilibrium equation of the slightly deformed configuration, an energy method approach and using finite element modelling are presented by Aydin et al. (2013). Solutions are presented for both doubly and singly symmetric cross sections with six loading cases used to demonstrate application of the methods. The choice of displacement functions for the energy method solution is discussed. A new dimensionless analytical solution for the buckling of I-beams has been presented by Zhang et al (2017). This was done to resolve challenges presented by some researchers on existing theories used. The performance of the new equations was verified using a numerical study. A design formula was also presented.

The post-buckling behaviour of monosymmetric I-beams was investigated by Ioannidis and Kounadis (1994). It was confirmed through this study that these beams are imperfection insensitive exhibiting post-buckling strength but with a shallow equilibrium path. The load carrying capacity above the critical load is, hence, not significant. The case of discrete lateral braces was investigated by Wang et al (1987) for monosymmetric cantilever beams. The influence of brace type and location was investigated with the influence of load height also incorporated. The buckling behaviour of parallel girders joined at their midspan by secondary beams was investigated by Gengshu and Shaofan (1989). Conditions under which the secondary beams increase the buckling moment were reported. The effect of discrete torsional bracing placed along the length of a simply supported monosymmetric beam subjected to end moments was investigated by Mohammadi et al. (2016). Proposed equations were put forward based on an analytical solution verified numerically. A predictive equation for the lateral-torsional buckling load of a monosymmetric beam-column subjected to a known load has been presented by Yilmaz and Kirac (2016). The Ritz method was used to formulate the proposed equation.

As with doubly symmetric beams the inelastic buckling behaviour must be determined to establish the ultimate strengths of these beams. For an inelastic buckling study to be carried out the constitutive material behaviour is required. Also, the magnitude of both geometric and material imperfections needs to be known. Studies on the inelastic behaviour of beams have typically been intended for the determination of real beam behaviour and subsequently, once ultimate strength is known, for development of design procedures to be included in design standards. A solution approach taking into account the elastic-plastic stress-strain relationship, spread of plastification in the longitudinal direction and as well as residual stress was used by Lindner (1976) to determine the ultimate load of a monosymmetric I-shaped beams due to lateral-torsional buckling. The loading used was that of a central point load. It was indicated that the more unfavorable case of uniform moment at the ends is seldom encountered in real members. Results were presented for a monosymmetric beam as well as for a doubly symmetric beam for comparison. It was found that the ECCS (1976) manual on stability gave safe predictions for ultimate strength of doubly symmetric beams but for monosymmetric beams could only be used for a given validity range. A marked difference in the trendline is observed for monosymmetric beams when compared to doubly symmetric beams studied. The inelastic buckling of welded monosymmetric I-beams has been investigated by Kitipornchai and Wong-Chung (1987). The inelastic buckling capacity was found to be affected by degree of monosymmetry as well as residual stress pattern. Theoretical capacities compared well with previous test results. A simple method for determining the inelastic buckling moment was presented with existing design rules reviewed.

A study of the lateral-torsional buckling provisions for monosymmetric beams in the draft Eurocodes (ENV 1993, ENV 1999) was presented by Baláž and Koleková (1999). Errors in existing solutions were highlighted and corrections were suggested. Validity for some of the given formulas was discussed. The Eurocode 3 (EC3) approach to design of monosymmetric beams was also investigated by Djurić-Mijović and Trajković (2007). The authors focused on the influence of cross-section shape and also the accuracy of the proposed approximate method in EC3 versus the approximate formulas proposed by Kitipornchai and Trahair (1980). Monosymmetric I and T-section beams were studied. It was concluded that the approach by Kitipornchai and Trahair (1980) was much more accurate compared to the exact formula in EC3 than the proposed approximate method in EC3. Recommendations on different types of sections suitable for different length and loading conditions were made. Use of the 3-factor formula was extended in domain to include I-section doubly and singly symmetric cantilevers by Andrade et al. (2007). A numerical study based on the Rayleigh-Ritz method was carried out to develop analytical expressions for the three required factors for various loading and boundary conditions. It was noted in the publication that although the 3-factor formula was included in the ENV version of Eurocode 3 (1992), the completed version of the Eurocode (2005), the EN version, provides no information on the determination of the critical elastic moment, M_{cr}. It has, however, been implied by Ekström and Wesley (2017) that the formula is retained in some form in non-contradictory complementary information (NCCI) to Eurocodes documents. This suggests that the formula still finds use, possibly also in some country specific annexes as well. The authors also provide an explanation of the three factors. Approximate equations for the inelastic buckling design of monosymmetric I-beams have been given by Trahair (2012). It was noted in this study that design approaches taken by some mentioned codes of practice did not appear well supported by research. Accurate approximations for uniform bending and less accurate but conservative approximations for moment gradient were suggested. An indication of the approach used for monosymmetric sections by two different codes of practice, CSA S16 and AISC 360 has been outlined by Manarin et al. (2019). The authors carried out a numerical investigation on the lateral buckling of T-shaped steel beams with a focus on applicable moment gradient factors for elastic critical loads.

Bradford et al (2002) described a procedure for the design of crane runway beams subject to lateral-torsional buckling failure. These beams consisted of an I-section with a channel cap. The procedure involved first finding the elastic critical buckling moment and then converting this to an ultimate strength using an approach known as 'design by buckling analysis' permitted in the Australian code AS4100 (1998). It was stated that the procedure could be easily modified to meet other limit state design code requirements. It was emphasized again in this study that moment modification factors for monosymmetric beams are different to those used for doubly symmetric beams. A design aid for determining the moment strength of crane runway girders consisting of built-up sections was provided by Hsu et al. (2012) based on the provisions of the American (AISC) code. To overcome the difficulty in calculation of torsional parameters, and to avoid crude estimations based on approximate formulas developed for I-section beams, these were calculated for various standard combinations of I-section beam and channel cap. A simplified rational design approach was also proposed. In recent years the strengthening of crane runway beams by introducing stiffeners to the I-section beam top flange has been investigated by Bijak et al. (2019) as well as Movaghati (2019). The motivation was increased capacity of the ordinary beam prior to use for the former and increased capacity due to change of use for the latter. Bijak et al. (2019) sought to develop a simple design approach, based on Eurocode 3, for the type of section investigated.

Over the years various studies have been reported on the buckling behaviour of web tapered beams. The use of these types of members does not seem to be widespread. Their merits are however frequently presented. A study on the lateral-torsional buckling behaviour of prismatic as well as tapered steel members with doubly or singly symmetric cross-sections has been presented by Lue et al. (2007). The study not only looked at the development of equations for predicting the elastic buckling moment but also for inelastic buckling behaviour to give design strengths. Results were reported as having consistent accuracy while maintaining simplicity for structural design use. A recent study by Yuan et al (2013) has been presented on the topic of tapered webs but focusing on T-section cantilever beams. It was reported that web tapering of cantilevers can lead to either a decrease or increase in buckling load depending on the flange width of the beam.

2.3.1.2 Design Code Equations for Monosymmetric Beams

One of the drawbacks on the use of laterally unrestrained monosymmetric beams is the lack of extensive or sufficient, and in some cases accurate, design guidance in practice. The design of monosymmetric beams has largely been approached in the same manner to that of doubly symmetric beams. In this vein design codes of practice take an approach of first determining the critical elastic moment in laterally unrestrained segments and then using this value to determine the ultimate moment which would then be directly related to the design moment by use of a partial safety factor. The critical elastic moment equation is usually cast in the form obtained for the case of a simply supported beam under uniform moment with factors then added to account for conditions deviating from these. These are usually in the form of a moment gradient factor and an effective length factor respectively. A factor that accounts for load position relative to shear centre may also be introduced as appropriate. It must also be noted that codes of practice generally aim to take a conservative approach. Routine extension of approaches developed for doubly symmetric beams to monosymmetric beams has been challenged by some authors such as Lindner (1976) and Trahair (2012) who have shown that the behaviour of monosymmetric sections is unique and thus approaches used with doubly symmetric sections do not always hold for monosymmetric sections.

In the South African standard for steel design SANS10162-1 (2011) which is based on the Canadian Standard CSA S16 (*Limit states design of steel structures*) the clause that deals with unrestrained monosymmetric beams, clause 13.6 (d), provides no equations. The user is required to use a 'rational method of analysis' such as that given in the Structural Stability Council's Guide to Stability Design for Metal Structures. This would refer to publications such as Ziemian (2010) and Galambos (1998). Although these guides address the critical elastic moment, guidance on ultimate moment is little. It has been reported by Xie and Mohareb (2022) that the Canadian Standards (CSA, 2009, 2014, 2019) provide equations for determining the critical elastic moment for monosymmetric beams subjected to general loading and/or end moments. The authors did, however, find an anomaly when applying the equation to determine elastic critical moment for monosymmetric beams subjected to end moments. The problem was noted when the moment diagram changed from one causing single curvature to one causing double curvature.

In the draft versions of the European standard, Eurocode 3, an expression for the critical elastic moment of monosymmetric sections was presented in the form of a three-factor formula. Mohri (2003) reports the equation as being of the form given in (2.7) for the critical elastic moment, M_b.

$$M_b = C_1 \frac{\pi^2 E I_z}{L^2}\left[(C_2 e_z + C_3 \beta_z) \pm \sqrt{(C_2 e_z + C_3 \beta_z)^2 + \frac{I_\omega}{I_z}\left(1 + \frac{G J L^2}{\pi^2 E I_\omega}\right)}\right] \qquad (2.7)$$

The coefficients depend on the load case applied to the beam. The critical elastic moment is then a function of bending distribution (C_1), load height effect ($C_2 e_z$) and Wagner's coefficient ($C_3 \beta_z$) which defines the degree of monosymmetry.

The expression was however, left out of the final version of the code (CEN, 2005). In the literature, it appears that there was lack of agreement on the values of the coefficients to be used (Balasz and Kolekova, 2009, Mohri, 2003, Tong and Zhang, 2003) and unsurprisingly so as they are determined numerically for most load cases. Depending on the method used results are likely to always have some variation. In the book by Trahair et al (2008) it has been indicated that no design provisions are given by the code on the design of monosymmetric sections. However, there is implied practice that as long as a correct elastic critical moment is obtained, the simplified (or 'general case'), but conservative, method in EC3 can be used for monosymmetric sections. This would imply that an approach used for doubly symmetric beams is extended to monosymmetric beams as well. In this case the critical elastic moment is typically obtained from analytical approaches outlined in the literature, specialized software or by using equations provided in National Annexes if available. Use of this approach is confirmed by Taras (2013). Trahair et al (2008) indicated that this approach has been questioned and may lead to less safe results in some cases. In reporting on work done to update Eurocode 3, Knobloch et al (2020) reported that both the 'general case' as applied to monosymmetric sections and the 'specific' case for rolled or welded doubly symmetric sections have inaccuracies based on results from computer modelling with models that incorporate all imperfections. This was reported as part of the process of reviewing the code and updating of design rules. One of the areas addressed in the new design rules is the design of monosymmetric sections. In this regard the peculiarity of the moment diagram coefficient (C_m), which accounts for effects of non-uniform bending moment diagram, has been acknowledged for monosymmetric sections in that the available coefficients for doubly symmetric beams are no longer directly applicable. The new rules provide a simplified approach where the moment diagram coefficient does not consider a change in sign but must be calculated assuming an equivalent bending moment diagram of the same sign along the entire member length. This becomes a safe and relatively easy approach. It is recommended, by the authors, that if more accurate solutions are desired then a second order analysis taking all imperfections into account would have to be carried out.

For the Canadian standard CAN-CSA S16 (CSA, 2014, 2019) it has been reported by Xie and Mohareb (2022) that the expression for the critical elastic moment is given as presented in equation (2.8) . The coefficient ω_3 is reported as being a modified moment gradient factor that accounts for non-uniform moment distribution and degree of monosymmetry of the section.

$$M_{cr} = \omega_3 \frac{\pi^2 E I_y}{2L^2}\left[\beta_x + \sqrt{\beta_x^2 + 4\left(\frac{GJL^2}{\pi^2 E I_y} + \frac{C_w}{I_y}\right)}\right] \tag{2.8}$$

It appears that the Canadian standard has made some effort in trying to deal with monosymmetric sections where there is change of sign in the moment diagram (also know as members in double curvature). The study by Xie and Mohareb (2022) sought to rectify an anomaly that was observed when applying the provisions of the code to determine the elastic critical moment for monosymmetric beams subjected to end moment loading. The versions of the coefficient ω_3 in equation (2.8) for the 2014 and 2019 versions of the code are given in equations (2.9) and (2.10) respectively.

$$\omega_{3\text{-}14} = \begin{cases} \omega_2 & \text{single curvature} \\ \omega_2\left[0.5+2\left(I_{yc}/I_y\right)^2\right] & \text{double curvature} \end{cases} \tag{2.9}$$

The variable I_{yc} in equation (2.9) is the second moment of area of the compression flange. A challenge arises for the double curvature case as both flanges will be partly in compression and two values become possible for this expression. An attempt to rectify this ambiguity resulted in equation (2.10) in the 2019 version of the code.

$$\omega_{3\text{-}19} = \begin{cases} \omega_2 & \text{single curvature} \\ \omega_2\left[0.5+2\left(I_{ym}/I_y\right)^2\right] & \text{double curvature} \end{cases} \tag{2.10}$$

In this equation I_{ym} is the second moment of area of the smaller flange about the y-axis (minor axis of section). Although the 2019 adjustment was still found to have an anomaly for the double curvature domain it at least produced results that were conservative when compared to results from finite element analysis. Conversely the 2014 equation produced non-conservative results in this domain. A similar challenge is also reported by the authors for the determination of the monosymmetry constant using the simplified equations given in the code due to use of I_{yc}. The simplified equation also has a validity range.

It is worth noting that the moment gradient factor ω_2 used in equations (2.9) and (2.10) is applied in the code for the case of elastic critical moment of doubly symmetric sections. Here, in these two equations, it is applied for monosymmetric sections where there is no change in sign of the bending moment diagram (i.e., members in single curvature). Two values are reported with one being applicable for members with a general moment diagram and another for members having a linear moment gradient. The anomaly that the authors set out to address arises particularly with the transition from a single curvature state to that of double curvature. This is similar to the challenge with monosymmetric sections reported by Knobloch (2020) for the Eurocode 3 design rules that were being updated. Therefore, this study highlighted some of the challenges that remain persistent in the design of monosymmetric sections. Although no mention is made of how the resistance moment is obtained, an equation has been provided for this in the software STAAD.Pro help files (n.d.).

For the American Institute of Steel Construction standard ANSI/AISC 360 (2010) its application to monosymmetric sections has been reported by MacCrimmon (2004). The author presents the approach from this code as a rational method for the design of monosymmetric compound sections formed from the welding on of a channel cap to an I-shaped section. It is reported as an approach also proposed by Ellifritt and Lue (1998). The moment diagram used has three regions; plastic, inelastic and elastic. In the inelastic region the relationship between unbraced length and critical elastic moment is approximately linear from the transition from elastic at M_i to fully plastic at M_p.

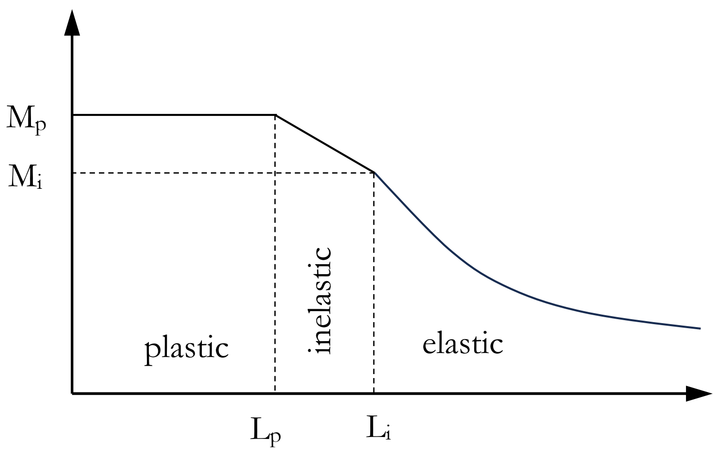

Fig.2-5 Moment resistance for unbraced length, L (MacCrimmon, 2004)

The moment M_i is equal to the critical elastic moment at L_i. Many of the beams used in practice are likely to fall in the inelastic range. The following equations are given by MacCrimmon (2004) for an unbraced length (L) and partial material factor (ϕ):

For L ≤ L_p: $$M_r = \phi M_p \quad (2.11)$$

For L > L_i: $$M_r = \phi M_{cr} \quad (2.12)$$

For $L_p < L \leq L_i$: $$\frac{M_r}{\phi} = M_p - \left(M_p - M_i\right)\left[\frac{L - L_p}{L_i - L_p}\right] \quad (2.13)$$

Using the critical elastic moment for a monosymmetric beam provided by Galambos (1998) and shown in (2.14) with effective length factor (K) and a moment modification factor (C_b), the cases that deviate from uniform moment or with loading at shear centre can be accommodated.

$$M_{cr} = \frac{\pi C_b}{KL}\left[\sqrt{EI_yGJ} \quad \left(B_1 + \sqrt{1 + B_2 + B_1^2}\right)\right] \quad (2.14)$$

$$B_1 = \frac{\pi \beta_x}{2KL}\sqrt{\frac{EI_y}{GJ}} \quad (2.15)$$

$$B_2 = \frac{\pi^2 EC_w}{(KL)^2 GJ} \quad (2.16)$$

$M_i = F_L S_{xc}$ *or* $F_y S_{xt}$ whichever is the lesser (2.17)

$$F_L = F_y - F_r \quad (2.18)$$

The length L_i cannot be solved for directly but by trial and error. These equations have also been reported by Surla et al (2015). Symbols S_{xc} and S_{xt} are the section moduli of the compression and tension flange respectively. Symbols F_y and F_r are the member yield stress and residual stress in the compression flange respectively.

It would appear that these equations have worked acceptably so far because crane beams are predominantly used as simply supported beams meaning that they do not experience double curvature bending. In this case, as shown previously, it seems code equations can give accurate results for specific cases. However, there is no evidence to suggest that these equations would not suffer from the same anomaly reported by Xie and Mohareb (2022) and Knobloch (2020) for the case of double curvature bending.

For the Australian standard AS4100 (1998), the authors of the Steel Structures Design Manual to AS 4100, Kirke and Al-Jamel (2004) indicate that the design guidance for monosymmetric sections provided in the code is unconservative. This is attributed to an erroneous moment modification factor. This is again not surprising given that in much of the literature there is a tendency to extend applications for doubly symmetric sections to monosymmetric sections with concomitant errors. The authors recommend following the proposals by Bradford et al (1999) in lieu of avoiding monosymmetric sections altogether. The equation used for the monosymmetry constant is the simplified equation of Kitipornchai and Trahair (1980).

In developing design proposals for monosymmetric beams, Trahair (2012) highlighted that methods for designing monosymmetric I-beams against lateral-torsional buckling are not well supported by research. It was indicated that design methods in the American standard AISC (2010), Eurocode 3 (CEN, 2005) and Australian standard AS4100 (1998) appeared to be generally based on extrapolation from well researched studies on doubly symmetric sections. Such an approach was stated as being questionable.

2.3.2 Experimental Studies – monosymmetric beams

As has been indicated in preceding sections experimental work on monosymmetric beams has in some cases been carried out concurrently with analytical and numerical work. Dedicated experiments are rare due to cost considerations and difficulty in assembling an appropriate test setup. However, some experimental work has been carried out. Because tests are carried out on real members, with imperfections, the failure loads are the ultimate strengths of the members and these results aid in the formulation of strength determination approaches in design standards. The lateral buckling behaviour of simply supported welded monosymmetric plate girders was carried out by O'hEachteirn and Nethercot (1988a) and O'hEachteirn and Nethercot (1988b) . In the first study, full scale models were used. It was confirmed that welded monosymmetric sections with larger flange in tension possess lower buckling strengths than equivalent rolled or equal flange sections. In the second study one-third scaled models were utilized. Results from the study confirmed the need for a lower design curve for welded sections. An experimental study of singly symmetric and non-symmetric sections has been reported by Bajer et al. (2017). The study sought to overcome limitations encountered with finite element models in correctly predicting real behaviour of beams. Experimental work was presented by Zhang et al (2017) who carried out tests on high strength steel (Q460GJ) beams with results being used to calibrate a numerical model. The calibrated models were then used to carry out a parametric analysis. Results from the study were compared with predictions from various codes of practice. It has been stated and demonstrated by Mandal and Calladine (2002) that the elastic critical load for a beam can be determined experimentally using an approach known as the 'Southwell plot'.

2.3.3 Numerical Studies – monosymmetric beams

Limitations with the classical procedures of obtaining buckling loads for beams have been outlined by Powell and Klingner (1970). Closed form solutions for governing differential equations are limited to a few cases, suitable displacement functions for use with energy equations may be limited by insufficient foreknowledge of the buckled shape and solutions to nonlinear differential equations can be tedious. Therefore, the solution to many buckling problems entails the use of approximate or numerical methods of solution. Several numerical methods have emerged over the years; some seemingly more widely reported than others. Some methods include the method of finite differences, method of finite integrals, power series approaches and more recently the finite element method. A background to the finite difference method as well as discussion on solution error has been presented by Nishino (1965). The merits of the finite integral method over the finite difference method have been argued by Brown and Trahair (1968) and have been used by, among others, Anderson and Trahair (1972), Kitipornchai et al (1986) and Trahair (2016) in finding solutions for governing differential equations. Because of the development of the digital computer from the 70s onwards the implementation of the finite element method has gained popularity and widespread use. Application of this matrix-based approach lends itself well to application on the digital computer and the complexity of problems that can be handled by the method continues to expand. The work of authors whose main study was based on the use of numerical methods is explored here.

Powell and Klingner (1970) present a numerical solution method based on the finite element method. The method is argued to be more general and possessing the following desirous features:

1. Continuous beams, web-tapered beams and beams with monosymmetric geometries can be modelled easily.
2. Various loading scenarios can be accommodated.
3. Different forms of lateral supports can be considered and modelled.
4. Both elastic and inelastic behavior can be analyzed or modelled.
5. Software can be developed for routine use in a design office.

Stiffness matrices based on the matrix displacement method were presented by Barsoum and Gallagher (1970) for the analysis of torsional and lateral stability of structures composed of flexural members. Accuracy was demonstrated by way of example problems whose exact solutions are known. A finite element approach for studying nonlinear instability of steel I-section members was presented by Bild et al. (1992). This was used to study the out-of-plane strength of steel beams with imperfections. Accuracy was evaluated by comparing with results from known solutions.

A finite element formulation for lateral-torsional buckling analysis of non-prismatic I-beams was developed by Gupta et al. (1996). Both linear and quadratic taper were considered. The finite element solution convergence was checked based on available experimental and numerical results. Finite element analysis was used by Helwig et al. (1997) to study both the effect of load height as well as moment gradient on singly symmetric I-shaped beams. A comparison of moment gradient factors based on the results of the study with traditional values used for doubly symmetric I-beams at the time was made. It was shown that moment gradient factors for doubly symmetric beams could be used for singly symmetric beams provided effect of load height was measured relative to mid-height of the cross section.

A study on the lateral-torsional buckling behaviour of continuous stepped I-beams using the finite element method has been presented by Park and Stallings (2003). The steps are considered for the case of change in flange width and/or thickness. The authors noted that North American design guides at the time only accounted for prismatic and web-tapered beams. New design equations for stepped beams were proposed as was a new equation for the moment gradient factor. The study on lateral-torsional buckling behaviour of stepped I-beams was extended to singly symmetric sections by Gelera and Park (2012). This study was based on beam geometries taken from real bridges. Uniform moment loading as well as various other loadings were considered. New design equations and approached were proposed for beams with monosymmetry ratio between 0.1 and 0.9. The application of the finite difference method in determining the elastic buckling load of cantilever beams subjected to various loading has been presented by Özbaşaran (2013). Results from the finite difference approach were compared to those from finite element analysis and were found to compare well. As is expected with numerical methods it was found that dividing the beam into more parts improves the accuracy of the solution but also increases calculation time. A similar study has been carried out by Soltani and Asgarian (2018) who used the finite difference method to determine the critical buckling load of a simply supported beam subjected to an arbitrary transverse load causing flexure. The finite difference solution is compared to results of some benchmark cases and found to be acceptably accurate to below 1% difference and showing even greater accuracy with an increase in the number of segments. Mohri et al. (2003) and, Mohri et al. (2010) have also applied numerical approaches in the study of lateral buckling stability of monosymmetric beams. Bijak (2019) applied a numerical approach; the Bubnov-Galerkin method to determine the stability of laterally unrestrained monosymmetric beams. Prebuckling displacements were not considered. Beams were simply supported and subjected to concentrated and distributed loads. The results showed consistency with results obtained from finite element analysis.

2.4 OTHER STUDIES

Some studies have not necessarily focused on instability of doubly symmetric or monosymmetric sections but have nonetheless contributed to understanding of the buckling behaviour of these members. These studies are highlighted here together with the contribution to the state of knowledge on lateral-torsional buckling.

Hoff (1944) validated the work of Wagner (1936) and others who had solved the buckling problem by making use of the Rayleigh-Ritz-Timoshenko energy method. This method obviated the derivation of the governing differential equations as well as having to consider the 'Wagner hypothesis'. The strain-energy due to shear associated with bending and that associated with non-uniform warping were neglected. Only that associated with flexural buckling, torsional buckling and non-uniform torsion (warping) was considered. The author derived the equations for buckling of a thin-walled member under compression consistent with the results from the static-kinematic approach where governing differential were used. This helped to validate the work of Goodier (1941 and 1942) and others who argued on the validity of the 'Wagner effect'. Goodier had initially presented solutions for compressed bars and then extended this to bars under compression and bending. This laid the foundation for the approaches used in beam lateral buckling analysis to this day.

State of the art literature surveys have been presented by Lee (1960) and Trahair (1996) who looked at the state of the current research on lateral-torsional buckling at the time. The study be Lee (1960) tracks the early research on elastic buckling and transition into inelastic buckling to model real behaviour. The study also looks at efforts on understanding the behavior and strength requirements for lateral restraints to beams susceptible to lateral-torsional buckling in the plastic range. Trahair (1996) presented the outcomes of a comprehensive survey of literature under two broad parts: 'present state of knowledge' and 'research needs'. Studies carried out on lateral-torsional buckling were reviewed under specific topics with areas still requiring further research outlined. Cross section types were one of those areas itemized.

Studies of other sections other than I-shaped sections susceptible to lateral-torsional buckling have been carried out for tee shaped sections (Kitipornchai and Wang, 1986, and Manarin, 2019), channel sections (Seah and Khong, 1990, la Poutré, 2000, Snijder, 2002, Dahmani, 2015, Ekström, 2017), and angle sections (Trahair, 2003, Trahair, 2002 and Hussain et al, 2018). The studies range from elastic to inelastic buckling with design recommendations. Guidance has been provided on the treatment of these sections in Galambos (1998) and Ziemian (2010). These sections are not explored further. Other novel forms of beams such as hybrid sections, corrugated web sections, stepped beams, beams with open sections flanges and castellated beams have been the subject of research interest but are not explored here. Coped (notched) beams are also outside of the scope of the current study.

2.5 SUMMARY OF LITERATURE REVIEW

The literature review has presented some of the significant studies on the lateral-torsional buckling of beams carried out to date; from the early work based on classical methods to current work largely carried out with the aid of the digital computer using finite element analysis to carry out large scale parametric analyses. It was noticed from early on that monosymmetric sections presented behaviour that was peculiar and different in some significant respects to that observed with doubly symmetric beams. These sections therefore had to be treated as a unique set of members with their own governing behavior including the nature of generalized treatments such as moment gradient factors. The research work has progressed from elastic analysis on to inelastic analysis to capture the real behaviour of members that have imperfections. The imperfections are both geometric, in the form of initial deformation, and material in the form of residual stress. This has made it easier to predict behaviour of beams under various conditions without resorting to expensive and time-consuming experiments. It has been shown that factors such as effect of load height relative to shear center, effect of elastic restraints and effect of moment gradient can be conveniently determined using the finite element method. This means that the importance of finite element analysis continues to grow as does the need to understand how new proposed sections, materials and forms behave under conditions that may cause buckling. Classical analytical and numerical methods continue to be important as does experimental testing, in order for finite element models to be correctly calibrated. Once calibrated, large scale parametric studies can then proceed using finite element analysis. The behaviour of monosymmetric sections does present some curious behaviour for example that observed by Camotim et al. (2012), and therefore the behaviour of these type of sections needs to be thoroughly understood so that their use can be enhanced and where necessary optimized. Despite the number of studies conducted on steel monosymmetric sections, design code guidance remains largely limited compared to that on doubly symmetric sections.

Despite all the work highlighted on monosymmetric sections, no studies have been found that consider the use of flange stiffeners to convert doubly symmetric sections into monosymmetric sections and exploit the beneficial effects of monosymmetry. Even though it is known that position of load relative to the shear center influences the critical elastic moment, there does not appear to be a specific study that has demonstrated how this may be exploited particularly for cross section optimization as well as in the case of strengthening existing members. The current study seeks to fill this gap in knowledge.

2.6 STATEMENT OF CURRENT STUDY

The area of strengthening existing I-shaped sections for the case of flexure, whether uni-axial or bi-axial, is a relatively under-explored area. However, it presents opportunities not only for finding unique ways to strengthen existing beams but also to present optimized geometries as alternatives to the I-section member for the flexural loading case. From the factors highlighted in Table 2-1 it can be seen that various opportunities exist for improving lateral-torsional buckling strength based on the listed factors. Optimization of the cross-section is one of these opportunities. Given that constraints may exist for the case of welding downstands onto flanges of I-section beams the option of using upstands as stiffeners is explored in the current study. The current research is focused on the behaviour of a monosymmetric section formed from stock hot-rolled I-beams strengthened with upstand stiffeners. Existing beams can be strengthened for various reasons such as change in use of the member which translates into a change in loading. The requirement for strength may also be accompanied by a requirement for greater stiffness. Degraded members could also be candidates for strengthening. Beams with stiffening are also created through routine practices such as kick plates introduced for safety reasons and yet the effect of these upstands welded onto existing beams is not quite understood nor appropriately accounted for in design. The current study also tracks the movement of the shear center with change in upstand height to understand how this influences behaviour.

2.7 JUSTIFICATION OF STUDY

The main motivations of the study are the strengthening of existing members as well as investigating a potential optimized cross section for flexure in the case of beams susceptible to lateral torsional buckling. It has been indicated in the introductory chapter that the use of upstand stiffeners on existing beams may be necessitated by different factors. One important one is the strengthening of existing beams. The strengthening of existing beams may arise for various reasons such as a change in the use of the structure. It may also happen that a member is used in a configuration where other strengthening methods such as flange downstands cannot be utilized or as in the case of certain alternatives such as fiber reinforcement, stiffness requirements are not met. In this case flange upstands as stiffeners may be the resort of choice. Understanding the behaviour of beams thus stiffened becomes imperative. The ultimate strength of such beams becomes paramount so that the effect of introducing upstands is understood and exploited if positive and any undesirable effects avoided.

Meeting sustainable development goals also requires re-thinking how infrastructure is developed by actively pursuing reduced carbon emissions. One way this can be done is by carrying out 'lean design' which includes the concept of optimizing the use of materials so that members employed are safe and efficient. Studying the behaviour of these types of monosymmetric sections promises to help achieve these aspirations.

2.8 AIM AND OBJECTIVES OF STUDY

It is the aim of the study to provide information on the behaviour and strength of laterally unrestrained monosymmetric steel beams formed by the introduction of flange upstands as stiffeners to I-section steel beams.

The study, therefore, has the following objectives:

(i) Study the movement of the shear center relative to the geometric centroid as upstand stiffeners are introduced and observe whether any peculiarities associated with the movement of the shear center exist.

(ii) Study the elastic and inelastic lateral-torsional buckling behaviour of monosymmetric beams having the monosymmetry introduced by way of upstand stiffeners on an I-section beam.

(iii) Observe the effects of upstands on the resistance moment and determine the applicability of using these stiffeners.

2.9 METHODOLOGY OF STUDY

Methodology in achieving the stated objectives involved the following listed activities:

a. Classical methods were used to develop equations for determination of section properties pertinent to the study of the lateral-torsional buckling behaviour of the proposed cross-section.

b. A mathematical model was developed to predict the critical buckling loads for point load and uniformly distributed loads. Results were compared to those obtained from finite element analysis (FEA).

c. Geometrical imperfections were determined based on provisions in the South African standards for steel structures (workmanship) as well as international best practice.

d. A finite element model was calibrated using benchmark problems on the elastic lateral-torsional buckling of beams. Once calibrated the model was used to carry out a study of elastic lateral-torsional buckling to verify the model developed in (b). The effect of varying the upstand height was observed throughout.

e. Nonlinear, inelastic buckling analysis was carried out using a properly calibrated finite element model with imperfections included to determine the ultimate strength of the beams with upstands. The effect of upstand height on ultimate strength was examined. Residual stresses were not considered in this study. Geometric imperfections and material constitutive laws were incorporated into the models.

f. Results from the nonlinear analysis were used to evaluate the member behaviour of 'real' beams.

g. The outcome of the study is discussed with appropriate recommendations made.

CHAPTER 3 SECTION PROPERTIES

3.1 INTRODUCTION

Two forms of the critical elastic buckling moment equations for monosymmetric cross sections are prevalent in the literature; one form found predominantly in North American and Australian literature as given in (3.1), and another from found predominantly in European literature as given in (3.2) and referred to as the 3-factor formula.

$$M_{cr} = \frac{\pi^2 E I_y \beta_x}{2L^2}\left\{1 \pm \sqrt{1 + \frac{4}{\beta_x^2}\left[\frac{C_w}{I_y} + \frac{GJL^2}{\pi^2 E I_y}\right]}\right\} \tag{3.1}$$

$$M_{cr} = K_1 \frac{\pi^2 E I_z}{(k_z L)^2}\left[\left(K_3 z_j + K_2 z_g\right) + \sqrt{\left(K_3 z_j + K_2 z_g\right)^2 + \frac{I_\omega}{I_z}\left(\frac{k_z}{k_\omega}\right)^2 + \frac{G I_t}{E I_z}\left(\frac{k_z L}{\pi}\right)^2}\right] \tag{3.2}$$

In order to determine the critical buckling load of a beam it can therefore be seen that several important section properties need to be determined first. These are (based on equation 3.1):

(i) The second moment of area of the minor axis (I_y)
(ii) The torsional constant (J)
(iii) The warping constant (C_w)
(iv) The monosymmetry constant (β_x)

These are presented in equation 3.2 as I_z, I_t, I_ω and in the $K_3 z_j$ factor respectively. Procedures and methods for determining these section properties exist and are generally easy to apply for the first two properties but complex for the last two. Moreover, determination of the warping constant as well as the monosymmetry constant requires that the shear center of the cross section be located first; this can be a cumbersome undertaking itself and may add to the complexity. The procedures for determination of these parameters are reviewed in this chapter. Equations for determination of the essential geometric properties for the cross section used in the current study are then derived and presented.

Procedures for the determination of some of the key properties highlighted can be found in books such as those by Timoshenko and Goodier (1951), Galambos (1968) and Heinz (1975) and appear in various forms either formulated for specific geometries or in a more general form applicable to arbitrary cross sections. Some equations have been derived for standard geometries such as I-shapes, tees, angles and channels. For other types of cross sections, such as the ones considered in the current study, the equations must be derived from first principles. These are presented in sections 3.3 to 3.6 that follow. The cross section considered in the current study is shown in Fig.3-1. This is a typical I-shaped section with upstands introduced on the upper flange ends. The section is monosymmetric with the shear center and centroid shown arbitrarily and not in the absolute positions.

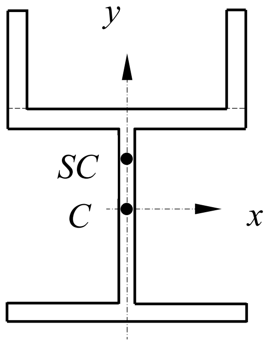

SC = Shear center

C = Centroid

Fig.3-1 I-shaped section geometry with flange upstands

The cross-section is assumed to conform to standard hot rolled beam members so that the plates can be considered to be thin walled. The applications can be extended to welded sections fabricated from plates that can be considered as ‘thin’. In the current study the derivatives of existing hot rolled geometries will be considered with the corner radii neglected. This simplification is not considered to cause any significant loss of accuracy. Benchmark comparisons will be made to verify this. The equations formulated will contain terms relating to the geometry as presented in Fig.3-2. Part (a) shows the overall dimensional parameters and part (b) shows the midline dimension parameters.

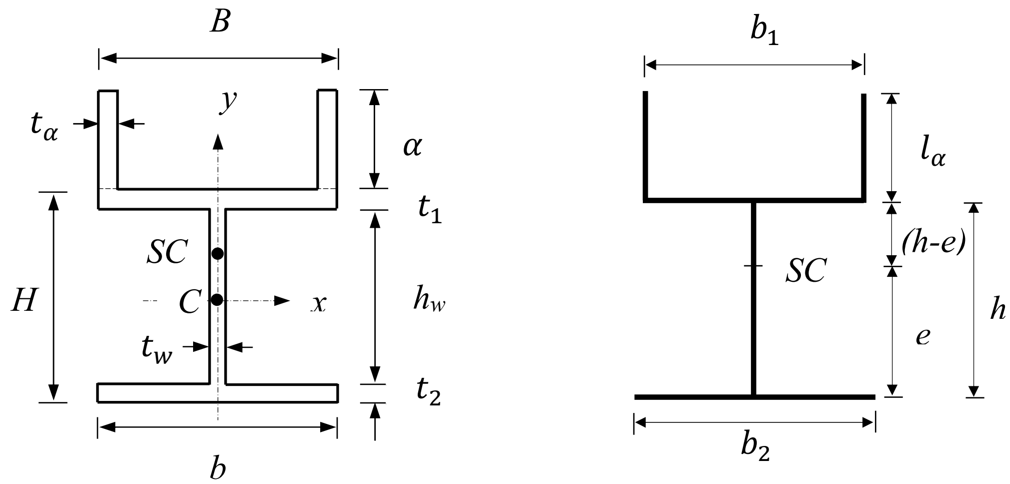

(a) Cross section parameters (b) midline parameters

Fig.3-2 I-Section geometry with flange upstands geometrical parameters

3.2 SECOND MOMENT OF AREA

For the cartesian coordinate systems shown in Fig.3-2 the second moments of area of the cross section are given as:

$$I_x = \int_A y^2 \, dA \qquad (3.3)$$

$$I_y = \int_A x^2 \, dA \qquad (3.4)$$

Equation 3.4, minor axis second moment of area, is of interest for determining the critical load. For a section consisting of plated sections the parallel axis theorem is utilized to find the second moment of area about the axis of symmetry. This is given in Equations (3.5) with the evaluated polynomial form of the equation given as equation (3.6).

$$I_y = I_i + Ax_i^2 \qquad (3.5)$$

$$\boxed{I_y = \frac{1}{12}\left[t_1 B^3 + t_2 b^3 + h_w t_w^3\right] + \left[\frac{\alpha t_\alpha^3}{6} + 2\alpha t_\alpha \left(\frac{B}{2} - \frac{t_\alpha}{2}\right)^2\right] \qquad (3.6)}$$

As indicated previously, the parameters in equation (3.6) are given with reference to dimensions and symbols indicated in Fig.3-2 (a).

3.3 TORSIONAL CONSTANT

The derivation of the torsional constant has been provided by Timoshenko and Goodier (1951) and also presented in Heins (1975). It is stated in Timoshenko and Goodier (1951) that the correct solution to the problem of torsion of prismatic bars by couples applied at the ends was given by St. Venant in 1855. Thus, pure torsion has also come to be known as St. Venant torsion. However, the solution for the torsional stress caused by the applied moment on different cross sections, and by consequence also the torsional constant, only became easy to solve after Prandtl (1903) presented the membrane analogy. Many of the torsional constant formulas in use today for various cross sections are thus derived on the basis of applying the membrane analogy.

The membrane analogy technique involves visualization of a stress function based on the equilibrium of torsion by considering the inflation of a hypothetical thin membrane over the exact cross section which is subjected to the torsional moment (Heins, 1975). This membrane, inflated by a pressure 'q', when equilibrium is considered results in an equation similar to the torsion equation. The stress function in the torsion equation is directly related to the resulting height of the membrane whereas the volume under the membrane is related to the applied torque. The similarity in the two equations is thus used to determine the stress in the member as well as the torsional constant.

Determining the torsion equilibrium equations is based on first considering the equilibrium of forces in the cross section and then considering the relationship between the rotation of the section and the resulting displacements. This yields two equations with three unknowns; two stress components and a rotation. This is remedied by assuming the stresses are related by a stress function denoted as $\psi(x, y)$ and known as Airy's stress function. The first part is based on Fig.3-3 and yields equation (3-7) based on equilibrium. If the relationship between stresses and the stress function is as given in equation (3-8) then the resulting torque equation is as given on equation (3-9). The resulting differential equation obtained from the rotation and resulting displacements is shown in Table 3-1.

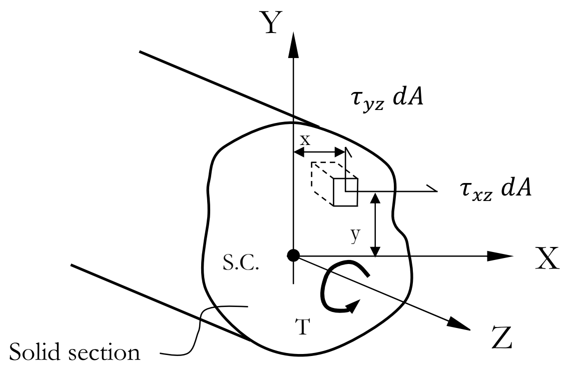

Fig.3-3 Equilibrium of torsion for a solid section (Adapted from Heins, 1975)

$$T = \int_0^A \left(\tau_{xz} y - \tau_{yz} x\right)\, dA \tag{3.7}$$

$$\tau_{xz} = \frac{\partial \psi}{\partial y} \qquad and \qquad \tau_{yz} = \frac{\partial \psi}{\partial x} \tag{3.8}$$

Resulting in:

$$T = \int_0^A \left(\tau_{xz} y - \tau_{yz} x\right)\, dA$$

$$= \int_0^A \left(\frac{\partial \psi}{\partial y} y + \frac{\partial \psi}{\partial x} x\right)\, dA$$

$$= 2 \iint \psi \, dxdy \tag{3.9}$$

Similarities between the torsion equilibrium equations and those arising from the membrane are summarized in Table 3-1 (Heins, 1975).

Table 3-1 similarities between membrane equations and torsion equations

Function	*Membrane Deflection 'z'*	*Torsion Stress Function 'ψ'*
Differential Equation	$\frac{\partial^2 z}{\partial x^2} + \frac{\partial^2 z}{\partial y^2} = -\frac{q}{S}$	$\frac{\partial^2 \psi}{\partial x^2} + \frac{\partial^2 \psi}{\partial y^2} = -2G\phi'$
	$Slopes \quad \frac{\partial z}{\partial x}, \quad \frac{\partial z}{\partial y}$	$Stresses \quad \tau_{xz}, \ \tau_{yz}$
	$Volume \quad V = \iint z \, dx \, dy$	$T = 2 \iint \psi \, dxdy$

S = membrane force, q = membrane pressure

Application of the membrane analogy for a plate of thickness 't' and width 'b' leads to a torsional constant equation as given in (3.10)

$$J = \frac{bt^3}{3} \tag{3.10}$$

Where *b* = plate width and *t* = plate thickness for the rectangular element.

It has been shown in Heins (1975) that for a member consisting of a collection of plates, such as the one considered in the current study, the torsional constant can be approximated by a summation of the contributions from the individual plate elements as given in equation (3-11).

$$J = \frac{1}{3} \sum_{i=1}^{n} b_i t_i^3 \tag{3.11}$$

Where 't' is the smaller plate dimension. It has been implied in Timoshenko and Goodier (1951) that when there are plate junctions then the midline dimension should be considered to improve the approximation. The work of Trayer and March (1930) is referenced. These authors carried out soap film experiments as well as member tests to obtain torsional properties. An illustration of the soap film contours from an applied pressure reveals the source of error when the plate equation is applied to the case of plate junctions in Fig.3-4.

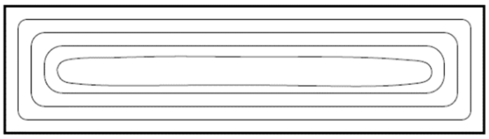

(a) Rectangular plate - PLAN

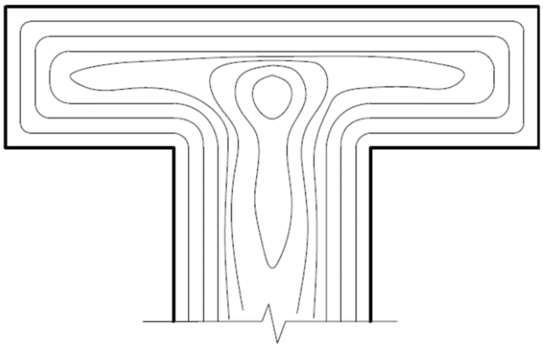

(b) Plate junction - PLAN

Fig.3-4 Soap film contours on (a) rectangular plate and (b) rectangular plate junctions

The 'bulge' at the junction in (b) shows the source of error. Trayer and March (1930) have provided a way of estimating the error. This depends on the diameter, D, of the largest circle that can be inscribed at the junction of the plates. The fourth power of this diameter is combined with a factor gives the additional component to the stiffness considered for the intersecting plates only. A graph for reading off the factor is provided by the authors and depends on two ratios; the junction fillet radius divided by the flange thickness and the ratio of widths of the narrower rectangle plate to wider rectangle. This means that the error will vary depending on the intersecting plate sizes.

The use of midline dimensions goes some way in reducing the magnitude of the error. The use of the equation in (3.11) is widely accepted in literature (Timoshenko and Gere, 1961; Heins, 1975; Trahair, 1993). Because the membrane effect at the junction is not completely captured it is anticipated that equation (3.11) yields a lower value of the torsion constant as an approximation. The torsional constant equation for the section used in the current study is presented in polynomial form in equation (3.12) with midline dimensions used for the plates making up the section.

$$J = \sum \frac{b_i t_i^3}{3} = \frac{2 l_\alpha t_\alpha^3}{3} + \frac{b_1 t_1^3}{3} + \frac{h\, t_w^3}{3} + \frac{b_2 t_2^3}{3} \qquad (3.12)$$

For areas where plates intersect, the midline dimension is used as shown in the shaded parts of Fig.3-5 (a).

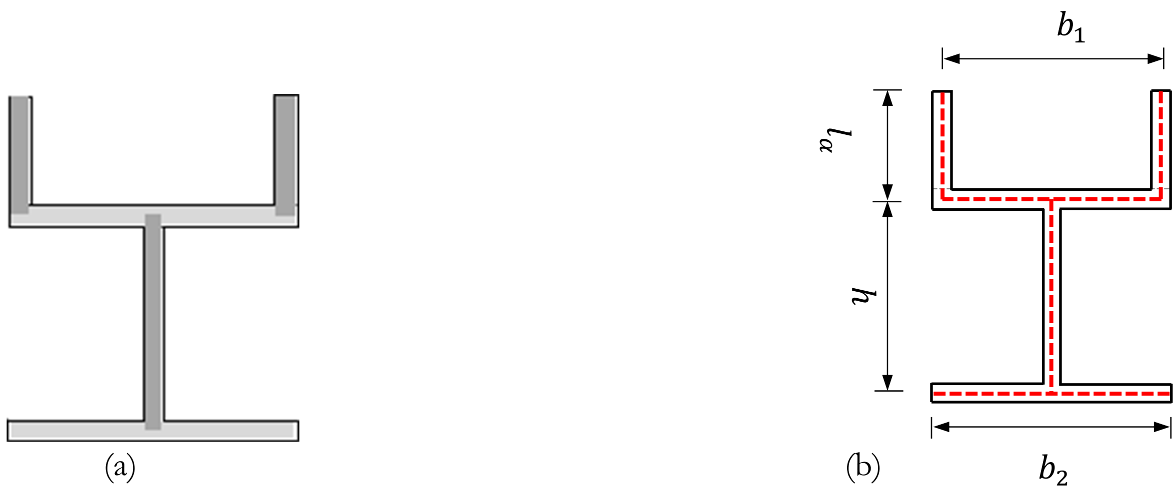

(a) (b)

Fig.3-5 Effective plate dimension regions for vertical and horizontal plates

The midline dimensions given in Fig.3-5 (b) and relationship with overall dimensions given in Fig.3-2 are summarized in Table 3-2. These dimensions are also used in other equations that follow.

Table 3-2 Midline dimensions

Midline dimensions	$l_\alpha = \left(\alpha + \frac{t_1}{2}\right)$	$b_1 = (B - t_\alpha)$
	$h = \left(H - \frac{t_1}{2} - \frac{t_2}{2}\right)$	$b_2 = b$

3.4 SHEAR CENTER

The shear center must first be located before the warping constant or the monosymmetry constant can be determined. In determining the location of the shear center several approaches are available. These are based on the characteristics of the shear center such as:

1. The shear center is the point through which a transverse load must act for the member to experience bending only with no twist. In this instance the shear flow through the member is used to locate the shear center.

2. When a torque is applied to a prismatic cross section, the shear center is the axis about which the member cross section rotates.

These fundamental characteristics, and many other associated ones, can be exploited to locate the shear center of a prismatic cross section. The approach used to generate a general equation for the location of the shear center for the section considered in the current study is the one presented in Heins (1975). This is carried out on the basis of a section subjected only to bending type stresses with transverse forces acting through the shear center. The section not being subjected to any axial or torsional loads. Since the plates are thin the shear stress generated in them is taken as uniform across the plate thickness. The shear flow is obtained by multiplying the shear stress by the thickness at any point. It is assumed that the cross section retains its shape during loading.

Considering the state of stress of a small element located along an open cross section as shown in Fig.3-6 (a) the forces on the element are shown in Fig.3-6 (b). The forces are in equilibrium with σ_z arising from the bending stress and τ the shear stress.

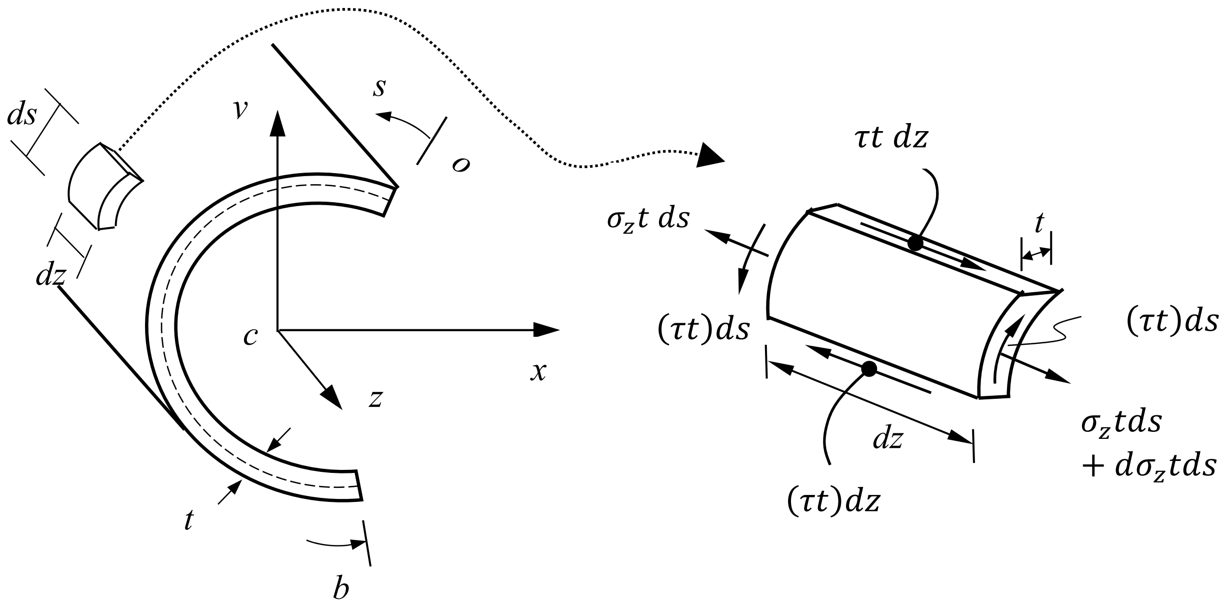

(a) (b)

Fig.3-6 Model for shear center location (Adapted from Heins, 1975)

By taking a summation of forces on the axis (z) direction for the element equation (3.13) is obtained.

$$t\frac{\partial \sigma_z}{\partial z} + \frac{\partial (\tau t)}{\partial s} = 0 \tag{3.13}$$

Replacing the bending stress with equations relating σ_z to the applied moments M_x and M_y and noting that derivatives of the moments give resultant shear forces, equation (3.13) can be re-written with respect to the shear flow as:

$$\tau t = \frac{1}{\left[I_{xy}^2 - I_x I_y\right]} \left[V_x \left(I_y \int_0^s y\, tds - I_{xy} \int_0^s x\, tds \right) + V_y \left(I_x \int_0^s x\, tds - I_{xy} \int_0^s y\, tds \right) \right] \tag{3.14}$$

If the centroidal coordinates are principal, then $I_{xy} = 0$ and the equation simplifies. Reference is now made to Fig.3-7 which shows the shear flow generated from applied transverse forces at the shear center. By taking only one of the forces at a time an equation can be written relating the applied force to the shear flow based on moment equilibrium with moments taken about the centroid 'c'. The lever arm for the shear flow being given by 'ρ'.

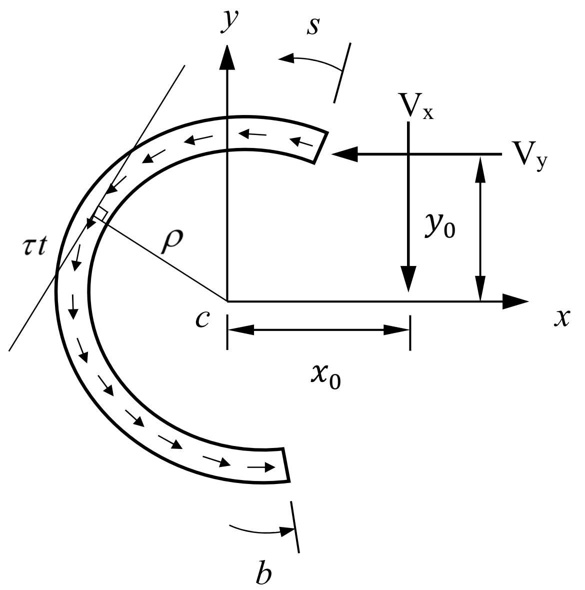

Fig.3-7 Shear flow in arbitrary thin-walled section subjected to transvers forces through shear center (Adapted from Heins, 1975)

The following equations are obtained:

$$x_0 = \frac{1}{V_x} \int_0^b \rho \, (\tau t) \, ds \tag{3.15}$$

and,

$$y_0 = \frac{1}{V_y} \int_0^b \rho \, (\tau t) \, ds \tag{3.16}$$

With a further term introduced:

$$\omega = \int_0^s \rho \, ds \tag{3.17}$$

Replacing the shear flow equation (3.14) in equations (3.15) and (3.16) gives expressions for the shear center location relative to the centroid; x_0 and y_0 in terms of cross section properties $I_{\omega x}$ and $I_{\omega y}$ where:

$$I_{\omega x} = \int_0^b \omega x \, t \, ds \tag{3.18}$$

$$I_{\omega y} = \int_0^b \omega y \, t \, ds \tag{3.19}$$

The expressions for the shear center location then become, with reference to Fig. 3-6:

$$x_0 = \frac{I_{\omega y}}{I_x} \tag{3.20}$$

$$y_0 = \frac{I_{\omega x}}{I_y} \tag{3.21}$$

Since the second moments of area are straightforward to determine, the determination of the shear center location requires only the determination of the geometric properties $I_{\omega x}$ and $I_{\omega y}$.

The approach used in the current study follows a similar approach presented in Jenkins (1990) with the only difference being the selection of an arbitrary reference point other than the centroid to simplify the calculation procedure. The distance to the shear center is now presented as:

$$y = \frac{I_{\omega x}}{I_y} \tag{3.22}$$

Being the distance from the reference pole to the shear center position. Because the shear center always lies on a line of symmetry the distance '*x*' has a value of zero in the sections considered under the current study. In determining the value of $I_{\omega x}$ it is recognized that the equation (3.18) is an integral containing two functions 'ω' and '*x*'. As long as these two functions are linearly varying along the plate length then a standard integration table found in some mechanics textbooks can be used to evaluate the integral. The functions are indeed linearly varying in the case of our cross section and therefore this approach is employed.

The reference pole, O is selected at the intersection of the web and lower flange midlines. The distance 'y' in equation (3.22) is thus measured from the pole to the shear center (S.C.) position. The distance from a chosen datum, in this case the base of the bottom flange, to the shear center is given by 'y_{sc}' and is obtained by adding half the bottom flange thickness to 'y' as is shown in equation (3.27). The graphical presentation of the two functions 'ω' and '*x*' are shown in Fig.3-8 (a) and (b) as is the position of the reference pole. The value of 'γ' is ${b_1}/{2} \cdot h$.

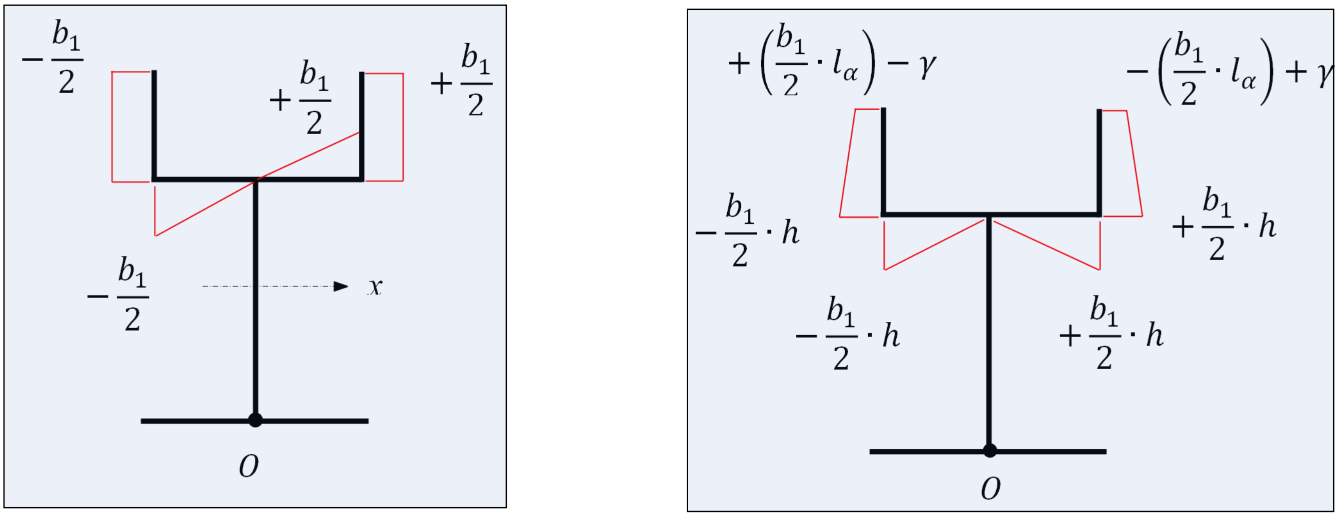

(a) Function for 'x' in graphical form

(b) Function for 'ω' in graphical form

Fig.3-8 Graphical representation of linear functions applicable to I-Section with upstands

The integration tables are then used to evaluate the integral in 3.18. The equations are evaluated separately for the flange ($I_{\omega x1}$) and upstands ($I_{\omega x2}$) and summed. These are given in equations (3.23) to (3.27).

$$I_{\omega x1} = \frac{b_1^3}{12} \cdot h \cdot t_1 \tag{3.23}$$

$$I_{\omega x2} = \frac{l_\alpha b_1 t_\alpha}{2} \cdot \left[b_1 h - \frac{b_1 l_\alpha}{2}\right] \tag{3.24}$$

$$I_{\omega x} = I_{\omega x1} + I_{\omega x2} \tag{3.25}$$

$$y_{sc} = \frac{I_{\omega x}}{I_y} + \frac{t_2}{2} \tag{3.26}$$

$$y_{sc} = y + \frac{t_2}{2} \tag{3.27}$$

The shear center can thus be located for the section considered in the current study using the equations derived in (3.23) to (3.27). The second term in (3.27) is added to measure the distance to the shear center from the base of the bottom flange. This is selected so that both the shear center and the centroid position $\bar{y}$ can be expressed from a common reference point, in this case the base of the lower flange. This is shown in Fig.3-9.

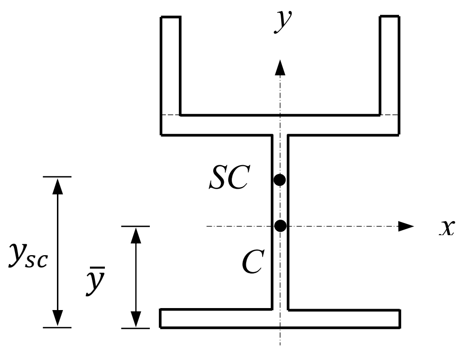

Fig.3-9 Shear center and centroid position for the I-section with upstands

This will be particularly important for the determination of the monosymmetry constant where the difference between the centroid and shear center is required. Determination of the centroid position is based on the equation:

$$\bar{y} = \frac{\sum A_i y_i}{\sum A_i} \tag{3.28}$$

A_i = *plate sub element area*, y_i = *distance from datum to plate sub-element.*

resulting in;

$$\boxed{\bar{y} = \frac{4\alpha t_\alpha H + 2\alpha^2 t_\alpha + 2Bt_1 H - Bt_1^2 + 2t_w h_w t_2 + h_w^2 t_w + bt_2^2}{4\alpha t_\alpha + 2Bt_1 + 2h_w t_w + 2bt_2} \quad (3.29)}$$

with $(h_w = H - t_1 - t_2)$

Once the shear center is determined it becomes possible to determine the warping constant and the monosymmetry constant.

3.5 WARPING CONSTANT

The warping constant is obtained by considering the approach given by Timoshenko and Gere (1961). In this approach a relationship is first derived between the warping displacements in the longitudinal direction, *w*, and the angle of twist rotation of the member along its axis, ϕ, when subjected to a torque. This relationship is expressed in equations (3.30) and (3.31).

$$\frac{\partial w}{\partial s} = -\rho_0 \phi' \tag{3.30}$$

$$w = w_0 - \phi' \int_0^s \rho_0 \, ds \tag{3.31}$$

Equation (3.31) gives the magnitude of displacement of points along the cross section in the longitudinal, 'z', direction with w_0 being the displacement in the 'z' direction of the point from which 's' is measured along 'm' the total distance. The integral in (3.31) represents twice the sectorial area, $\left(\frac{1}{2}\rho_0 \, ds\right)$ shown as the shaded portion in Fig.3-10 (a). Formulation of the warping constant solution is presented with reference to Fig. 3-10 for an arbitrary cross section with shear center located at SC.

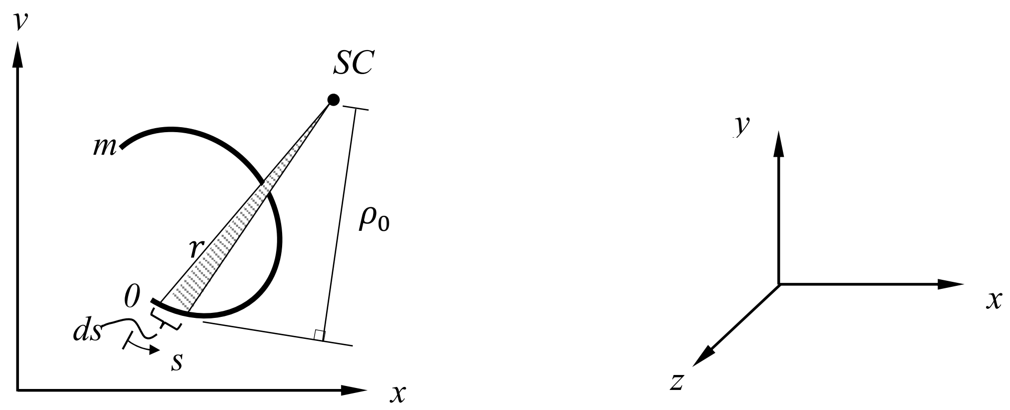

(a) Cross section

(b) Cartesian coordinate system

Fig.3-10 Cross section detail for the derivation of the warping constant

Timoshenko and Gere (1961) have shown that the average value of the warping displacement, $\bar{w}$, is:

$$\bar{w} = \frac{1}{m}\int_0^m w \, ds = w_0 - \frac{\phi'}{m}\int_0^m \left[\int_0^s \rho_0 \, ds\right] ds \tag{3.32}$$

Subtracting this from equation (3.31) gives the warping displacement with respect to the plane of average warping. The new displacement relative to this average plane is given in equation (3.33).

$$w = \frac{\phi'}{m}\int_0^m \left[\int_0^s \rho_0 \, ds\right] ds - \phi' \int_0^s \rho_0 \, ds \tag{3.33}$$

The expression in (3.33) can be simplified by introducing two new functions, the warping function and the average warping function given in (3.34) and (3.35) respectively.

$$\omega_s = \int_0^s \rho_0 \, ds \tag{3.34}$$

$$\bar{\omega}_s = \frac{1}{m}\int_0^m \omega_s \, ds \tag{3.35}$$

The warping function represents double the sectorial area corresponding to the arc 's' of the midline of the cross section shown in Fig.3-9 (a). The equation (3.33) can now be expressed as:

$$w = \phi'(\bar{\omega}_s - \omega_s) \tag{3.36}$$

By considering the longitudinal stresses arising from an applied torque with non-uniform torsion taking place in the section, an expression is developed relating the applied torque to the rate of twist. These longitudinal stresses can arise due to restraints placed on warping displacements at some point on the member or due to forms of transverse loading. From this relationship an expression for the warping constant was obtained by Timoshenko and Gere (1961) as:

$$C_w = \int_0^m (\bar{\omega}_s - \omega_s)^2 \, t \, ds \tag{3.37}$$

In carrying out the evaluation of the integrals (3.34), (3.35) and (3.37) the sequence shown in Fig.3-11 has been used for the section in the current study. For the upper part of the section s_1, s_2 and s_3 are integrated as a continuous function over the full length indicated. This means the start value for the next segment integral follows from the end value of the previous segment as shown in the general representation of equation (3.38).

$$\int_0^m f_n ds = \int_0^{l_\alpha} f_1 ds + \int_{l_\alpha}^{l_\alpha + b_1} f_2 ds + \int_{l_\alpha + b_1}^{2l_\alpha + b_1} f_3 ds \tag{3.38}$$

The integrals are based on the midline dimensions just as for the shear centre. The integral for s_4 is evaluated separately and added to the result from the upper part of the section.

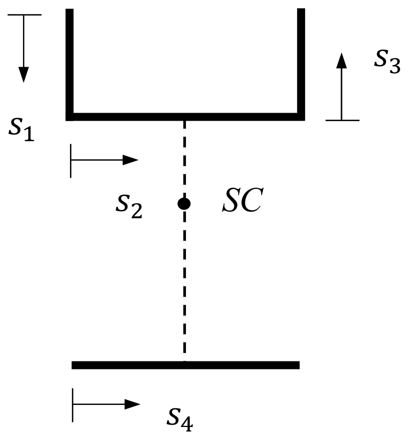

Fig.3-11 Integration sequence for determination of the warping constant

The evaluation of equation (3.37) using the approach described leads, after a significant amount of mathematical computation, to the general equation (3.39) for the warping constant of the section considered in the current study.

$$\boxed{C_w = \frac{t_1 b_1^3 (h-e)^2}{12} + \frac{t_\alpha b_1^2 {l_\alpha}^3}{6} - \frac{t_\alpha b_1^2 (h-e) l_\alpha^2}{2} + \frac{t_\alpha b_1^2 (h-e)^2 l_\alpha}{2} + \frac{t_2 e^2 b_2^3}{12}} \quad (3.39)$$

where e = y from equation (3.22) and shown in Fig.3-2 (b).

The equation incorporates full thickness dimensions as well as midline plate dimensions. The parameter '*e*' corresponds to the shear center location, hence the need indicated earlier to determine this.

It is worth noting that extending the approach to the case of an I-shaped cross section also yields an advantageous result over that contained in Timoshenko and Gere (1961). The authors give a general equation in Table A-3 as shown in equation (3.40) with reference to Fig.3-12 and with t_f as the flange thickness for both flanges.

$$C_w = \frac{t_f h^2}{12} \cdot \frac{B^3 b^3}{B^3 + b^3} \quad (3.40)$$

Applying the approach used in the current study leads to the equation given in (3.41).

$$C_w = \frac{(e-h)^2 t_1 B^3}{12} + \frac{e^2 b^3 t_2}{12} \quad (3.41)$$

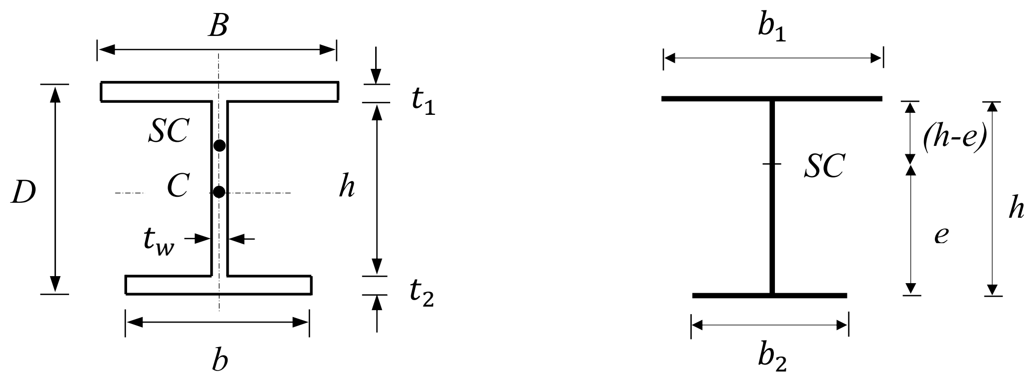

Fig.3-12 I-Section beam overall and midline dimensions

The advantage of the equation (3.41) developed in the current study is immediately obvious as it accommodates the solution for the case then the two flange thicknesses are not identical. The solution from Timoshenko and Gere (1961) is only valid for the case where the two flanges have the same thickness. In this case no attempt has been made to verify whether (3.41) simplifies to (3.40) when $t_1 = t_2 = t_f$. The generality of equation (3.41) holds an advantage in the form given. A verification has been carried out to show that the two equations generate the same result for both doubly and singly symmetric cross sections. For the singly symmetric section the value of $\frac{B}{b}$ is adjusted to 2. The results are presented in Table 3-3. Doubly symmetric section geometries from the Southern African Steel Construction Handbook (SASCH), (SAISC 2016) are employed but with corner radii neglected.

Table 3-3: Comparison of warping constant from equations (3.40) and (3.41)

Section	**B (mm)**	**b (mm)**	$\boldsymbol{\frac{B}{b}}$	$\boldsymbol{C_w}$ – Equation (3.40) - (10^9)	$\boldsymbol{C_w}$ – Equation (3.41) - (10^9)	**% Difference**
203x133x25	133.2	133.2	1	29.32	29.32	0.0
	133.2	66.6	2	6.52	6.52	0.0
533x210x122	211.9	211.9	1	2312.40	2312.40	0.0
	211.9	105.95	2	513.87	513.87	0.0
152x152x23	152.4	152.4	1	21.26	21.26	0.0
	152.4	76.2	2	4.72	4.72	0.0
305x305x158	310.6	310.6	1	2850.50	2850.50	0.0
	310.6	155.3	2	633.45	633.45	0.0

The results in Table 3-3 show that the equation developed in the current study for the I-section case yields the same results as the ones obtained from the equation by Timoshenko and Gere (1961). This helps to verify the approach used in generating the general equation for the I-shaped section with flange upstands given in (3.39).

3.6 MONOSYMMETRY CONSTANT

The monosymmetry constant equation in (3.42) was shown to be the correct one by Anderson and Trahair (1972) and is still used widely in this form to this day. This is the form in which it appears in the equations derived by Goodier (1942). v

$$\beta_x = \frac{1}{I_x}\int_A y(y^2 + x^2)dA - 2y_0 \qquad (3.42)$$

This equation is not easy to apply in routine design. A simplified approach for members consisting of an assemblage of plates has been proposed by Hsu et al (2012). This approach leads to a simplification of equation (3.42) into polynomial form which is easy to implement in routine design. In order to simplify the form of the equation it must first be recognized that the integral can be re-written as a double integral as shown in (3.43).

$$\beta_x = \frac{1}{I_x}\int_{x_1}^{x_2}\int_{y_1}^{y_2}(y^3 + yx^2)\,dy\,dx - 2y_0 \qquad (3.43)$$

Recognizing the coordinates (x_1, y_1) and (x_2, y_2), with respect to the centroid, as occurring on diagonally opposite ends of a plate the integration can be performed separately over each plate and then summed up. In this was a cross section which can be depicted as an assemblage of plates can be divided into suitable plate geometries, the integration carried out over each plate sub-assembly and then the parts summed up for the complete solution. This is shown mathematically in equation (3.44) after the integration and simplification of (3.43) using the limits shown.

$$\boxed{\beta_x = \frac{1}{I_x}\left\{\sum\left[\frac{1}{6}(x_2^3 - x_1^3)(y_2^2 - y_1^2) + \frac{1}{4}(x_2 - x_1)(y_2^4 - y_1^4)\right]\right\} - 2y_0 \qquad (3.44)}$$

where $y_0 = y_{sc} - \bar{y}$

The equation for the major axis second moment of area for the section with flange upstands is given in equation (3.45).

$$\begin{aligned} I_x = \frac{\alpha^3 t_\alpha}{6} &+ \left[2\alpha t\left(H - \bar{y} + \frac{\alpha}{2}\right)^2\right] + \frac{Bt_1^3}{12} + \left[Bt_1\left(H - \bar{y} - \frac{t_1}{2}\right)^2\right] + \frac{t_w h_w^3}{12} \\ &+ \left[h_w t_w\left(\frac{H}{2} - \bar{y}\right)^2\right] + \frac{bt_2^3}{12} \\ &+ \left[bt_2\left(\bar{y} - \frac{t_2}{2}\right)^2\right] \qquad (3.45) \end{aligned}$$

The procedure is shown diagrammatically in Fig.3-13. This shows how the cross section in the current study can be broken into five (5) plate sub-assemblies and also shows the integration limits for a single plate. These limits are applied to each successive plate and the results for the individual sub-assemblies summed up.

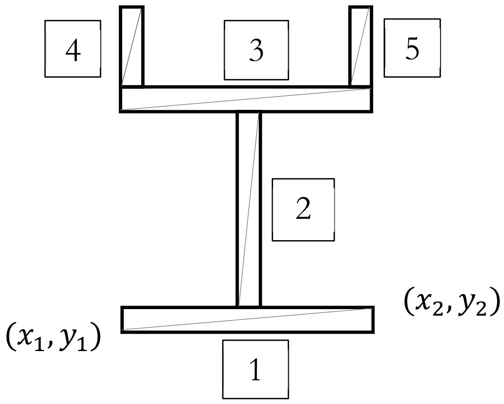

Fig.3-13 Plate sub-assemblies for monosymmetric cross section in current study

A suitable coordinate system needs to be used when applying equation (3.44) and must be consistent with the coordinate system used when deriving the equation. This is also important so that the sign of y_0 is correctly determined. The coordinate system used in this case is similar to that adopted by Hsu et al (2012) and is shown in Fig.3-14. The polynomial equation can be efficiently and conveniently applied with the aid of a spreadsheet to get the value of the monosymmetry constant. Once the spreadsheet is set up correctly for the required number of plates one needs only to enter the coordinate values for the relevant plate diagonal end points to get the required output. An example of the spreadsheet input and output for a 203x133x25 narrow flange beam with radii neglected is shown in Fig.3-14.

MONOSYMMETRY CONSTANT

Beam: 203x133x25

Plate #	x1	y1	x2	y2	PART - A	PART - B	PART (A+B)
1	66,60	114,18	-66,60	106,38	169 403 886,0	1 395 190 944,4	1 564 594 830,3
2	2,85	106,38	-2,85	-81,22	36 421,8	120 487 348,4	120 523 770,2
3	66,60	-81,22	-66,60	-89,02	-130 754 575,4	-642 099 250,3	-772 853 825,7
4	66,60	-89,02	58,80	-114,02	-77 925 644,1	-207 120 138,5	-285 045 782,6
5	-58,80	-89,02	-66,60	-114,02	-77 925 644,1	-207 120 138,5	-285 045 782,6
							342 173 209,6

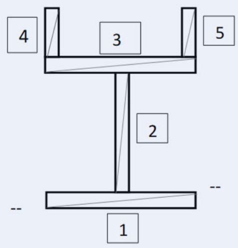

I_x	27 518 844,4	mm^4
y_0	-13,6	mm
β_x	**39,7**	

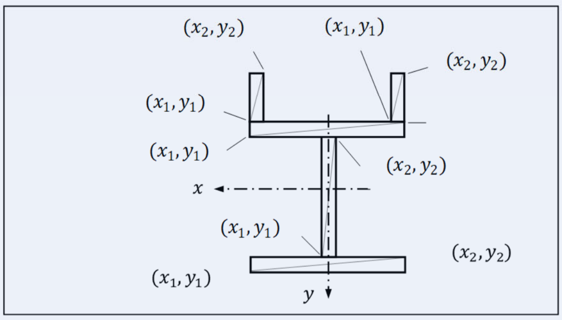

Fig.3-14 Spreadsheet implementation of equation (3.44) for coordinate system of Hsu et al (2012)

This concludes the derivations for the key geometrical properties of the I-shaped cross section with top flange end upstands or stiffeners. The approaches used here can be applied to any other cross-sections which can be idealized as an assemblage of plate elements.

3.7 APPLICATION OF DERIVED EQUATIONS

3.7.1 Introduction

Having derived the necessary equations for key geometric parameters and presented them in an easy to apply polynomial form their use is now demonstrated, and their accuracy verified. An initial verification is carried out to verify the loss of accuracy produced by neglecting the radii on the 'base' i.e. I-shaped cross section prior to introduction of upstands. This is done simply to verify the applicability of equations formulated for a plated case to that were the section has corner radii as contained in the steel handbook standard sections. After this, all other comparisons are based only on the plated section with radii neglected. The results from the equations are compared to software output from a commercially available software, Prokon ver.3.1(2019). Prokon uses the following approaches for determining the section properties:

- **Centroid, Moments of area:** The program calculates the bending section properties using a method of division into sub-sections. Circles and arcs are first converted to polygons with approximately the same shapes. The program uses lines at 1° angle increments for this purpose. The section is then sub-divided into a series of trapeziums and the properties are calculated for each trapezium. The global section properties are finally calculated through summation of the values obtained for each trapezium.

For calculating the shear and torsional section properties, the program uses a finite difference analysis method.

- **Shear center:** The shear stress distributions in the Y and X-directions are determined for a unit load applied in the Y-direction. The shear centre is then calculated by considering the moment of shear stresses about the centre of mass.

- **St. Venant Torsional Constant:** Prandtl membrane analogy is used. The torsional constant, J, is taken as twice the volume below the membrane. The maximum slope of the membrane then gives the torsional modulus.

- **Warping Constant:** Warping torsion is evaluated by using the relationship between shear and axial deformation from classical elastic theory. The shear deformation is obtained from the pure torsion analysis. The warping constant, C_w, is then determined from the longitudinal displacements.

- **Monosymmetry Constant:** The finite difference method is used to evaluate this.

3.7.2 Comparison with SASCH sections

A comparison of outputs from the equations derived in the preceding sections for four section properties with those from the steel handbook (SAISC, 2016) are presented here. Where applicable the full width for the top flange, B, is used in place of the midline width, b_1. The results are intended to show the effects of neglecting the corner radii. Six beams are considered; three narrow flange and three wide flange beams. The selections are from the smallest, largest and a median size. Results from the comparison are shown in Tables 3-4 to 3-9. The difference is negative when the absolute equation value is lesser of the two.

Table 3-4 Comparison of section property values for a 203x133x25 UB – Narrow Flange

Member		**I_x (mm^4)**	**I_y (mm^4)**	**J (mm^4)**	**C_w (mm^6)**
203x133x25	Equation output	22.98×10^6	3.07×10^6	54.2×10^3	29.3×10^9
	SASCH value	23.5×10^6	3.09×10^6	62.1×10^3	29.5×10^9
	% Difference	-2.3	-0.65	-14.6	-0.6

Table 3-5 Comparison of section property values for a 406x140x39 UB – Narrow Flange

Member		**I_x (mm^4)**	**I_y (mm^4)**	**J (mm^4)**	**C_w (mm^6)**
406x140x39	Equation output	121×10^6	4.09×10^6	93×10^3	154×10^9
	SASCH value	124×10^6	4.10×10^6	108×10^3	155×10^9
	% Difference	-2.5	-0.24	-16	-0.6

Table 3-6 Comparison of section property values for a 533x210x122 UB – Narrow Flange

Member		**I_x (mm^4)**	**I_y (mm^4)**	**J (mm^4)**	**C_w (mm^6)**
533x210x122	Equation output	753×10^6	33.86×10^6	1731×10^3	2312×10^9
	SASCH value	762×10^6	33.90×10^6	1810×10^3	2320×10^9
	% Difference	-1.2	-0.12	-4.6	-0.4

Table 3-7 Comparison of section property values for a 152x152x23 UC – Wide Flange

Member		**I_x (mm^4)**	**I_y (mm^4)**	**J (mm^4)**	**C_w (mm^6)**
152x152x23	Equation output	12.4×10^6	4.01×10^6	42.96×10^3	21.26×10^9
	SASCH value	12.6×10^6	4.02×10^6	51.1×10^3	21.3×10^9
	% Difference	-1.6	-0.25	-18.9	-0.2

Table 3-8 Comparison of section property values for a 254x254x73 UC – Wide Flange

Member		**I_x (mm^4)**	**I_y (mm^4)**	**J (mm^4)**	**C_w (mm^6)**
254x254x73	Equation output	112×10^6	38.79×10^6	535.73×10^3	558.47×10^9
	SASCH value	114×10^6	38.8×10^6	578×10^3	559×10^9
	% Difference	-1.8	-0.03	-7.9	-0.1

Table 3-9 Comparison of section property values for a 305x305x158 UC – Wide Flange

Member		**I_x (mm^4)**	**I_y (mm^4)**	**J (mm^4)**	**C_w (mm^6)**
305x305x158	Equation output	383×10^6	124.94×10^6	3625.2×10^3	2850×10^9
	SASCH value	387×10^6	125×10^6	3810×10^3	2850×10^9
	% Difference	-1.0	-0.05	-5.1	0.0

It is clear from the results presented in Tables 3-4 to 3-9 that the neglecting of the radii leads only to minor differences for three of the parameters; the second moments of area and the warping constant with a maximum difference always less than 2%. For one of the parameters; the St. Venant torsional constant, large differences are observed. For this parameter with differences of up to 19% observed. However, it is worth noting that the values obtained from the equations are generally conservative with only one case where the values were equal. This means that ignoring the corner radii results in a conservative estimate for the case of rolled sections with corner radii. From here onwards the equation outputs will be compared to similar sections i.e., plated section geometries with no corner radii generated from a commercially available software, Prokon.

3.7.3 Comparison of equation outputs with software output

The six beams used in section 3.7.2 are now employed for comparison with software output. the software utilized is Prokon ver.3.1 (2019), the underlying assumptions of which were explained in Section 3.7.1. The designation 'NF' for narrow flange and 'WF' for wide flange will be employed to differentiate them from the standard rolled members in the SASCH from which they are derived. This will make any future comparison with standard rolled sections easier. The properties relevant to determination of the critical elastic moment are considered. The first set of Tables will compare the second moment of area about the minor axis, centroid location, shear center location, St. Venant torsional constant and warping constant. The next set of tables then presents a comparison for the monosymmetry constant. Equation outputs are indicated as 'Eqn.', software outputs as 'Soft.' and the difference as '% Diff.' given as a percentage of the difference between equation and software output. Negative values indicate a smaller absolute equation output value.

Table 3-10 Comparison of section property values for a NF203x133x25 UB

Section	Upstand Height		I_y x10^6(mm^4)	$\bar{y}$ (mm)	y_{sc} (mm)	J x10^3 (mm^4)	C_w x10^9 (mm^6)	β_x
NF203x133x25	0	Eqn.	3.075	101.6	101.5	54.20	29.33	0
		Soft.	3.075	101.6	102	53.27	29.32	0
		% Diff.	0,0%	0,0%	-0,5%	1,7%	0,0%	--
	25	Eqn.	4.610	114.2	127.8	62.11	36.03	39.7
		Soft.	4.610	114.2	129	61.79	36.27	41.6
		% Diff.	0,0%	0,0%	-0,9%	0,5%	-0,7%	-4,8%
	50	Eqn.	6.146	126.7	135.3	70.02	37.11	37.7
		Soft.	6.146	126.7	136	69.62	37.34	39.4
		% Diff.	0,0%	0,0%	-0,5%	0,6%	-0,6%	-4,5%
	75	Eqn.	7.680	139.3	134.8	77.93	37.20	16.6
		Soft.	7.681	139.3	136	77.66	37.37	18.19
		% Diff.	0,0%	0,0%	-0,9%	0,4%	-0,5%	-9,6%
	100	Eqn.	9.216	151.8	130.3	85.84	38.23	-14.7
		Soft.	9.216	151.8	131	85.56	38.50	-13.23
		% Diff.	0,0%	0,0%	-0,5%	0,3%	-0,7%	10,0%
	125	Eqn.	10.751	164.4	123.5	93.75	41.30	-52.1
		Soft.	10.751	164.4	124	93.43	41.77	-50.7
		% Diff.	0,0%	0,0%	-0,4%	0,3%	-1,1%	2,7%

Table 3-11 Comparison of section property values for a NF406x140x39 UB

Section	Upstand Height		I_y x10⁶(mm⁴)	$\bar{y}$ (mm)	y_{sc} (mm)	J x10³ (mm⁴)	C_w x10⁹ (mm⁶)	β_x
NF406x140x39	0	Eqn.	4.095	198.7	198.3	92.53	154.36	0
		Soft.	4.095	198.7	199	91.31	154.32	0
		% Diff.	0,0%	0,0%	-0,4%	1,3%	0,0%	--
	25	Eqn.	6.005	215.9	253.2	103.13	194.86	95.0
		Soft.	6.005	215.9	255	102.73	195.69	99.1
		% Diff.	0,0%	0,0%	-0,7%	0,4%	-0,4%	-4,3%
	50	Eqn.	7.915	232.4	276.7	113.73	208.47	125.8
		Soft.	7.914	232.4	278	113.16	209.18	129.3
		% Diff.	0,0%	0,0%	-0,5%	0,5%	-0,3%	-2,8%
	75	Eqn.	9.824	248.8	286.3	124.33	212.15	126.7
		Soft.	9.824	248.4	288	123.94	213.03	129.8
		% Diff.	0,0%	0,2%	-0,6%	0,3%	-0,4%	-2,4%
	100	Eqn.	11.734	263.9	288.6	134.93	212.55	111.6
		Soft.	11.734	263.9	290	134.63	213.30	114.5
		% Diff.	0,0%	0,0%	-0,5%	0,2%	-0,4%	-2,6%
	125	Eqn.	13.644	279	286.8	145.53	212.95	86.9
		Soft.	13.644	279	288	145.20	214.28	89.6
		% Diff.	0,0%	0,0%	-0,4%	0,2%	-0,6%	-3,1%

Table 3-12 Comparison of section property values for a NF533x210x122 UB

Section	Upstand Height		I_y x10⁶(mm⁴)	$\bar{y}$ (mm)	y_{sc} (mm)	J x10³ (mm⁴)	C_w x10⁹ (mm⁶)	β_x
NF533x210x122	0	Eqn.	33.865	272.3	271.6	17300	2310	0
		Soft.	33.865	272.3	272	1668.6	2312	0
		% Diff.	0,0%	0,0%	-0,1%	3,5%	-0,1%	--
	25	Eqn.	43.577	290.7	318.2	1890	2710	78.4
		Soft.	43.577	290.7	326	1859.9	2752	93.6
		% Diff.	0,0%	0,0%	-2,5%	1,6%	-1,6%	-19,2%
	50	Eqn.	53.290	308.3	348.4	2050	2920	123.6
		Soft.	53.290	308.3	355	2021	2958	137.2
		% Diff.	0,0%	0,0%	-1,9%	1,4%	-1,3%	-11,0%
	75	Eqn.	63.003	325.4	365.5	2210	3020	141.0
		Soft.	63.003	325.4	372	2183	3046	153.6
		% Diff.	0,0%	0,0%	-1,8%	1,2%	-0,9%	-8,9%
	100	Eqn.	72.716	342.0	374.6	2380	3060	141.2
		Soft.	72.716	342	381	2342	3091	153.1
		% Diff.	0,0%	0,0%	-1,7%	1,6%	-1,0%	-8,4%
	125	Eqn.	82.428	358.1	378.7	2540	3070	130.1
		Soft.	82.428	358.1	384	2506	3102	141.3
		% Diff.	48,5%	0,0%	-1,4%	1,3%	-1,0%	-8,6%

Table 3-13 Comparison of section property values for a WF15x152x23 UC

Section	Upstand Height		I_y x10⁶(mm⁴)	$\bar{y}$ (mm)	y_{sc} (mm)	J x10³ (mm⁴)	C_w x10⁹ (mm⁶)	β_x
WF152x152x23	0	Eqn.	4.014	76.2	76.2	42.96	21.26	0
		Soft.	4.014	76.2	76.2	42.63	21.23	0
		% Diff.	0,0%	0,0%	0,0%	0,8%	0,2%	--
	25	Eqn.	5.817	85.5	93.4	48.20	25.30	20.3
		Soft.	5.817	85.4	93.9	48.13	25.41	21.2
		% Diff.	0,0%	0,1%	-0,5%	0,2%	-0,4%	-4,5%
	50	Eqn.	7.621	95.3	96.6	53.44	25.68	8.5
		Soft.	7.621	95.3	97.3	53.36	25.77	9.3
		% Diff.	0,0%	0,0%	-0,7%	0,1%	-0,4%	-9,8%
	75	Eqn.	9.424	105.6	94.2	58.68	26.06	-18.6
		Soft.	9.424	105.6	94.6	58.68	26.15	-17.8
		% Diff.	0,0%	0,0%	-0,4%	0,0%	-0,4%	4,2%
	100	Eqn.	11.227	116.3	88.4	63.92	28.15	-53.9
		Soft.	11.227	116.3	88.8	63.89	28.36	-53.2
		% Diff.	0,0%	0,0%	-0,5%	0,1%	-0,8%	1,3%
	125	Eqn.	13.030	127.2	80.8	69.17	33.01	-93.9
		Soft.	13.030	127.2	81.1	69.20	33.23	-93.2
		% Diff.	0,0%	0,0%	-0,4%	0,0%	2,4%	0,7%

Table 3-14 Comparison of section property values for a WF254x254x73 UC

Section	Upstand Height		I_y x10⁶(mm⁴)	$\bar{y}$ (mm)	y_{sc} (mm)	J x10³ (mm⁴)	C_w x10⁹ (mm⁶)	β_x
WF254x254x73	0	Eqn.	38.795	127.1	127.1	535.73	558.47	0
		Soft.	38.795	127.1	127	523.32	558.83	0
		% Diff.	0,0%	0,0%	0,1%	2,3%	-0,1%	--
	25	Eqn.	49.014	137.1	146.9	583.46	636.75	26.7
		Soft.	49.014	137.1	148	577.64	641.13	29.2
		% Diff.	0,0%	0,0%	-0,7%	1,0%	-0,7%	-9,2%
	50	Eqn.	59.232	147.5	156.4	631.18	662.86	29.9
		Soft.	59.232	147.5	158	625.91	667.89	32.2
		% Diff.	0,0%	0,0%	-1,0%	0,8%	-0,8%	-7,5%
	75	Eqn.	69.451	158.2	159.5	678.90	667.06	17.5
		Soft.	69.451	158.2	161	673.15	670.51	19.7
		% Diff.	0,0%	0,0%	-0,9%	0,8%	-0,5%	-12,5%
	100	Eqn.	79.670	169.0	158.6	726.62	668.09	-4.9
		Soft.	79.670	169	160	720.91	672.38	-2.9
		% Diff.	0,0%	0,0%	-0,9%	0,8%	-0,6%	41,6%
	125	Eqn.	89.889	180.1	155.0	774.34	677.61	-34.1
		Soft.	89.889	180.1	156	768.31	684.11	-32.2
		% Diff.	0,0%	0,0%	-0,6%	0,8%	-1,0%	5,6%

Table 3-15 Comparison of section property values for a WF305x305x158 UC

Section	Upstand Height		I_y x10⁶(mm⁴)	$\bar{y}$ (mm)	y_{sc} (mm)	J x10³ (mm⁴)	C_w x10⁹ (mm⁶)	β_x
WF305x305x158	0	Eqn.	124.941	163.6	163.5	3630	2850	0
		Soft.	124.940	163.6	164	3509	2850	0
		% Diff.	0,0%	0,0%	-0,3%	3,3%	0,0%	--
	25	Eqn.	150.496	174.0	182.0	3890	3150	23.9
		Soft.	150.500	174.0	185	3826	3193	30.4
		% Diff.	0,0%	0,0%	-1,6%	1,6%	-1,4%	-27,3%
	50	Eqn.	176.051	184.7	193.9	4150	3290	32.4
		Soft.	176.050	184.7	197	4093	3344	38.5
		% Diff.	0,0%	0,0%	-1,6%	1,4%	-1,6%	-18,8%
	75	Eqn.	201.605	195.5	199.6	4410	3340	26.4
		Soft.	201.610	195.5	203	4352	3370	32.1
		% Diff.	0,0%	0,0%	-1,7%	1,3%	-0,9%	-21,7%
	100	Eqn.	227.160	206.5	201.3	4670	3340	10.3
		Soft.	227.160	206.5	204	4610	3385	15.8
		% Diff.	0,0%	0,0%	-1,3%	1,3%	-1,3%	-53,2%
	125	Eqn.	252.715	217.7	200.0	4930	3350	-13.1
		Soft.	252.720	217.7	203	4873	3400	-7.7
		% Diff.	0,0%	0,0%	-1,5%	1,2%	-1,5%	41,1%

It is clear for both narrow flange and wide flange sections that the derived equation outputs agree with the software outputs for all properties except the monosymmetry constant. The outputs for the second moment of area about the minor axis and the centroid show no or very minute difference with a maximum of 0.1%. Outputs for the shear center, torsional constant and warping constant are generally within a difference of 2%, with a few values falling out to a maximum of 3.5%. For the monosymmetry constant the difference varies from a few percent to a maximum of 53%. Although it is clear that the equations derived under the current study give accurate values for the second moment of area about the minor axis, centroid, shear center, St. Venant torsional constant and warping constant, the discrepancy with the monosymmetry constant warrants further investigation. The discrepancy with the monosymmetry constant is thus addressed in the section that follows.

3.7.4 Normalization with Prokon for Monosymmetry Constant

It must be recognized that the two section properties particularly dependent on the value of the shear center are the warping constant and the monosymmetry constant. A study on the sensitivity of the warping constant and the monosymmetry constant to the shear center reveals that the monosymmetry constant is particularly sensitive to the value of the shear center. The study was carried out by introducing an error in the shear center value and observing the error change in the values of the warping and monosymmetry constants.

Therefore, in order to verify the derived equation outputs the shear center values obtained from the software were input into the equations for section properties derived from the current study and the new outputs then compared to the software output. The results are now presented in Table 3-16 to 3-21.

Table 3-16 Comparison of monosymmetry constant value for a NF 203x133x25 UB with software (y_{sc}) in equation

Section	Upst. Height (α)						y_{sc}	β_x
NF 203x133x25	25	Eqn.	Original Comparison	127,8	39,7	New Equation Input based on software value	129	42,1
		Software		129	41,6		129	41,6
		% Diff.		-0,9%	-4,8%		0,0%	1,2%
	50	Eqn.		135,3	37,7		136	39,2
		Software		136	39,4		136	39,4
		% Diff.		-0,5%	-4,5%		0,0%	-0,5%
	75	Eqn.		134,8	16,6		136	19,1
		Software		136	18,2		136	18,2
		% Diff.		-0,9%	-9,6%		0,0%	4,7%
	100	Eqn.		130,3	-14,7		131	-13,2
		Software		131	-13,2		131	-13,2
		% Diff.		-0,5%	10,0%		0,0%	0,0%
	125	Eqn.		123,5	-52,1		124	-51,0
		Software		124	-50,7		124	-50,7
		% Diff.		-0,4%	2,7%		0,0%	0,6%

Table 3-17 Comparison of monosymmetry constant value for a NF 406x140x39 UB with software (y_{sc}) in equation

Section	Upst. Height (α)						y_{sc}	β_x
NF 406x140x39	25	Eqn.	Original Comparison	253,2	95,0	New Equation Input based on software value	255	98,7
		Software		255	99,1		255	99,1
		% Diff.		-0,7%	-4,3%		0,0%	-0,4%
	50	Eqn.		276,7	125,8		278	128,4
		Software		278	129,3		278	129,3
		% Diff.		-0,5%	-2,8%		0,0%	-0,7%
	75	Eqn.		286,3	126,7		288	130,2
		Software		288	129,8		288	129,8
		% Diff.		-0,6%	-2,4%		0,0%	0,3%
	100	Eqn.		288,6	111,6		290	114,4
		Software		290	114,5		290	114,5
		% Diff.		-0,5%	-2,6%		0,0%	-0,1%
	125	Eqn.		286,8	86,9		288	89,3
		Software		288	89,6		288	89,6
		% Diff.		-0,4%	-3,1%		0,0%	-0,3%

Table 3-18 Comparison of monosymmetry constant value for a NF 533x210x122 UB with software (y_{sc}) in equation

Section	Upst. Height (α)			y_{sc}	β_x		y_{sc}	β_x
NF 533x210x122	25	Eqn.	Original Comparison	318,2	78,5	New Equation Input based on software value	326	94,0
		Software		326	93,6		326	93,6
		% Diff.		-2,5%	-19,2%		0,0%	0,5%
	50	Eqn.		348,4	123,6		355	136,8
		Software		355	137,2		355	137,2
		% Diff.		-1,9%	-11,0%		0,0%	-0,3%
	75	Eqn.		365,5	141,0		372	154,1
		Software		372	153,6		372	153,6
		% Diff.		-1,8%	-8,9%		0,0%	0,3%
	100	Eqn.		374,6	141,2		381	154,0
		Software		381	153,1		381	153,1
		% Diff.		-1,7%	-8,4%		0,0%	0,6%
	125	Eqn.		378,7	130,1		384	140,7
		Software		384	141,3		384	141,3
		% Diff.		-1,4%	-8,6%		0,0%	-0,5%

Table 3-19 Comparison of monosymmetry constant value for a WF 152x152x23 UC beam with software (y_{sc}) in equation

Section	Upst. Height (α)			y_{sc}	β_x		y_{sc}	β_x
WF 152x152x23	25	Eqn.	Original Comparison	93,4	20,3	New Equation Input based on software value	93,9	21,3
		Software		93,9	21,2		93,9	21,2
		% Diff.		-0,5%	-4,5%		0,0%	0,4%
	50	Eqn.		96,6	8,5		97,3	9,4
		Software		97,3	9,3		97,3	9,3
		% Diff.		-0,7%	-9,8%		0,0%	0,7%
	75	Eqn.		94,2	-18,6		94,6	-17,8
		Software		94,6	-17,8		94,6	-17,8
		% Diff.		-0,4%	4,2%		0,0%	-0,2%
	100	Eqn.		88,4	-53,9		88,8	-53,1
		Software		88,8	-53,2		88,8	-53,2
		% Diff.		-0,5%	1,3%		0,0%	-0,2%
	125	Eqn.		80,8	-93,9		81,1	-93,2
		Software		81,1	-93,2		81,1	-93,2
		% Diff.		-0,4%	0,7%		0,0%	0,0%

Table 3-20 Comparison of monosymmetry constant value for a WF 254x254x73UC beam with software (y_{sc}) in equation

Section	Upst. Height (α)			y_{sc}	β_x		y_{sc}	β_x
WF 254x254x73	25	Eqn.	Original Comparison	146,9	26,7	New Equation Input based on software value	148	28,9
		Software		148	29,2		148	29,2
		% Diff.		-0,7%	-9,2%		0,0%	-0,9%
	50	Eqn.		156,4	29,9		158	33,0
		Software		158	32,2		158	32,2
		% Diff.		-1,0%	-7,5%		0,0%	2,6%
	75	Eqn.		159,5	17,5		161	20,5
		Software		161	19,7		161	19,7
		% Diff.		-0,9%	-12,5%		0,0%	4,0%
	100	Eqn.		158,6	-4,9		160	-2,1
		Software		160	-2,9		160	-2,9
		% Diff.		-0,9%	41,6%		0,0%	-36,3%
	125	Eqn.		155	-34,1		156	-32,2
		Software		156	-32,2		156	-32,2
		% Diff.		-0,6%	5,6%		0,0%	0,0%

Table 3-21 Comparison of monosymmetry constant value for a WF 305x305x158UC beam with software (y_{sc}) in equation

Section	Upst. Height (α)			y_{sc}	β_x		y_{sc}	β_x
WF 305x305x158	25	Eqn.	Original Comparison	182	23,9	New Equation Input based on software value	185	29,9
		Software		185	30,4		185	30,4
		% Diff.		-1,6%	-27,3%		0,0%	-1,8%
	50	Eqn.		193,9	32,4		197	38,6
		Software		197	38,5		197	38,5
		% Diff.		-1,6%	-18,8%		0,0%	0,3%
	75	Eqn.		199,6	26,4		203	33,1
		Software		203	32,1		203	32,1
		% Diff.		-1,7%	-21,7%		0,0%	2,9%
	100	Eqn.		201,3	10,3		204	15,7
		Software		204	15,8		204	15,8
		% Diff.		-1,3%	-53,2%		0,0%	-0,5%
	125	Eqn.		200	-13,1		203	-7,2
		Software		203	-7,7		203	-7,7
		% Diff.		-1,5%	41,1%		0,0%	-7,1%

It is observed from the comparison that with the software shear center values input into the derived equations from the current study the outputs obtained are mostly within 1% of the software values, with only a few exceptions. These exceptions may arise due if the software rounds off some of its outputs. Whether it does this or not is not clear. The results of this study give confidence that the equations developed under the current study are accurate and give credible results. The sensitivity of the monosymmetry constant to the shear center value is clearly demonstrated.

A separate study on the sensitivity of the critical elastic moment to errors in the monosymmetry constant and the warping constant reveals a low sensitivity. This in part vindicates the use of simplified equations for these two parameters. Simplified equations must not be used to locate the shear center due to the previous stated sensitivity of the warping constant and monosymmetry constant to the shear center position accuracy.

3.7.5 Conclusion on section property comparisons

The preceding sections have presented a validation of the outputs obtained from the equations derived in the current study. Thus, it has been shown that the equations produce reliable and accurate outputs and will be used going forward. These equations will form the basis for cross-section property determination in the sections that follow. Sufficient confidence in their accuracy has been attained.

3.8 SECTION PROPERTIES WITH VARYING UPSTAND HEIGHT

The study by Anderson and Trahair (1972) showed the effects that load application height relative to the shear center position had on the critical elastic moment of a monosymmetric cross section. The further the distance between the two, when the load is applied above the shear center for a simply supported beam, the lower the critical moment. In order to optimize the height of upstands on the section in the current study an investigation into the behaviour of the shear center as the upstand height is adjusted was carried out. The study is based on the narrow flange and wide flange sections used in the previous sections. The position of the shear center as well as that of the centroid are plotted as the upstand height is adjusted. The results are given in Fig.3-15 to Fig.3-20.

In order to capture any similar behavior, plots are made not only for the shear center and centroid position as the upstand height is adjusted but also against a non-dimensionalized parameter, 'eta'. The value of eta is given by the ratio of upstand height (α) to beam height (H), for beam with no upstands, and given mathematically in equations (3.46).

$$\alpha = \eta H \tag{3.46}$$

The values of η considered are in increments of 0.05 up to a value of one (1) for the results shown in figures 3-15 to 3-20. This provides sufficient points for the plots and for observation of trends to be made. It is recognized that the upstand values generated at this interval choice do not necessarily conform to practical dimensions and therefore the exercise is carried out simply to study the movement of the shear center and centroid as the flange upstand height is adjusted.

Four plots are provided; two based on the shear center and centroid position movement with change in upstand height and two tracking the change in the value of the monosymmetry constant as the upstand height is varied. For each of the two, one is plotted against change in upstand height and the other with respect the non-dimensional factor, eta (η). The non-dimensional factor allows for observing the general pattern of behaviour. Plots are presented for three narrow flange sections and three wide flange sections in figures 3-15 to 3-20. As a reminder, all plots are based on the equations that have been presented in the preceding sections.

Beam: NF 203x133x25 H= 203,2 mm

η	α	$\bar{y}$	y_{sc}	β_x
0,00	0,0	101,6	101,5	0,0
0,05	10,2	106,7	115,6	23,2
0,10	20,3	111,8	124,8	36,4
0,15	30,5	116,9	130,5	41,7
0,20	40,6	122,0	133,7	41,4
0,25	50,8	127,1	135,3	37,3
0,30	61,0	132,3	135,7	30,1
0,35	71,1	137,3	135,2	20,7
0,40	81,3	142,5	133,9	9,5
0,45	91,4	147,5	132,1	-3,1
0,50	101,6	152,6	129,9	-16,9
0,55	111,8	157,8	127,3	
0,60	121,9	162,8	124,4	
0,65	132,1	167,9	121,3	
0,70	142,2	173,0	118,0	
0,75	152,4	178,1	114,4	
0,80	162,6	183,2	110,8	
0,85	172,7	188,3	107,0	
0,90	182,9	193,4	103,1	
0,95	193,0	198,5	99,1	
1,00	203,2	203,6	95,0	

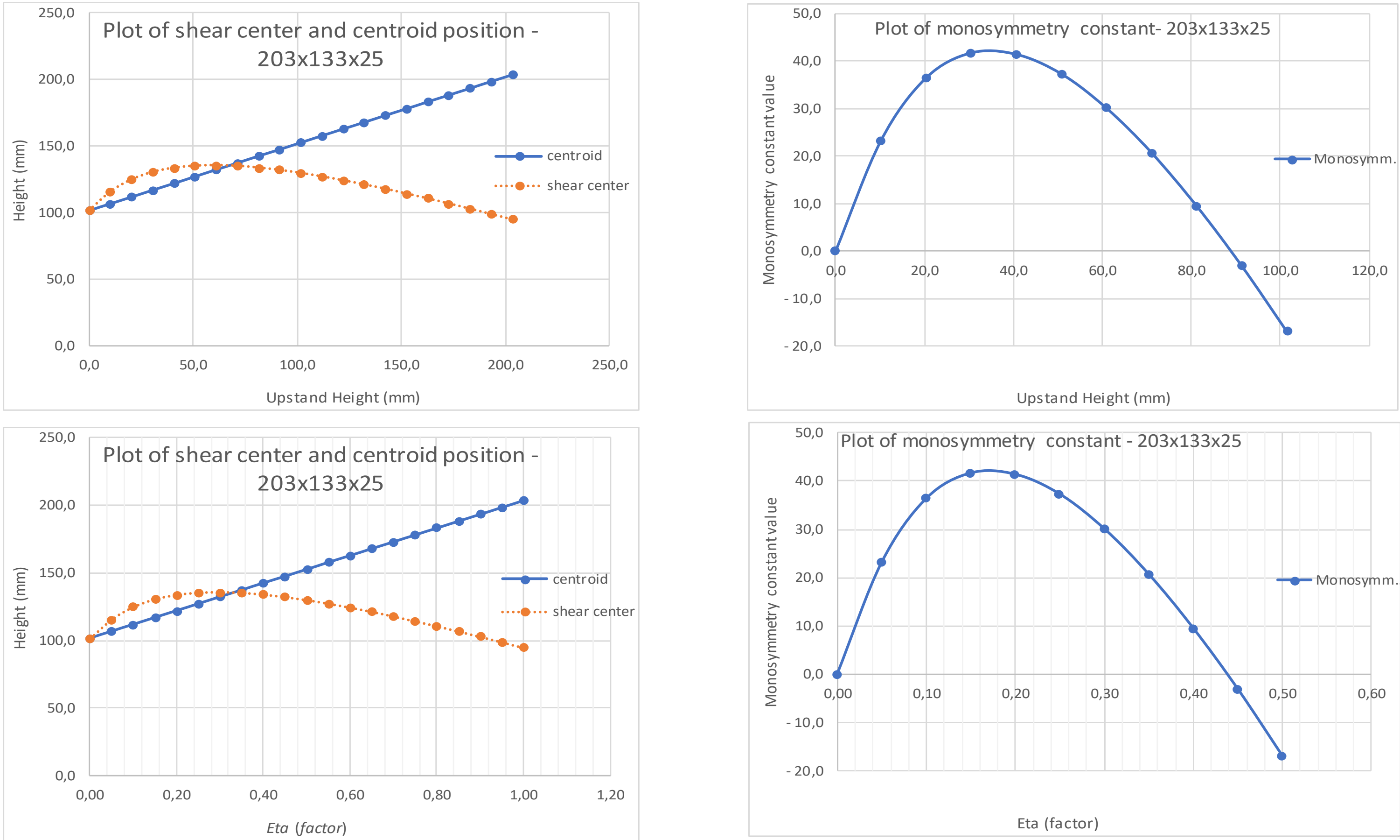

Fig.3-15 Plot of shear center and centroid movement with increasing upstand height for a NF 203x133x25 beam

Beam: NF 406x140x39 H= 397,3 mm

η	α	$\bar{y}$	y_{sc}	β_x
0,00	0,0	198,7	198,3	0,0
0,05	19,9	212,4	245,4	82,5
0,10	39,7	225,7	269,4	118,1
0,15	59,6	238,6	281,5	128,7
0,20	79,5	251,2	287,1	124,9
0,25	99,3	263,5	288,6	112,2
0,30	119,2	275,6	287,5	93,3
0,35	139,1	287,4	284,6	70,0
0,40	158,9	299,1	280,4	43,6
0,45	178,8	310,7	275,2	14,6
0,50	198,7	322,1	269,2	-16,5
0,55	218,5	333,2	262,7	-48,9
0,60	238,4	344,5	255,7	
0,65	258,2	355,6	248,4	
0,70	278,1	366,6	240,7	
0,75	298,0	377,6	232,8	
0,80	317,8	388,4	224,7	
0,85	337,7	399,2	216,3	
0,90	357,6	410,0	207,8	
0,95	377,4	420,7	199,3	
1,00	397,3	431,4	190,5	

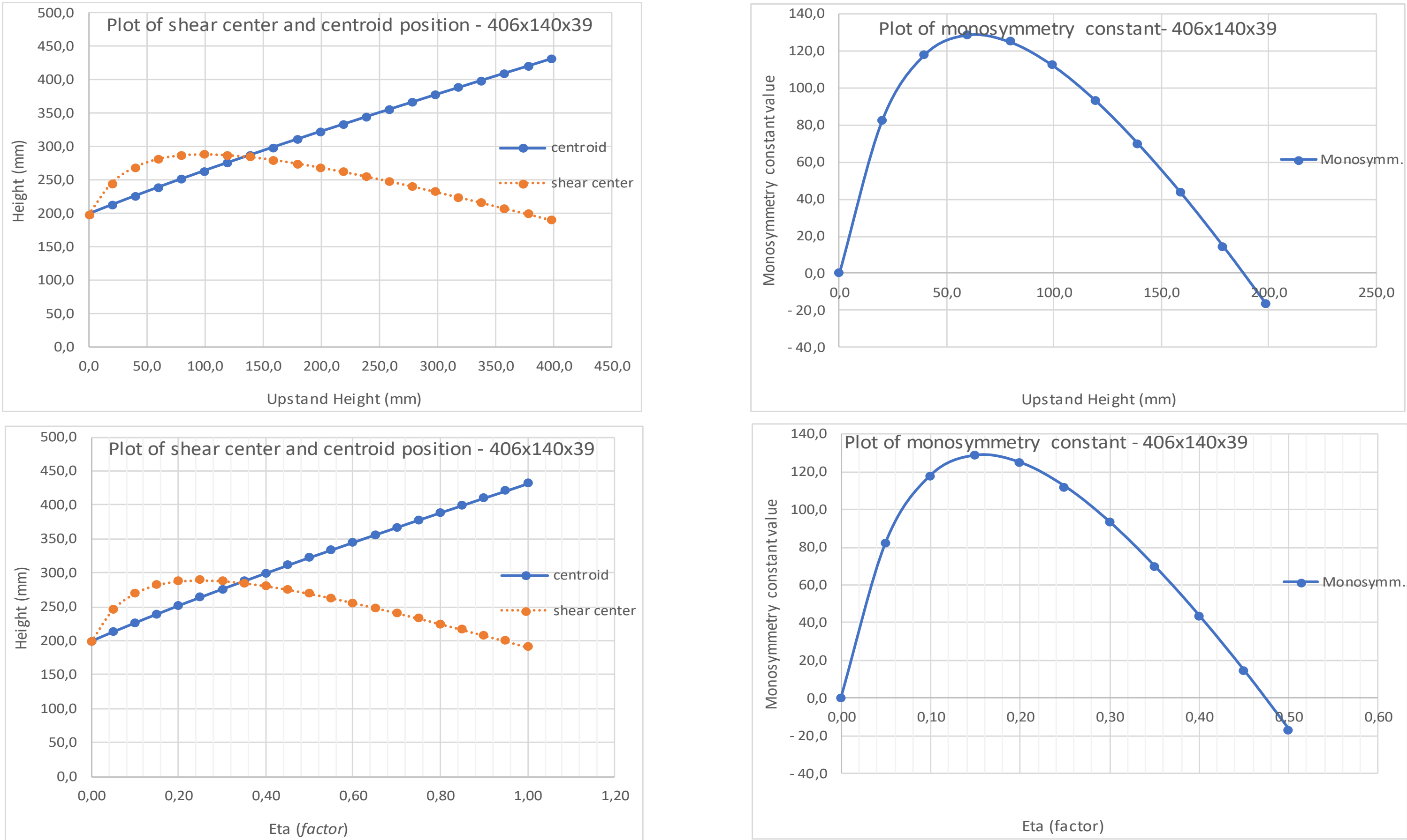

Fig.3-16 Plot of shear center and centroid movement with increasing upstand height for a NF 406x140x39 beam

Beam: NF 533x210x122 H= 544,6 mm

η	α	$\bar{y}$	y_{sc}	β_x
0,00	0,0	272,3	271,6	0,0
0,05	27,2	292,2	321,6	84,0
0,10	54,5	311,4	352,2	128,4
0,15	81,7	329,9	368,5	142,4
0,20	108,9	347,7	376,5	138,4
0,25	136,2	365,2	379,3	122,4
0,30	163,4	382,2	378,5	98,1
0,35	190,6	398,9	375,2	67,9
0,40	217,8	415,3	370,1	33,0
0,45	245,1	431,5	363,6	-5,6
0,50	272,3	447,4	356,0	-46,8
0,55	299,5	463,2	347,6	-90,4
0,60	326,8	478,8	338,5	
0,65	354,0	494,2	328,8	
0,70	381,2	509,5	318,8	
0,75	408,5	524,7	308,2	
0,80	435,7	539,8	297,5	
0,85	462,9	554,7	286,4	
0,90	490,1	569,6	275,1	
0,95	517,4	584,5	263,6	
1,00	544,6	599,2	251,9	

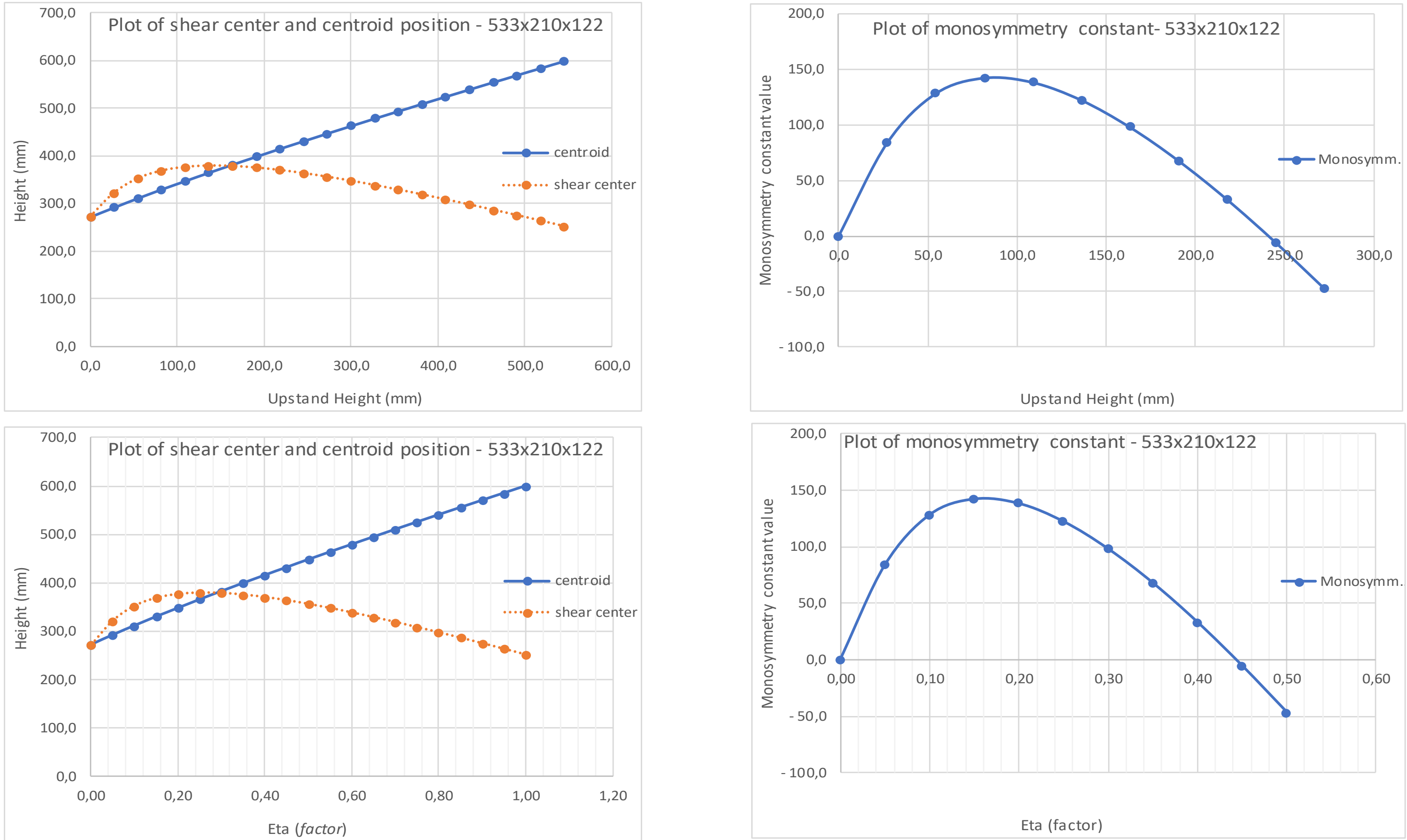

Fig.3-17 Plot of shear center and centroid movement with increasing upstand height for a NF 533x210x122 beam

Beam: WF 152x152x23 H= 152,4 mm

η	α	$\bar{y}$	y_{sc}	β_x
0,00	0,0	76,2	76,2	0,0
0,05	7,6	78,9	83,6	11,0
0,10	15,2	81,7	89,0	17,6
0,15	22,9	84,6	92,7	20,2
0,20	30,5	87,6	95,0	19,6
0,25	38,1	90,6	96,3	16,7
0,30	45,7	93,6	96,8	11,9
0,35	53,3	96,7	96,8	5,6
0,40	61,0	99,8	96,2	-2,0
0,45	68,6	103,0	95,3	-10,6
0,50	76,2	106,1	94,0	-20,1
0,55	83,8	109,4	92,5	
0,60	91,4	112,6	90,7	
0,65	99,1	115,9	88,7	
0,70	106,7	119,2	86,5	
0,75	114,3	122,5	84,2	
0,80	121,9	125,9	81,8	
0,85	129,5	129,2	79,2	
0,90	137,2	132,7	76,6	
0,95	144,8	136,1	73,8	
1,00	152,4	139,5	71,0	

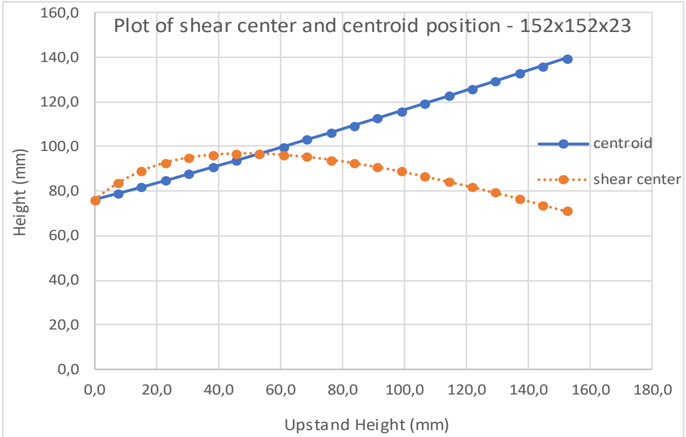

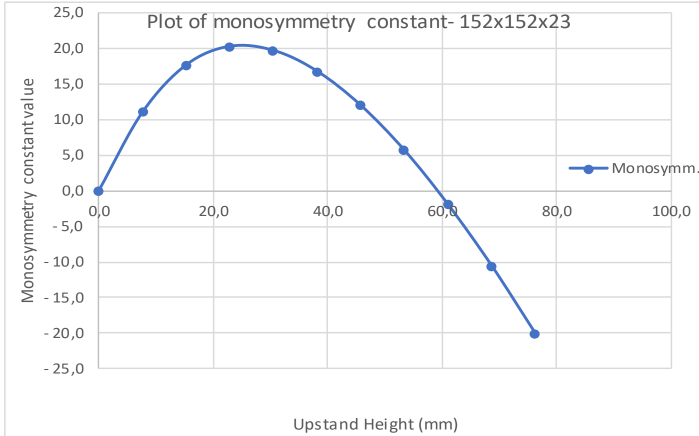

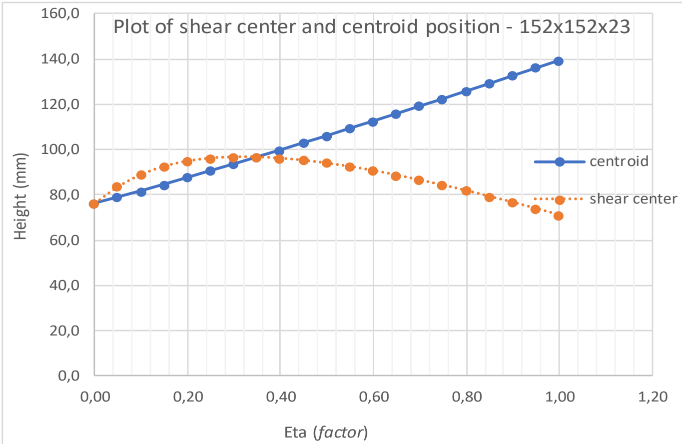

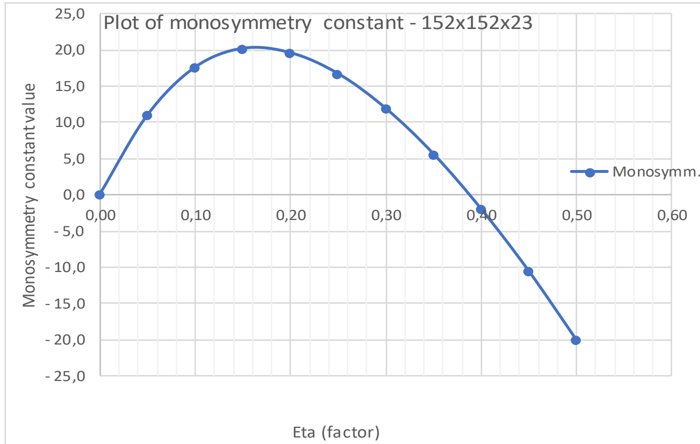

Fig.3-18 Plot of shear center and centroid movement with increasing upstand height for a WF 152x152x23 beam

Beam: WF 254x254x73 H= 254,2 mm

η	α	$\bar{y}$	y_{sc}	β_x
0,00	0,0	127,1	127,1	0,0
0,05	12,7	132,2	138,4	16,5
0,10	25,4	137,3	147,1	26,9
0,15	38,1	142,5	152,9	30,8
0,20	50,8	147,9	156,6	29,7
0,25	63,6	153,3	158,7	24,7
0,30	76,3	158,7	159,5	16,6
0,35	89,0	164,2	159,4	6,0
0,40	101,7	169,8	158,4	-6,7
0,45	114,4	175,4	156,8	-21,1
0,50	127,1	181,0	154,6	-36,8
0,55	139,8	186,7	152,0	
0,60	152,5	192,4	149,0	
0,65	165,2	198,2	145,7	
0,70	177,9	203,9	142,1	
0,75	190,7	209,8	138,3	
0,80	203,4	215,6	134,2	
0,85	216,1	221,5	129,9	
0,90	228,8	227,3	125,5	
0,95	241,5	233,3	121,0	
1,00	254,2	239,2	116,3	

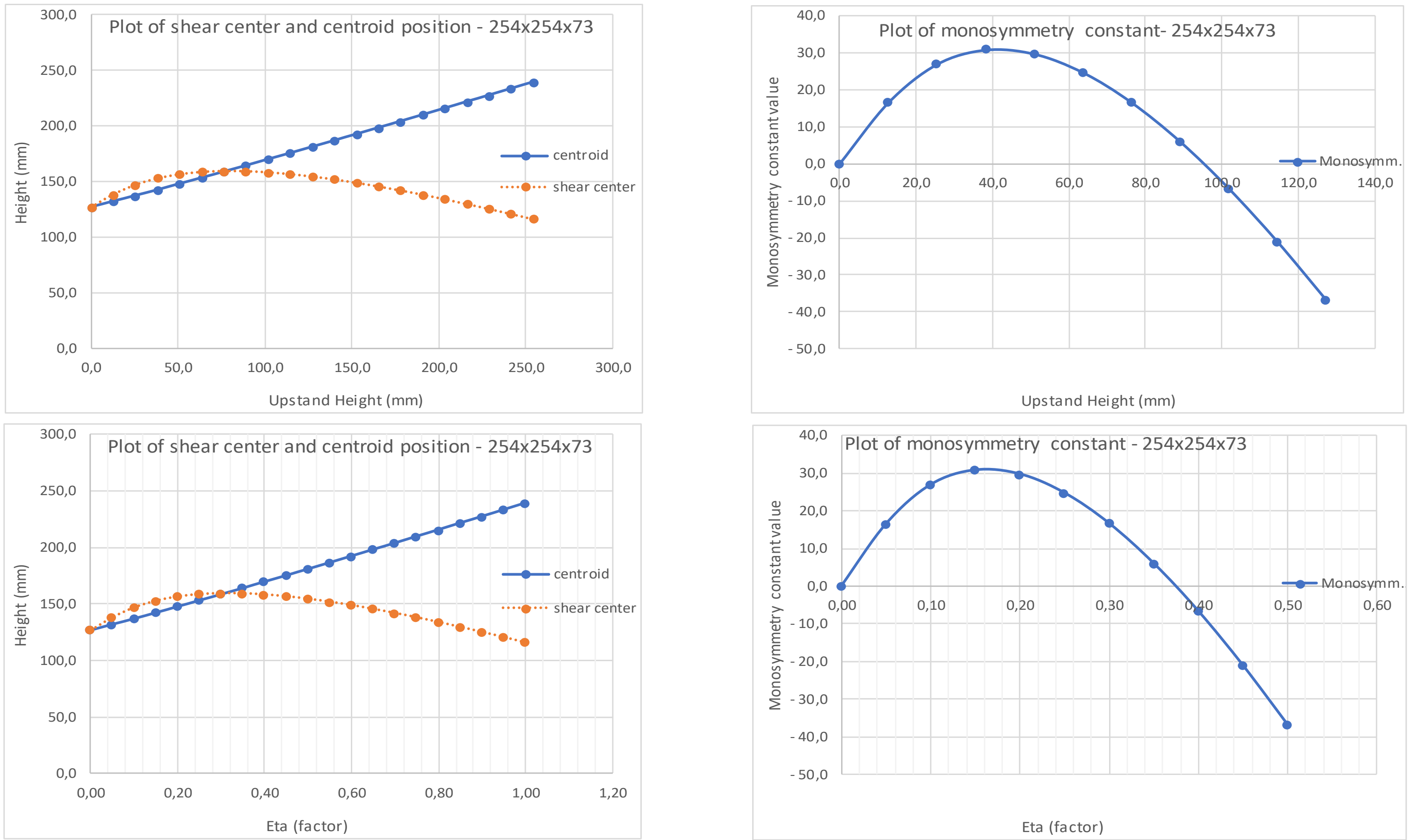

Fig.3-19 Plot of shear center and centroid movement with increasing upstand height for a WF 254x254x73 beam

Beam: WF 305x305x158 H= 327,2 mm

η	α	$\bar{y}$	y_{sc}	β_x
0,00	0,0	163,6	163,5	0,0
0,05	16,4	170,4	175,8	16,3
0,10	32,7	177,3	186,5	28,4
0,15	49,1	184,3	193,6	32,4
0,20	65,4	191,3	198,0	30,1
0,25	81,8	198,5	200,4	22,8
0,30	98,2	205,7	201,2	11,7
0,35	114,5	213,0	200,8	-2,5
0,40	130,9	220,3	199,4	-19,4
0,45	147,2	227,7	197,2	-38,4
0,50	163,6	235,1	194,3	-59,2
0,55	180,0	242,6	190,8	
0,60	196,3	250,1	186,9	
0,65	212,7	257,7	182,5	
0,70	229,0	265,2	177,8	
0,75	245,4	272,9	172,8	
0,80	261,8	280,5	167,5	
0,85	278,1	288,2	161,9	
0,90	294,5	295,9	156,2	
0,95	310,8	303,5	150,3	
1,00	327,2	311,3	144,2	

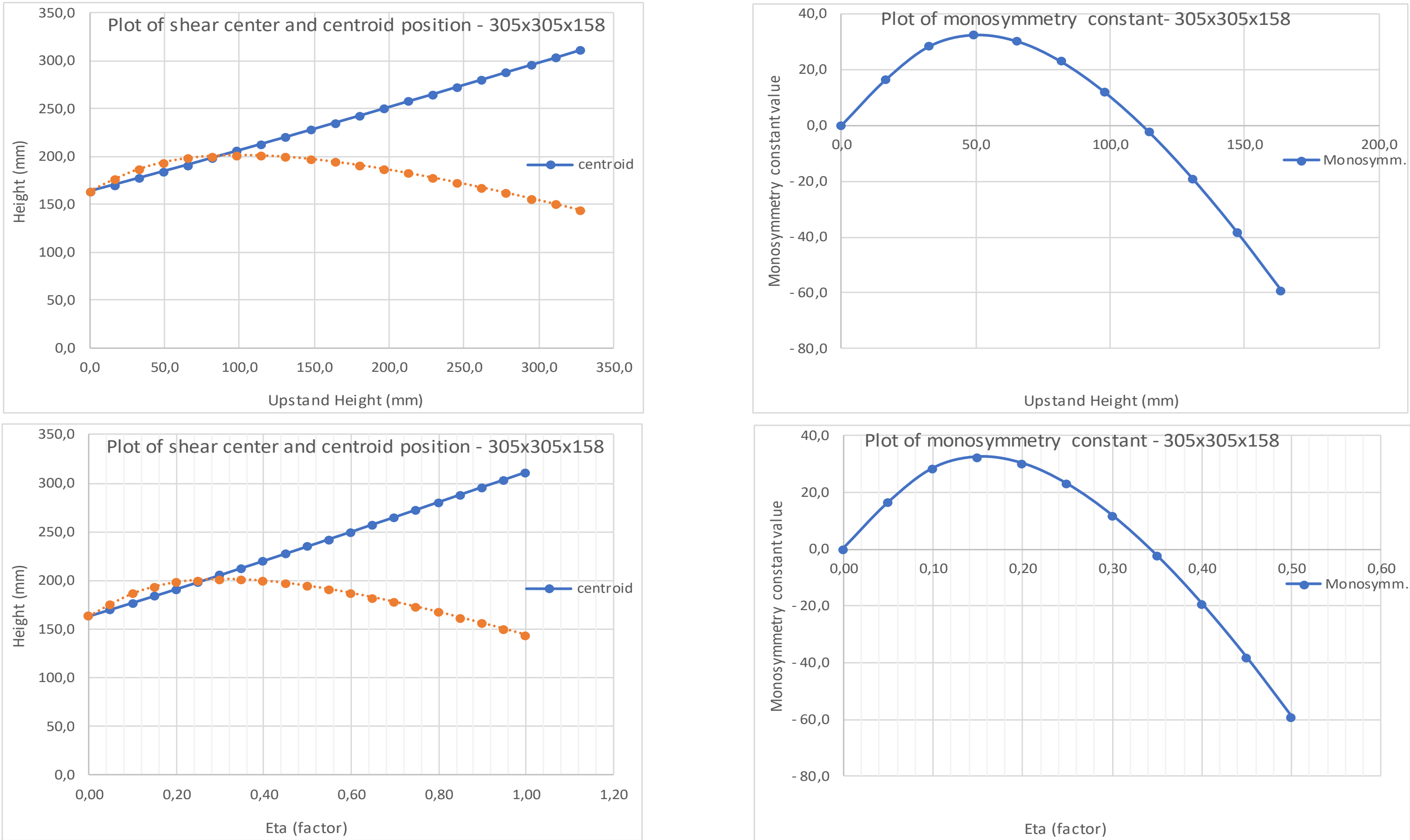

Fig.3-20 Plot of shear center and centroid movement with increasing upstand height for a WF 305x305x158 beam

The plots reveal that there exists an upstand height where the monosymmetric sections have a coincident shear center and centroid i.e., $y_{sc} = \bar{y}$; something typically only associated with bisymmetric or point symmetric cross sections. It has been stated in many texts such as Ziemian (2010) that monosymmetric sections have a shear center lying away from the centroid. However, it can now be shown that there exists monosymmetric cross sections that have a coincident shear center and centroid. Another important peculiarity of these sections is that there exist upstand heights where the value of the monosymmetry constant has a value of zero; again, another property typically associated with bisymmetric cross sections. The following conclusions can thus be drawn from the observations:

1. Monosymmetric cross sections employing top flange upstands can attain two properties typically associated with bi-symmetric cross sections; a coincident shear center and centroid, as well as a monosymmetry constant whose value is zero.

2. The upstand height at which the cross section attains a coincident shear center and centroid appears to be different from the upstand height at which the sections has a monosymmetry constant value of zero.

3. The coincidence of the shear center and the centroid occurs for the six cross sections presented lies between 'η' values of 0.25 and 0.35.

4. The maximum value of the monosymmetry constant appears for the six cross sections to occur between 'η' values of 0.1 and 0.2.

5. For the three narrow flange (NF) beams the value of 'η' where the monosymmetry constant takes on a value of zero occurs between 0.4 and 0.5.

6. For the three wide flange (WF) beams the value of 'η' where the monosymmetry constant takes on a value of zero occurs between 0.3 and 0.4.

The peculiarity observed with the shear center and centroid is illustrated in Fig.3-21. A similar peculiarity has also been illustrated for the monosymmetry constant in Fig.3-22. The effect of these observations on the critical buckling load of a beam with upstands is the subject of the studies that follow in chapter 5. Because the critical elastic moment for a monosymmetric section is dependent, among other factors, on the position of the shear center relative to the centroid, on the distance of applied load from the shear center and on the monosymmetry constant it is anticipated that these observed peculiarities will have implications on the critical elastic moment as well as the flexural strength and this merits further investigation. It is for this reason that the elastic moment behaviour and the flexural strength characteristics are investigated in the chapters that follow.

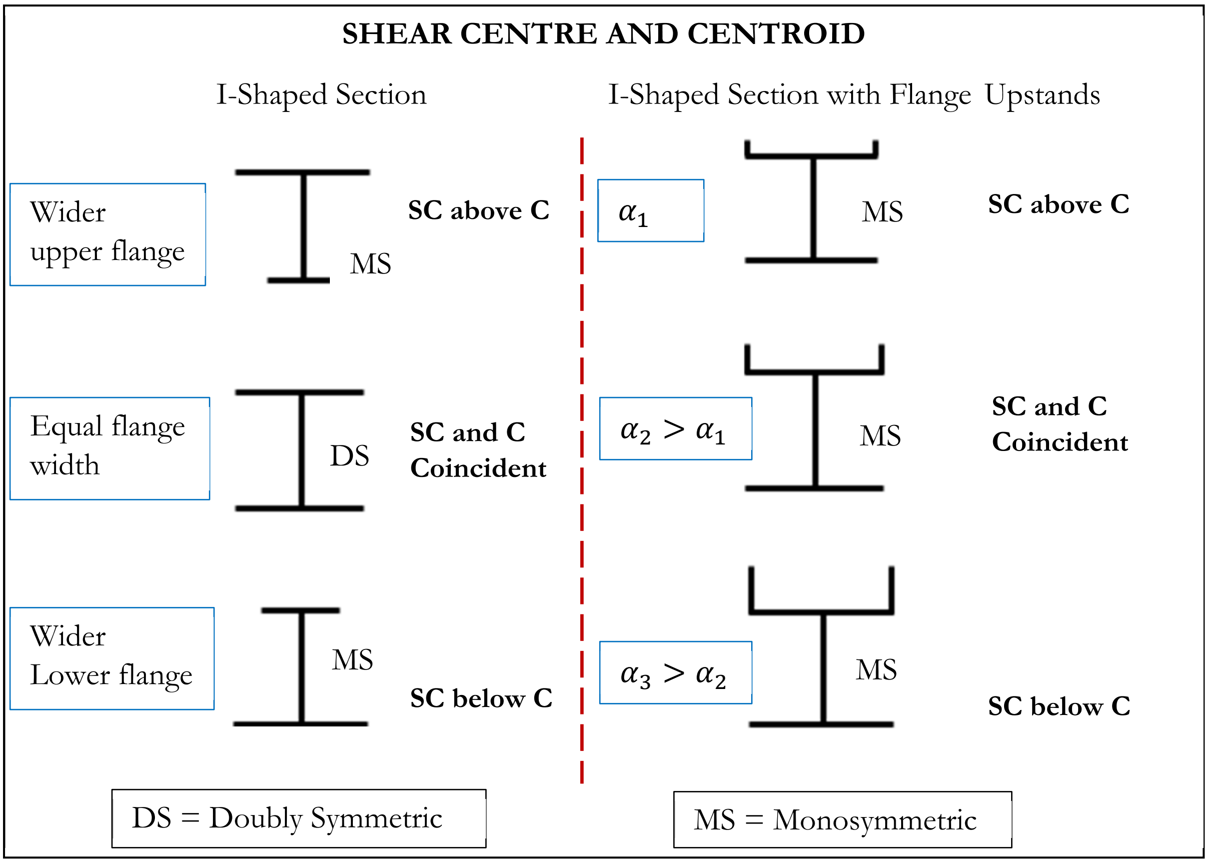

Fig.3-21 Illustration of observed behaviour of beams with upstands compared to an I-shaped section for the shear center and centroid

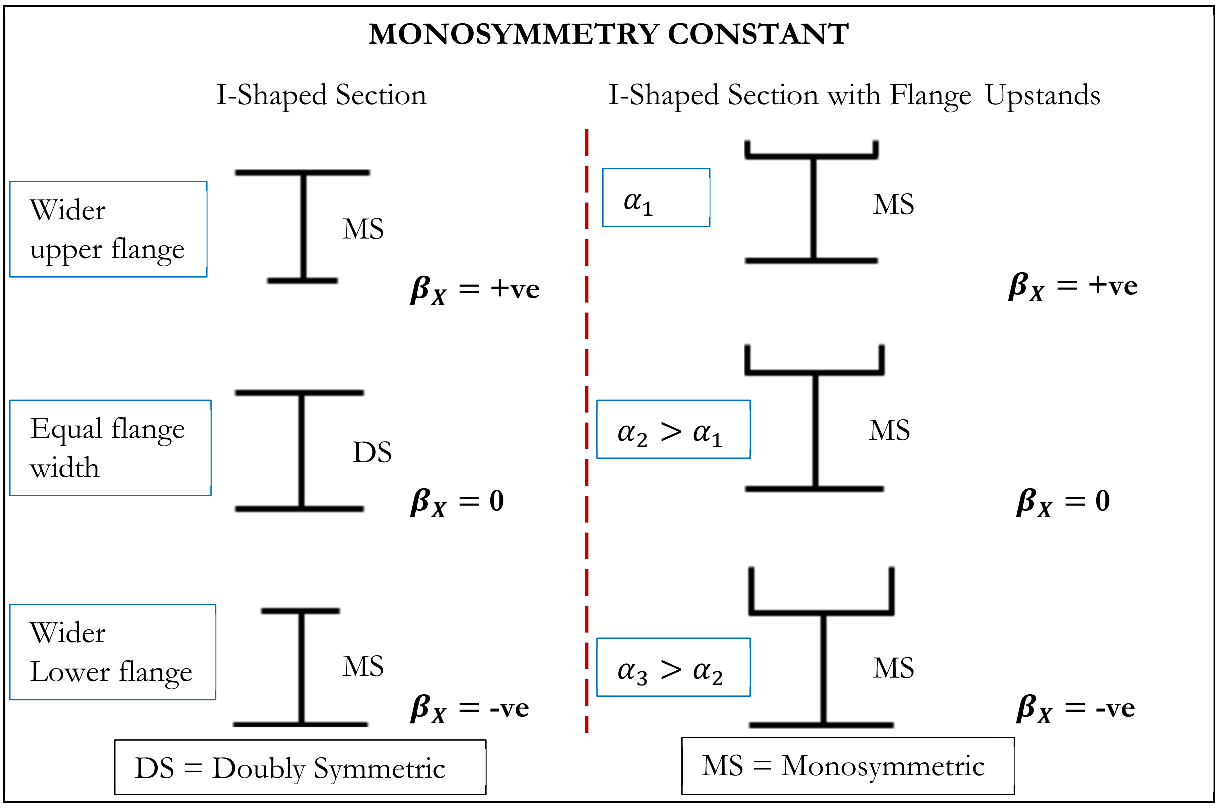

Fig.3-22 Illustration of observed behaviour of beams with upstands compared to an I-shaped section for the monosymmetry constant

Of further interest at this stage is the point of coincidence of the shear center and the centroid. This will also be denoted in the text as the SC = C point with 'SC' standing for the shear center and 'C' the centroid. A further study of this point is provided in section 3.9 which follows.

3.9 COINCIDENCE POINT (SHEAR CENTER AND CENTROID)

The coincident shear center and geometric centroid has already been shown to exist for the type of monosymmetric section investigated in this study. In order to establish the exact upstand height at which the coincidence occurs the equation for the location of the shear center must be equated to the equation for the centroid. Equations devoted to these two parameters, including their derivations, are presented from equation (3.6) to (3.29). It is desirable to have the equations in a compact form when they are equated. The simplified form is given in equations (3.47) and (3.48) for the centroid and shear center position respectively. As in previous cases the base of the section is the reference point for the distances. In this form once the numerical values are obtained from the geometrical parameters it becomes easy to obtain the upstand height, α, from the resulting high order polynomial obtained. A spreadsheet package can also be used to solve for the desired upstand height.

$$\bar{y} = \frac{2\alpha^2 t_\alpha + 4H\alpha t_\alpha + \gamma_1}{4\alpha t_\alpha + \gamma_2} \tag{3.47}$$

$$y_{sc} = \frac{\alpha(2x_1 + t_1 x_4) - \alpha^2 2x_2 + (2x_3 + t_1 x_5)}{\alpha 2x_4 + 2x_5} \tag{3.48}$$

where,

$$\gamma_1 = 2Bt_1H - Bt_1^2 + 2t_w h_w t_2 + h_w^2 t_w + bt_2^2 \tag{3.49}$$

$$\gamma_2 = 2Bt_1 + 2h_w t_w + 2bt_2 \tag{3.50}$$

$$x_1 = \frac{b_1^2 t_\alpha h}{2} - \frac{t_1 t_\alpha b_1^2}{4} \tag{3.51}$$

$$x_2 = \frac{b_1^2 t_\alpha}{4} \tag{3.52}$$

$$x_3 = \frac{b_1^2 t_\alpha t_1 h}{4} - \frac{b_1^2 t_1^2 t_\alpha}{16} + \frac{b_1^3 t_1 h}{12} \tag{3.53}$$

$$x_4 = \frac{t_\alpha^3}{6} + 2t_\alpha \left[\frac{B}{2} - \frac{t_\alpha}{2}\right]^2 \tag{3.54}$$

$$x_5 = \frac{t_1 B^3}{12} + \frac{t_2 b^3}{12} + \frac{h_w t_w^3}{12} \tag{3.55}$$

The values from equations (3.49) to (3.55) are used to determine the numerical values to be used in the two equations, (3.47) and (3.48), leaving only the upstand height, α, at coincidence as the unknown variable to be determined.

Given the two equations (3.47) and (3.48) a spreadsheet software such as Microsoft Excel© can be used to find the required value of the upstand height by way of a 'goal seek' function whereby the 'goal' required is the value of, α, the upstand height such that the numerical value for equation (3.47) exactly matches the numerical value for (3.48). This is an alternative to solving the resulting third-degree polynomial obtained from equating the two equations. The nature of the polynomial obtained from equating the two equations also makes it difficult to formulate a general equation for the value of 'α' sought. The values in Table 3-22 have been obtained using a spreadsheet with selected values verified by solving the polynomial that is generated from equating equations (3.47) and (3.48).

The values for the upstand height at which the shear center and centroid are coincident have been determined for all the sections in the South African steel design handbook (SASCH, 2016). These are presented in Table 3-22a for narrow flange beams and Table 3-22b for wide flange beams. It is seen from the results presented in the tables that the mean value of the ratio of upstand height to section height (eta) is 0.31, with a coefficient of variation (CoV) of 0.055 and a standard deviation of 0.017 for the Narrow Flange members (NF) or universal beams. The mean value of the ratio of upstand height to section height (eta) is 0.28, with a coefficient of variation (CoV) of 0.149 and a standard deviation of 0.042 for the Wide Flange members (WF) or universal columns. The variability is thus observed to be higher for the wide flange sections. These mean values reflect the range seen in the previous examples for the six members considered in section 3.8.

Table 3-22a Coincidence point of shear center and centroid for monosymmetric sections based on members in the South African steel handbook (SASCH, 2016) – Narrow Flange members

	Designation	**H**	$\alpha/_{H}$
	mm x mm x kg/m	mm	
1	IPE-AA 100	97,6	0,32
2	IPE 100	100,0	0,28
3	IPE-AA 120	117,0	0,32
4	IPE 120	120,0	0,29
5	IPE-AA 140	136,6	0,32
6	IPE 140	140,0	0,29
7	IPE-AA 160	156,4	0,32
8	IPE 160	160,0	0,30
9	IPE-AA 180	176,4	0,32
10	IPE 180	180,0	0,30
11	IPE-AA 200	196,4	0,32
12	IPE 200	200,0	0,30
13	203x133x25	203,2	0,33
14	203x133x30	206,8	0,31
15	254x146x31	251,5	0,33
16	254x146x37	256,0	0,30
17	254x146x43	259,6	0,29
18	305x102x25	304,8	0,35
19	305x102x28	308,9	0,32
20	305x102x33	312,7	0,29
21	305x165x40	303,8	0,32
22	305x165x46	307,1	0,30
23	305x165x54	310,9	0,29
24	356x171x45	352,0	0,34
25	356x171x51	355,6	0,32
26	356x171x57	358,6	0,31
27	356x171x67	364,0	0,29
28	406x140x39	397,3	0,34
29	406x140x46	402,3	0,31
30	406x178x54	402,6	0,34
31	406x178x60	406,4	0,31
32	406x178x67	409,4	0,31
33	406x178x74	412,8	0,30

Table 3-22a CTD'

	Designation	H	$^{\alpha}/_{H}$
34	457x191x67	453,6	0,33
35	457x191x74	457,2	0,31
36	457x191x82	460,2	0,31
37	457x191x89	463,6	0,30
38	457x191x98	467,6	0,28
39	533x210x82	528,3	0,34
40	533x210x92	533,1	0,32
41	533x210x101	536,7	0,31
42	533x210x109	539,5	0,30
43	533x210x122	544,6	0,29
		Mean	**0,31**
		St.Dev	**0,017**
		CoV	**0,055**

Table 3-22b Coincidence point of shear center and centroid for monosymmetric sections based on members in the South African steel handbook (SASCH, 2016) – Wide Flange members

	Designation	H	$^{\alpha}/_{H}$
	mm x mm x kg/m	mm	
1	152x152x23	152,4	0,35
2	152x152x30	157,5	0,31
3	152x152x37	161,8	0,28
4	203x203x46	203,2	0,31
5	203x203x52	206,2	0,30
6	203x203x60	209,6	0,29
7	203x203x71	215,9	0,25
8	203x203x86	222,3	0,23
9	254x254x73	254,2	0,31
10	254x254x89	260,4	0,29
11	254x254x107	266,7	0,27
12	254x254x132	276,4	0,23
13	254x254x167	289,1	0,17
14	305x305x97	307,8	0,32
15	305x305x118	314,5	0,30
16	305x305x137	320,5	0,29
17	305x305x158	327,2	0,27
		Mean	**0,28**
		St.Dev	**0,042**
		CoV	**0,149**

The values for the upstand height at which the shear center and centroid are coincident have also been determined for selected sections found in a United States historical Steel database of section (USS, 1946). These are presented in Table 3-23.

Table 3-23a Coincidence point of shear center and centroid for monosymmetric sections based on members in the US database (USS, 1946) – Selected narrow flange beams

SUMMARY OF NARROW FLANGE (NF) - CB SECTIONS (USS SECTIONS)

	Designation	H	α	α/H
1	NF-14 x 12-78	351,7	108,05	0,31
2	NF-14 x 10 - 61	353,3	108,38	0,31
3	NF-14 x 8 - 43	347,5	107,71	0,31
4	NF-14 x 6.75 - 30	352	118,51	0,34
5	NF-12 x 12 - 65	307,8	98,84	0,32
6	NF-12 x 10 - 53	306,3	95,64	0,31
7	NF-12 x 8 - 40	303,3	93,00	0,31
8	NF-12 x 6.5	303,8	96,64	0,32
			Mean	**0,31**
			ST.DEV	**0,010**
			CoV	**0,033**

Table 3-23b Coincidence point of shear center and centroid for monosymmetric sections based on members in the US database (USS, 1946) – Selected wide flange beams

SUMMARY OF WIDE FLANGE (H-BEAM) - SECTIONS (USS SECTIONS)

	Designation	H	α	$^{\alpha}/_{H}$
1	H4 - 8x8	203,2	65,46	0,32
2	H3a - 6x6	152,4	40,06	0,26
3	H3 - 6x6	152,4	45,38	0,30
4	H2 - 5x5	127,0	33,55	0,26
5	H1 - 4x4	101,6	23,84	0,23
			Mean	**0,28**
			ST.DEV	**0,034**
			CoV	**0,123**

It is seen from the results presented in the tables that the mean value of the ratio of upstand height to section height (eta) for eight (8) narrow flange beam sections is 0.31, with a coefficient of variation (CoV) of 0.033 and a sample standard deviation of 0.010. This is similar to the figures obtained from the South African database. The mean value of the ratio of upstand height to section height (eta) for five (5) H-Beams or wide flange sections is 0.28, with a coefficient of variation (CoV) of 0.149 and a sample standard deviation of 0.042. This is also similar to figures obtained from the South African sections although only a sample of the database has been considered here.

The values for the upstand height at which the shear center and centroid are coincident have also been further determined for sections found in the database of United Kingdom beams (narrow flange sections) presented as UKB as well as United Kingdom columns presented as UKC which are wide flange sections (SCI, 2015). Because some of the sections have the exact same properties as the SASCH (2016) sections only the ones not already covered by Table 3-22 from (SASCH, 2016) are presented here. This means that the (SASCH, 2016) sections are a subset of the entire UK database. The results for the UK sections are presented in Table 3-24.

Table 3-24a Coincidence point of shear center and centroid for monosymmetric sections based on members in the UK database (SCI, 2015) – Selected narrow flange beams

UK - NARROW FLANGE (NF-UKB) SECTIONS

S/N	Designation	mass/m	H	α	α/H
1	1016 x 305	487	1 036,30	234,00	0,23
2		437	1 026,10	247,00	0,24
3		393	1 015,90	260,40	0,26
4		349	1 008,10	264,70	0,26
5		314	999,90	273,40	0,27
6		272	990,10	282,60	0,29
7		249	980,10	305,80	0,31
8		222	970,30	329,30	0,34
9	914 x 419	388	921,00	271,80	0,30
10		343	911,80	280,00	0,31
11	914 x 305	289	926,60	272,20	0,29
12		253	918,40	280,00	0,30
13		224	910,40	291,60	0,32
14		201	903,00	306,40	0,34
15	838 x 292	227	850,90	256,50	0,30
16		194	840,70	272,70	0,32
17		176	834,90	283,80	0,34
18	762 x 267	197	769,80	231,20	0,30
19		173	762,20	241,80	0,32
20		147	754,00	254,20	0,34
21		134	750,00	260,70	0,35
22	686 x 254	170	692,90	207,90	0,30
23		152	687,50	213,40	0,31
24		140	683,50	218,40	0,32
25		125	677,90	228,10	0,34
26	610 x 305	238	635,80	176,70	0,28
27		179	620,20	188,80	0,30
28		149	612,40	193,80	0,32
29	610 x 229	140	617,20	181,70	0,29
30		125	612,20	186,60	0,30
31		113	607,60	192,70	0,32
32		101	602,60	201,30	0,33

Table 3-24a CTD'

S/N	Designation	mass/m	H	α	$^{\alpha}/_{H}$
33	610 x 178	100	607,40	188,10	0,31
34		92	603,00	197,30	0,33
35		82	598,60	204,70	0,34
36	533 x 312	273	577,10	141,70	0,25
37		219	560,30	159,90	0,29
38		182	550,70	166,30	0,30
39		151	542,50	171,50	0,32
40	533 x 165	85	534,90	161,20	0,30
41		75	529,10	172,20	0,33
42		66	524,70	179,90	0,34
43	457 x 191	161	492,00	106,00	0,22
44		133	480,60	120,70	0,25
45		106	469,20	133,10	0,28
46	457 x 152	82	465,80	126,40	0,27
47		74	462,00	130,40	0,28
48		67	458,00	136,10	0,30
49		60	454,60	139,30	0,31
50		52	449,80	148,10	0,33
51	406 x 178	85	417,20	119,20	0,29
52	406 x 140	53	406,60	123,40	0,30
53	305 x 127	48	311,00	88,20	0,28
54		42	307,20	91,95	0,30
55		37	304,40	84,10	0,28
56	254 x 102	28	260,40	77,10	0,30
57		25	257,20	82,30	0,32
58		22	254,00	88,10	0,35
59	203 x 102	23	203,20	58,30	0,29
60	178 x 102	19	177,80	53,30	0,30
61	152 x 89	16	152,40	43,50	0,29
62	127 x 76	13	127,00	33,00	0,26
				Mean	**0,30**
				St. Dev	**0,030**
				CoV	**0,098**

It is seen from the results presented in the tables that the mean value of the ratio of upstand height to section height (eta) for sixty-two (62) narrow flange beam sections is 0.30, with a coefficient of variation (CoV) of 0.098 and a sample standard deviation of 0.030. This mean value is slightly lower than the mean obtained from the South African database.

Table 3-24b Coincidence point of shear center and centroid for monosymmetric sections based on members in the UK database (SCI, 2015) – Selected wide flange beams

UK - WIDE FLANGE (WF-UKC) SECTIONS

S/N	Designation	mass/m	H	α	$^{\alpha}/_{H}$
1	152x152	51	170,20	39,75	0,23
2		44	166,00	43,03	0,26
3	203x203	114	235,00	34,84	0,15
4		100	228,60	44,25	0,19
5	305x305	240	352,50	63,51	0,18
6		198	339,90	76,66	0,23
7	356x368	202	374,60	103,88	0,28
8		177	368,20	107,57	0,29
9		153	362,00	110,72	0,31
10		129	355,60	114,08	0,32
11	356x406	393	419,00	63,32	0,15
12		340	406,40	80,21	0,20
13		287	393,60	91,95	0,23
14		235	381,00	100,84	0,26
				Mean	**0,23**
				St. Dev	**0,055**
				CoV	**0,236**

The mean value of the ratio of upstand height to section height (eta) for five (14) wide flange sections is 0.23, with a coefficient of variation (CoV) of 0.240 and a sample standard deviation of 0.056. This mean value is also lower than was obtained from the South African sections database. As with the South African sections the variation for the wide flange beams is higher than that for the narrow flange beams.

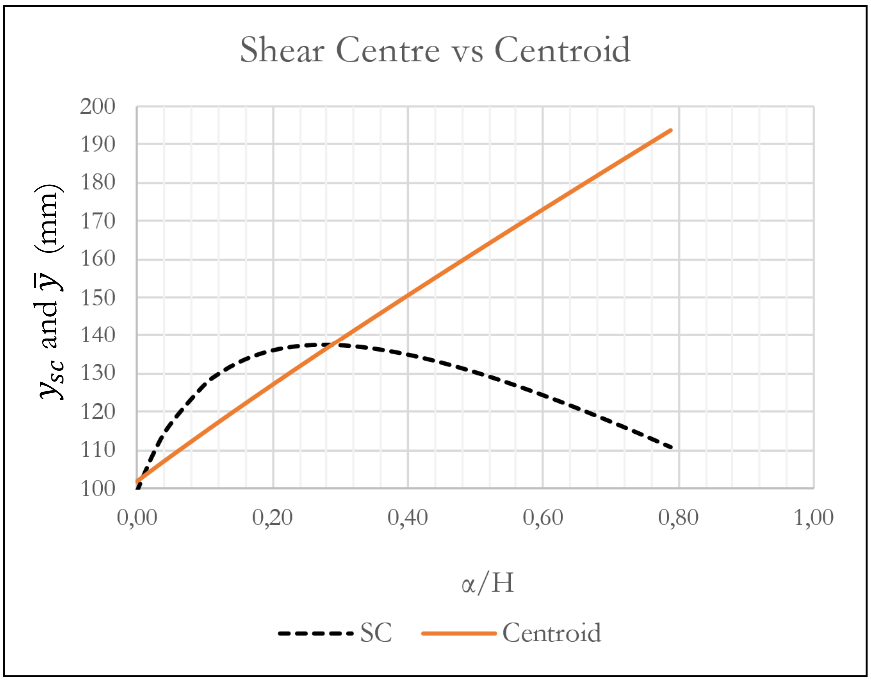

Fig.3-23 Shear center vs centroid plot for a UK-NF section (203x102x23)

A plot for a UK-NF section is shown in Fig.3-23 consistent with observations from plots in section 3.8 and results presented in Table 3-24(a).

A statistical analysis based on a two-tail hypothesis test indicates that for all cases considered for the observed behaviour of the coincidence point, and based on the tables presented the following conclusions can be made with a 95% level of confidence:

1. For **narrow flange** beams the coincidence point occurs in the range of an upstand height of **a third** of the member height for the standard sections in the sources considered. This gives a good starting point for determining the coincidence point. Investigations in the following chapters will establish whether there is correlation of this point to the optimum critical elastic moment. A value of 0.305 for 'η' was obtained as an acceptable mean value for the coincidence point.
2. For **wide flange** beams the coincidence point is in the range of upstand height of **a quarter** of the member height. This gives a good starting point for determining the coincidence point and for determining the optimum stiffener height should it be determined that the critical moment is correlated to this. A value of 0.26 for 'η' was obtained as an acceptable mean value for the coincidence point. However, due to high variability for these sections, as shown by a higher coefficient of variation than for narrow flange sections, it is proposed that a range be used when determining the optimum stiffener height. A range of 'η' from 0.15 to 0.30 is proposed.

3.10 CONCLUSION

In this chapter the general equations for obtaining relevant section properties for I-shaped sections with top flange upstands have been derived, verified and applied to obtain values. These values have been used to observe trends as the upstand height is varied and have revealed some peculiarities with the cross section. These peculiarities in particular have to do with the movement of the shear center relative to the centroid as well as the change in the value of the monosymmetry constant. These monosymmetric members also exhibit the peculiarity of taking on properties of doubly symmetric sections such as a coincident shear center and centroid and a monosymmetry constant whose value is zero. These peculiarities have been consistently observed both for narrow flange (NF) as well as for wide flange (WF) sections. A non-dimensional parameter '*eta*' (η) has been used to identify the broad ranges of upstand height in which the observed peculiarity of coincidence of shear center and centroid generally fall. The effect of this on the critical buckling load as well as beam strength will be investigated in the sections that follow. There is an indication that the peculiarities observed could point to a situation where application of upstands on a beam of this nature, to increase strength, becomes an optimization problem. Higher upstand heights may only offer advantages within a limited range. This will be investigated and established in the sections that follow.

CHAPTER 4 FORMULATION FOR THE ELASTIC BUCKLING PROBLEM

4.1 INTRODUCTION

Buckling is a form of instability that members under compressive stress are particularly susceptible to. The design of structures is typically based on material strength and member stiffness requirements. However, a structure may become unstable before strength and stiffness requirements are violated. Buckling instability, as a failure mode, needs to be considered as it may govern for slender and lightweight members. In the study of the buckling phenomenon two general modes of failure are identified; one is the bifurcation buckling type of failure and the other is a limit load type of failure. Lateral-torsional buckling of the beams considered in the current study are prone to failure by the former (i.e. bifurcation buckling) and thus solution methods adopted are based on this failure mode and this must be borne even though not specifically stated going forward. Limit load buckling is unique to specific structures such as shallow arches and certain types of shell structures and is not considered further. Bifurcation buckling is associated with the concept of equilibrium paths. As the load on a member is increased the displacement proceeds in a configuration consistent with the applied loading and thus consisting of a stable equilibrium path until a critical value is reached. Once the critical load value is reached the displacement changes into a different configuration, and thus follows a new path. A bifurcation of equilibrium is said to have taken place. In beams and columns, the load associated with this bifurcation point, simply referred to as the critical buckling load, is an upper-bound of elastic load capacity. In small displacement theory, once the critical load is attained displacement in the new configuration will continue without any increase in the applied load. This represents transition to an unstable equilibrium configuration and is an undesirable condition for a loaded member. This therefore also becomes a point of interest. An illustration of bifurcation buckling for a column is illustrated in Fig.4-1. Initially the column experiences a displacement in the load direction (δL). Once the critical load is attained the displacement changes to a lateral displacement (in a different direction from 'δL') accompanied by bending rotation θ. A plot of the applied load to the bending rotation is shown in Fig.4-2.

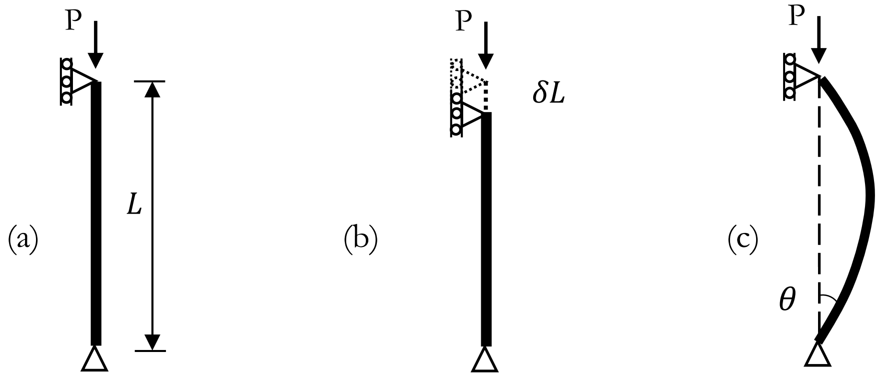

Fig.4-1 Column deformations prior to [(a), (b)] and after bifurcation [(c)]

The stable part of Fig4-2 corresponds to (a) and (b) in the illustration of Fig.4-1. In this configuration the displacement is in the direction of load application. Once the bifurcation point is reached the nature of the displacement changes. This is illustrated in Fig.4-1 (c) were the column, initially deforming along its axis, now bends and displaces in a direction perpendicular to the initial deformation direction.

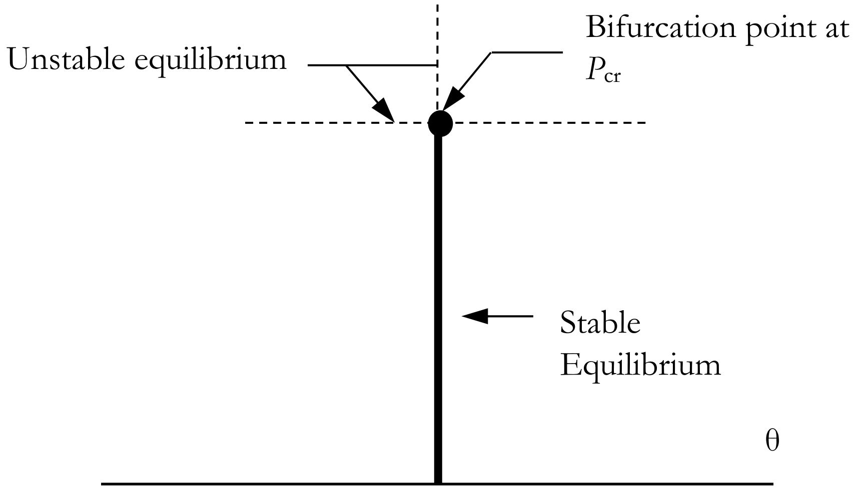

Fig.4-2 Illustration of equilibrium path of load with respect to member rotation (Galambos and Surovek, 2008)

The bifurcation point is also associated with a loss of stiffness since the deformation in the new direction continues to increase at a constant load. This property of the bifurcation point also aids in the theoretical formulation for the buckling load. Another important property of the bifurcation point is given in the paragraph that follows.

To determine the critical buckling load, the concept of equilibrium states is of particular importance. This relates to how the buckling problem is formulated for determination of critical loads. A rolling ball analogy is used to describe three types of equilibrium.

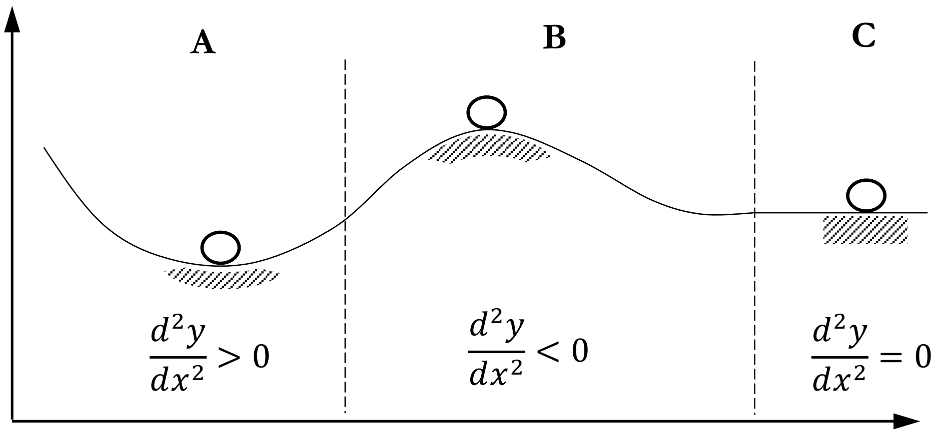

Fig.4-3 Analogy of equilibrium states relating to critical buckling

Some properties associated with the surface that the ball rests on are used in equilibrium computations; the nature of the change of slope is used to determine whether the equilibrium is stable or unstable. Illustrated in Fig.4-3 are the different types of equilibrium states with accompanying analytical interpretations.

Derivatives of functions indicate stationery points when they are equal to zero. The second derivative then gives an indication of the nature of the function on either side of the stationery point. The ball shown in Fig.4-3 (A) when disturbed will return to its original position after the disturbance is removed. This is analogous to stable equilibrium. For Fig.4-3 (B) once the ball is displaced from its original position it continues to move away from this position and does not return. This is analogous to unstable equilibrium. For case Fig.4-3 (C) the ball once disturbed neither moves further away nor returns to its original position when the disturbance is removed and is analogous to neutral equilibrium. In buckling studies, it is of interest to find the critical load when the equilibrium state changes from one of stable equilibrium to one of unstable equilibrium; that point is considered a point of instability failure. As indicated, these points where equilibrium states change are also known as bifurcation points. The state of neutral equilibrium is particularly important because it allows the formulation of buckling problem equations based on a 'slightly deformed' configuration of the member because at neutral equilibrium a slight displacement does not lead to the member moving away. Writing the equations in the slightly deformed configuration allows for the formulation of the eigenvalue problem necessary for solution of the buckling problem.

Two theories are employed in determining the elastic buckling behaviour of structural members: small displacement theory as well as large displacement theory. Small displacement theory is useful for determining the critical buckling load but does not necessary reveal the full nature of behaviour once buckling has occurred. Large displacement theory is used to not only indicate the buckling load but also to reveal elastic behaviour beyond the critical load point or beyond the bifurcation point (post-buckling behaviour). In small displacement theory the expression used for d^2x/dy^2 in the member curvature expression is approximate, with nonlinear terms in the differential equation expression neglected. For large displacement analysis the exact expression for curvature is utilised. Members that may have stable post-buckling behaviour, i.e. accompanied by stiffness gain, can be identified using this type of analysis. This behaviour type is shown in Fig.4-4 (a). Some other members can only maintain a stable post-buckling configuration with reduction in applied load. These members are said to have an unstable post-buckling behaviour and are depicted in Fig.4-4 (b). Beams, columns and frames largely exhibit a very shallow stable post-buckling behaviour which in the elastic range can be approximated by a horizontal line similar to that predicted from bifurcation theory. The member can still therefore be considered unstable since it will fail from combined stresses of the loads acting in the deformed state causing the member to reach its material failure strength before any increase in load capacity is achieved.

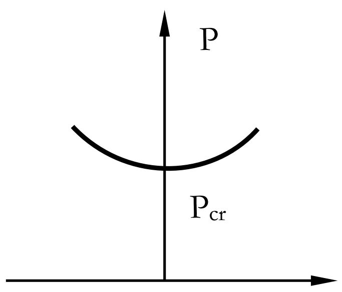

Fig.4-4 Bifurcation models of symmetric buckling from large displacement analysis showing (a) stable post-buckling and (b) unstable post-buckling (Ziemian, 2010)

It is important to note that one of the assumptions made in determining the critical load is that the member is initially straight. This assumption, although theoretically providing useful results, does not reflect reality. In reality members have imperfections and these have an impact on the load displacement behaviour. The presence of 'out-of-straightness' for instance results in the member starting to deform in a direction perpendicular to the applied load right from the onset of load application. This results in a slightly different load path for all possible post-buckling cases as shown in Fig.4-5.

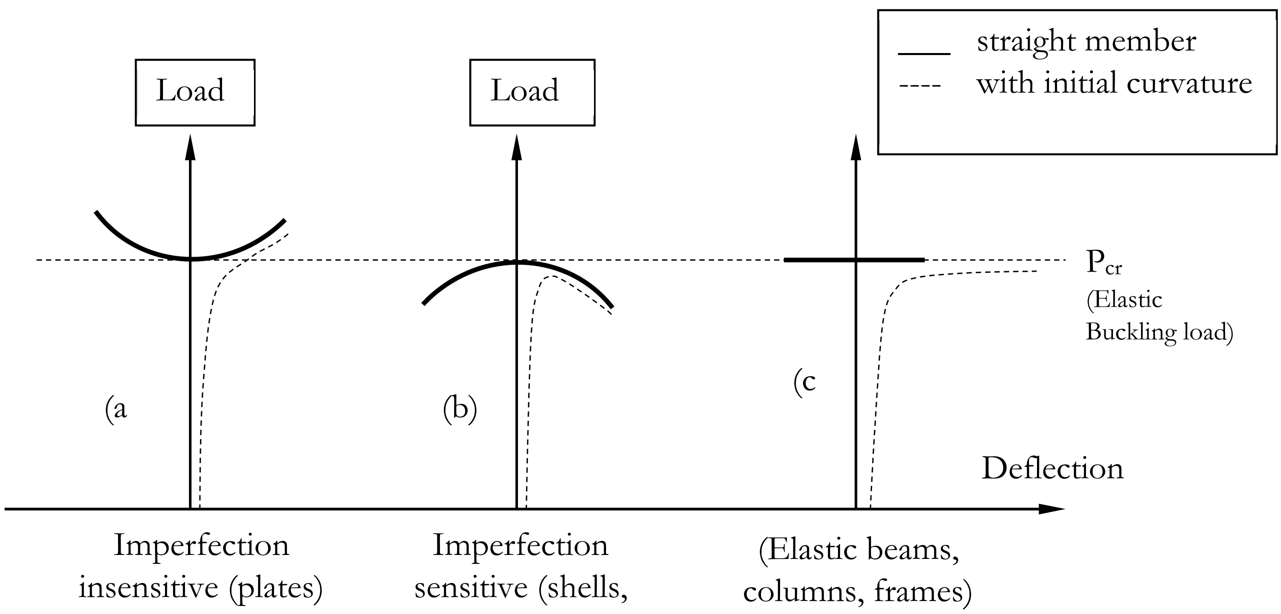

Fig.4-5 Illustration of load displacement curves for members with imperfections

The inelastic behaviour of the beams considered in the current study, which incorporates imperfections, will form part of the work in later chapters in determining the true strength of real beams.

A summary of important points with regards buckling instability and the critical loads is provided by Galambos and Surovek (2008) and listed here:

- Instability occurs when a small change in load causes a large change in displacement
- The critical load, or buckling load, is the load at which the system passes from a stable to an unstable state
- The critical load is obtained by considering equilibrium or potential energy of the system in a deformed configuration
- Small displacement theory may be used to simplify the calculations if only the critical load is of interest.

The following additional points are given:

- Three methods of stability evaluation are typically considered:
  i. The small deflection method, giving only the buckling load
  ii. The large displacement method for the perfect system, giving information about post-buckling behaviour
  iii. The large displacement method for the imperfect system, giving the complete deformation history, including the reduction of stiffness in the vicinity of the critical load

- Two methods of solution are used
  i. Static equilibrium methods, and
  ii. Energy methods

In the current study bifurcation buckling is first considered, based on small deflection theory, to obtain the elastic critical loads. In subsequent chapters large displacement of the imperfect system (nonlinear analysis) is then applied to obtain the actual strength of the beams.

4.2 DETERMINATION OF CRITICAL BUCKLING LOAD IN BEAMS

Over the years many approaches for solving for the critical buckling loads have been developed. Many classical texts such as those by Timoshenko and Gere (1961), Salvadori (1955) and Chajes (1974) present approaches that can be used to solve for the critical load. Some of the solution approaches will be presented here. The benefits of having many approaches for determining the buckling load are that the researcher or designer has an option to use the method most suitable for their situation and that the solution from one approach can be checked with that from another approach (Wang and Kitipornchai, 1991). The solution approaches presented by three different authors are posed in the sections that follow. Subsequently the methods explored for use in the current study are discussed further; these are the closed form solution from the static-kinematic method for uniform moment and the energy method.

One classical approach to finding the critical buckling load is to employ a procedure carried out in two steps; first the governing differential equation (DE) for the particular case under review is determined. Once the governing DE has been determined it is then solved to obtain the critical load. The solution to the governing differential equations can take one of two courses. Depending on the nature of the DE there may exist an exact solution or the case may be that an exact solution cannot be obtained based on available mathematical methods. Methods for finding exact solutions for linear homogeneous and non-homogeneous DEs are available in existing literature. When an exact solution cannot be obtained for a given DE a numerical or approximate solution approach must be employed. Many numerical methods have been developed and are available to the designer or researcher. Recognising that differential equations describe a continuous system over a given interval, numerical methods simplify the solution by reducing the system from having infinite degrees of freedom (continuous system) to a system with finite degrees of freedom by discretising the system within the domain (i.e. made up of several discrete points) or by approximating the form of the dependent variable with a simple function. Numerical methods that are based on discretising the domain usually converge to the correct solution as the discretisation interval is reduced but with a corresponding increase in computational effort as a penalty.

Other classical approaches bypass the need to formulate the governing DE and can proceed to the solution directly. There are some methods that are amenable to application by hand calculations and other methods that require the use of calculators or computers due to the sheer quantity and complexity of the mathematical operations that need to be applied to arrive at a solution. As indicated in earlier chapters initial research was based on simplified loading and boundary conditions and the methods that were appropriate for these cases may not be applicable to more complex cases. It is no surprise therefore that over the years as the complexity of problems, loading and boundary conditions investigated has expanded the compendium of available solution methods has grown.

4.2.1 Methods from Nemir (1985)

A list of available solution methods for buckling problems was presented by Nemir (1985). Three different analysis methods were presented. For cases where a governing differential equation needs to be solved four (4) different solution methods were presented. The governing differential equations need only be determined under method 1. For the other methods the solution can be obtained directly without resorting to determination of the governing differential equations first. The different methods and summarised details of the approaches are given in Table 4-1. Functions that approximate the deformed shape must be chosen such that they satisfy the boundary conditions (BCs) of the structural member under consideration. Boundary conditions are of two types: geometric (deflection and shape) and natural (shear and bending moment). (Chajes, 1974). In some cases approximate functions that do not necessarily satisfy natural boundary conditions may be considered but geometric boundary conditions must always be satisfied.

Table 4-1 Buckling solution methods according to Nemir (1985)

<table>
<tr><th>Method 1</th><th>Procedure to obtain governing DE</th><th colspan="2">Solution Methods</th></tr>
<tr><td></td><td></td><td>Exact solution (closed form)</td><td>Approximate solution</td></tr>
<tr><td rowspan="2">Equilibrium Methods</td><td>(1) Calculation of internal forces caused by load acting on displaced member</td><td rowspan="2">(1) Smallest root obtained by setting the determinant of coefficients matrix to zero
(2) Use of a suitable function that satisfies the deformed shape and BCs</td><td rowspan="2">(1) Solution by a suitable finite series e.g. Taylors series
(2) Iterative integration (Stodolla-Vianello) method
(3) Finite difference method
(4) Finite Integral method</td></tr>
<tr><td>(2) Principle of stationery energy and use of the calculus of variations</td></tr>
<tr><td>Method 2</td><td></td><td colspan="2">Solution approach</td></tr>
<tr><td>Energy Methods</td><td>Not required</td><td colspan="2">- Based on the principle of the stationery value of energy
- Use approximate deformation shapes that satisfy BCs of the problem.
- A common general method used is the Ritz method
- Various modifications to the Ritz method can be found in the literature</td></tr>
<tr><td>Method 3</td><td></td><td colspan="2"></td></tr>
<tr><td rowspan="2">Numerical Methods</td><td rowspan="2">Not required</td><td rowspan="2"></td><td>(1) Member stiffness-matrix method</td></tr>
<tr><td>(2) Finite element method (FEM)</td></tr>
</table>

In the current study the method of first determining the governing differential equations is discussed for the uniform moment case. In these DEs the coefficients are obtained from the geometric and elastic characteristics of the members as well as the load effects. As indicated in Table 4-1 there are two (2) main ways of obtaining these governing DEs. In the first approach we must calculate internal forces caused by loads acting on the slightly displaced member and considering equilibrium of external and internal forces at the point of buckling (Nemir, 1985).

In the second approach the governing DEs of equilibrium are obtained by applying the principle of stationery energy. The concept of the calculus of variations is then used to derive the DEs of equilibrium from the energy expression.

4.2.2 Methods from Wang & Kitipornchai (1991)

An integrated view of numerical techniques available for determining the critical load at the time was presented by Wang and Kitipornchai (1991). The authors stated that one advantage of having many methods for obtaining the buckling load solution is that various methods can be used to independently solve the same problem and thus confirm accuracy, validity and convergence of solutions. In the current study two of these methods are employed, the Rayleigh-Ritz method and the finite element method. It is observed, as has been indicated by many others in the literature, that apart from a few problems, it is generally laborious and, in some cases, impossible to obtain exact analytical solutions. It therefore becomes imperative to resort to numerical techniques.

In the articulation of the available methods the authors grouped them into two categories; static-kinematic methods and work-energy methods, corresponding to different strategies used to satisfy the state of neutral equilibrium for the deformed member. A summary of the solution process and the applicable methods as given is provided in Table 4-2.

It has been stated that obtaining the governing DEs using the calculus of variations is easier compared to the conventional approach of analysing a free body diagram (FBD) of the deformed member and obtaining the equilibrium equations from statical and geometrical considerations. This is likely to be particularly true for loading conditions that deviate from the simple cases of loads through the shear centre and acting in isolation. The authors also indicate that the methods outlined present varying advantages and disadvantages. For instance, it is stated that the most efficient methods for nonlinear problems are the shooting method and the finite element method. Some methods that are efficient for elastic problems are not suitable for inelastic problems. In terms of formulation the finite difference method offers the convenience of having to work with polynomials which can also be easily programmed in software for obtaining a solution. They therefore present a relatively straightforward application and with convergence schemes will give accurate results without having to resort to a high number of discrete points in the solution domain.

Table 4-2 Solutions methods according to Wang and Kitipornchai (1991)

1. Static-Kinematic Approach	
Characteristics	*Methods*
- Field DEs are derived based on static and geometric considerations of the free body diagram of the slightly bent form of the member - Boundary conditions used to solve a two-point boundary value problem (BVP) for the buckling load - Some types of DEs give closed form solutions such as the Bessel's and Legendre's forms - Power series may be used to solve some problems - Numerical techniques most convenient for most problems	- Finite difference method - Finite integral method - Least mean squared error method - Galerkin's method - Finite element Galerkin method - Shooting method
2. Work-Energy Approach	
Characteristics	*Methods*
- In this approach the conditions of equilibrium of the deformed member are satisfied via the virtual work concept - Either the principle of virtual work or that of complementary virtual work is used - In buckling the two principles are reduced to the principle of stationery potential energy (PE) or the principle of stationery complementary PE - A functional of the energy is minimised to obtain the buckling load - The principle of energy conservation also applies	- Rayleigh-Timoshenko method - Rayleigh-Ritz method - Finite element method

When considering the work-energy approach the potential of the loads is taken as the negative value of the work done by the loads. It has been stated in the literature such as (Kitipornchai et al, 1986) that energy methods give an upper-bound solution. A convergence check involving the selected displacement function or number of terms in a series is therefore critical.

4.2.3 Methods from Trahair (2016)

In correcting a governing differential equation formulation by Eamon and Lamb (2015), Trahair (2016) provided a list of and applied several methods to generate the governing differential equation as well as to solve for the buckling load. Although the intention was to solve a specific problem, in this case correcting an erroneous governing DE, it gives a good indication of available methods and how they can be applied. For the derivation of the governing DE both consideration of equilibrium in the slightly displaced configuration as well as use of the calculus of variations were employed. The solution methods employed are listed in Table 4-3.

Table 4-3: Solution methods employed by Trahair (2016)

1. Determination of the governing DE	
(i)	Calculus of variations (with second variation of total potential energy)
(ii)	Consideration of equilibrium of the deflected and twisted beam
2. Solution Methods	
2(a) Solutions based on the governing DE	
(i)	A numerical method – The finite integral method
(ii)	A single term approximation (trigonometric function) of the buckled shape based on a half sine wave
2(b) Solutions based on energy equations for buckling	
(i)	Limited series (terms) for the buckled shape
(ii)	Finite element analysis based on cubic deformation fields

The incorrect equation that was presented by Eamon and Lamb (2015) for an open section doubly symmetric beam loaded with a uniformly distributed load is shown in equation (4.1). The correct equation verified using both methods presented in Table 4-3 is shown in equation (4.2).

$$EI_w\frac{d^4\phi}{dz^4} - GJ\frac{d^2\phi}{dz^2} - V_y y_q\frac{d\phi}{dz} - \frac{M_x^2}{EI_y}\phi = 0 \tag{4.1}$$

$$(EI_w\phi'')'' - (GJ\phi')' - \left(\frac{M_x^2}{EI_y} - qy_q\right)\phi = 0 \tag{4.2}$$

An expected term 'qy_q' appears in equation (4.2) and an unexpected term '$V_y q_y$' does not appear in the presented correct equation.

4.3 GOVERNING EQUATIONS FOR THE UNIFORM MOMENT CASE

Derivation of the governing differential equations for a monosymmetric section loaded by a uniform moment is presented here. It is worth noting that in the literature the governing DEs presented by different authors may vary slightly depending on where the origin of the coordinate system is taken. For instance, Timoshenko and Gere (1961) use the midspan of the beam as the origin for a simply supported beam under point load whereas for a similar load case Anderson and Trahair (1972) use one of the supports as the origin. A local coordinate system is also used so that the load effects on the member in its slightly displaced configuration can be established with respect to its local axes. The equilibrium condition is then enforced on the member in the slightly deformed configuration.

The following assumptions are made for the derivation of the governing DEs:

(1) Deflections and angles of twist are small
(2) Material is elastic, homogeneous and isotropic
(3) There is no local buckling in the flanges, web or stiffeners
(4) The section does not experience distortion while buckling takes place

Derivation of the governing differential equation for a monosymmetric cross section member subjected to uniform moment has been given by Galambos and Surovek (2008). The beam elevation, plan and cross-section with orientation of x-, y- and z- axes are shown in Figure 4-6. Displacements in the 'x' and 'y' directions are indicated as '*u*' and '*v*' respectively with rotation about the shear centre indicated as ϕ in subsequent figures. This shows the case for equal end moment loading and for this particular loading case the compression flange will be subjected to a uniform compressive stress along the entire length of the beam. For doubly symmetric beams this is the worst-case loading for LTB but not necessarily so for monosymmetric cross section beams (Camotim *et al*, 2012).

The elastic curve for both the vertical and horizontal displacements is shown as a dotted line.

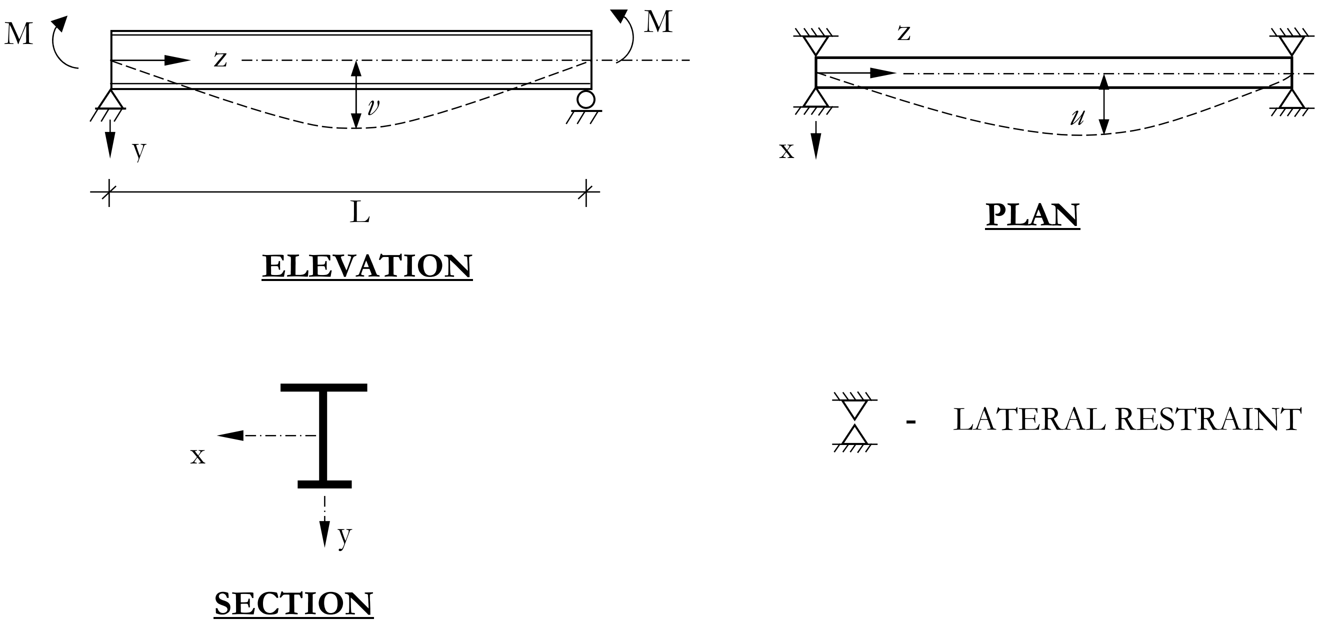

Fig.4-6 Basic case of lateral-torsional buckling due to uniform moment

The cross section in the slightly deformed shape is shown in Fig.4-7 (a). The governing differential equations are formulated from this. To begin with the major axis bending moment is decomposed into components $M_{y'}$ and $M_{x'}$ acting on the slightly bent section. This is illustrated in Fig.4-7 (b).

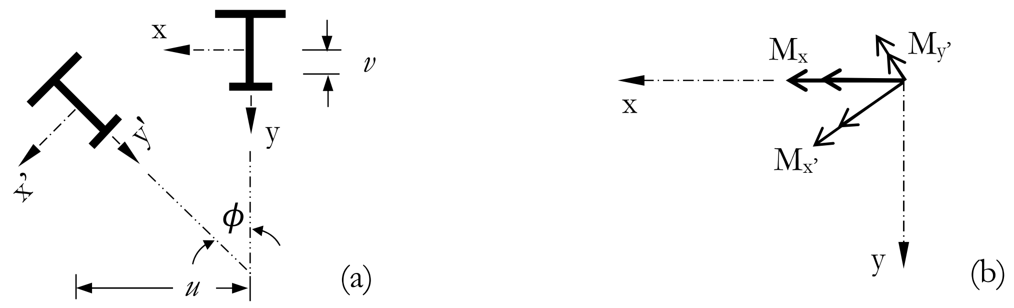

Fig.4-7 Slightly bent cross section configuration and major axis moment decomposition

As indicated in earlier sections the small displacement theory is utilised in which consideration of small angles results in cos ϕ = 1 and sin ϕ = ϕ. The components of moment on the slightly deformed section can therefore be written in terms of the major axis applied moment which is M. The equations are given below:

$$M_{x'} = \ M_x \ \cos\phi \ \approx \ M_x \tag{4.3}$$

$$M_{y'} = \ -M_x \ \sin\phi \ \approx \ -M_x\phi \tag{4.4}$$

M_x in equations (4.3) and (4.4) can be replaced by M since M_x = M along the length of the beam. This is illustrated in Fig.4-8.

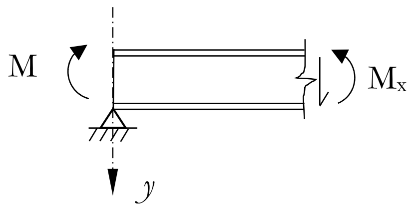

Fig.4-8 Moment M_x along beam length

The two governing differential equations for bending about the major and minor axes as obtained from the elastic curve are:

$$M_{x'} = -EI_x \frac{d^2v}{dz^2} \ = \ -EI_x v'' \ = \ -M$$

$$EI_x v'' \ - \ M \ = 0 \tag{4.5}$$

$$M_{y'} = -EI_y \frac{d^2u}{dz^2} \ = \ -EI_x u'' \ = \ M\phi$$

$$EI_y u'' \ + \ M\phi = 0 \tag{4.6}$$

An additional DE is required to complete the description of the lateral movement and twist of the member. Equations (4.5) and (4.6) account for the lateral movements. The addition DE will account for the twist. This equation is derived on the basis of the torsional component of the major axis moment M_x along the length of the beam. This is illustrated in Fig.4-9.

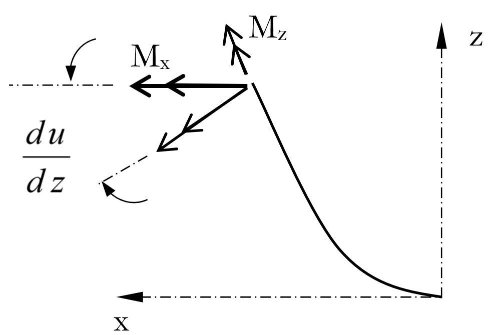

Fig.4-9 Torsional component of major axis moment M_x

The torsional moment component is given by:

$$M_z = M_x \sin\frac{du}{dz} \approx -M u'$$

$$M_z = -M u' \tag{4.7}$$

The St. Venant and warping torsional stiffnesses, and twist angle are related to the applied torsion M_z. We can therefore re-write equation (4.7) as:

$$EC_w\phi'' - (GJ + M\beta_x)\phi' = M_z$$

$$EC_w\phi'' - (GJ + M\beta_x)\phi' + Mu' = 0 \tag{4.8}$$

Equation (4.8) has a term $M\beta_x$, the *Wagner* term, in addition to '*GJ*', the St. Venant torsional stiffness, for the torsion expression. This term arises due to the effect of monosymmetry. This term has an effect of either increasing or decreasing the torsional stiffness of the beam depending on the value of the monosymmetry constant, β_x. The two differential equations containing the coupled displacements *u* and ϕ are equations (4.6) and (4.8). These two equations are the governing DEs for lateral-torsional buckling (LTB). They can be solved to find the critical buckling moment (M_{cr}). To solve the DEs the two are first combined into one equation by differentiating (4.8) with respect to 'z' and substituting equation (4.6).

Re-write (4.6) as:

$$u'' = \frac{-M\phi}{EI_y} \tag{4.9}$$

Differentiating (4.8) and replacing with (4.9) for u'' gives:

$$EC_w\phi^{iv} - (GJ + M\beta_x)\phi'' - \frac{M^2\phi}{EI_y} = 0 \tag{4.10}$$

We now solve (4.10) with the boundary conditions at the two ends being given in terms of *u* and ϕ as:

$$u(0) = u(L) = \phi(0) = \phi(L) = 0$$

$$u''(0) = u''(L) = \phi''(0) = \phi''(L) = 0$$

The supports used are simply supported 'fork-type' supports, as illustrated in Fig.4-10, which prevent rotation and lateral movement but permit warping.

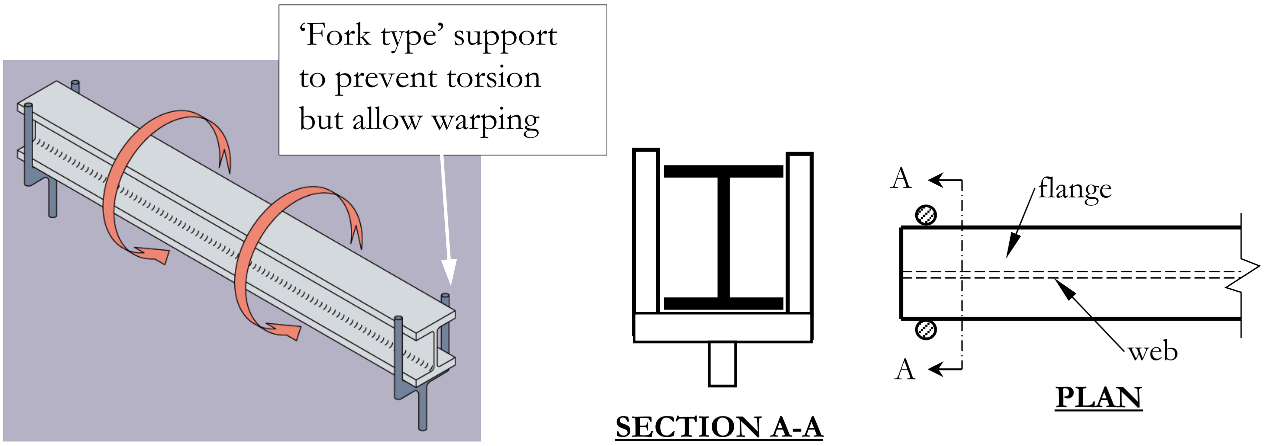

Fig.4-10 ‘Fork type’ supports for a simply supported beam (Adapted from SCI, 2011)

Equation (4.10) is re-written in the form given in (4.11) by rearranging terms to have a unit (1) coefficient to the highest derivative.

$$\phi^{iv} - \frac{GJ + M\beta_x}{EC_w}\phi'' - \frac{M^2}{E^2 C_w I_y}\phi = 0 \qquad (4.11)$$

The equation (4.11) is simplified by setting: $\lambda_1 = \frac{GJ+M\,\beta_x}{EC_w}$ and $\lambda_2 = \frac{M^2}{E^2 I_y C_w}$.

This gives: $\phi^{iv} - \lambda_1 \phi'' - \lambda_2 \phi = 0$ (4.12)

The auxiliary equation for this homogeneous fourth-order DE is:

$$m^4 - \lambda_1 m^2 - \lambda_2 = 0 \qquad (4.13)$$

Galambos and Surovek (2008) present the complete solution to the DE in two forms Depending on which expressions from (4.14) and (4.15) are chosen.

$$\phi = A_1 e^{\alpha_1 z} + A_2 e^{-\alpha_1 z} + A_3 e^{i\alpha_2 z} + A_4{}^{-i\alpha_2 z} \qquad (4.14)$$

$$\phi = C_1 \cosh \alpha_1 z + C_2 \sinh \alpha_1 z + C_3 \sin \alpha_2 z + C_4 \cos \alpha_2 z \qquad (4.15)$$

A_1, A_2, A_3, A_4 and C_1, C_2, C_3, C_4 are constants of integration and their values are obtained from the boundary conditions. The value of $i = \sqrt{-1}$. It is stated by Galambos and Surovek (2008) that it is more convenient to work with the equation containing trigonometric and hyperbolic functions, i.e. equation (4.16). Substituting for the boundary conditions involving ϕ i.e. ϕ *(0)* = ϕ *(L)* = ϕ*” (0)* = ϕ*” (L)* =*0*, four homogeneous simultaneous equations are obtained and can be expressed in matrix form. One of the roots from the auxiliary equation is:

$$\alpha_2 = \sqrt{\frac{\sqrt{\lambda_1^2 + 4\lambda_2} - \lambda_1}{2}} \tag{4.16}$$

Thus, solving for the nontrivial solution and the lowest eigenvalue results in the equation:

$$\frac{M^2}{E^2 I_y C_w} = \frac{\pi^2}{L^2}\left[\frac{GJ + M\beta_x}{EC_w} + \frac{\pi^2}{L^2}\right] \tag{4.17}$$

Solving the quadratic equation in (4.17) for 'M' using the well-known quadratic formula gives the critical elastic buckling moment (M_{cr}) for a monosymmetric section loaded in the plane of symmetry as given by (4.18). An alternative equation for M_{cr} is given in (4.19) by Galambos & Surovek (2008) and yields the same results as the previous equation.

$$M_{cr} = \frac{\pi^2 E I_y \beta_x}{2L^2}\left[1 \pm \sqrt{1 + \frac{4}{\beta_x^2}\left(\frac{GJL^2}{\pi^2 E I_y} + \frac{C_w}{I_y}\right)}\right] \tag{4.18}$$

$$M_{cr} = \frac{\pi}{L}\sqrt{EI_y GJ}\left[\frac{\pi\beta_x}{2L}\sqrt{\frac{EI_y}{GJ}} \pm \sqrt{1 + \frac{\pi^2 EC_w}{GJL^2} + \frac{\pi^2\beta_x^2}{4L^2}\left(\frac{EI_y}{GJ}\right)}\right] \tag{4.19}$$

The positive sign is for the case of the top flange in compression. The negative sign for the top flange in tension. For doubly symmetric cross sections equation (4.18) or (4.19) reduces to (4.20), since $\beta_x = 0$.

$$M_{cr} = \frac{\pi}{L}\sqrt{EI_y GJ}\sqrt{1 + \frac{\pi^2 EC_w}{GJL^2}} \tag{4.20}$$

The critical moment for beams with other end conditions can be found and catered for by means of a suitable factor to the equations in (4.18) to (4.20). For instance, a beam with torsion and warping fixed at the ends can be determined by first finding the solution to the DE in (4.11) with the boundary conditions for torsion changed to: $\phi(0) = \phi(L) = 0$ *and* $\phi'(0) = \phi'(L) = 0$. From the resulting critical elastic moment value, a boundary condition factor can then be determined and incorporated into equations (4.18 to 4.20).

The solution to problems where boundary conditions are changed from the basic case of simple, fork-type, supports with free warping are not easy to obtain directly. In some cases, closed form solutions may not even exist. The solutions for these problems would have to be obtained by trial-and-error methods or approximated by numerical methods. Approximate formulas can then be obtained by fitting equations to the numerically obtained discrete values from parametric studies. The approach taken by design standards is to keep a standard equation such as those from (4.18) to (4.20) and use appropriate factors to account for the different boundary conditions. A similar approach is used for load conditions that differ from that of uniform moments at the ends. This simplified approach is sufficient for day-to-day design office use. Additional factors may also be incorporated for cases such as loads that do not act at the shear centre. In this way factors affecting the lateral-torsional buckling behaviour are appropriately accounted for. A separate set of equations is used to account for inelastic lateral-torsional buckling.

A method that does not require determination of the governing differential equations is the Rayleigh-Ritz energy method. In this method minimization of the potential energy function is used to obtain the critical load. The accuracy of the method is dependent on the selection of a suitable function that estimates the displacement configuration of the member at buckling as accurately as possible. The selection of a suitable function is a critical part of effective application of the Rayleigh-Ritz method. This method is used for the current study for the two cases of transverse loads: a uniformly distributed load and the case of a central point load. The approach for a uniform moment given in 4.3.1 gives a closed form solution and therefore equation (4.18) or (4.19) is used to obtain the critical load for this particular case.

4.4 SOLUTION BY THE RAYLEIGH-RITZ ENERGY METHOD

4.4.1 Introduction

As described by Kitipornchai et al (1986), in the Raleigh-Ritz method there is no need to formulate or find the solution to the governing differential equations. In this approach the total potential energy is first determined as the sum of the strain energy, *U*, stored in the beam during buckling and the work done by the loads, *V*. The potential energy function, Π, is then minimised with respect to the assumed buckled shape (function) to obtain the critical load. The derivative of the potential energy function with respect to the unknown terms in the approximating function leads to several algebraic equations, equal to the number of unknown coefficients, which are solved to obtain the critical load.

$$\Pi = U + V \qquad (4.21)$$

$$\partial\Pi_i \rightarrow \ (solve)$$

It has been stated that the energy approach generally gives an upper bound solution to the exact value when boundary conditions are satisfied (Timoshenko and Gere, 1961), (Kitipornchai et al., 1986), (Chajes, 1974). However, this can be mitigated by the selection of a suitable approximating mathematical function, or in the case of a series function by selecting a suitable number of terms. Typically functions that are relatively easy to integrate such as trigonometric functions and polynomials, are most suitable.

Several authors have used the Rayleigh-Ritz approach to determine the critical loads for different and varying applications or cases. Chajes (1974) used the Rayleigh-Ritz method for both the case of uniform moment and a central point load for a simply supported beam. However, the solution method for obtaining the critical load is different from the one that will be applied here. The energy equation used by Chajes (1974) was shown to be slightly flawed by Pi and Trahair (1992) who attributed the flaw to some missing terms. This had led to the use of the term $\frac{1}{2}\int_0^l 2M_x u'\phi'\ dz$ for work done by centroidal loads which differs from the classical term $\frac{1}{2}\int_0^l 2M_x u''\phi\ \ dz$. Although the former term gives correct results for the case of uniform moment, it would be in error for other non-uniform moment load cases. Agreement of the classical equation with experimental results was demonstrated by the authors. The derivation of the classical term has been presented by Bleich (1952) [in Tong and Zhang (2003)] and Galambos (1968). The classical term is thus retained in the current study. Kitipornchai et al (1986) applied both the Rayleigh-Ritz and the finite integral methods to obtain critical loads for simply supported beams subjected to moment gradient loading. No transverse loads were considered in this study. Galambos and Surovek (2008) present an application of the method to solve the problem of a doubly symmetric simply supported beam subjected to a uniformly distributed load as well as a central point load. A similar study with more load cases is presented by Yilmaz et al (2017). The method has been applied as a 'strain-energy method' for the case of a central point load for a doubly symmetric cross section by Timoshenko and Gere (1961). Mohri et al (2003) applied the method to determine the three factors for the monosymmetric member 3-factor formula which was proposed for use in the Eurocode at the time. The results from the Rayleigh-Ritz method were compared to those from the method of Galerkin. Although the method used in the current study is like that of Mohri et al (2003) the monosymmetry constant equation used is slightly different. These authors use a value that is half of the one used in the current study. The Rayleigh-Ritz energy method has also been applied by Yuan et al (2013) to determine analytically the critical load for tapered tee-section cantilever beams. Mohammadi et al (2016) have applied the method to determine the critical load for beams under uniform moment but provided with discrete torsional restraints along its length. The stiffness contribution of the restraints is simply added to the strain energy portion of the potential energy equation. Apart from Mohri et al (2003) none of these studies discussed have specifically applied the Rayleigh-Ritz method to determination of the critical load for monosymmetric beams subjected to transverse loads. However, the work of Mohri et al (2003), as indicated earlier, used a monosymmetric constant formula that was based on half the value used in the current study. The difference in the equations means the energy equations used are slightly different with the $\int_0^L M_x\beta_x(\phi')^2 dz$ term replaced with

$\frac{1}{2}\int_0^L M_x\beta_x(\phi')^2 dz$ in the energy equation used in the current study. The work of Roberts and Azizian (1984) presented equations for monosymmetric sections subject to transverse loads but in this case the energy equation was solved based on the second variation of the total potential energy. A similar approach has been used by Pi and Trahair (1992) albeit for doubly symmetric sections.

In generating the potential energy equation, it is recognised that at the point of buckling strain energy is stored in the beam due to minor axis bending, torsion and warping. At the same time as the member moves into the slightly deformed configuration, work is done by the applied loads. The total potential energy equation is given by the sum of the two. The equations for a doubly symmetric section subject to transverse loads at a height, a, from the shear centre have been given by Yilmaz et al (2017). The strain energy equation is given in (4.22) and the general work equation for the loads in (4.23).

$$U = \frac{1}{2}\int_0^L \left(EI_y(u'')^2 + EC_w(\phi'')^2 + GJ(\phi')^2\right) dz \tag{4.22}$$

$$V = \frac{1}{2}\int_0^L 2M_x(u'')\,\phi\, dz + \frac{1}{2}\int_0^L aw\phi^2\, dz + \frac{1}{2}\sum Pa{\phi_L}^2 \tag{4.23}$$

The rotation angle for the point load, ϕ_L, must be evaluated at the location of the point load hence the subscript. In the current study half sine waves are used as approximation functions for the displacement terms u and ϕ. These equations are presented in (4.24) and (4.25) respectively.

$$u = A\sin\left(\frac{\pi z}{L}\right) \tag{4.24}$$

$$\phi = B\sin\left(\frac{\pi z}{L}\right) \tag{4.25}$$

In selecting the approximation function it is essential that it satisfies the kinematic degrees of freedom or boundary conditions (BCs) at the supports while also approximating the displaced configuration between supports as accurately as possible. For instance, in this case at the supports: $\phi(z) = 0, u(z) = 0\ at\ z = 0\ and\ z = L$. In between the supports both displacement and rotation take on non-zero values as would be expected.

The two components in the work done by external loads equation for the lowering of the transverse loads have been demonstrated by Aydin et al (2013) as shown in Fig.4-12 and its interpretation given in equations (4.26) to (4.28). Two of the work done by external loads terms are accounted for in the illustration in Fig.4-12. The third term in the energy equation is for the work done by the major axis bending moment during buckling and its derivation has been provided by Galambos (1968) as indicated earlier.

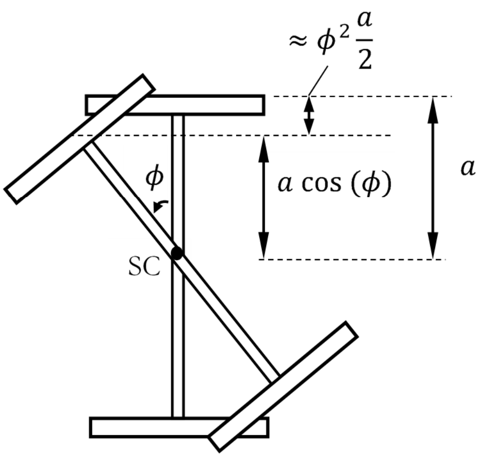

Fig.4-12 Lowering of a point from shear center during twisting (Adapted from Aydin et al, 2013)

For a transverse load located at a distance, a, from the shear centre, the lowering of the external load as shown in Fig.4-12, Δ, is given as:

$$\Delta = a\,(1 - cos\phi) \approx \frac{\phi^2 a}{2} \tag{4.26}$$

As it moves, the external load does work. The work done by a UDL and point load respectively would be:

$$V_{UDL} = \frac{a}{2}\int_0^L \phi^2 w\, dz \tag{4.27}$$

$$V_{PL} = \frac{a}{2}\sum_{i=1}^{n} \phi_i^2 P_i \tag{4.28}$$

Some key trigonometric identities are required to find the solution to the potential energy equation, and these are listed in (4.29) to (4.36).

$$\int_0^L sin^2\left(\frac{\pi z}{L}\right) dz = \int_0^L cos^2\left(\frac{\pi z}{L}\right) dz = \frac{L}{2} \tag{4.29}$$

$$\int_{\frac{L}{2}}^L sin^2\left(\frac{\pi z}{L}\right) dz = \frac{L}{4} \tag{4.30}$$

$$\int_0^L z\, sin^2\left(\frac{\pi z}{L}\right) dz = \frac{L^2}{4} \tag{4.31}$$

$$\int_0^L z^2\, sin^2\left(\frac{\pi z}{L}\right) dz = \left(\frac{1}{6} - \frac{1}{4\pi^2}\right) L^3 \tag{4.32}$$

$$\int_0^{\frac{L}{2}} z\, sin^2\left(\frac{\pi z}{L}\right) dz = \left(\frac{1}{16} + \frac{1}{4\pi^2}\right) L^2 \tag{4.33}$$

$$\int_{\frac{L}{2}}^{L} z\, sin^2\left(\frac{\pi z}{L}\right) dz = \left(\frac{3}{16} - \frac{1}{4\pi^2}\right) L^2 \tag{4.34}$$

$$\int_0^{\frac{L}{2}} z\, cos^2\left(\frac{\pi z}{L}\right) dz = \left(\frac{1}{16} - \frac{1}{4\pi^2}\right) L^2 \tag{4.35}$$

$$\int_{\frac{L}{2}}^{L} z\, cos^2\left(\frac{\pi z}{L}\right) dz = \left(\frac{3}{16} + \frac{1}{4\pi^2}\right) L^2 \tag{4.36}$$

The solution to the energy equations is presented in the sections that follow for the case of a point load as well as for a UDL. The Rayleigh-Ritz method is thus applied in the current study to obtain the critical load for the two cases of a point load at midspan and that of a uniformly distributed load (UDL) for a simply supported monosymmetric beam.

4.4.2 Point Load

For the monosymmetric section a term incorporating the monosymmetry constant must be introduced in the energy equation to account for the Wagner effect. The potential energy equation for point loads acting at any distance, a, from the shear centre is written in the form of equation (4.37) and solved in the current study.

$$\Pi = \frac{1}{2}\int_0^L \left(EI_y(u'')^2 + EC_w(\phi'')^2 + GJ(\phi')^2 + M_x\beta_x(\phi')^2\right) dz + \frac{1}{2}\int_0^L 2M_x(u'')\,\phi\, dz + \frac{1}{2}\sum Pa{\phi_L}^2 \tag{4.37}$$

The approximating functions in (4.24) and (4.25) are replaced in (4.37) and after integration the following potential energy equation is obtained:

$$\Pi = \frac{EI_yA^2\pi^4}{4L^3} + \frac{GJB^2\pi^2}{4L} + \frac{EC_wB^2\pi^2}{4L^3} + \frac{AB\pi^2P}{2}\left(\frac{3\pi^2-4}{16\pi^2}\right) - \frac{AB\pi^2P}{8} - \frac{AB\pi^2P}{2}\left(\frac{\pi^2+4}{16\pi^2}\right) + \frac{B^2\pi^2P\beta_x}{4}\left(\frac{\pi^2-4}{16\pi^2}\right) + \frac{B^2\pi^2\beta_xP}{16} + \frac{B^2\pi^2\beta_xP}{4}\left(\frac{3\pi^2+4}{16\pi^2}\right) + \frac{PaB^2}{2} \tag{4.38}$$

The potential energy equation in (4.38) is then minimised with respect to 'A' and 'B'. Two equations are then obtained by equating the minimisation function to zero.

$$\frac{\partial \Pi}{\partial A} = \frac{2EI_y A\,\pi^4}{4L^3} - 0.866850256\,BP = 0 \qquad (4.39)$$

$$\frac{\partial \Pi}{\partial B} = -0.866850256\,AP + \frac{2GJB\,\pi^2}{4L} + \frac{2EC_w B\,\pi^2}{4L^3} + 0.366850274\,B\beta_x P + \frac{2PaB}{2} = 0 \qquad (4.40)$$

The two equations can be expressed in matrix form:

$$\begin{bmatrix} \frac{EI_y\pi^4}{2L^3} & -0.866850256\,P \\ -0.866850256\,P & \left(\frac{GJ\,\pi^2}{2L} + \frac{EC_w\,\pi^2}{2L^3} + 0.366850274\,\beta_x P + Pa\right) \end{bmatrix} \begin{bmatrix} A \\ B \end{bmatrix} = \begin{bmatrix} 0 \\ 0 \end{bmatrix} \qquad (4.41)$$

The non-trivial solution for the critical load is obtained by setting the determinant of the coefficients to zero. This gives a quadratic equation as presented in (4.42). Solution of this quadratic equation then gives the critical buckling load, P_{cr}.

$$0.715429366\,P^2 - \frac{EI_y\pi^4}{2L^3}\left(\frac{GJ\;\pi^2}{2L} + \frac{EC_w\;\pi^2}{2L^3}\right) - \frac{EI_y\pi^4 P}{2L^3}(0.366850274\,\beta_x + a) = 0 \qquad (4.42)$$

Equation (4.42) is verified for accuracy in section 4.4.5 by comparing outputs from this equation to some benchmark problems and to those obtained from the finite element analysis method.

4.4.3 Uniformly Distributed Load (UDL)

As for the case of a point load, for a monosymmetric section a term incorporating the monosymmetry constant must be introduced in the energy equation to account for the Wagner effect. The potential energy equation for a UDL acting at any distance, a, from the shear centre is:

$$\Pi = \frac{1}{2}\int_0^L \left(EI_y(u'')^2 + EC_w(\phi'')^2 + GJ(\phi')^2 + M_x\beta_x(\phi')^2\right) dz + \frac{1}{2}\int_0^L 2M_x(u'')\,\phi\, dz + \frac{1}{2}\int_0^L aw\phi^2\, dz \qquad (4.43)$$

The approximating functions in (4.24) and (4.25) are replaced in (4.43) and after performing the integration the following potential energy equation is obtained:

$$\Pi = \frac{EI_yA^2\pi^4}{4L^3} + \frac{GJB^2\pi^2}{4L} + \frac{EC_wB^2\pi^2}{4L^3} + \frac{AB\pi^2wL}{2}\left(\frac{1}{6} - \frac{1}{4\pi^2}\right) - \frac{AB\pi^2wL}{8} + \frac{B^2\pi^2\beta_xwL}{16} - \frac{B^2\pi^2\beta_xwL}{4}\left(\frac{1}{6} + \frac{1}{4\pi^2}\right) + \frac{wLaB^2}{4} \qquad (4.44)$$

The potential energy equation in (4.44) is then minimised with respect to 'A' and 'B'. Two equations are then obtained by equating the minimisation function to zero.

$$\frac{\partial\Pi}{\partial A} = \frac{2EI_yA\,\pi^4}{4L^3} - \frac{wLB\pi^2}{8}\left(\frac{\pi^2+3}{3\pi^2}\right) = 0 \qquad (4.45)$$

$$\frac{\partial\Pi}{\partial B} = -\frac{wLA\pi^2}{8}\left(\frac{\pi^2+3}{3\pi^2}\right) + \frac{2GJB\,\pi^2}{4L} + \frac{2EC_wB\,\pi^2}{4L^3} + \frac{2B\,\pi^2\beta_xwL}{16} - \frac{2B\,\pi^2\beta_xwL}{4}\left(\frac{1}{6} + \frac{1}{4\pi^2}\right) + \frac{2wLaB}{4} = 0 \qquad (4.46)$$

The two equations can be expressed in matrix form:

$$\begin{bmatrix} \frac{EI_y\pi^4}{2L^3} & -\frac{wL}{8}\left(\frac{\pi^2+3}{3}\right) \\ -\frac{wL}{8}\left(\frac{\pi^2+3}{3}\right) & \left(\frac{GJ\,\pi^2}{2L} + \frac{EC_w\,\pi^2}{2L^3} + \frac{wL}{8}\left(\frac{\pi^2-3}{3}\right)\beta_x + \frac{wL}{2}a\right) \end{bmatrix} \begin{bmatrix} A \\ B \end{bmatrix} = \begin{bmatrix} 0 \\ 0 \end{bmatrix} \qquad (4.47)$$

The non-trivial solution for the critical load is obtained by setting the determinant of the coefficients to zero. This gives a quadratic equation in the load as presented in (4.48). Solution of this quadratic equation then gives the critical buckling load, w_{cr}.

$$\frac{w^2L^2}{64}\left(\frac{\pi^2+3}{3}\right)^2 - w\left[\frac{EI_y\pi^4}{2L^2}\left(\frac{\beta_x}{8}\left(\frac{\pi^2-3}{3}\right)+\frac{a}{2}\right)\right] - \frac{EI_y\pi^4}{2L^3}\left(\frac{GJ\,\pi^2}{2L}+\frac{EC_w\,\pi^2}{2L^3}\right) = 0 \tag{4.48}$$

Equation (4.48) is verified for accuracy in section 4.4.5 by comparing outputs from this equation to some benchmark problems and to those obtained from the finite element analysis method.

4.4.4 The Finite Element Method

The finite element method is a powerful numerical analysis method that has seen considerable growth in application and solution of complex problems as the improvements in the digital computer have progressed. The method lends itself well to implementation on a digital computer. The basic idea of the finite element method (FEM) is to divide a body into smaller parts known as the finite elements which are connected by nodes (Fish and Belytschko, 2007). The required field over the domain, such as displacements, are determined mathematically at the nodes using an approximate solution method. The value of the field at any point other than the nodes is determined by appropriate interpolation from the determined nodal values. The nodal unknowns are determined by generating a system of linear equations where the number of unknowns is equal to the number of nodes. Where other numerical analysis approaches are based around solving the governing differential equations and their boundary conditions this approach is known as the 'strong form'. The finite element method does not follow this approach. Instead, it is formulated based on integral forms of equations in what is mathematically known as the 'weak form'. Approximation functions are combined with the weak form to obtain the discrete finite element equations. The equations are solved for the unknowns. Generally, the accuracy of the solution improves as the number of elements (and nodes) is increased but this comes at a penalty of computation time or effort, a familiar effect with numerical methods.

From a mathematical standpoint the determination of the critical load is premised on the property that the stiffness of the member vanishes at the critical load. This is because at the critical load displacements increase without a corresponding increase in applied load. For the displacements to increase without bound the stiffness matrix must become singular. For this to happen the determinant of the matrix must be zero. This property is used to obtain the eigenvalues corresponding to the critical load. Because at buckling theoretically the member can be in two different states at the same load an eigenvalue problem is created.

The steps in implementation of a finite element model have been given by Fish and Belytschko (2007) as:

1. Pre-Process: subdivide the problem domain into finite elements
2. Element formulation: development of equations for the elements
3. Assembly: obtain equations of entire system from equations of individual elements
4. Solving the equations
5. Post-Processing: determining quantities of interest e.g. stress, strains and their visualisations etc.

In the implementation steps indicated the users of most modern finite element programs only interact with steps 1 and 5, with the intermediate steps performed by the computer in the background. For step 2 various elements are present in the element library of software packages and are selected based on the problem to be investigated as the formulations differ for the different elements. In the current study the software Abaqus is used for carrying out the finite element analysis. The commonly used elements found in the software library are:

1. Beam/Truss elements
2. Solid elements, and
3. Shell elements

The approximation functions used with the elements are generally either linear or quadratic. The elements are shown in Fig.4-13.

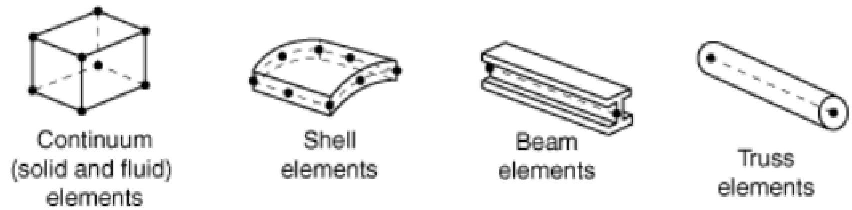

Fig.4-13 Abaqus finite elements (from Simulia, n.d.)

The characteristics and element formulations are discussed in the software documentation (Simulia, n.d.). One of the important characteristics of the elements is the degrees of freedom (DOF) at the nodes. These are fundamental variables used in the solution analysis. Shell elements are generally modelled as being applied at the midline of thin-walled elements whereas solid elements fill up the form of the object being modelled. Use of the midline on beams results in overlap of material at junctions and corner radii cannot be modelled unless a hybrid model of shell and beam elements is considered. The use of shells for beam modelling has been shown to incur some errors (Vales and Stan, 2017) including change in torsional stiffness when corner radii are omitted. For this reason, the current study adopts the use of solid elements for most cases with shell models used only occasionally, particularly where computer time becomes 'expensive' i.e. computer run time becomes excessive for solid models. For the same member, the shell model will have significantly less elements than its solid counterpart. Generally, also, more slender sections are best modelled using shell elements. For these sections the torsional strength is low and the loss of accuracy therefore not significant.

To obtain the optimum mesh size for a finite element analysis study a mesh convergence study needs to be carried out. This helps to determine the most optimum element size or mesh density for accurate results but without unduly lengthy computational time. A mesh convergence study for the solid element C3D8 is presented in Fig.4-14. Analysis run times for a 7.5mm (with one element through flange thickness), 7.5mm (with two elements through flange/stiffener thickness) and 5mm element size (seed) respectively are shown in Fig.4-14.

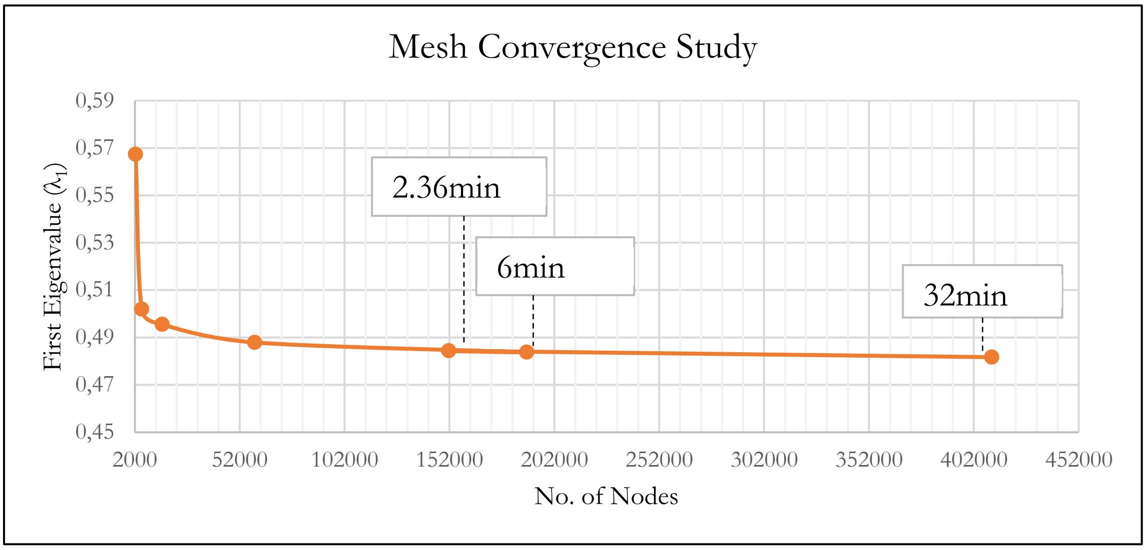

Fig.4-14 Mesh convergence study for the C3D8 solid element

As the number of nodes (and hence number of elements) increases the run time increases and the solution converges. It was determined from the study that a mesh seed of 7.5mm with at least two elements across the flange and stiffener elements gives sufficiently converged results. With a further 33% reduction in seed size (5mm) only a 0.43% change in the obtained first eigenvalue is observed.

4.4.5 Results from Derived Equations

Results from the equations derived in 4.4.2 and 4.4.3 for point load and uniformly distributed load i.e., Equations (4.42) and (4.48) respectively are checked against some existing results in the literature and then against results from finite element analysis. The first check, presented in 4.4.5.1, is for the point load equation and is carried out against the results presented by Mohri *et al* (2003) for a monosymmetric I-shaped section, simply supported at different spans. The authors did not provide the final equation used for the point load case but provided the governing differential equation that was solved using the method of Galerkin, and a description of the solution steps applied. The governing differential equation was obtained from an energy equation of the form in (4.22) and (4.23) by determining the stationery condition of the potential function ($\delta\Pi$) and considering variation of the total potential in relation to virtual displacements and their derivatives. The uncoupled governing differential equation obtained after some calculations is shown in equation (4.49)

$$EI_\omega \theta_x^{(4)} - \left(GJ + 2\beta_z M_y\right)\theta_x'' - 2\beta_z M_y' \theta_x' + q_z e_z \theta_x - \frac{M_y^2}{EI_z}\theta_x = 0 \qquad (4.49)$$

In the equation, β_z is the monosymmetry constant, M_y the major axis bending moment, I_z the minor axis second moment of area, θ_x the rotation about member axis, 'q_z' the applied load, e_z the distance above centroid where the load is applied and I_ω the warping constant. Other parameters are already previously defined. For the point load case the load 'q_z' applied at a distance 'a' from the reference end was written as $q_z = Q_z \Delta(x - a)$, where 'Δ' is Dirac's function ($\Delta = 1$ if $x = a$ and $\Delta = 0$ elsewhere).

The details of the cross section used for the comparison are given below each table. The check was made against the results obtained from the equation developed by the authors and also against the finite element results against which they checked their results.

The following check, in 4.4.5.2 is for the UDL equation. The results from the equation developed in the current study are checked against results by Aydin *et al* (2013). The outputs from the equation developed by the authors was used for the check and not the finite element results against which their equation was checked. The beam case used is that of simple supports and results at various spans are checked. In their check against outputs from the finite element analysis, based on a shell model, the authors reported results that compared well with their equation.

The buckling load equation used by Aydin *et al* (2013) is presented in equation (4.50) and is based on an energy method approach. The work done by external loads was equated to the strain energy. A suitable function satisfying boundary conditions was selected. The integrals from torsion and warping terms were evaluated directly as they yielded closed form solutions. The integrals from the work done terms were evaluated using a Simpson integration rule which is a numerical approach. Stepwise change in the moment diagram was assumed and the beam was divided into twenty-four (24) segments. A general equation in equivalent point load form 'P' was obtained.

$$P = \frac{P_{cr}}{2\pi^2 L\sqrt{D_1}}\left[-\frac{kH_A+2D_2\beta_x}{\sqrt{D_1}} + \sqrt{\frac{(kH_A+2D_2\beta_x)^2}{D_1} + \frac{2\pi^2 GJ}{P_{cr}}\left(1+\frac{\pi^2 EC_W}{L^2 GJ}\right)}\right] \tag{4.50}$$

All other loads had to be converted to 'P' using appropriate conversion factors given in a table by the authors. For a UDL the factors D1, D2 and k are given as $6.0915\text{x}10^{-3}$, 0.14312 and 0.50 respectively. The buckling load is of the form 'qL' where 'q' is the UDL.

In the sections that follow from 4.4.5.3 to 4.4.5.6 the results from the equations developed in the current study are then checked against outputs from finite element analysis for a 6m span beam. This is arbitrarily selected for the check. In the first two sections (4.4.5.3, 4.4.5.4) the results are checked for the I-shaped section used in the previous sections where upstands are introduced to the top flange in 25mm increments up to 100mm. One check is for the point load case and the other for the UDL. Three load positions are investigated for the point load (above shear centre, at shear centre and below shear centre) whereas for the UDL only two load positions are considered (above shear centre and below shear centre) owing to the difficulty of placing a UDL at the shear centre in a finite element solid model. In sections 4.4.5.5 and 4.4.5.6 the equation outputs are checked against finite element analysis results based on an I-shaped wide flange section taken from the South African steel handbook, SASCH (2016) a WF152x152x30. Upstands are introduced at 25mm height intervals up to a height of 100mm.

The commercially available software Abaqus was used for the finite element analysis. The finite element model used was a solid model with eight (8) node linear, fully integrated brick elements (designated as C3D8 in the Abaqus element library). A mesh convergence study was carried out as presented in 4.4.4 in order to determine the optimum element/mesh size. The supports were applied such that a 'fork type' support was created. These permit bending about the major and minor axis but restricts rotation about the longitudinal axis at the supports. Warping is allowed to take place freely. One end was held from displacement along the axis to avoid rigid body translation. The smallest positive eigenvalue as well as the absolute lowest negative eigen value are reported. These are used in the current study for comparison with the results reported in the literature.

4.4.5.1 Point Load equation results against Mohri et al (2003)

Results for the point load case applied at shear centre (S.C.) are presented in Table 4-4.

Table 4-4 Comparison of results from point load equation (4.42) to results from Mohri et al (2003)

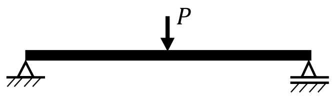

No.	Span (m)	Load	Load at S.C. (kNm)						
			Current Eqn.	Mohri et al. Eqn	% Diff.		Current Eqn.	Mohri et al. (S8R5)	% Diff.
1	4	+ve value	139,90	134,43	3,9%		139,90	130,89	6,4%
		-ve value	-84,40	-83,05	1,6%		-84,40	-78,34	7,2%
2	5	+ve value	102,20	98,52	3,6%		102,20	97,36	4,7%
		-ve value	-66,70	-65,64	1,6%		-66,70	-63,45	4,9%
3	6	+ve value	80,20	77,48	3,4%		80,20	77,41	3,5%
		-ve value	-55,50	-54,65	1,5%		-55,50	-53,99	2,7%
4	7	+ve value	65,90	63,78	3,2%		65,90	64,40	2,3%
		-ve value	-47,70	-47,00	1,5%		-47,70	-47,40	0,6%
5	8	+ve value	55,90	54,17	3,1%		55,90	55,32	1,0%
		-ve value	-42,00	-41,32	1,6%		-42,00	-42,52	-1,2%

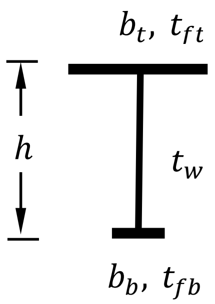

$h = 300mm$ $\qquad I_y = 3.3939\ x\ 10^6 mm^4$

$b_t = 150mm$ $\qquad J = 125.1\ x\ 10^3 mm^4$

$b_b = 75mm$ $\qquad C_w = 27.985\ x\ 10^9 mm^6$

$t_{ft} = t_{fb} = 10.7mm$ $\qquad \beta_x = 209.6$

$t_w = 7.1mm$ $\qquad E = 210\ GPa$

For comparison with Mohri *et al.* (2003) equation the correlation is good with difference between results less than 4% in all cases. The results from Mohri *et al.* (2003) used are those from the equations developed in that study based on the Galerkin method as well as the finite element analysis results obtained from a shell model employed in that study. Eight node shell elements with reduced degrees of freedom at nodes (S8R5) elements were used in their study. Comparison of results from current study equation to the FEM results from the authors stated above reveal a close correlation as well with differences generally less than 5% with only two exceptions.

4.4.5.2 UDL equation results against Aydin et al (2013)

Results for the UDL case are presented in Table 4-5.

Table 4-5 Comparison of results from UDL equation (4.48) to results from Aydin et al (2013)

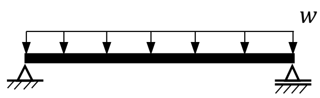

No.	Span		Below S.C. (kNm)			At S.C. (kNm)			Above S.C. (kNm)		
			EQN.	Aydin et al. EQN.	% Diff.	EQN.	Aydin et al. EQN.	% Diff.	EQN.	Aydin et al. EQN.	% Diff.
1	5		202,10	201,11	0,5%	276,20	272,47	1,4%	400,80	392,31	2,1%
2	6		156,60	156,21	0,2%	206,60	204,28	1,1%	290,30	284,78	1,9%
3	7		127,50	127,40	0,1%	163,30	161,83	0,9%	223,00	219,17	1,7%
4	9		92,80	92,91	-0,1%	113,60	112,91	0,6%	147,80	145,79	1,4%
5	10		81,70	81,82	-0,1%	98,20	97,76	0,4%	125,30	123,79	1,2%
6	11		72,90	73,10	-0,3%	86,40	86,09	0,4%	108,30	107,16	1,1%
7	12		65,90	66,06	-0,2%	77,00	76,84	0,2%	95,10	94,23	0,9%

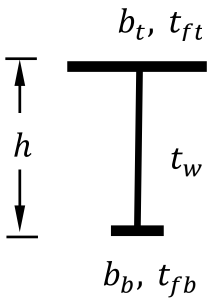

$h = 400mm$

$b_t = 180mm$

$b_b = 90mm$

$t_{ft} = t_{fb} = 13.5mm$

$t_w = 8.6mm$

$I_y = 7.401\ x\ 10^6 mm^4$

$J = 303.379x\ 10^3 mm^4$

$C_w = 108.90\ x\ 10^9 mm^6$

$\beta_x = 278.3$

$E = 210\ GPa$

The equation is observed to give results that are very close to those obtained by Aydin *et al* (2013). It is worth noting that the results by the authors, though showing good correlation with shell finite element results they obtained, for the bottom flange loading had up to 10% difference whereas for top flange loading the difference in obtained results did not exceed about 5%.

4.4.5.3 I-Section Beam vs FEM (Point Load)

Results for the point load case where current equation outputs are compared to those from a finite element analysis are presented in Table 4-6.

Table 4-6 Comparison of results from Point Load equation (4.42) to results from FEM solid model (I-section) – 6m span

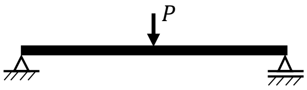

kN

No.	Upstand Height	Load	Below S.C.			At S.C.			Above S.C.		
			EQN.	FEM	% Diff.	EQN.	FEM	% Diff.	EQN.	FEM	% Diff.
1	0	Point. L	-20,6	-21,15	-2,7%	-35,9	-37,2	-3,6%	-39,2	-40,66	-3,7%
		Point. L	89,4	84,8	5,1%	51,4	50,9	1,0%	47	46,89	0,2%
2	25	Point. L	-24,1	-24,7	-2,5%	-48,2	-47,23	2,0%	-52,7	-51,48	2,3%
		Point. L	130,8	145,8	-11,5%	74,8	72,13	3,6%	68,4	66,46	2,8%
3	50	Point. L	-29,2	-28,2	3,4%	-60,4	-58,9	2,5%	-68	-65,81	3,2%
		Point. L	193,8	172,06	11,2%	93,5	90,84	2,8%	83,1	81,4	2,0%
4	75	Point. L	-34,7	-33	4,9%	-74,5	-71,81	3,6%	-87,4	-83,51	4,5%
		Point. L	233,6	204,9	12,3%	108,8	106	2,6%	92,7	91,22	1,6%
5	100	Point. L	-39,9	-40,81	-2,3%	-85,9	-91,25	-6,2%	-105,7	-110,75	-4,8%
		Point. L	276,3	240,11	13,1%	128,1	123,75	3,4%	104,2	101,91	2,2%

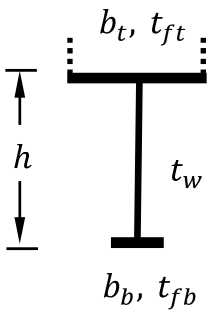

$h = 300mm$

$b_t = 150mm$

$b_b = 75mm$

$t_{ft} = t_{fb} = 10.7mm$

$t_w = 7.1mm$

The results from the equation from the current study give results close to those obtained from the finite element analysis model except for some of the cases for the load at the bottom flange. A possible explanation for this is provided in the discussion section for this chapter.

4.4.5.4 I-Section Beam vs FEM (UDL)

Results for the UDL case where current equation outputs are compared to those from a finite element analysis are presented in Table 4-7.

Table 4-7 Comparison of results from UDL equation (4.48) to results from FEM solid model (I-section) – 6m span

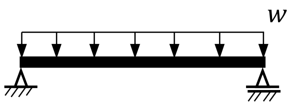

No.	Upstand Height	Load	Below S.C.				Above S.C.		
			EQN.	FEM	% Diff.		EQN.	FEM	% Diff.
1	0	UDL	-5,9	-6,15	-4,2%		-9,9	-10,05	-1,5%
		UDL	22,8	22,1	3,1%		13,5	13,11	2,9%
2	25	UDL	-7,49	-7,1	5,2%		-13,2	-13,2	0,0%
		UDL	36,28	36,7	-1,2%		19,9	19,68	1,1%
3	50	UDL	-8,2	-8,9	-8,5%		-16,9	-16,84	0,4%
		UDL	49,8	47,9	3,8%		24,3	24,24	0,2%
4	75	UDL	-10,2	-10,56	-3,5%		-21,7	-21,34	1,7%
		UDL	57,7	56,97	1,3%		27,1	27,3	-0,7%
5	100	UDL	-12,3	-13,25	-7,7%		-27,9	-28,48	-2,1%
		UDL	64,9	66,3	-2,2%		28,7	30,53	-6,4%

kN/m

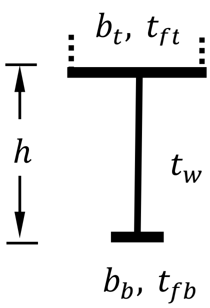

$$h = 300mm$$

$$b_t = 150mm$$

$$b_b = 75mm$$

$$t_{ft} = t_{fb} = 10.7mm$$

$$t_w = 7.1mm$$

A good agreement is obtained between the developed equation and the results from the finite element analysis results. Only a few values are greater than 5% in difference, with none greater than 8.5%.

4.4.5.5 H152 Beam (wide flange) vs FEM (Point Load)

Table 4-8 Comparison of results from Point Load equation (4.42) to results from FEM solid model (H152)

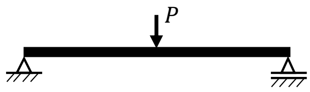

kN

SPAN = 6m

No.	Upstand Height	Load	Below S.C.			At S.C.			Above S.C.		
			EQN.	FEM	% Diff.	EQN.	FEM	% Diff.	EQN.	FEM	% Diff.
1	0	Point. L	-22	-21,6	1,8%	-29,8	-29,1	2,3%	-40,3	-39,41	2,2%
		Point. L	40,3	38,4	4,7%	29,8	28,4	4,7%	22	21,09	4,1%
2	25	Point. L	-24,5	-23,96	2,2%	-37	-35,8	3,2%	-48,3	-46,73	3,3%
		Point. L	59,7	56,43	5,5%	39,6	37,86	4,4%	30,3	29,31	3,3%
3	50	Point. L	-28,1	-27,6	1,8%	-44,9	-43,09	4,0%	-59,1	-56,6	4,2%
		Point. L	73,9	69,08	6,5%	46,3	44,08	4,8%	35,2	33,79	4,0%
4	75	Point. L	-33,4	-31,86	4,6%	-54,6	-51,1	6,4%	-74,1	-69,56	6,1%
		Point. L	82,8	76,35	7,8%	50,7	47,81	5,7%	37,3	35,53	4,7%
5	100	Point. L	-41	-38,38	6,4%	-66,9	-61,66	7,8%	-94,4	-86,4	8,5%
		Point. L	87,3	79	9,5%	53,6	49,94	6,8%	38	35,8	5,8%

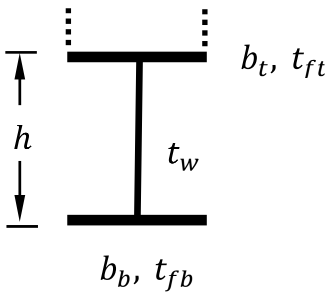

∗Section properties vary due to varying upstand height

**Base section: WF 152x152x23*

The agreement is again generally good with excessive differences observed only for the high upstand values. All differences are still generally below 5% for most cases and even for the cases with high difference this does not exceed 9.5%.

4.4.5.6 H152 Beam (wide flange) vs FEM (UDL)

Table 4-9 Comparison of results from UDL equation (4.48) to results from FEM solid model (H152)

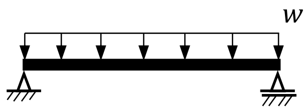

kN/m

No.	Upstand Height	Load	Below S.C.			6m SPAN	Above S.C.		
			EQN.	FEM	% Diff.		EQN.	FEM	% Diff.
1	0	UDL	-6,3	-6,3	0,0%		-10,3	-10,4	-1,0%
		UDL	10,3	10,1	1,9%		6,3	6,2	1,6%
2	25	UDL	-7,1	-7,49	-5,5%		-12,3	-12,24	0,5%
		UDL	15	15,5	-3,3%		8,7	8,63	0,8%
3	50	UDL	-8,2	-8,25	-0,6%		-14,7	-14,89	-1,3%
		UDL	18,4	17,92	2,6%		10,3	9,95	3,4%
4	75	UDL	-9,9	-9,79	1,1%		-19	-18,52	2,5%
		UDL	20,2	19,45	3,7%		10,6	10,44	1,5%
5	100	UDL	-12,4	-13,13	-5,9%		-24,5	-23,37	4,6%
		UDL	20,9	21,65	-3,6%		10,6	10,46	1,3%

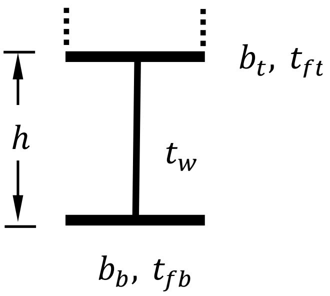

∗*Section properties vary due to varying upstand height*

**Base section: WF 152x152x23*

For the UDL case (6m beam) difference between equation and finite element analysis results are below 5%. For the few that exceed this value they still fall below 6% difference.

4.5 DISCUSSION

Based on comparison with some results in the existing literature and those from finite element analysis, it appears that the developed equations (i.e., Equations (4.42) and (4.48)) predict the critical load to satisfaction. The loads obtained from the equations developed in the current study appear generally to give slightly non-conservative results when compared to finite element analysis results. This is not surprising as energy equations generally give critical values higher than the exact values. These results highlight the expressed need for a judicious selection of functions to predict the displacements.

The result from the point load case where high differences are observed may be attributed to the observations by Roberts and Azizian (1984) who noted that agreement of their numerical solutions based on energy considerations were not good when negative values of the monosymmetry constant were used or when the load was applied below the shear centre. This was attributed to the choice of a single halve sine wave as an approximating function. It is still, however, clear from the presented results that the existing approaches for obtaining equations for monosymmetric sections do predict the behaviour of the monosymmetric cross section considered in the current study acceptably.

Kitipornchai et al (1986) studied monosymmetric beams subjected to moment gradients and proposed the use of Fourier sine series as shown in equation (4.51) to approximate the deflected shapes of u and ϕ. Equations (4.52) and (4.53) were presented as giving accurate approximations (two terms for the displacement and one term for the rotation):

$$u = \sum_{r=1}^{n} \Delta_r \, sin \frac{r\pi z}{L} \tag{4.51}$$

$$u = \Delta_1 \, sin \frac{\pi z}{L} + \Delta_2 \, sin \frac{2\pi z}{L} \tag{4.52}$$

$$\phi = \theta_1 \, sin \frac{\pi z}{L} \tag{4.53}$$

where, Δ_1, Δ_2 and ϕ are arbitrary constants to be determined.

Timoshenko and Gere (1961) proposed a trigonometric function with two terms as being sufficiently accurate although this was used for a doubly symmetric section loaded with a point load at the shear centre. In their proposed function the authors suggested a two-term trigonometric function based on having expressed the energy function in terms of the rotation term (ϕ) only, after suitable substitution of the deflection term 'u'. The equation used is shown in equation (4.54). The trigonometric function was based on cosine terms since the coordinates were chosen such that the origin was placed at the mid-span of the simply supported beam considered. The authors indicated that taking only the first term, in their case, gave an error of only half of 1%. The error then reduced to one tenth on 1% for the two-term equation.

$$\phi = a_1 \cos \frac{\pi z}{l} + a_2 \cos \frac{3\pi z}{l} \tag{4.54}$$

4.6 CONVERGENCE OF THE ONE TERM SINE FUNCTION

It can be shown that the use of one term for the numerical solution is appropriate due to convergence of the solution even if more terms are considered. The complexity of using two terms for both the rotation term (ϕ) and the displacement term (u) is eliminated by using the approach reported by Timoshenko & Gere (1961) where all terms in the energy equation are expressed in terms of the rotation term function by employing an appropriate relationship. Unlike the approach used by Timoshenko & Gere (1961) which utilised cosine functions due to the position of the origin at midspan in the current study sine terms are used since the origin is at one end of the member. The two single term functions are given in equations (4.24) and (4.25). The relationship between (ϕ) and the displacement term (u) is given in equation (4.56) and is obtained from the kinematic-static approach. This is used to adjust the energy equation so that it is expressed in terms of the rotation term only. The adjusted energy equation is shown in (4.57). The two-term sine function to be used in the numerical determination is presented in equation (4.55). This is the function that will be used in the energy equation to obtain the critical load. Only the point load case is considered here.

$$\phi = B\sin\frac{\pi z}{l} + C\sin\frac{3\pi z}{l} \tag{4.55}$$

$$u'' = -\frac{M\phi}{EI_y} \tag{4.56}$$

$$\Pi = \frac{1}{2}\int_0^L \left(GJ(\phi')^2 + EC_w(\phi'')^2 + M_x\beta_x(\phi')^2\right) dz + \frac{1}{2}\sum Pa{\phi_L}^2 - \int_0^{\frac{L}{2}} \frac{P^2z^2}{4EI_y}\,\phi^2\, dz \tag{4.57}$$

Terms for ϕ, ϕ^2, ϕ', $(\phi')^2$, ϕ'' and $(\phi'')^2$ are required to perform the integrations.

The five terms in (4.57) yield the following after performing the integration:

$$Term\ 1\colon \frac{GJB^2\pi^2}{4L} + \frac{GJC^2\pi^2}{4L} \tag{4.58}$$

$$Term\ 2\text{: } \frac{EC_w B^2 \pi^4}{4L^3} + \frac{81EC_w C^2 \pi^4}{4L^3} \tag{4.59}$$

$$Term\ 3\text{: } \frac{B^2 \pi^2 P \beta_x}{8}\left(\frac{1}{4} - \frac{1}{\pi^2}\right) - \frac{3BCP\beta_x}{4} + \frac{9C^2 \pi^2 P \beta_x}{8}\left(\frac{1}{4} - \frac{1}{9\pi^2}\right) \tag{4.60}$$

$$Term\ 4\text{: } \frac{Pa}{2}(B^2 - 2BC + C^2) \tag{4.61}$$

$$Term\ 5\text{: } \frac{5BCP^2 L^3}{64EI_Y \pi^2} - \frac{B^2 P^2}{4EI_y}\left(\frac{L^3}{48} + \frac{L^3}{8\pi^2}\right) - \frac{C^2 P^2}{4EI_y}\left(\frac{L^3}{48} + \frac{L^3}{72\pi^2}\right) \tag{4.62}$$

Taking the partial derivatives $\frac{\partial \pi}{\partial B}$ and $\frac{\partial \pi}{\partial C}$ to minimize the potential energy function and collecting terms yields the equations presented in matrix form on the page that follows.

$$\begin{bmatrix} \frac{-P^2}{2EI_y}\left(\frac{L^3}{48}+\frac{L^3}{8\pi^2}\right)+P\left(\frac{\pi^2\beta_x}{4}\left[\frac{1}{4}-\frac{1}{\pi^2}\right]+a\right)+\frac{GJ\pi^2}{2L}+\frac{EC_w\pi^4}{2L^3} & \frac{5BCP^2L^3}{64EI_Y\pi^2}-\frac{3BCP\beta_x}{4}-Pa \\ \frac{5BCP^2L^3}{64EI_Y\pi^2}-\frac{3BCP\beta_x}{4}-Pa & \left(\frac{-P^2L^3}{96EI_y}-\frac{P^2L^3}{144\pi^2}\right)+\left(\frac{9P\pi^2\beta_x}{4}\left[\frac{1}{4}-\frac{1}{9\pi^2}\right]+Pa\right)+\frac{9GJ\pi^2}{2L}+\frac{81EC_w\pi^4}{2L^3} \end{bmatrix}\begin{bmatrix} B \\ C \end{bmatrix}=\begin{bmatrix} 0 \\ 0 \end{bmatrix}$$

Setting the determinant equal to zero for the non-trivial solution and solving for 'P' yields a fourth order polynomial. The smallest root of the polynomial gives the desired critical buckling load.

This is tested for a **NF-203x133x25** Beam with top flange loading. The beam has the following properties:

$C_w = 29\ 325\ 507\ 672\ mm^3$	$L = 10\ 000mm$
$I_y = 3\ 075\ 141\ mm^4$	$\alpha = 0$
$J = 54\ 202\ mm^3$	$\beta_x = 0$

One Term Solution: P = 9.28kN

Two-Term solution: P = 9.22kN

*Difference between one-term and two-term solution is 0.65%.

This gives the necessary confidence that the one-term solution has sufficiently converged to be used in the current study.

4.7 THE WAGNER EFFECT IN MONOSYMMETRIC SECTIONS

In this section a brief discussion regarding the source of the Wagner effect in beams is discussed with the derivation of the monosymmetry constant given. During twisting at the critical buckling load, the state of forces is as shown in a slightly twisted fibre in Fig.4-15.

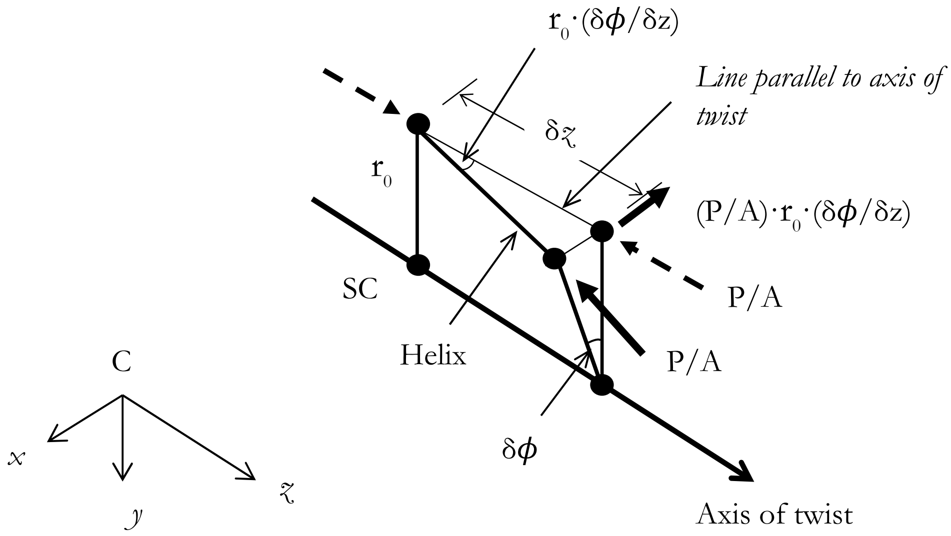

Fig.4-15. Torque exerted by axial stress during twisting. *(Adapted from Trahair, 2011)*

The twisted fibre develops transverse force components in both the compressive side as well as the tensile side. These transverse forces set up moment couples which either increase or decrease the twist. The developed transverse forces with their lever arms are shown in Fig.4-16. In doubly symmetric sections, with similar distance to shear centre, these moments couples cancel out and thus give a monosymmetry constant value of zero.

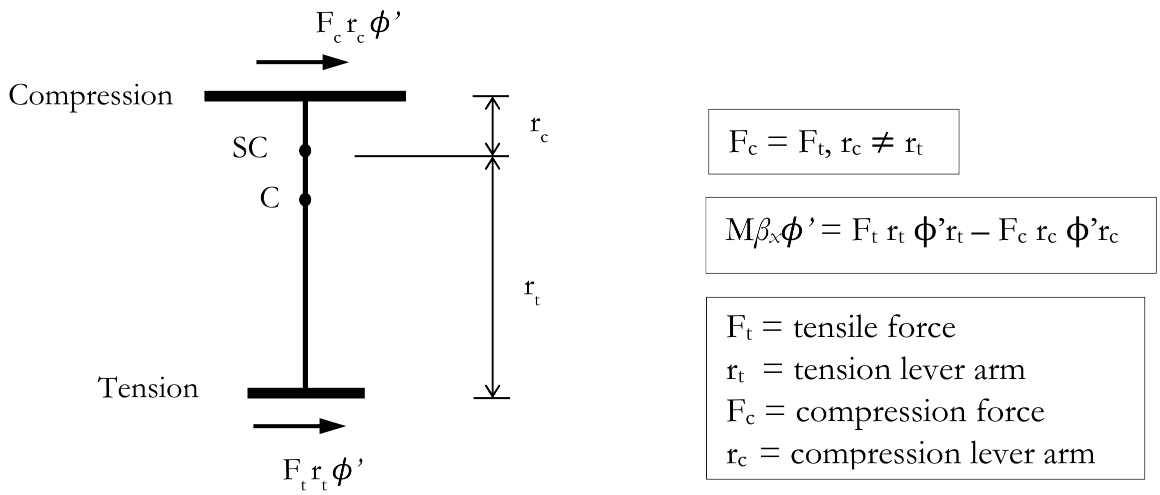

Fig.4-16. Wagner effect in monosymmetric beams. *(Adapted from Trahair, 2011)*

For monosymmetric I-shaped sections when the larger flange is in compression the Wagner effect results in a positive monosymmetry constant which increases the torsional rigidity and thus increase the critical load. A negative monosymmetry constant value results in a decrease in torsional rigidity and an accompanying decrease in the critical load. The derivation of the monosymmetry constant given in equation (3.42) is now presented. The stress from the major axis bending is given in (4.63) and the inclination angle, θ, of the fibre leading to formation of a transverse force component is given by (4.64).

$$\sigma = \frac{M}{I_x} y \tag{4.63}$$

$$\theta = r_0 \frac{\delta \phi}{\delta z} \tag{4.64}$$

The transverse force component becomes:

$$dF = \sigma \, dA \, r_0 \frac{\delta \phi}{\delta z} \tag{4.65}$$

This force forms a moment about the shear centre given by the force magnitude multiplied by the tangential distance to the shear centre. Noting that the rotation moment induced $dT = dF \times r_0$, equation (4.63) can be substituted in (4.65) to give:

$$dT = \frac{M}{I_x} (y \, r_0) dA \, \phi' r_0 \tag{4.66}$$

or

$$dT = \frac{M}{I_x} (y \, {r_0}^2) dA \, \phi' \tag{4.67}$$

Noting that $(y \, r_0^2) = y \, [(x_0 - x)^2 + (y_0 - y)^2]$ relative to the centroidal axis we replace this in (4.67). We also note that $x_0 = 0$ for the section considered in the current study. This results in:

$$dT = \frac{M}{I_x} [(yx^2 + y^3) + (yy_0^2) - (2y_0 y^2)] dA \, \phi' \tag{4.68}$$

Integrating both sides gives the total twist effect:

$$T = \frac{M}{I_x} \left[\int_A yx^2 + y^3 \, dA + y_0 \int_A y \, dA - 2y_0 \int_A y^2 dA \right] \phi' \tag{4.69}$$

The integral $\int_A y \, dA$ becomes zero when evaluated at the centroid and $\int_A y^2 dA$ gives I_x. The equation can therefore be simplified to:

$$T = M \left[\frac{1}{I_x} \int_A yx^2 + y^3 \, dA - 2y_0 \right] \phi' \tag{4.70}$$

The part in the square brackets in (4.70) is the monosymmetry constant, β_x, as given in equation (3.42) earlier. The twist rigidity 'GJ' is therefore adjusted by the effect of ($M\beta_x$).

4.8 CONCLUSION

In this chapter the concept of elastic critical buckling has been introduced and the methods used to determine the critical elastic buckling load discussed. Equations for determining the elastic critical loads for three load cases applied to a simply supported monosymmetric beam were then presented. An existing closed form solution for the load case of uniform moment based on the static-kinematic approach has been discussed. For the other two load cases the Rayleigh-Ritz method was used to solve the potential energy equation and obtain the critical loads. These two solutions have been obtained and presented in the current study for a monosymmetric section beam.

The equations obtained were checked against benchmark problems and finite element analysis results to validate them. It was found that using the existing approaches for obtaining critical loads does generate acceptably accurate equations that predict the critical load for a monosymmetric section with upstands. The convergence of the solution for the selected approach and approximation functions was demonstrated. These equations are applied in the chapter that follows for parametric studies.

In the chapter that follows the trend in critical elastic moment value with change in upstand height was investigated. This was then compared to the point of coincidence of the shear center and centroid determined in Chapter 3. The comparison was essential to determine whether there was any observable correlation between the two. Any correlation would then render the coincidence point a critical parameter in the treatment of these sections.

CHAPTER 5 ELASTIC BUCKLING ANALYSIS OF SELECTED BEAMS

5.1 INTRODUCTION

Having obtained the elastic critical buckling load equations in Chapter 4, these together with the geometric property equations from Chapter 3 are used to study the elastic critical buckling load trends for monosymmetric steel beams stiffened with upstands. The two load cases that are studied are that of a central point load applied on the top flange and that of a uniformly distributed load (UDL) also applied on the top flange. These two load cases are more likely to be encountered in real life structures than that of a uniform moment which is more of a theoretical load case adopted for mathematical expedience. For the point load case equation (4.42) is used to generate the elastic critical moment and for the UDL case equation (4.48) is used. These are used as they facilitate generation of large sets of results compared to finite element analysis which is limited by the amount of time it takes to generate and run the models. The equations have been validated using finite element analysis results in section 4.4.5.

The trends observed are reported based on beams that are grouped according to specific geometric properties such as ratio of upstand height to initial member depth or upstand thickness to flange thickness ratio. It is recognised that in future other parameters for grouping may prove more suitable such as on the basis of the torsional parameter ratio i.e., a ratio involving the St. Venant torsional stiffness to warping torsional stiffness for a given section. This study is a concept study upon whose findings further investigations can be justified. The members selected for the study are chosen from the Southern African Steel Construction Handbook (SASCH, 2016). This contains sizes and properties of all hot-rolled narrow flange and wide flange beams available in South Africa as stock items. Sizes match closely those that are available in the United Kingdom (UK).

5.2 SELECTION OF MEMBERS FOR STUDY

The members selected for the study are shown in Table 5.1. These consist of ten (10) members from the list of narrow flange (NF) sections and four (4) from the list of wide flange (WF) sections. The total number of sections in the SASCH is forty-three (43) NF sections and seventeen (17) WF sections. This therefore represents a sample of 23% from both categories. The selection is based on the ratio of breadth (b) to depth or height (h) of the beam. Two beams each conforming to the following ratios are selected: 0.3, 0.4, 0.5, 0.6, 0.7, 0.9 and 1.0 giving a total of fourteen (14) members. Table 5.1 lists the members in the order that they are presented in the SASCH.

The trends obtained from analysing the members in Table 5.1 are presented in section 5.3 with applications discussed in section 5.4. Discussion on the applications presented is carried out in section 5.5. The corner radii are neglected when applying equations (4.42) and (4.48) for elastic critical loads as well as in the application of equations for cross-section properties from Chapter 3. The prefixes 'NF' and 'WF' are applied to the section designations in the handbook to denote sections used with corner radii neglected.

Table 5.1 Members from SASCH selected for current study

DATABASE OF STRUCTURAL STEEL SECTIONS

I-sections (Parallel flange)

Narrow Flange

Designation	**m**	**H**	**b**	**t_w**	**t_f**			**A**	About x-x	
									I	**Z_e**
mmxmmxkg/m	**kg/m**	**mm**	**mm**	**mm**	**mm**	**b/h**		**10^3 mm^2**	**10^6 mm^4**	**10^3mm^3**
IPE 100	8,10	100	55	4,1	5,7	0,6		1,03	1,71	34,2
IPE 160	15,8	160	82	5	7,4	0,5		2,01	8,69	109
203x133x25	25,1	203,2	133,4	5,7	7,8	0,7		3,22	23,5	231
203x133x30	30,0	206,8	133,8	6,4	9,6	0,7		3,80	28,9	279
254x146x31	31,1	251,5	146,1	6	8,6	0,6		3,99	44,3	352
305x102x25	24,8	304,8	101,6	5,8	7	0,3		3,12	43,6	286
305x102x28	28,2	308,9	101,9	6	8,8	0,3		3,64	54,4	352
305x165x40	40,3	303,8	165,1	6,1	10,2	0,5		5,16	85,5	563
406x140x39	39,0	397,3	141,8	6,3	8,6	0,4		4,92	124	625
533x210x122	122	544,6	211,9	12,8	21,3	0,4		15,6	762	2800

Table 5.1 Members from SASCH selected for current study (CTD')

H-sections (Parallel flange)

Wide Flange

Designation	m	H	b	t_w	t_f			A	About x-x	
									I	Z_e
mmxmmxkg/m	kg/m	mm	mm	mm	mm	b/h		10^3 mm^2	10^6 mm^4	10^3mm^3
152x152x23	23,0	152,4	152,4	6,1	6,8	1,0		2,97	12,6	165
254x254x73	73,1	254,2	254	8,6	14,2	1,0		9,29	114	896
254x254x167	167	289,1	264,5	19,2	31,7	0,9		21,2	299	2070
305x305x158	158	327,2	310,6	15,7	25,0	0,9		20,1	387	2360

The ratio of b/H is indicated in the seventh (7th) column. Beam pairs can be easily identified. A spreadsheet was developed for ease of generating section properties as well as determination of critical loads. For the stiffened beams the upstand height was varied at 10mm intervals up to a value of 130mm. The upper limit was selected to accommodate trends for the deeper sections that have high critical load values.

5.3 TRENDS FROM STUDY OF SELECTED BEAMS

The behaviour with change in simply supported beam span is observed for each beam and results compared. The following spans are considered to try and cover the entire spectrum from stocky to slender: 2m, 4m, 6m, 8m and 10m. The movement of the shear centre and centroid is as per the observations reported in Chapter 3. The point load case is reported first followed by the UDL case.

5.3.1 Trends for the Point Load case

The point load case considered, as before, is that of midspan loading and acting on the top flange. Summaries for all 14 beams are presented in the Figures and Tables that follow based on the (b/H) value of the beams. The trend results for the beams are presented in three sets. First as tabulated results for all spans (Set 1), then results plot of M_{cr} for all spans (Set 2) and finally graphs of normalised M_{cr} against upstand height (Set 3) for the 2m case only. For each beam the increase in the critical elastic moment is tracked with respect to the increase in upstand height.

5.3.1.1 Trends for Beams with (b/H) = 0.3 & 0.4

The sets of results are presented in the sequence indicated in Table 5.2 for the four members considered.

Table 5.2 First group of four 'NF' members

Member	***Beam***	***b/H***	***Set 1***	***Set 2***	***Set 3***
NF 305x102x25	B_1	0.3	Tabulated results for all spans	Plots of M_{cr} for all spans	Graph of normalised M_{cr} against upstand height for 2m span
NF 305x102x28	B_2	0.3			
NF 406x140x39	B_3	0.4			
NF 533x210x122	B_4	0.4			

Table 5.3 Results for NF-305x102x25 with (b/H = 0.3) for all spans considered

Beam: B305x102x25 — 2m

		Upstand Height (mm)													
	Load Position:	0	10	20	30	40	50	60	70	80	90	100	110	120	130
		Critical Moment (kNm)													
B305x102x25	ABOVE FLANGE	85,8	116,9	144,5	167,4	186,1	200,9	212,1	220,1	225,2	228,0	228,8	228,0	226,2	223,8
	% Increase:	-	36,2%	23,6%	15,9%	11,2%	7,9%	5,6%	3,8%	2,3%	1,2%	0,4%	-0,3%	-0,8%	-1,1%
	Cumulative % Inc.	-	36,2%	68,3%	95,1%	116,9%	134,1%	147,2%	156,4%	162,4%	165,6%	166,6%	165,7%	163,6%	160,7%

4m

		Upstand Height (mm)													
	Load Position:	0	10	20	30	40	50	60	70	80	90	100	110	120	130
		Critical Moment (kNm)													
B305x102x25	ABOVE FLANGE	29,9	39,0	47,2	54,3	60,3	65,4	69,5	72,9	75,4	77,4	78,7	79,6	80,1	80,3
	% Increase:	-	30,5%	21,1%	15,0%	11,1%	8,4%	6,3%	4,8%	3,5%	2,6%	1,8%	1,1%	0,6%	0,3%
	Cumulative % Inc.	-	30,5%	58,0%	81,7%	101,9%	118,7%	132,6%	143,7%	152,4%	158,8%	163,4%	166,4%	168,1%	168,8%

6m

		Upstand Height (mm)													
	Load Position:	0	10	20	30	40	50	60	70	80	90	100	110	120	130
		Critical Moment (kNm)													
B305x102x25	ABOVE FLANGE	18,4	23,2	27,7	31,6	35,1	38,1	40,7	42,9	44,8	46,4	47,6	48,7	49,5	50,2
	% Increase:	-	26,3%	19,1%	14,2%	10,9%	8,6%	6,8%	5,5%	4,4%	3,5%	2,8%	2,2%	1,7%	1,3%
	Cumulative % Inc.	-	26,3%	50,5%	71,8%	90,6%	106,9%	121,1%	133,2%	143,5%	152,0%	159,0%	164,7%	169,2%	172,7%

8m

		Upstand Height (mm)													
	Load Position:	0	10	20	30	40	50	60	70	80	90	100	110	120	130
		Critical Moment (kNm)													
B305x102x25	ABOVE FLANGE	13,6	16,9	19,9	22,5	25,0	27,1	29,1	30,8	32,3	33,6	34,8	35,8	36,6	37,4
	% Increase:	-	23,7%	17,7%	13,6%	10,7%	8,7%	7,1%	5,9%	4,9%	4,1%	3,4%	2,9%	2,4%	2,0%
	Cumulative % Inc.	-	23,7%	45,6%	65,4%	83,1%	99,0%	113,2%	125,8%	136,9%	146,6%	155,1%	162,4%	168,7%	174,1%

10m

		Upstand Height (mm)													
	Load Position:	0	10	20	30	40	50	60	70	80	90	100	110	120	130
		Critical Moment (kNm)													
B305x102x25	ABOVE FLANGE	11,0	13,4	15,6	17,7	19,5	21,2	22,8	24,2	25,5	26,6	27,6	28,6	29,4	30,1
	% Increase:	-	22,0%	16,8%	13,1%	10,6%	8,7%	7,3%	6,2%	5,3%	4,5%	3,9%	3,3%	2,9%	2,5%
	Cumulative % Inc.	-	22,0%	42,4%	61,1%	78,1%	93,6%	107,7%	120,6%	132,1%	142,6%	152,0%	160,4%	167,9%	174,5%

Table 5.4 Results for NF-305x102x28 with (b/H = 0.3) for all spans considered

Beam: B305x102x28 2m

		Upstand Height (mm)													
	Load Position:	0	10	20	30	40	50	60	70	80	90	100	110	120	130
		Critical Moment (kNm)													
B305x102x28	ABOVE FLANGE	113,1	150,6	185,0	213,9	237,7	256,8	271,6	282,5	290,1	294,7	296,9	297,2	296,0	293,9
	% Increase:		33,1%	22,8%	15,6%	11,1%	8,0%	5,8%	4,0%	2,7%	1,6%	0,7%	0,1%	-0,4%	-0,7%
	Cumulative % Inc.		33,1%	63,5%	89,1%	110,1%	127,0%	140,0%	149,7%	156,4%	160,4%	162,4%	162,6%	161,6%	159,8%

4m

		Upstand Height (mm)													
	Load Position:	0	10	20	30	40	50	60	70	80	90	100	110	120	130
		Critical Moment (kNm)													
B305x102x28	ABOVE FLANGE	41,2	52,7	63,4	72,8	81,0	88,0	93,9	98,8	102,9	106,1	108,7	110,6	112,0	113,0
	% Increase:		27,9%	20,4%	14,8%	11,2%	8,6%	6,7%	5,3%	4,1%	3,2%	2,4%	1,8%	1,3%	0,9%
	Cumulative % Inc.		27,9%	54,0%	76,9%	96,7%	113,7%	128,1%	140,1%	149,9%	157,8%	163,9%	168,6%	172,1%	174,5%

6m

		Upstand Height (mm)													
	Load Position:	0	10	20	30	40	50	60	70	80	90	100	110	120	130
B305x102x28	ABOVE FLANGE	25,9	32,2	38,2	43,6	48,5	52,8	56,6	60,0	63,0	65,6	67,8	69,7	71,4	72,8
	% Increase:		24,4%	18,6%	14,1%	11,1%	8,9%	7,3%	6,0%	5,0%	4,1%	3,4%	2,8%	2,4%	2,0%
	Cumulative % Inc.		24,4%	47,6%	68,4%	87,1%	103,7%	118,5%	131,6%	143,1%	153,1%	161,7%	169,2%	175,5%	180,9%

8m

		Upstand Height (mm)													
	Load Position:	0	10	20	30	40	50	60	70	80	90	100	110	120	130
		Critical Moment (kNm)													
B305x102x28	ABOVE FLANGE	19,4	23,7	27,8	31,6	35,1	38,2	41,1	43,7	46,1	48,3	50,2	51,9	53,5	54,9
	% Increase:		22,3%	17,4%	13,6%	10,9%	9,0%	7,5%	6,4%	5,4%	4,7%	4,0%	3,5%	3,0%	2,6%
	Cumulative % Inc.		22,3%	43,5%	63,0%	80,8%	97,1%	112,0%	125,5%	137,8%	148,9%	158,9%	167,9%	176,0%	183,2%

10m

		Upstand Height (mm)													
	Load Position:	0	10	20	30	40	50	60	70	80	90	100	110	120	130
		Critical Moment (kNm)													
B305x102x28	ABOVE FLANGE	15,7	18,9	22,1	25,0	27,7	30,2	32,5	34,7	36,6	38,5	40,2	41,7	43,2	44,5
	% Increase:		20,9%	16,6%	13,2%	10,8%	9,0%	7,7%	6,6%	5,7%	5,0%	4,4%	3,9%	3,4%	3,1%
	Cumulative % Inc.		20,9%	40,9%	59,5%	76,7%	92,6%	107,4%	121,2%	133,8%	145,6%	156,4%	166,3%	175,5%	183,9%

Table 5.5 Results for NF-406x140x39 with (b/H = 0.4) for all spans considered

Beam: B406x140x39

2m

		Upstand Height (mm)													
	Load Position:	0	10	20	30	40	50	60	70	80	90	100	110	120	130
		Critical Moment (kNm)													
B406x140x39	ABOVE FLANGE	340,4	437,6	527,5	606,0	673,6	731,0	778,5	817,0	847,0	869,3	884,6	893,8	897,6	897,0
	% Increase:		28,6%	20,6%	14,9%	11,2%	8,5%	6,5%	4,9%	3,7%	2,6%	1,8%	1,0%	0,4%	-0,1%
	Cumulative % Inc.		28,6%	55,0%	78,0%	97,9%	114,7%	128,7%	140,0%	148,8%	155,4%	159,9%	162,6%	163,7%	163,5%

4m

		Upstand Height (mm)													
	Load Position:	0	10	20	30	40	50	60	70	80	90	100	110	120	130
		Critical Moment (kNm)													
B406x140x39	ABOVE FLANGE	100,7	126,9	151,3	172,9	191,8	208,2	222,1	233,8	243,4	251,0	256,9	261,2	264,0	265,7
	% Increase:		26,0%	19,3%	14,3%	10,9%	8,5%	6,7%	5,3%	4,1%	3,1%	2,3%	1,7%	1,1%	0,6%
	Cumulative % Inc.		26,0%	50,3%	71,8%	90,6%	106,8%	120,7%	132,3%	141,8%	149,4%	155,2%	159,4%	162,3%	163,9%

6m

		Upstand Height (mm)													
	Load Position:	0	10	20	30	40	50	60	70	80	90	100	110	120	130
		Critical Moment (kNm)													
B406x140x39	ABOVE FLANGE	55,1	68,0	80,2	91,1	100,7	109,3	116,8	123,3	128,9	133,6	137,5	140,6	143,1	145,0
	% Increase:		23,4%	17,8%	13,6%	10,6%	8,5%	6,9%	5,6%	4,5%	3,6%	2,9%	2,3%	1,8%	1,3%
	Cumulative % Inc.		23,4%	45,4%	65,2%	82,7%	98,3%	111,9%	123,7%	133,8%	142,3%	149,3%	155,1%	159,6%	163,0%

8m

		Upstand Height (mm)													
	Load Position:	0	10	20	30	40	50	60	70	80	90	100	110	120	130
		Critical Moment (kNm)													
B406x140x39	ABOVE FLANGE	38,2	46,3	54,0	61,0	67,3	73,0	78,1	82,6	86,6	90,1	93,1	95,7	97,9	99,8
	% Increase:		21,3%	16,6%	12,9%	10,3%	8,4%	7,0%	5,8%	4,8%	4,0%	3,4%	2,8%	2,3%	1,9%
	Cumulative % Inc.		21,3%	41,4%	59,6%	76,2%	91,0%	104,3%	116,2%	126,6%	135,8%	143,7%	150,5%	156,2%	161,0%

10m

		Upstand Height (mm)													
	Load Position:	0	10	20	30	40	50	60	70	80	90	100	110	120	130
		Critical Moment (kNm)													
B406x140x39	ABOVE FLANGE	29,7	35,5	41,0	46,1	50,7	55,0	58,8	62,3	65,5	68,3	70,8	73,1	75,1	76,8
	% Increase:		19,6%	15,6%	12,4%	10,1%	8,4%	7,0%	5,9%	5,1%	4,3%	3,7%	3,2%	2,7%	2,3%
	Cumulative % Inc.		19,6%	38,3%	55,4%	71,0%	85,3%	98,3%	110,1%	120,7%	130,2%	138,7%	146,3%	152,9%	158,8%

Table 5.6 Results for NF-533x210x122 with (b/H = 0.4) for all spans considered

Beam: B533x210x122 2m

		Upstand Height (mm)													
	Load Position:	0	10	20	30	40	50	60	70	80	90	100	110	120	130
		Critical Moment (kNm)													
B533x210x122	ABOVE FLANGE	3 812,2	4 355,6	4 982,7	5 553,3	6 069,5	6 533,4	6 946,9	7 311,9	7 630,8	7 905,6	8 138,7	8 332,6	8 489,9	8 613,1
	% Increase:		14,3%	14,4%	11,5%	9,3%	7,6%	6,3%	5,3%	4,4%	3,6%	2,9%	2,4%	1,9%	1,5%
	Cumulative % Inc.		14,3%	30,7%	45,7%	59,2%	71,4%	82,2%	91,8%	100,2%	107,4%	113,5%	118,6%	122,7%	125,9%

4m

		Upstand Height (mm)													
	Load Position:	0	10	20	30	40	50	60	70	80	90	100	110	120	130
		Critical Moment (kNm)													
B533x210x122	ABOVE FLANGE	1 164,9	1 317,7	1 492,9	1 654,2	1 802,1	1 937,1	2 059,7	2 170,4	2 269,6	2 358,0	2 436,0	2 504,1	2 563,0	2 613,1
	% Increase:		13,1%	13,3%	10,8%	8,9%	7,5%	6,3%	5,4%	4,6%	3,9%	3,3%	2,8%	2,4%	2,0%
	Cumulative % Inc.		13,1%	28,2%	42,0%	54,7%	66,3%	76,8%	86,3%	94,8%	102,4%	109,1%	115,0%	120,0%	124,3%

6m

		Upstand Height (mm)													
	Load Position:	0	10	20	30	40	50	60	70	80	90	100	110	120	130
		Critical Moment (kNm)													
B533x210x122	ABOVE FLANGE	656,4	735,4	824,9	908,3	985,8	1 057,6	1 124,1	1 185,2	1 241,4	1 292,7	1 339,4	1 381,7	1 419,8	1 453,9
	% Increase:		12,0%	12,2%	10,1%	8,5%	7,3%	6,3%	5,4%	4,7%	4,1%	3,6%	3,2%	2,8%	2,4%
	Cumulative % Inc.		12,0%	25,7%	38,4%	50,2%	61,1%	71,2%	80,6%	89,1%	96,9%	104,0%	110,5%	116,3%	121,5%

8m

		Upstand Height (mm)													
	Load Position:	0	10	20	30	40	50	60	70	80	90	100	110	120	130
		Critical Moment (kNm)													
B533x210x122	ABOVE FLANGE	464,0	515,8	573,9	628,5	679,8	728,0	773,1	815,3	854,7	891,3	925,4	956,9	986,0	1 012,8
	% Increase:		11,2%	11,3%	9,5%	8,2%	7,1%	6,2%	5,5%	4,8%	4,3%	3,8%	3,4%	3,0%	2,7%
	Cumulative % Inc.		11,2%	23,7%	35,5%	46,5%	56,9%	66,6%	75,7%	84,2%	92,1%	99,4%	106,2%	112,5%	118,3%

10m

		Upstand Height (mm)													
	Load Position:	0	10	20	30	40	50	60	70	80	90	100	110	120	130
		Critical Moment (kNm)													
B533x210x122	ABOVE FLANGE	364,5	402,9	445,5	485,8	524,0	560,2	594,4	626,7	657,3	686,0	713,1	738,5	762,4	784,8
	% Increase:		10,5%	10,6%	9,1%	7,9%	6,9%	6,1%	5,4%	4,9%	4,4%	3,9%	3,6%	3,2%	2,9%
	Cumulative % Inc.		10,5%	22,2%	33,3%	43,8%	53,7%	63,1%	71,9%	80,3%	88,2%	95,6%	102,6%	109,2%	115,3%

Tabulated results for all spans for the four members under consideration have been presented in Tables 5.3 to 5.6. These results are for five (5) different spans considered. These are 2m, 4m, 6m, 8m and 10m. It is observed from the tables that a similar trend emerges for each member. At short upstand heights the increase in the critical elastic moment is relatively high. As the upstand height increases the increase in the critical elastic moment diminishes. In some cases, for the large upstand heights the critical elastic moments reaches a peak and starts to diminish with increasing upstand height. It can also be noted that with increase in span the rate at which the critical elastic moment increases with increase in upstand height diminishes. This means that the observed trend in terms of the change in critical elastic moment is not only sensitive to upstand height but also to the span of the member. The observed trend matches that observed with the movement of the shear centre relative to the centroid in Chapter 3. In that case the shear centre moves upwards away from the centroid reaches a peak and then starts to migrate downwards. It appears that the trend for the critical elastic moment mimics that observed with the shear centre movement and therefore there is a correlation that can be observed. Again, this will be examined for the cases that follow.

It appears from the tabulated results that the gain in critical elastic moment appears to diminish with an increase in the (b/H) value. This trend will be monitored for the cases that follow to determine whether this sensitivity to the degree of member width to height ratio is consistent. It must be indicated though that the plate thicknesses are not accounted for in the ratio used.

.

Table 5.7 Results for NF-305x102x25 with (b/H = 0.3) – All spans consolidated trend (M_{cr})

	Updtand height (m)													
Span (m)	0	10	20	30	40	50	60	70	80	90	100	110	120	130
	M_{cr} (kNm)													
2	85,8	116,9	144,5	167,4	186,1	200,9	212,1	220,1	225,2	228,0	228,8	228,0	226,2	223,8
4	29,9	39,0	47,2	54,3	60,3	65,4	69,5	72,9	75,4	77,4	78,7	79,6	80,1	80,3
6	18,4	23,2	27,7	31,6	35,1	38,1	40,7	42,9	44,8	46,4	47,6	48,7	49,5	50,2
8	13,6	16,9	19,9	22,5	25,0	27,1	29,1	30,8	32,3	33,6	34,8	35,8	36,6	37,4
10	11,0	13,4	15,6	17,7	19,5	21,2	22,8	24,2	25,5	26,6	27,6	28,6	29,4	30,1

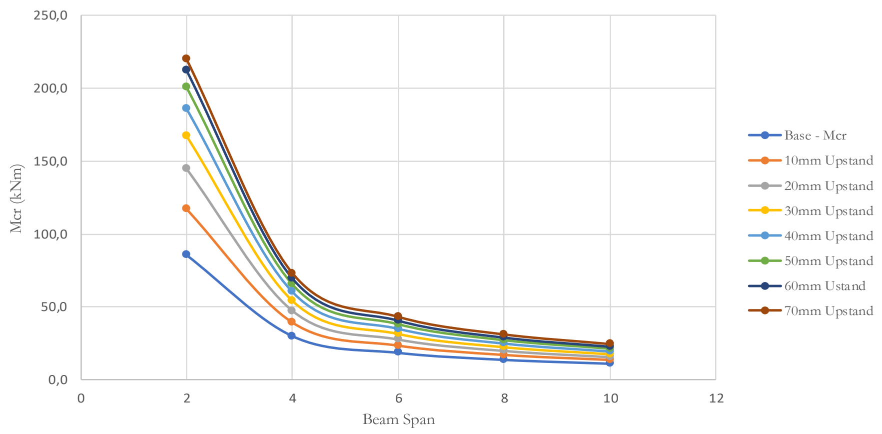

Table 5.8 Results for NF-305x102x28 with (b/H = 0.3) – All spans consolidated trend (M_{cr})

	Upstand Height (m)													
Span (m)	0	10	20	30	40	50	60	70	80	90	100	110	120	130
	M_{cr} (kNm)													
2	113,1	150,6	185,0	213,9	237,7	256,8	271,6	282,5	290,1	294,7	296,9	297,2	296,0	293,9
4	41,2	52,7	63,4	72,8	81,0	88,0	93,9	98,8	102,9	106,1	108,7	110,6	112,0	113,0
6	25,9	32,2	38,2	43,6	48,5	52,8	56,6	60,0	63,0	65,6	67,8	69,7	71,4	72,8
8	19,4	23,7	27,8	31,6	35,1	38,2	41,1	43,7	46,1	48,3	50,2	51,9	53,5	54,9
10	15,7	18,9	22,1	25,0	27,7	30,2	32,5	34,7	36,6	38,5	40,2	41,7	43,2	44,5

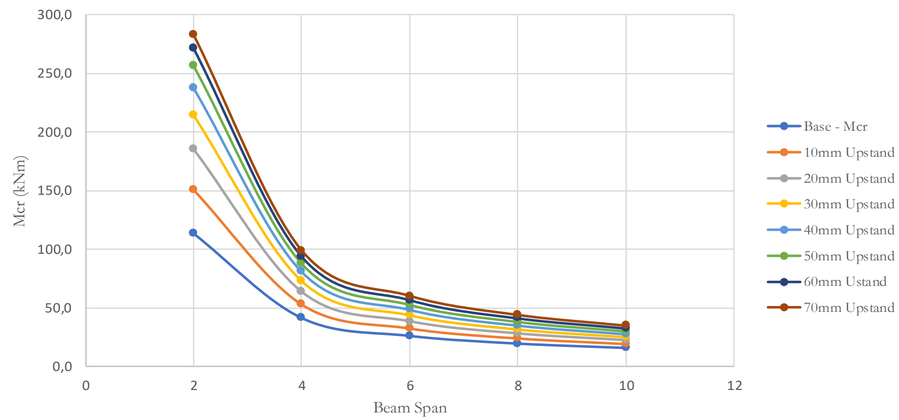

Table 5.9 Results for NF-406x140x39 (b/H = 0.4) – All spans consolidated trend (M_{cr}) - UDL

Span	Upstand Height (mm)													
	0	10	20	30	40	50	60	70	80	90	100	110	120	130
	Mcr (kNm)													
2	302,9	391,6	474,4	547,3	610,6	664,7	709,8	746,5	775,3	796,6	811,1	819,4	822,4	820,7
4	88,8	112,5	134,8	154,6	172,0	187,2	200,1	211,0	219,9	227,0	232,3	236,1	238,5	239,7
6	48,2	59,7	70,6	80,4	89,2	97,0	103,8	109,7	114,7	119,0	122,4	125,2	127,3	128,8
8	33,1	40,2	47,1	53,3	58,9	64,0	68,5	72,5	76,1	79,2	81,8	84,1	85,9	87,4
10	25,5	30,5	35,4	39,9	43,9	47,7	51,1	54,1	56,9	59,4	61,5	63,4	65,1	66,5

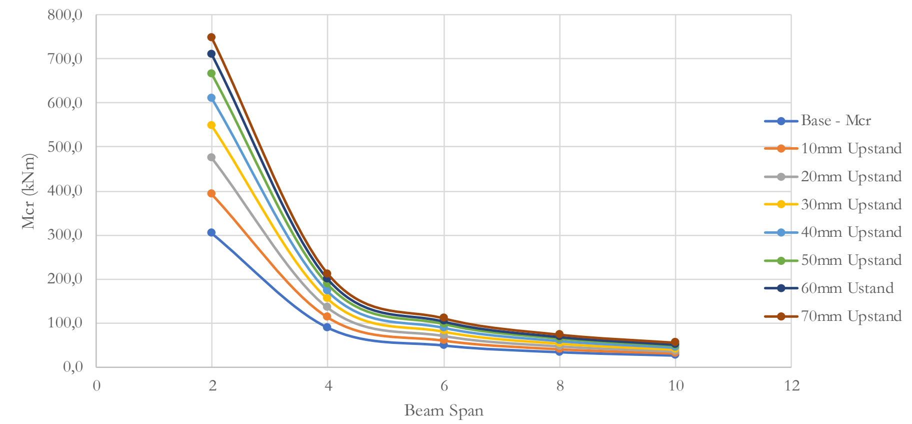

Table 5.10 Results for NF-533x210x122 (b/H = 0.4) – All spans consolidated trend (M_{cr}) – UDL

Span	Upstand Height (mm)													
	0	10	20	30	40	50	60	70	80	90	100	110	120	130
	Mcr (kNm)													
2	3 394,8	3 890,3	4 464,7	4 990,4	5 468,5	5 900,1	6 286,5	6 629,0	6 929,0	7 188,1	7 408,0	7 590,6	7 737,9	7 852,1
4	1 026,8	1 164,6	1 323,0	1 469,4	1 604,1	1 727,4	1 839,7	1 941,2	2 032,3	2 113,3	2 184,7	2 246,8	2 300,2	2 345,2
6	572,0	642,2	721,9	796,4	865,8	930,1	989,7	1 044,6	1 094,9	1 140,8	1 182,5	1 220,0	1 253,7	1 283,6
8	400,1	445,6	496,7	544,8	590,0	632,5	672,2	709,4	744,0	776,2	806,0	833,5	858,8	881,9
10	311,6	345,0	382,0	417,1	450,3	481,8	511,6	539,7	566,2	591,1	614,5	636,4	656,9	676,0

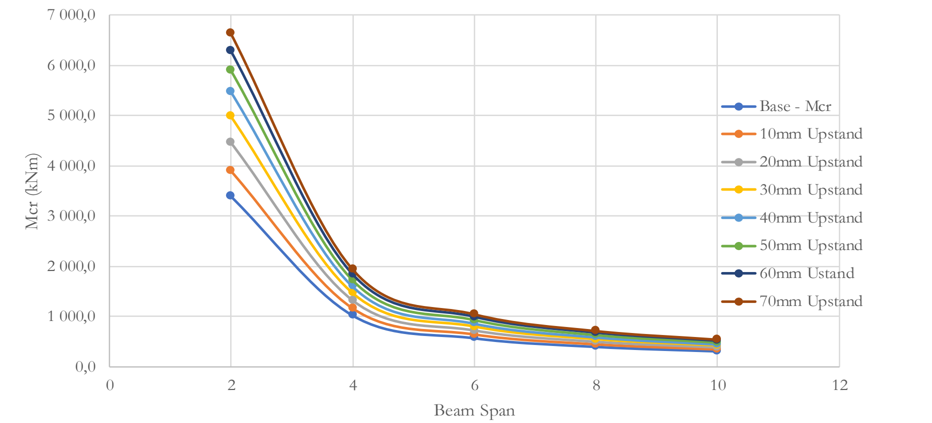

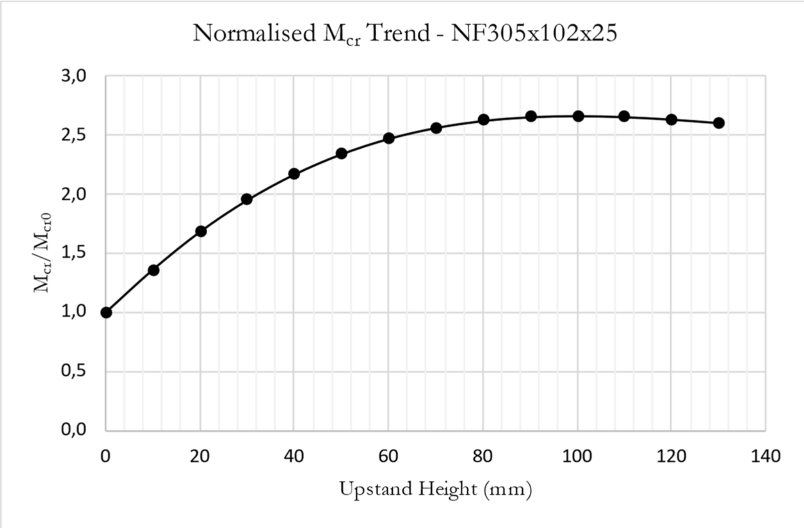

Fig.5-1 Normalised critical moment vs upstand height - B_1

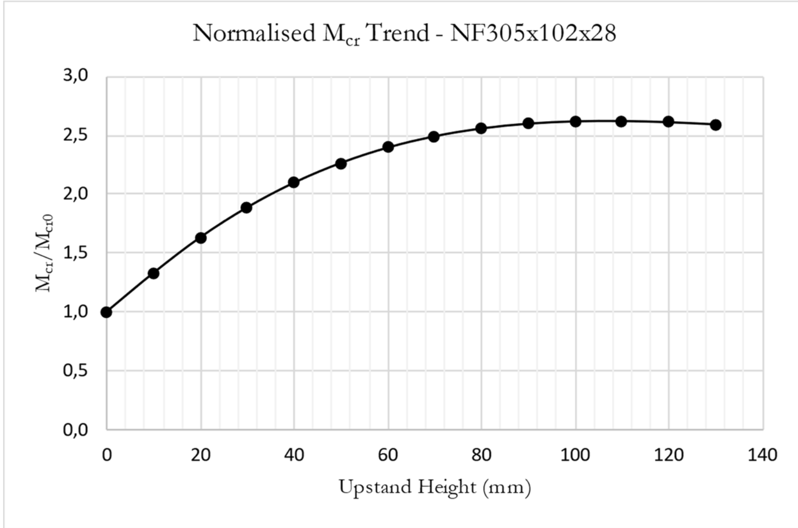

Fig.5-2 Normalised critical moment vs upstand height – B2

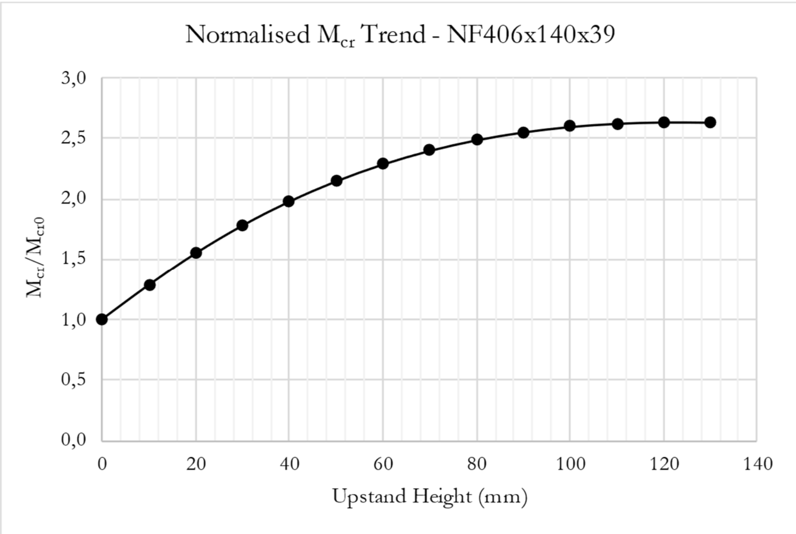

Fig.5-3 Normalised critical moment vs upstand height - B_3

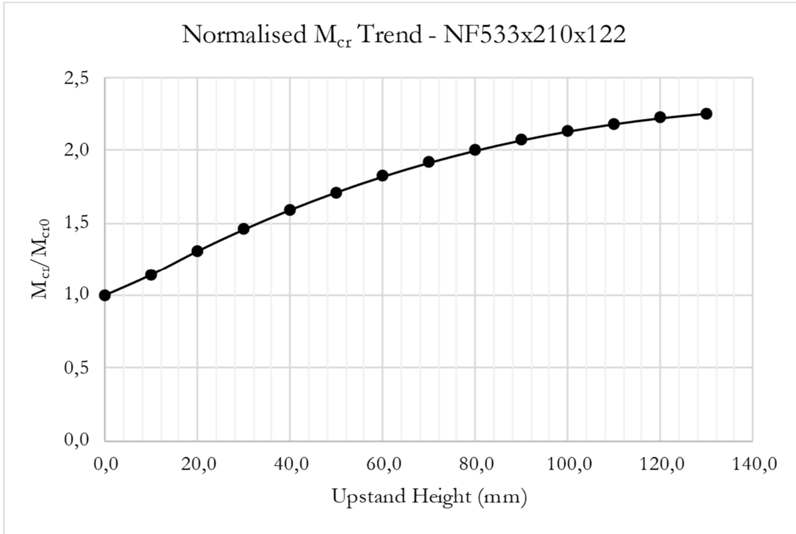

Fig.5-4 Normalised critical moment vs upstand height – B_4

The results presented in the Tables 5.7 to 5.10 illustrate how as the span length increases the relative increase in the critical elastic moment decreases. This shows that the greatest strength gain for a given increase in upstand height is obtained for shorter spans than for longer ones for the beams considered. This is consistent for all four members. The converging curves illustrate this reduced increase at the higher spans. However, for all spans considered there is a change in the critical elastic moment for a corresponding change in the upstand height. The fact that this change is diminishing with increase in upstand height can be observed for the 2m span case.

Fig's 5.1 to 5.4 also illustrate the increase in critical elastic moment with upstand height. Here the diminishing increase with upstand height is clearly illustrated. Very distinct with a peak value appearing to be reached for Beams B1, B2 and B3. No peak value but a similar trend observed for B4. The implications of this trend for member performance and design are addressed later.

5.3.1.2 Trends for Beams with (b/H) = 0.5 & 0.6

The sets of results are presented in the sequence indicated in Table 5.11 for the four members considered.

Table 5.11 Second group of four 'NF' members

Member	***Beam***	***b/H***	***Set 1***	***Set 2***	***Set 3***
NF IPE 160	B_5	0.5	Tabulated results for all spans	Plots of M_{cr} for all spans	Graph of normalised M_{cr} against upstand height for 2m span
NF 305x165x40	B_6	0.5			
NF IPE 100	B_7	0.6			
NF 254x146x31	B_8	0.6			

Table 5.12 Results for NF-IPE 160 with (b/H = 0.5) for all spans considered

Beam: IPE 160 — 2m

		Upstand Height (mm)													
	Load Position:	0	10	20	30	40	50	60	70	80	90	100	110	120	130
		Critical Elastic Moment (kNm)													
IPE 160	ABOVE FLANGE	35,4	47,1	56,8	64,2	69,5	73,0	75,2	76,3	76,7	76,8	76,6	76,6	76,6	77,0
	% Increase:		32,8%	20,7%	13,0%	8,2%	5,1%	3,0%	1,5%	0,6%	0,0%	-0,2%	-0,1%	0,1%	0,4%
	Cumulative % Inc.		32,8%	60,3%	81,1%	96,0%	106,0%	112,1%	115,3%	116,5%	116,6%	116,3%	116,1%	116,3%	117,3%

4m

		Upstand Height (mm)													
	Load Position:	0	10	20	30	40	50	60	70	80	90	100	110	120	130
		Critical Elastic Moment (kNm)													
IPE 160	ABOVE FLANGE	16,5	21,0	25,1	28,5	31,3	33,7	35,6	37,2	38,4	39,4	40,2	40,8	41,4	41,8
	% Increase:		27,1%	19,1%	13,6%	10,0%	7,6%	5,7%	4,4%	3,4%	2,6%	2,0%	1,6%	1,3%	1,1%
	Cumulative % Inc.		27,1%	51,4%	72,0%	89,3%	103,6%	115,3%	124,8%	132,3%	138,3%	143,1%	146,9%	150,1%	152,8%

6m

		Upstand Height (mm)													
	Load Position:	0	10	20	30	40	50	60	70	80	90	100	110	120	130
		Critical Elastic Moment (kNm)													
IPE 160	ABOVE FLANGE	11,3	14,1	16,6	18,9	20,9	22,7	24,2	25,6	26,8	27,8	28,7	29,5	30,2	30,8
	% Increase:		24,7%	18,2%	13,7%	10,7%	8,5%	6,9%	5,7%	4,7%	3,9%	3,3%	2,8%	2,3%	2,0%
	Cumulative % Inc.		24,7%	47,3%	67,4%	85,3%	101,1%	114,9%	127,1%	137,7%	146,9%	155,0%	162,0%	168,1%	173,5%

8m

		Upstand Height (mm)													
	Load Position:	0	10	20	30	40	50	60	70	80	90	100	110	120	130
		Critical Elastic Moment (kNm)													
IPE 160	ABOVE FLANGE	8,6	10,7	12,5	14,3	15,8	17,2	18,5	19,7	20,8	21,7	22,6	23,4	24,1	24,7
	% Increase:		23,3%	17,6%	13,6%	10,9%	9,0%	7,5%	6,3%	5,4%	4,6%	4,0%	3,5%	3,1%	2,7%
	Cumulative % Inc.		23,3%	45,1%	64,9%	82,9%	99,3%	114,2%	127,8%	140,1%	151,2%	161,2%	170,4%	178,6%	186,1%

10m

		Upstand Height (mm)													
	Load Position:	0	10	20	30	40	50	60	70	80	90	100	110	120	130
		Critical Elastic Moment (kNm)													
IPE 160	ABOVE FLANGE	7,0	8,6	10,1	11,5	12,8	13,9	15,0	16,0	17,0	17,8	18,6	19,4	20,1	20,7
	% Increase:		22,5%	17,3%	13,6%	11,1%	9,2%	7,8%	6,7%	5,8%	5,1%	4,5%	4,0%	3,5%	3,2%
	Cumulative % Inc.		22,5%	43,7%	63,3%	81,4%	98,1%	113,7%	128,1%	141,4%	153,7%	165,1%	175,6%	185,4%	194,4%

Table 5.13 Results for NF-305x165x40 with (b/H = 0.5) for all spans considered

Beam: B305x165x40 2m

		Upstand Height (mm)													
	Load Position:	0	10	20	30	40	50	60	70	80	90	100	110	120	130
		Critical Elastic Moment (kNm)													
B305x165x40	ABOVE FLANGE	491,1	604,5	708,4	796,2	868,6	926,6	971,4	1 004,0	1 025,8	1 038,3	1 042,9	1 041,1	1 034,4	1 024,3
	% Increase:		23,1%	17,2%	12,4%	9,1%	6,7%	4,8%	3,4%	2,2%	1,2%	0,4%	-0,2%	-0,6%	-1,0%
	Cumulative % Inc.		23,1%	44,2%	62,1%	76,9%	88,7%	97,8%	104,4%	108,9%	111,4%	112,3%	112,0%	110,6%	108,6%

4m

		Upstand Height (mm)													
	Load Position:	0	10	20	30	40	50	60	70	80	90	100	110	120	130
		Critical Elastic Moment (kNm)													
B305x165x40	ABOVE FLANGE	152,8	184,7	214,3	239,9	261,7	280,0	294,9	306,8	315,9	322,6	327,1	329,8	331,0	331,0
	% Increase:		20,8%	16,0%	12,0%	9,1%	7,0%	5,3%	4,0%	3,0%	2,1%	1,4%	0,8%	0,4%	0,0%
	Cumulative % Inc.		20,8%	40,2%	57,0%	71,2%	83,2%	93,0%	100,8%	106,7%	111,1%	114,0%	115,8%	116,6%	116,6%

6m

		Upstand Height (mm)													
	Load Position:	0	10	20	30	40	50	60	70	80	90	100	110	120	130
		Critical Elastic Moment (kNm)													
B305x165x40	ABOVE FLANGE	87,4	103,7	119,1	132,8	144,8	155,2	164,1	171,7	177,9	183,1	187,2	190,3	192,7	194,4
	% Increase:		18,7%	14,9%	11,5%	9,0%	7,2%	5,8%	4,6%	3,7%	2,9%	2,2%	1,7%	1,3%	0,9%
	Cumulative % Inc.		18,7%	36,4%	52,0%	65,7%	77,6%	87,8%	96,5%	103,7%	109,6%	114,2%	117,9%	120,6%	122,6%

8m

		Upstand Height (mm)													
	Load Position:	0	10	20	30	40	50	60	70	80	90	100	110	120	130
		Critical Elastic Moment (kNm)													
B305x165x40	ABOVE FLANGE	62,3	72,9	83,1	92,2	100,5	107,8	114,3	120,0	124,9	129,2	132,9	136,0	138,6	140,7
	% Increase:		17,1%	13,9%	11,0%	8,9%	7,3%	6,0%	5,0%	4,1%	3,4%	2,8%	2,3%	1,9%	1,5%
	Cumulative % Inc.		17,1%	33,4%	48,1%	61,3%	73,0%	83,5%	92,6%	100,6%	107,5%	113,4%	118,3%	122,5%	125,9%

10m

		Upstand Height (mm)													
	Load Position:	0	10	20	30	40	50	60	70	80	90	100	110	120	130
		Critical Elastic Moment (kNm)													
B305x165x40	ABOVE FLANGE	49,2	57,0	64,5	71,4	77,7	83,3	88,5	93,1	97,3	101,0	104,3	107,2	109,7	111,9
	% Increase:		15,9%	13,2%	10,6%	8,8%	7,3%	6,2%	5,2%	4,5%	3,8%	3,3%	2,8%	2,4%	2,0%
	Cumulative % Inc.		15,9%	31,2%	45,2%	57,9%	69,5%	80,0%	89,4%	97,9%	105,4%	112,1%	118,0%	123,2%	127,7%

Table 5.14 Results for NF-IPE 100 with (b/H = 0.6) for all spans considered

Beam: IPE 100 2m

		Upstand Height (mm)													
	Load Position:	0	10	20	30	40	50	60	70	80	90	100	110	120	130
		Critical Elastic Moment (kNm)													
IPE 100	ABOVE FLANGE	8,9	12,3	14,9	16,9	18,3	19,3	19,9	20,3	20,6	20,9	21,2	21,5	21,9	22,4
	% Increase:		37,8%	21,8%	13,2%	8,2%	5,2%	3,3%	2,1%	1,5%	1,3%	1,4%	1,5%	1,8%	2,1%
	Cumulative % Inc.		37,8%	67,8%	90,0%	105,6%	116,3%	123,4%	128,1%	131,6%	134,7%	137,9%	141,6%	146,0%	151,3%

4m

		Upstand Height (mm)													
	Load Position:	0	10	20	30	40	50	60	70	80	90	100	110	120	130
		Critical Elastic Moment (kNm)													
IPE 100	ABOVE FLANGE	4,6	6,2	7,5	8,7	9,6	10,5	11,1	11,7	12,2	12,6	13,0	13,3	13,6	13,9
	% Increase:		33,0%	21,7%	15,2%	11,2%	8,5%	6,6%	5,2%	4,2%	3,4%	2,8%	2,4%	2,1%	1,9%
	Cumulative % Inc.		33,0%	62,0%	86,6%	107,6%	125,2%	140,1%	152,6%	163,2%	172,2%	179,9%	186,7%	192,8%	198,4%

6m

		Upstand Height (mm)													
	Load Position:	0	10	20	30	40	50	60	70	80	90	100	110	120	130
		Critical Elastic Moment (kNm)													
IPE 100	ABOVE FLANGE	3,2	4,2	5,1	5,9	6,6	7,3	7,9	8,4	8,8	9,3	9,6	10,0	10,3	10,6
	% Increase:		31,3%	21,6%	15,8%	12,2%	9,8%	8,0%	6,6%	5,5%	4,7%	4,0%	3,5%	3,1%	2,7%
	Cumulative % Inc.		31,3%	59,7%	85,0%	107,6%	127,9%	146,0%	162,3%	176,8%	189,8%	201,6%	212,2%	221,8%	230,6%

8m

		Upstand Height (mm)													
	Load Position:	0	10	20	30	40	50	60	70	80	90	100	110	120	130
		Critical Elastic Moment (kNm)													
IPE 100	ABOVE FLANGE	2,4	3,2	3,9	4,5	5,1	5,6	6,1	6,5	6,9	7,3	7,7	8,0	8,3	8,6
	% Increase:		30,5%	21,4%	16,1%	12,8%	10,4%	8,7%	7,4%	6,3%	5,5%	4,8%	4,2%	3,8%	3,4%
	Cumulative % Inc.		30,5%	58,5%	84,0%	107,5%	129,1%	149,0%	167,3%	184,2%	199,7%	214,1%	227,4%	239,7%	251,1%

10m

		Upstand Height (mm)													
	Load Position:	0	10	20	30	40	50	60	70	80	90	100	110	120	130
		Critical Elastic Moment (kNm)													
IPE 100	ABOVE FLANGE	2,0	2,6	3,1	3,6	4,1	4,5	5,0	5,3	5,7	6,0	6,4	6,7	6,9	7,2
	% Increase:		30,0%	21,4%	16,3%	13,1%	10,8%	9,1%	7,8%	6,8%	6,0%	5,3%	4,7%	4,2%	3,8%
	Cumulative % Inc.		30,0%	57,7%	83,5%	107,4%	129,8%	150,7%	170,4%	188,7%	206,0%	222,1%	237,3%	251,6%	265,1%

Table 5.15 Results for NF-254x146x31 with (b/H = 0.6) for all spans considered

Beam: B254x146x31 2m

		Upstand Height (mm)													
	Load Position:	0	10	20	30	40	50	60	70	80	90	100	110	120	130
		Critical Elastic Moment (kNm)													
B254x146x31	ABOVE FLANGE	246,0	309,1	364,5	409,4	444,7	471,0	489,3	500,6	506,1	506,8	504,1	498,9	492,2	485,1
	% Increase:		25,6%	17,9%	12,3%	8,6%	5,9%	3,9%	2,3%	1,1%	0,2%	-0,5%	-1,0%	-1,3%	-1,4%
	Cumulative % Inc.		25,6%	48,1%	66,4%	80,7%	91,4%	98,9%	103,5%	105,7%	106,0%	104,9%	102,8%	100,1%	97,2%

4m

		Upstand Height (mm)													
	Load Position:	0	10	20	30	40	50	60	70	80	90	100	110	120	130
		Critical Elastic Moment (kNm)													
B254x146x31	ABOVE FLANGE	81,5	99,8	116,2	130,1	141,6	150,8	158,0	163,4	167,2	169,6	171,0	171,4	171,3	170,7
	% Increase:		22,5%	16,5%	11,9%	8,8%	6,5%	4,8%	3,4%	2,3%	1,5%	0,8%	0,3%	-0,1%	-0,3%
	Cumulative % Inc.		22,5%	42,7%	59,7%	73,8%	85,1%	94,0%	100,6%	105,3%	108,2%	109,9%	110,5%	110,3%	109,5%

6m

		Upstand Height (mm)													
	Load Position:	0	10	20	30	40	50	60	70	80	90	100	110	120	130
		Critical Elastic Moment (kNm)													
B254x146x31	ABOVE FLANGE	48,7	58,3	67,2	75,0	81,6	87,3	92,0	95,9	99,0	101,5	103,4	104,7	105,7	106,4
	% Increase:		19,9%	15,2%	11,5%	8,9%	6,9%	5,4%	4,2%	3,3%	2,5%	1,8%	1,3%	0,9%	0,6%
	Cumulative % Inc.		19,9%	38,1%	54,0%	67,7%	79,4%	89,1%	97,1%	103,6%	108,6%	112,5%	115,3%	117,3%	118,6%

8m

		Upstand Height (mm)													
	Load Position:	0	10	20	30	40	50	60	70	80	90	100	110	120	130
		Critical Elastic Moment (kNm)													
B254x146x31	ABOVE FLANGE	35,5	42,0	48,0	53,3	58,1	62,2	65,8	69,0	71,7	73,9	75,8	77,4	78,7	79,7
	% Increase:		18,1%	14,3%	11,1%	8,9%	7,2%	5,8%	4,8%	3,9%	3,2%	2,6%	2,1%	1,7%	1,3%
	Cumulative % Inc.		18,1%	35,0%	50,0%	63,3%	75,0%	85,2%	94,0%	101,6%	107,9%	113,3%	117,7%	121,3%	124,2%

10m

		Upstand Height (mm)													
	Load Position:	0	10	20	30	40	50	60	70	80	90	100	110	120	130
		Critical Elastic Moment (kNm)													
B254x146x31	ABOVE FLANGE	28,4	33,2	37,7	41,8	45,5	48,8	51,8	54,4	56,8	58,8	60,6	62,2	63,6	64,7
	% Increase:		16,9%	13,6%	10,8%	8,8%	7,3%	6,1%	5,1%	4,3%	3,6%	3,1%	2,6%	2,2%	1,8%
	Cumulative % Inc.		16,9%	32,8%	47,1%	60,1%	71,8%	82,2%	91,5%	99,8%	107,0%	113,3%	118,8%	123,6%	127,7%

Tabulated results for all spans for the four members under consideration have been presented in Tables 5.12 to 5.15. As for the previous four members considered at short upstand heights there is a high increase in the critical elastic moment and this diminishes as the upstand height increases. It can also be observed that in some cases, such as the 2m span case, at large upstand heights the critical elastic moment reaches a peak and starts to diminish with increasing upstand height. The diminishing trend observed with the larger spans suggests that if the upstand height is increased further similar trend to what is observed in the 2m span case would be observed.

It can be seen once again that the initial percentage change in the critical elastic moment decreases with an increase in the span for all four cases of (b/H). This shows that for shorter spans the change in the critical moment is more pronounced than for longer spans. However, the trend of diminishing increase with upstand height is consistent for all spans. Despite a change in the (b/H) value no noticeable change in the rate of percentage increase was noticed. This may indicate that the rate of increase is not necessarily dependent on the (b/H) parameter.

Table 5.16 Results for NF-IPE 160 with (b/H = 0.5) – All spans consolidated trend (M_{cr})

Span	Upstand Height (mm)													
	0	10	20	30	40	50	60	70	80	90	100	110	120	130
	Mcr (kNm)													
2	35,4	47,1	56,8	64,2	69,5	73,0	75,2	76,3	76,7	76,8	76,6	76,6	76,6	77,0
4	16,5	21,0	25,1	28,5	31,3	33,7	35,6	37,2	38,4	39,4	40,2	40,8	41,4	41,8
6	11,3	14,1	16,6	18,9	20,9	22,7	24,2	25,6	26,8	27,8	28,7	29,5	30,2	30,8
8	8,6	10,7	12,5	14,3	15,8	17,2	18,5	19,7	20,8	21,7	22,6	23,4	24,1	24,7
10	7,0	8,6	10,1	11,5	12,8	13,9	15,0	16,0	17,0	17,8	18,6	19,4	20,1	20,7

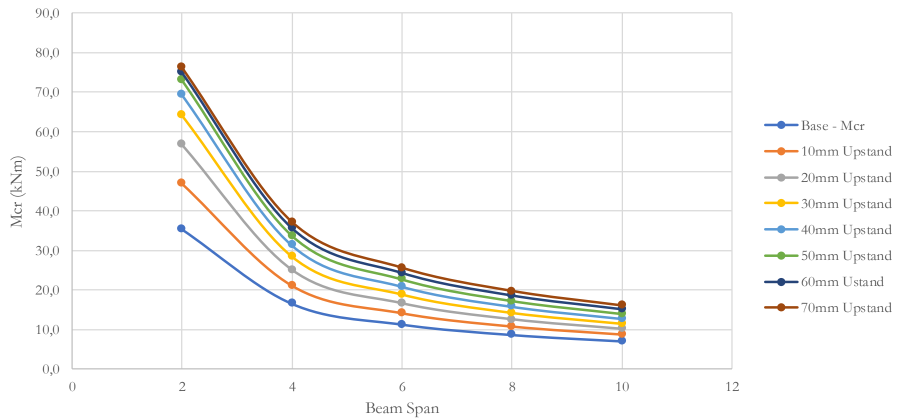

Table 5.17 Results for NF-305x165x40 with (b/H = 0.5) – All spans consolidated trend (M_{cr})

Span	Upstand Height (mm)													
	0	10	20	30	40	50	60	70	80	90	100	110	120	130
	Mcr (kNm)													
2	491,1	604,5	708,4	796,2	868,6	926,6	971,4	1 004,0	1 025,8	1 038,3	1 042,9	1 041,1	1 034,4	1 024,3
4	152,8	184,7	214,3	239,9	261,7	280,0	294,9	306,8	315,9	322,6	327,1	329,8	331,0	331,0
6	87,4	103,7	119,1	132,8	144,8	155,2	164,1	171,7	177,9	183,1	187,2	190,3	192,7	194,4
8	62,3	72,9	83,1	92,2	100,5	107,8	114,3	120,0	124,9	129,2	132,9	136,0	138,6	140,7
10	49,2	57,0	64,5	71,4	77,7	83,3	88,5	93,1	97,3	101,0	104,3	107,2	109,7	111,9

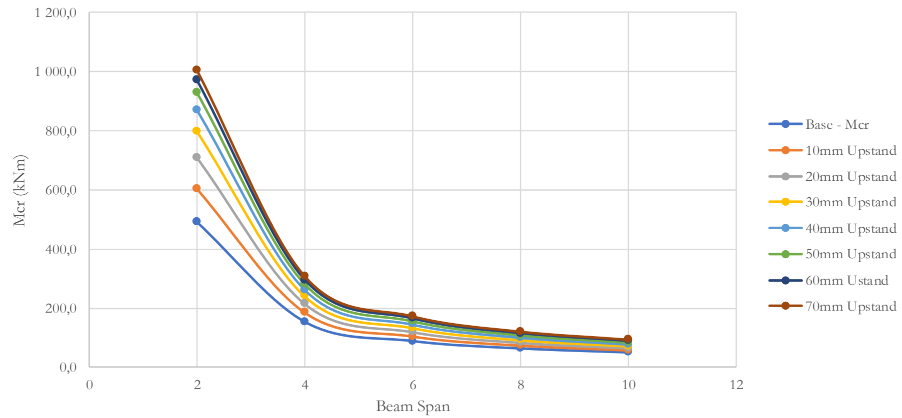

Table 5.18 Results for NF-IPE 100 with (b/H = 0.6) – All spans consolidated trend (M_{cr})

Span	Upstand Height (mm)													
	0	10	20	30	40	50	60	70	80	90	100	110	120	130
	Mcr (kNm)													
2	8,9	12,3	14,9	16,9	18,3	19,3	19,9	20,3	20,6	20,9	21,2	21,5	21,9	22,4
4	4,6	6,2	7,5	8,7	9,6	10,5	11,1	11,7	12,2	12,6	13,0	13,3	13,6	13,9
6	3,2	4,2	5,1	5,9	6,6	7,3	7,9	8,4	8,8	9,3	9,6	10,0	10,3	10,6
8	2,4	3,2	3,9	4,5	5,1	5,6	6,1	6,5	6,9	7,3	7,7	8,0	8,3	8,6
10	2,0	2,6	3,1	3,6	4,1	4,5	5,0	5,3	5,7	6,0	6,4	6,7	6,9	7,2

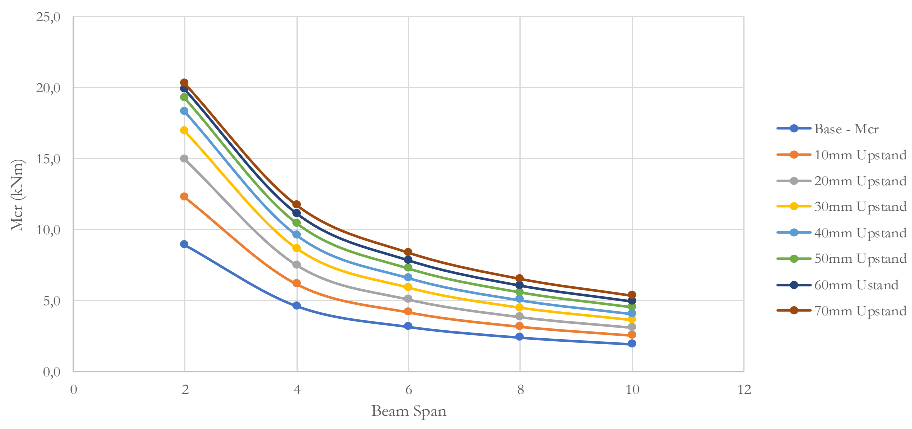

Table 5.19 Results for NF-IPE 100 with (b/H = 0.6) – All spans consolidated trend (M_{cr})

Span (m)	Upstand Height (mm)													
	0	10	20	30	40	50	60	70	80	90	100	110	120	130
	Mcr (kNm)													
2	246,0	309,1	364,5	409,4	444,7	471,0	489,3	500,6	506,1	506,8	504,1	498,9	492,2	485,1
4	81,5	99,8	116,2	130,1	141,6	150,8	158,0	163,4	167,2	169,6	171,0	171,4	171,3	170,7
6	48,7	58,3	67,2	75,0	81,6	87,3	92,0	95,9	99,0	101,5	103,4	104,7	105,7	106,4
8	35,5	42,0	48,0	53,3	58,1	62,2	65,8	69,0	71,7	73,9	75,8	77,4	78,7	79,7
10	28,4	33,2	37,7	41,8	45,5	48,8	51,8	54,4	56,8	58,8	60,6	62,2	63,6	64,7

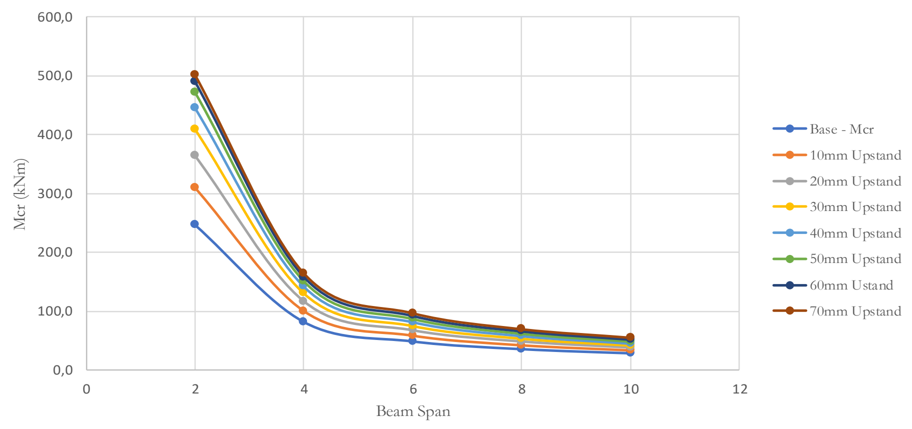

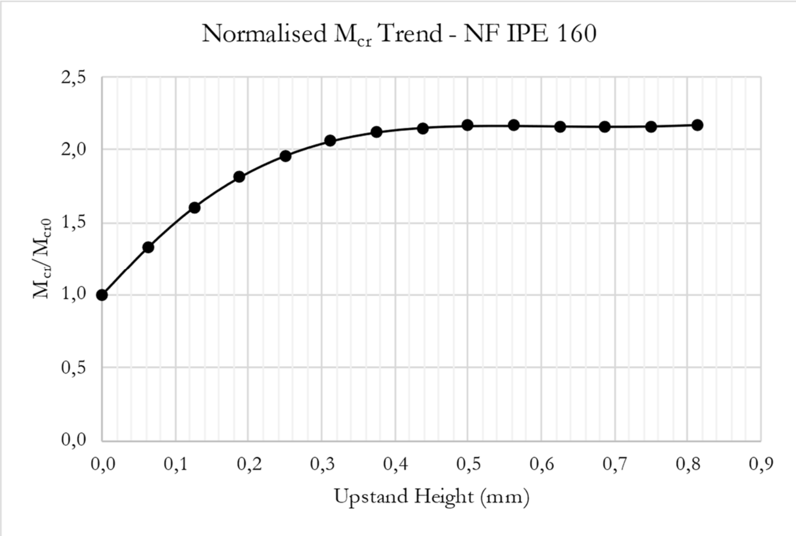

Fig.5-5 Normalised critical moment vs upstand height - B_5

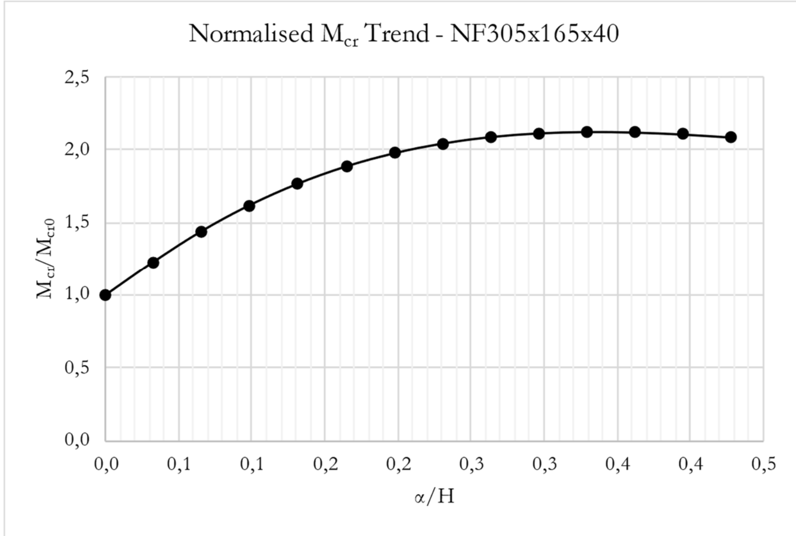

Fig.5-6 Normalised critical moment vs upstand height - B_6

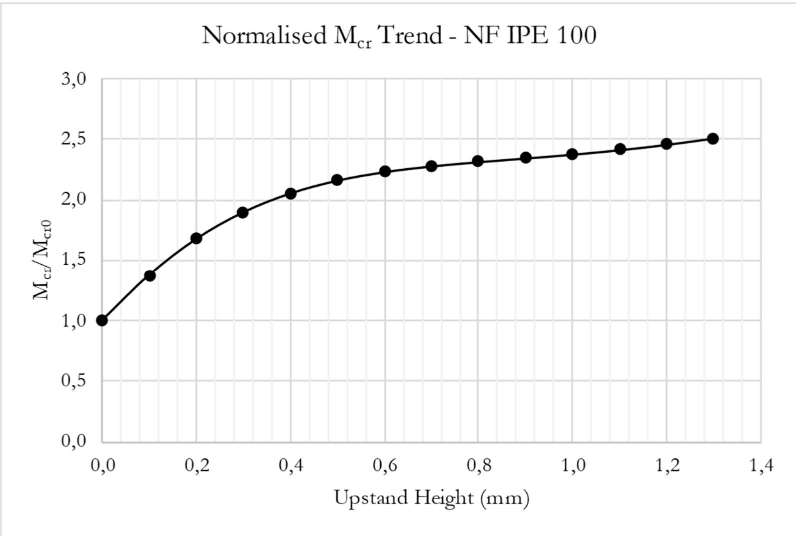

Fig.5-7 Normalised critical moment vs upstand height - B_7

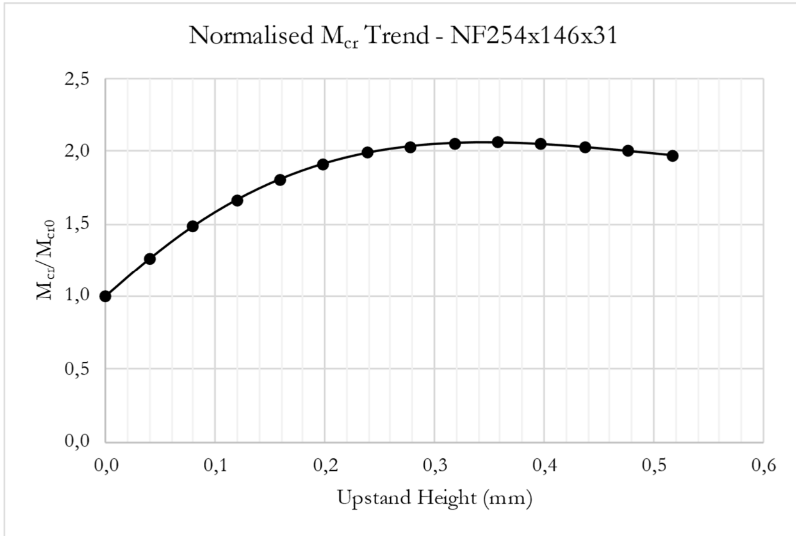

Fig.5-8 Normalised critical moment vs upstand height - B_8

The results presented in the Tables 5.16 to 5.19 illustrate how as the span length increases the relative increase in the critical elastic moment decreases. This shows that the greatest strength gain for a given increase in upstand height is obtained for shorter spans than for longer ones for the beams considered. This is consistent for all four members. The converging curves illustrate this reduced increase at the higher spans. However, for all spans considered there is a change in the critical elastic moment for a corresponding change in the upstand height. The fact that this change is diminishing with increase in upstand height can be observed for the 2m span case.

Fig's 5.5 to 5.8 also illustrate the increase in critical elastic moment with upstand height. Here the diminishing increase with upstand height is clearly illustrated just as was observed with the previous set of sections. For Beams B5, B6 and B8 the trend shows a peak at high upstand height followed by a reducing critical moment with increase in upstand height beyond this point. For beam B7 no peak value is observed but a similar trend of decreasing increase in critical moment with upstand height is observed like the other members.

5.3.1.3 Trends for Beams with (b/H) = 0.7

The sets of results are presented in the sequence indicated in Table 5.20 for the two members considered.

Table 5.20 Last group of two 'NF' members

Member	***Beam***	***b/H***	***Set 1***	***Set 2***	***Set 3***
NF 203x133x25	B_9	0.7	Tabulated results for all spans	Plots of M_{cr} for all spans	Graph of normalised M_{cr} against upstand height for 2m span
NF 203x133x30	B_{10}	0.7			

Table 5.21 Results for NF-203x133x25 with (b/H = 0.7) for all spans considered

Beam: 2m

		Upstand Height (mm)													
	Load Position:	0	10	20	30	40	50	60	70	80	90	100	110	120	130
		Critical Elastic Moment (kNm)													
203x133x25	ABOVE FLANGE	144,1	182,5	214,9	239,8	257,9	270,0	277,0	279,8	279,5	277,1	273,4	269,4	265,5	262,3
	% Increase:		26,7%	17,7%	11,6%	7,6%	4,7%	2,6%	1,0%	-0,1%	-0,9%	-1,3%	-1,5%	-1,4%	-1,2%
	Cumulative % Inc.		26,7%	49,1%	66,4%	78,9%	87,3%	92,2%	94,1%	93,9%	92,3%	89,7%	86,9%	84,2%	82,0%

4m

		Upstand Height (mm)													
	Load Position:	0	10	20	30	40	50	60	70	80	90	100	110	120	130
		Critical Elastic Moment (kNm)													
203x133x25	ABOVE FLANGE	51,9	63,7	74,1	82,5	89,3	94,6	98,4	101,1	102,8	103,8	104,2	104,2	103,9	103,5
	% Increase:		22,7%	16,2%	11,5%	8,2%	5,9%	4,1%	2,7%	1,7%	0,9%	0,4%	0,0%	-0,2%	-0,3%
	Cumulative % Inc.		22,7%	42,6%	59,0%	72,0%	82,1%	89,6%	94,8%	98,1%	99,9%	100,6%	100,6%	100,1%	99,4%

6m

		Upstand Height (mm)													
	Load Position:	0	10	20	30	40	50	60	70	80	90	100	110	120	130
		Critical Elastic Moment (kNm)													
203x133x25	ABOVE FLANGE	32,5	39,0	44,9	50,0	54,2	57,8	60,7	63,0	64,9	66,3	67,3	68,1	68,6	69,0
	% Increase:		20,0%	15,0%	11,2%	8,5%	6,6%	5,0%	3,9%	2,9%	2,2%	1,6%	1,1%	0,8%	0,5%
	Cumulative % Inc.		20,0%	38,1%	53,6%	66,7%	77,6%	86,6%	93,8%	99,5%	103,8%	107,0%	109,4%	111,0%	112,1%

8m

		Upstand Height (mm)													
	Load Position:	0	10	20	30	40	50	60	70	80	90	100	110	120	130
		Critical Elastic Moment (kNm)													
203x133x25	ABOVE FLANGE	24,3	28,8	32,8	36,5	39,6	42,4	44,8	46,8	48,5	49,9	51,1	52,1	52,9	53,6
	% Increase:		18,3%	14,2%	11,0%	8,7%	7,0%	5,6%	4,5%	3,7%	3,0%	2,4%	1,9%	1,5%	1,2%
	Cumulative % Inc.		18,3%	35,2%	50,0%	63,0%	74,4%	84,2%	92,5%	99,6%	105,5%	110,4%	114,5%	117,8%	120,5%

10m

		Upstand Height (mm)													
	Load Position:	0	10	20	30	40	50	60	70	80	90	100	110	120	130
		Critical Elastic Moment (kNm)													
203x133x25	ABOVE FLANGE	19,6	23,0	26,1	29,0	31,5	33,8	35,8	37,6	39,1	40,5	41,7	42,7	43,6	44,4
	% Increase:		17,2%	13,6%	10,8%	8,8%	7,2%	6,0%	5,0%	4,2%	3,5%	2,9%	2,5%	2,1%	1,8%
	Cumulative % Inc.		17,2%	33,2%	47,6%	60,5%	72,1%	82,3%	91,4%	99,4%	106,3%	112,4%	117,7%	122,2%	126,2%

Table 5.22 Results for NF-203x133x30 with (b/H = 0.7) for all spans considered

Beam: B203x133x30 2m

		Upstand Height (mm)													
	Load Position:	0	10	20	30	40	50	60	70	80	90	100	110	120	130
B203x133x30	ABOVE FLANGE	192,7	239,3	279,9	311,7	335,3	351,8	362,1	367,4	368,7	367,2	364,0	360,0	355,9	352,3
	% Increase:		24,2%	17,0%	11,3%	7,6%	4,9%	2,9%	1,4%	0,4%	-0,4%	-0,9%	-1,1%	-1,1%	-1,0%
	Cumulative % Inc.		24,2%	45,3%	61,8%	74,0%	82,6%	87,9%	90,7%	91,4%	90,6%	88,9%	86,8%	84,7%	82,8%

4m

		Upstand Height (mm)													
	Load Position:	0	10	20	30	40	50	60	70	80	90	100	110	120	130
B203x133x30	ABOVE FLANGE	74,3	89,5	103,3	115,0	124,5	132,2	138,3	142,9	146,2	148,5	150,0	150,9	151,4	151,6
	% Increase:		20,5%	15,4%	11,2%	8,3%	6,2%	4,6%	3,3%	2,3%	1,6%	1,0%	0,6%	0,3%	0,1%
	Cumulative % Inc.		20,5%	39,1%	54,7%	67,6%	77,9%	86,1%	92,2%	96,7%	99,9%	101,9%	103,1%	103,7%	103,9%

6m

		Upstand Height (mm)													
	Load Position:	0	10	20	30	40	50	60	70	80	90	100	110	120	130
B203x133x30	ABOVE FLANGE	48,0	56,8	64,9	72,0	78,2	83,6	88,2	92,0	95,2	97,9	100,0	101,7	103,1	104,3
	% Increase:		18,2%	14,3%	11,0%	8,6%	6,8%	5,5%	4,4%	3,5%	2,8%	2,2%	1,7%	1,4%	1,1%
	Cumulative % Inc.		18,2%	35,1%	50,0%	62,9%	74,1%	83,6%	91,6%	98,2%	103,7%	108,2%	111,8%	114,7%	117,1%

8m

		Upstand Height (mm)													
	Load Position:	0	10	20	30	40	50	60	70	80	90	100	110	120	130
B203x133x30	ABOVE FLANGE	36,3	42,4	48,2	53,4	58,1	62,2	65,9	69,2	72,1	74,6	76,8	78,6	80,3	81,7
	% Increase:		16,9%	13,6%	10,8%	8,7%	7,2%	5,9%	5,0%	4,1%	3,5%	2,9%	2,5%	2,1%	1,8%
	Cumulative % Inc.		16,9%	32,7%	47,0%	59,9%	71,3%	81,5%	90,5%	98,4%	105,3%	111,3%	116,6%	121,1%	125,0%

10m

		Upstand Height (mm)													
	Load Position:	0	10	20	30	40	50	60	70	80	90	100	110	120	130
B203x133x30	ABOVE FLANGE	29,5	34,2	38,7	42,8	46,5	49,9	53,1	55,9	58,4	60,7	62,8	64,7	66,3	67,8
	% Increase:		16,0%	13,1%	10,6%	8,8%	7,4%	6,2%	5,3%	4,6%	3,9%	3,4%	3,0%	2,6%	2,3%
	Cumulative % Inc.		16,0%	31,2%	45,1%	57,8%	69,4%	80,0%	89,6%	98,2%	106,0%	113,0%	119,3%	125,0%	130,1%

Table 5.23 Results for NF-203x133x25 (b/H = 0.7) – All spans consolidated trend (M_{cr})

	Upstand Height (mm)													
Span (m)	0	10	20	30	40	50	60	70	80	90	100	110	120	130
	Mcr (kNm)													
2	144,1	182,5	214,9	239,8	257,9	270,0	277,0	279,8	279,5	277,1	273,4	269,4	265,5	262,3
4	51,9	63,7	74,1	82,5	89,3	94,6	98,4	101,1	102,8	103,8	104,2	104,2	103,9	103,5
6	32,5	39,0	44,9	50,0	54,2	57,8	60,7	63,0	64,9	66,3	67,3	68,1	68,6	69,0
8	24,3	28,8	32,8	36,5	39,6	42,4	44,8	46,8	48,5	49,9	51,1	52,1	52,9	53,6
10	19,6	23,0	26,1	29,0	31,5	33,8	35,8	37,6	39,1	40,5	41,7	42,7	43,6	44,4

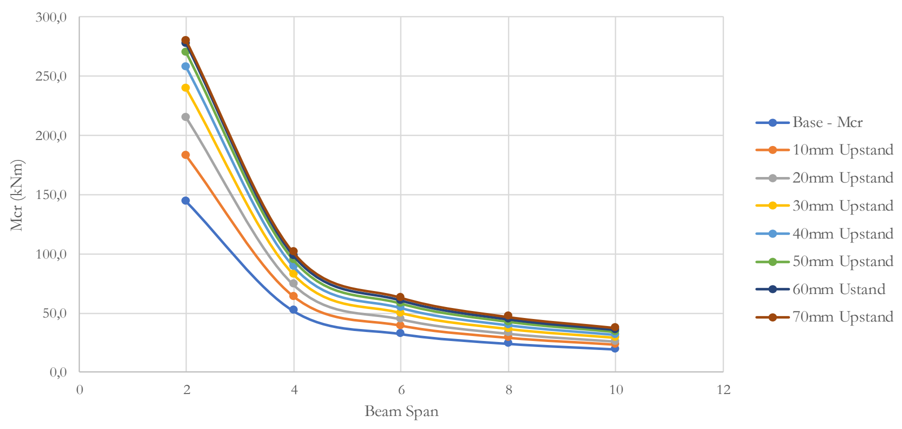

Table 5.24 Results for NF-203x133x30 (b/H = 0.7) – All spans consolidated trend (M_{cr})

	Upstand Height (mm)													
Span (m)	0	10	20	30	40	50	60	70	80	90	100	110	120	130
	Mcr (kNm)													
2	192,7	239,3	279,9	311,7	335,3	351,8	362,1	367,4	368,7	367,2	364,0	360,0	355,9	352,3
4	74,3	89,5	103,3	115,0	124,5	132,2	138,3	142,9	146,2	148,5	150,0	150,9	151,4	151,6
6	48,0	56,8	64,9	72,0	78,2	83,6	88,2	92,0	95,2	97,9	100,0	101,7	103,1	104,3
8	36,3	42,4	48,2	53,4	58,1	62,2	65,9	69,2	72,1	74,6	76,8	78,6	80,3	81,7
10	29,5	34,2	38,7	42,8	46,5	49,9	53,1	55,9	58,4	60,7	62,8	64,7	66,3	67,8

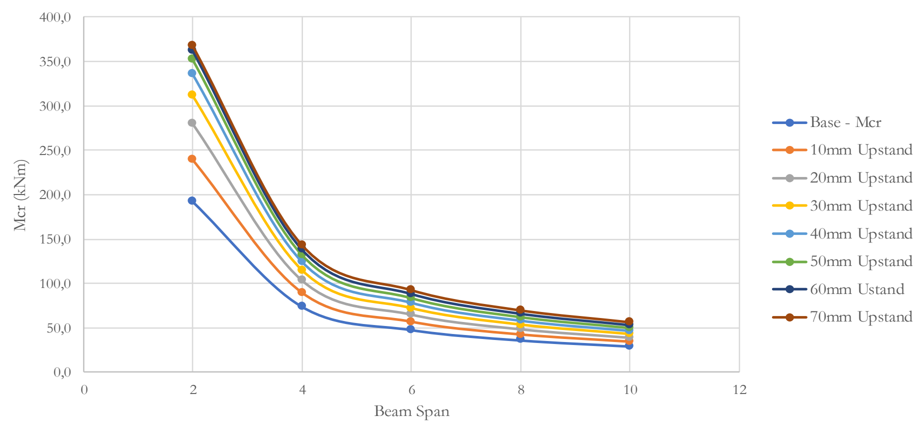

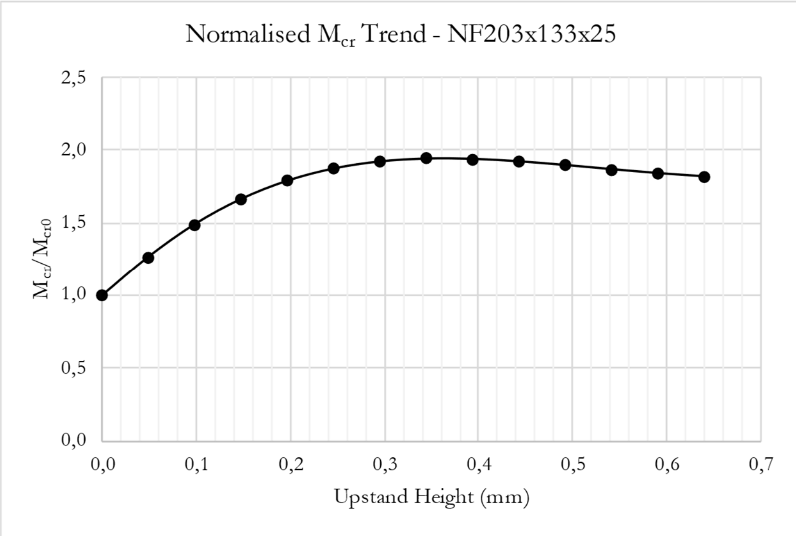

Fig.5-9 Normalised critical moment vs upstand height - B_9

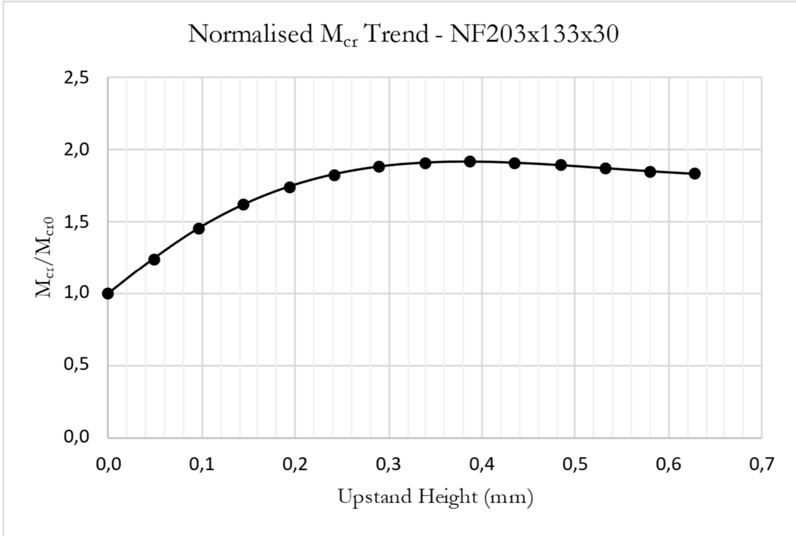

Fig.5-10 Normalised critical moment vs upstand height - B_{10}

Tabulated results in Table 5.21 and 5.22 show similar trends to that observed with the first sets of four members. The critical elastic moment increases at a decreasing rate with increase in upstand height. This is illustrated in Fig's 5-9 and 5-10 for the 2m span case. For this case it can be clearly observed that a peak value is reached for the critical elastic moment followed by a decreasing value with increase in upstand height. Tables 5.23 and 5.24 capture this trend across different spans considered.

5.3.1.4 Trends for Beams with (b/H) = 0.9 & 1.0

The four beams considered here fall under the category of wide flange (WF) members. The sets of results are presented in the sequence indicated in Table 5.25 for the four members considered. This covers beams B_{11} to B_{14}.

Table 5.25 Group of four 'WF' members

Member	***Beam***	***b/H***	***Set 1***	***Set 2***	***Set 3***
WF 254x254x167	B_{11}	0.9	Tabulated results for all spans	Plots of M_{cr} for all spans	Graph of normalised M_{cr} against upstand height for 2m span
WF 305x305x158	B_{12}	0.9			
WF 152x152x23	B_{13}	1.0			
WF 254x254x73	B_{14}	1.0			

Table 5.26 Results for WF-254x254x167 with (b/H = 0.9) for all spans considered

Beam: H254x254x167 2m

		Upstand Height (mm)													
	Load Position:	0	10	20	30	40	50	60	70	80	90	100	110	120	130
		Critical Elastic Moment (kNm)													
H254x254x167	ABOVE FLANGE	6 829,0	7 202,7	7 817,0	8 338,2	8 772,1	9 124,9	9 403,6	9 615,3	9 767,8	9 869,1	9 927,0	9 949,5	9 944,2	9 918,2
	% Increase:		5,5%	8,5%	6,7%	5,2%	4,0%	3,1%	2,3%	1,6%	1,0%	0,6%	0,2%	-0,1%	-0,3%
	Cumulative % Inc.		5,5%	14,5%	22,1%	28,5%	33,6%	37,7%	40,8%	43,0%	44,5%	45,4%	45,7%	45,6%	45,2%

4m

		Upstand Height (mm)													
	Load Position:	0	10	20	30	40	50	60	70	80	90	100	110	120	130
		Critical Elastic Moment (kNm)													
H254x254x167	ABOVE FLANGE	2 885,2	3 052,0	3 284,8	3 494,0	3 680,8	3 846,2	3 991,6	4 118,2	4 227,5	4 320,8	4 399,7	4 465,5	4 519,9	4 564,3
	% Increase:		5,8%	7,6%	6,4%	5,3%	4,5%	3,8%	3,2%	2,7%	2,2%	1,8%	1,5%	1,2%	1,0%
	Cumulative % Inc.		5,8%	13,8%	21,1%	27,6%	33,3%	38,3%	42,7%	46,5%	49,8%	52,5%	54,8%	56,7%	58,2%

6m

		Upstand Height (mm)													
	Load Position:	0	10	20	30	40	50	60	70	80	90	100	110	120	130
		Critical Elastic Moment (kNm)													
H254x254x167	ABOVE FLANGE	1 927,6	2 041,5	2 186,3	2 320,3	2 444,0	2 557,8	2 662,2	2 757,5	2 844,3	2 923,1	2 994,3	3 058,5	3 116,2	3 167,9
	% Increase:		5,9%	7,1%	6,1%	5,3%	4,7%	4,1%	3,6%	3,1%	2,8%	2,4%	2,1%	1,9%	1,7%
	Cumulative % Inc.		5,9%	13,4%	20,4%	26,8%	32,7%	38,1%	43,1%	47,6%	51,6%	55,3%	58,7%	61,7%	64,3%

8m

		Upstand Height (mm)													
	Load Position:	0	10	20	30	40	50	60	70	80	90	100	110	120	130
		Critical Elastic Moment (kNm)													
H254x254x167	ABOVE FLANGE	1 475,5	1 563,5	1 669,4	1 769,1	1 862,7	1 950,6	2 032,9	2 109,8	2 181,6	2 248,5	2 310,8	2 368,6	2 422,2	2 471,9
	% Increase:		6,0%	6,8%	6,0%	5,3%	4,7%	4,2%	3,8%	3,4%	3,1%	2,8%	2,5%	2,3%	2,1%
	Cumulative % Inc.		6,0%	13,1%	19,9%	26,2%	32,2%	37,8%	43,0%	47,9%	52,4%	56,6%	60,5%	64,2%	67,5%

10m

		Upstand Height (mm)													
	Load Position:	0	10	20	30	40	50	60	70	80	90	100	110	120	130
		Critical Elastic Moment (kNm)													
H254x254x167	ABOVE FLANGE	1 203,3	1 275,5	1 359,3	1 438,9	1 514,6	1 586,4	1 654,5	1 719,1	1 780,1	1 837,9	1 892,5	1 944,1	1 992,7	2 038,6
	% Increase:		6,0%	6,6%	5,9%	5,3%	4,7%	4,3%	3,9%	3,6%	3,2%	3,0%	2,7%	2,5%	2,3%
	Cumulative % Inc.		6,0%	13,0%	19,6%	25,9%	31,8%	37,5%	42,9%	47,9%	52,7%	57,3%	61,6%	65,6%	69,4%

Table 5.27 Results for WF-305x305x158 with (b/H = 0.9) for all spans considered

Beam: H305x305x158 2m

		Upstand Height (mm)													
	Load Position:	0	10	20	30	40	50	60	70	80	90	100	110	120	130
		Critical Elastic Moment (kNm)													
H305x305x158	ABOVE FLANGE	8 421,0	9 134,3	9 964,4	10 675,8	11 274,2	11 766,0	12 158,4	12 459,1	12 676,6	12 819,7	12 897,9	12 920,6	12 897,3	12 837,3
	% Increase:		8,5%	9,1%	7,1%	5,6%	4,4%	3,3%	2,5%	1,7%	1,1%	0,6%	0,2%	-0,2%	-0,5%
	Cumulative % Inc.		8,5%	18,3%	26,8%	33,9%	39,7%	44,4%	48,0%	50,5%	52,2%	53,2%	53,4%	53,2%	52,4%

4m

		Upstand Height (mm)													
	Load Position:	0	10	20	30	40	50	60	70	80	90	100	110	120	130
		Critical Elastic Moment (kNm)													
H305x305x158	ABOVE FLANGE	2 825,5	3 046,5	3 299,2	3 522,4	3 717,4	3 885,6	4 028,4	4 147,6	4 244,8	4 322,0	4 381,1	4 424,0	4 452,9	4 469,7
	% Increase:		7,8%	8,3%	6,8%	5,5%	4,5%	3,7%	3,0%	2,3%	1,8%	1,4%	1,0%	0,7%	0,4%
	Cumulative % Inc.		7,8%	16,8%	24,7%	31,6%	37,5%	42,6%	46,8%	50,2%	53,0%	55,1%	56,6%	57,6%	58,2%

6m

		Upstand Height (mm)													
	Load Position:	0	10	20	30	40	50	60	70	80	90	100	110	120	130
		Critical Elastic Moment (kNm)													
H305x305x158	ABOVE FLANGE	1 703,9	1 828,1	1 967,4	2 093,6	2 207,2	2 308,7	2 398,8	2 477,9	2 546,7	2 605,9	2 656,3	2 698,6	2 733,5	2 761,7
	% Increase:		7,3%	7,6%	6,4%	5,4%	4,6%	3,9%	3,3%	2,8%	2,3%	1,9%	1,6%	1,3%	1,0%
	Cumulative % Inc.		7,3%	15,5%	22,9%	29,5%	35,5%	40,8%	45,4%	49,5%	52,9%	55,9%	58,4%	60,4%	62,1%

8m

		Upstand Height (mm)													
	Load Position:	0	10	20	30	40	50	60	70	80	90	100	110	120	130
		Critical Elastic Moment (kNm)													
H305x305x158	ABOVE FLANGE	1 252,0	1 338,7	1 434,2	1 522,2	1 603,2	1 677,2	1 744,6	1 805,6	1 860,6	1 909,9	1 953,9	1 992,8	2 027,0	2 057,0
	% Increase:		6,9%	7,1%	6,1%	5,3%	4,6%	4,0%	3,5%	3,0%	2,7%	2,3%	2,0%	1,7%	1,5%
	Cumulative % Inc.		6,9%	14,5%	21,6%	28,0%	34,0%	39,3%	44,2%	48,6%	52,5%	56,1%	59,2%	61,9%	64,3%

10m

		Upstand Height (mm)													
	Load Position:	0	10	20	30	40	50	60	70	80	90	100	110	120	130
		Critical Elastic Moment (kNm)													
H305x305x158	ABOVE FLANGE	1 004,6	1 071,5	1 144,3	1 212,2	1 275,5	1 334,3	1 388,8	1 439,0	1 485,3	1 527,8	1 566,6	1 602,0	1 634,2	1 663,3
	% Increase:		6,7%	6,8%	5,9%	5,2%	4,6%	4,1%	3,6%	3,2%	2,9%	2,5%	2,3%	2,0%	1,8%
	Cumulative % Inc.		6,7%	13,9%	20,7%	27,0%	32,8%	38,2%	43,2%	47,9%	52,1%	55,9%	59,5%	62,7%	65,6%

Table 5.28 Results for WF-152x152x23 with (b/H = 1.0) for all spans considered

Beam: H152x152x23 2m

		Upstand Height (mm)													
	Load Position:	0	10	20	30	40	50	60	70	80	90	100	110	120	130
		Critical Elastic Moment (kNm)													
H152x152x23	ABOVE FLANGE	142,0	174,3	199,2	216,1	226,2	230,7	231,0	228,4	224,4	219,9	215,9	213,0	211,6	211,8
	% Increase:		22,8%	14,3%	8,5%	4,7%	2,0%	0,1%	-1,1%	-1,8%	-2,0%	-1,8%	-1,3%	-0,7%	0,1%
	Cumulative % Inc.		22,8%	40,3%	52,3%	59,4%	62,5%	62,7%	60,9%	58,1%	54,9%	52,1%	50,1%	49,0%	49,2%

4m

		Upstand Height (mm)													
	Load Position:	0	10	20	30	40	50	60	70	80	90	100	110	120	130
		Critical Elastic Moment (kNm)													
H152x152x23	ABOVE FLANGE	52,1	62,2	70,5	76,7	81,2	84,1	85,7	86,4	86,4	86,0	85,4	84,7	84,2	84,0
	% Increase:		19,4%	13,2%	8,9%	5,8%	3,6%	2,0%	0,8%	0,0%	-0,5%	-0,7%	-0,7%	-0,6%	-0,3%
	Cumulative % Inc.		19,4%	35,2%	47,2%	55,7%	61,3%	64,5%	65,8%	65,8%	65,0%	63,8%	62,6%	61,6%	61,1%

6m

		Upstand Height (mm)													
	Load Position:	0	10	20	30	40	50	60	70	80	90	100	110	120	130
		Critical Elastic Moment (kNm)													
H152x152x23	ABOVE FLANGE	33,0	38,6	43,4	47,3	50,4	52,7	54,4	55,6	56,3	56,8	56,9	57,0	57,0	56,9
	% Increase:		17,1%	12,5%	9,0%	6,5%	4,6%	3,2%	2,1%	1,3%	0,7%	0,3%	0,1%	0,0%	-0,1%
	Cumulative % Inc.		17,1%	31,7%	43,5%	52,9%	60,0%	65,1%	68,7%	70,9%	72,2%	72,8%	72,9%	72,8%	72,7%

8m

		Upstand Height (mm)													
	Load Position:	0	10	20	30	40	50	60	70	80	90	100	110	120	130
		Critical Elastic Moment (kNm)													
H152x152x23	ABOVE FLANGE	24,7	28,6	32,0	34,9	37,3	39,3	40,8	42,1	43,0	43,7	44,2	44,6	44,8	45,0
	% Increase:		15,7%	11,9%	9,0%	6,9%	5,3%	4,0%	3,0%	2,2%	1,6%	1,2%	0,8%	0,6%	0,4%
	Cumulative % Inc.		15,7%	29,5%	41,2%	50,9%	58,9%	65,3%	70,3%	74,1%	76,9%	78,9%	80,4%	81,4%	82,1%

10m

		Upstand Height (mm)													
	Load Position:	0	10	20	30	40	50	60	70	80	90	100	110	120	130
		Critical Elastic Moment (kNm)													
H152x152x23	ABOVE FLANGE	20,0	23,0	25,6	27,9	29,9	31,6	33,0	34,2	35,2	36,0	36,6	37,2	37,6	37,9
	% Increase:		14,8%	11,6%	9,0%	7,1%	5,7%	4,5%	3,6%	2,9%	2,3%	1,8%	1,4%	1,1%	0,9%
	Cumulative % Inc.		14,8%	28,1%	39,7%	49,6%	58,1%	65,2%	71,2%	76,1%	80,0%	83,2%	85,8%	87,8%	89,5%

Table 5.29 Results for WF-254x254x73 with (b/H = 1.0) for all spans considered

Beam: H254x254x73 2m

		Upstand Height (mm)													
	Load Position:	0	10	20	30	40	50	60	70	80	90	100	110	120	130
		Critical Elastic Moment (kNm)													
H254x254x73	ABOVE FLANGE	2 036,4	2 314,5	2 572,6	2 782,9	2 948,5	3 072,9	3 160,1	3 214,3	3 240,3	3 243,1	3 227,6	3 198,7	3 160,9	3 118,5
	% Increase:		13,7%	11,1%	8,2%	6,0%	4,2%	2,8%	1,7%	0,8%	0,1%	-0,5%	-0,9%	-1,2%	-1,3%
	Cumulative % Inc.		13,7%	26,3%	36,7%	44,8%	50,9%	55,2%	57,8%	59,1%	59,3%	58,5%	57,1%	55,2%	53,1%

4m

		Upstand Height (mm)													
	Load Position:	0	10	20	30	40	50	60	70	80	90	100	110	120	130
		Critical Elastic Moment (kNm)													
H254x254x73	ABOVE FLANGE	648,2	728,5	804,2	868,0	920,6	962,8	995,5	1 019,6	1 036,0	1 046,0	1 050,5	1 050,7	1 047,5	1 042,0
	% Increase:		12,4%	10,4%	7,9%	6,1%	4,6%	3,4%	2,4%	1,6%	1,0%	0,4%	0,0%	-0,3%	-0,5%
	Cumulative % Inc.		12,4%	24,1%	33,9%	42,0%	48,5%	53,6%	57,3%	59,8%	61,4%	62,1%	62,1%	61,6%	60,8%

6m

		Upstand Height (mm)													
	Load Position:	0	10	20	30	40	50	60	70	80	90	100	110	120	130
		Critical Elastic Moment (kNm)													
H254x254x73	ABOVE FLANGE	377,1	419,5	460,0	495,3	525,5	551,1	572,3	589,5	603,0	613,4	620,9	625,9	629,0	630,5
	% Increase:		11,3%	9,7%	7,7%	6,1%	4,9%	3,8%	3,0%	2,3%	1,7%	1,2%	0,8%	0,5%	0,2%
	Cumulative % Inc.		11,3%	22,0%	31,3%	39,4%	46,1%	51,8%	56,3%	59,9%	62,7%	64,6%	66,0%	66,8%	67,2%

8m

		Upstand Height (mm)													
	Load Position:	0	10	20	30	40	50	60	70	80	90	100	110	120	130
		Critical Elastic Moment (kNm)													
H254x254x73	ABOVE FLANGE	271,7	300,0	327,3	351,5	373,0	391,8	408,0	421,9	433,6	443,4	451,3	457,7	462,7	466,5
	% Increase:		10,4%	9,1%	7,4%	6,1%	5,0%	4,1%	3,4%	2,8%	2,2%	1,8%	1,4%	1,1%	0,8%
	Cumulative % Inc.		10,4%	20,4%	29,4%	37,3%	44,2%	50,2%	55,3%	59,6%	63,2%	66,1%	68,4%	70,3%	71,7%

10m

		Upstand Height (mm)													
	Load Position:	0	10	20	30	40	50	60	70	80	90	100	110	120	130
		Critical Elastic Moment (kNm)													
H254x254x73	ABOVE FLANGE	215,8	237,0	257,5	276,1	292,9	307,9	321,2	333,0	343,4	352,4	360,1	366,7	372,3	377,0
	% Increase:		9,8%	8,7%	7,2%	6,1%	5,1%	4,3%	3,7%	3,1%	2,6%	2,2%	1,8%	1,5%	1,3%
	Cumulative % Inc.		9,8%	19,3%	27,9%	35,7%	42,7%	48,8%	54,3%	59,1%	63,3%	66,8%	69,9%	72,5%	74,7%

Table 5.30 Results for WF-254x254x167 (b/H = 0.9) – All spans consolidated trend (M_{cr})

Span (m)	Upstand Height (mm)													
	0	10	20	30	40	50	60	70	80	90	100	110	120	130
	Mcr (kNm)													
2	6 829,0	7 202,7	7 817,0	8 338,2	8 772,1	9 124,9	9 403,6	9 615,3	9 767,8	9 869,1	9 927,0	9 949,5	9 944,2	9 918,2
4	2 885,2	3 052,0	3 284,8	3 494,0	3 680,8	3 846,2	3 991,6	4 118,2	4 227,5	4 320,8	4 399,7	4 465,5	4 519,9	4 564,3
6	1 927,6	2 041,5	2 186,3	2 320,3	2 444,0	2 557,8	2 662,2	2 757,5	2 844,3	2 923,1	2 994,3	3 058,5	3 116,2	3 167,9
8	1 475,5	1 563,5	1 669,4	1 769,1	1 862,7	1 950,6	2 032,9	2 109,8	2 181,6	2 248,5	2 310,8	2 368,6	2 422,2	2 471,9
10	1 203,3	1 275,5	1 359,3	1 438,9	1 514,6	1 586,4	1 654,5	1 719,1	1 780,1	1 837,9	1 892,5	1 944,1	1 992,7	2 038,6

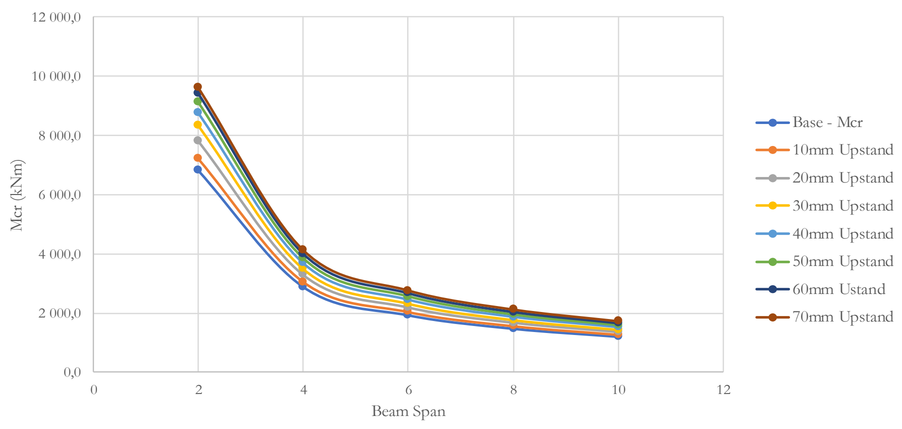

Table 5.31 Results for WF-305x305x158 (b/H = 0.9) – All spans consolidated trend (M_{cr})

Span (m)	Upstand Height (mm)													
	0	10	20	30	40	50	60	70	80	90	100	110	120	130
	Mcr (kNm)													
2	8 421,0	9 134,3	9 964,4	10 675,8	11 274,2	11 766,0	12 158,4	12 459,1	12 676,6	12 819,7	12 897,9	12 920,6	12 897,3	12 837,3
4	2 825,5	3 046,5	3 299,2	3 522,4	3 717,4	3 885,6	4 028,4	4 147,6	4 244,8	4 322,0	4 381,1	4 424,0	4 452,9	4 469,7
6	1 703,9	1 828,1	1 967,4	2 093,6	2 207,2	2 308,7	2 398,8	2 477,9	2 546,7	2 605,9	2 656,3	2 698,6	2 733,5	2 761,7
8	1 252,0	1 338,7	1 434,2	1 522,2	1 603,2	1 677,2	1 744,6	1 805,6	1 860,6	1 909,9	1 953,9	1 992,8	2 027,0	2 057,0
10	1 004,6	1 071,5	1 144,3	1 212,2	1 275,5	1 334,3	1 388,8	1 439,0	1 485,3	1 527,8	1 566,6	1 602,0	1 634,2	1 663,3

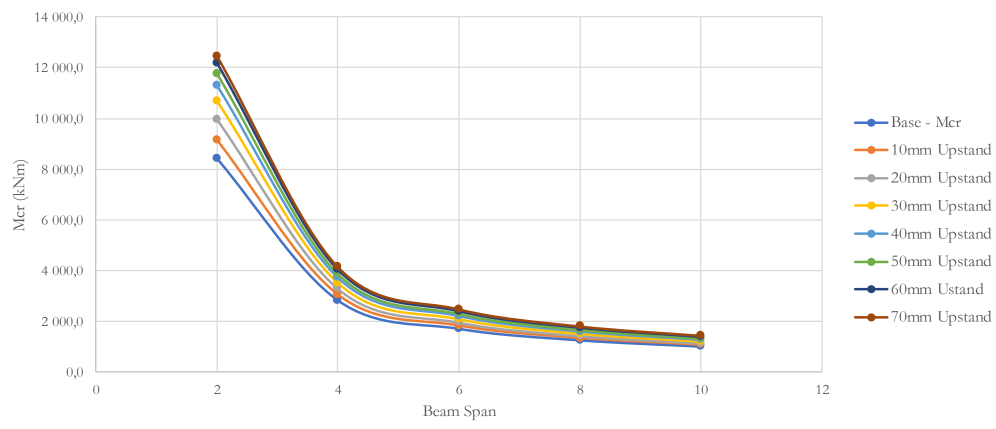

Table 5.32 Results for WF-152x52x23 (b/H = 1.0) – All spans consolidated trend (M_{cr})

	Upstand Height (mm)													
Span (m)	0	10	20	30	40	50	60	70	80	90	100	110	120	130
	Mcr (kNm)													
2	142,0	174,3	199,2	216,1	226,2	230,7	231,0	228,4	224,4	219,9	215,9	213,0	211,6	211,8
4	52,1	62,2	70,5	76,7	81,2	84,1	85,7	86,4	86,4	86,0	85,4	84,7	84,2	84,0
6	33,0	38,6	43,4	47,3	50,4	52,7	54,4	55,6	56,3	56,8	56,9	57,0	57,0	56,9
8	24,7	28,6	32,0	34,9	37,3	39,3	40,8	42,1	43,0	43,7	44,2	44,6	44,8	45,0
10	20,0	23,0	25,6	27,9	29,9	31,6	33,0	34,2	35,2	36,0	36,6	37,2	37,6	37,9

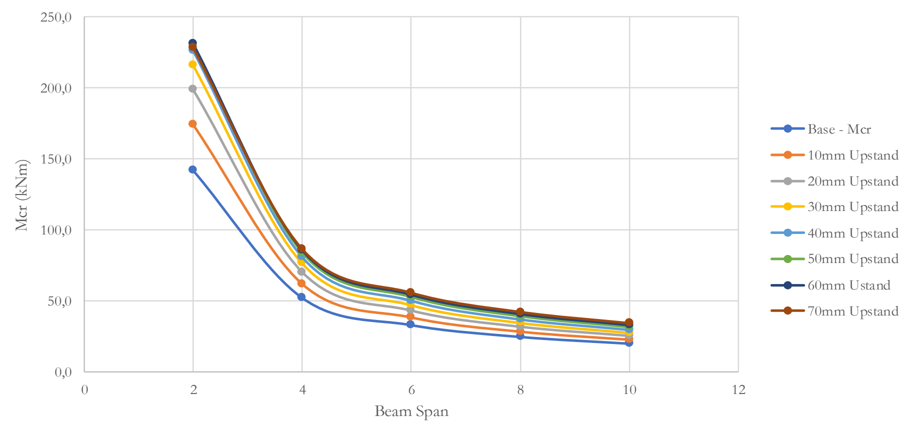

Table 5.33 Results for WF-254x254x73 (b/H = 1.0) – All spans consolidated trend (M_{cr})

	Upstand Height (mm)													
Span (m)	0	10	20	30	40	50	60	70	80	90	100	110	120	130
	Mcr (kNm)													
2	2 036,4	2 314,5	2 572,6	2 782,9	2 948,5	3 072,9	3 160,1	3 214,3	3 240,3	3 243,1	3 227,6	3 198,7	3 160,9	3 118,5
4	648,2	728,5	804,2	868,0	920,6	962,8	995,5	1 019,6	1 036,0	1 046,0	1 050,5	1 050,7	1 047,5	1 042,0
6	377,1	419,5	460,0	495,3	525,5	551,1	572,3	589,5	603,0	613,4	620,9	625,9	629,0	630,5
8	271,7	300,0	327,3	351,5	373,0	391,8	408,0	421,9	433,6	443,4	451,3	457,7	462,7	466,5
10	215,8	237,0	257,5	276,1	292,9	307,9	321,2	333,0	343,4	352,4	360,1	366,7	372,3	377,0

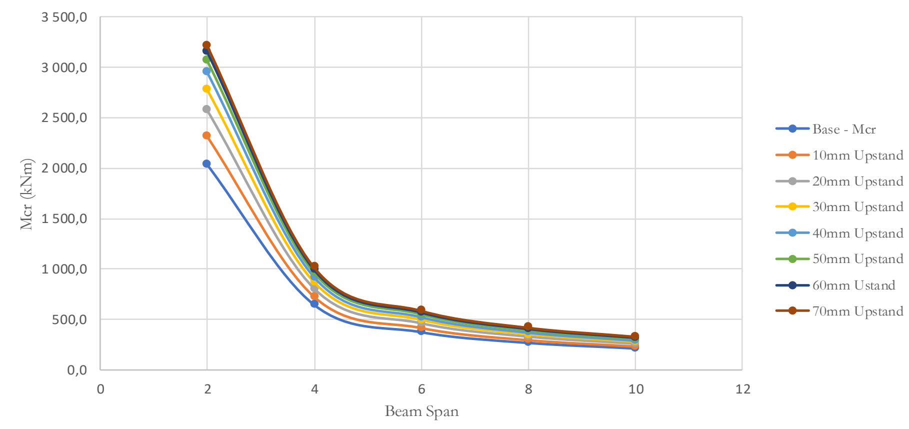

The observations for the wide flange sections considered here are similar to what was observed for the ten (10) narrow flange sections considered in the preceding sections. At low upstand heights there is greater change in the critical elastic moment and the rate of change diminishes with increase in upstand height. However, the changes in the critical elastic moment are more modest with these sections. Although the numerical increase can be significant, even in the hundreds of kilonewton-meter, the percentage values are small given that these wide flange sections have high critical elastic moment values to start with i.e., prior to introduction of the upstands. The reduction in percentage increase as the span increases is also consistent with observations from the narrow flange sections. Trends for the 2m span case are illustrated in Fig's 5-11 to 5-14 and are consistent with what has been observed for the narrow flange sections.

Having considered the member behaviour trends under central point loading, the section that follows considers members subjected to a uniformly distributed load (UDL).

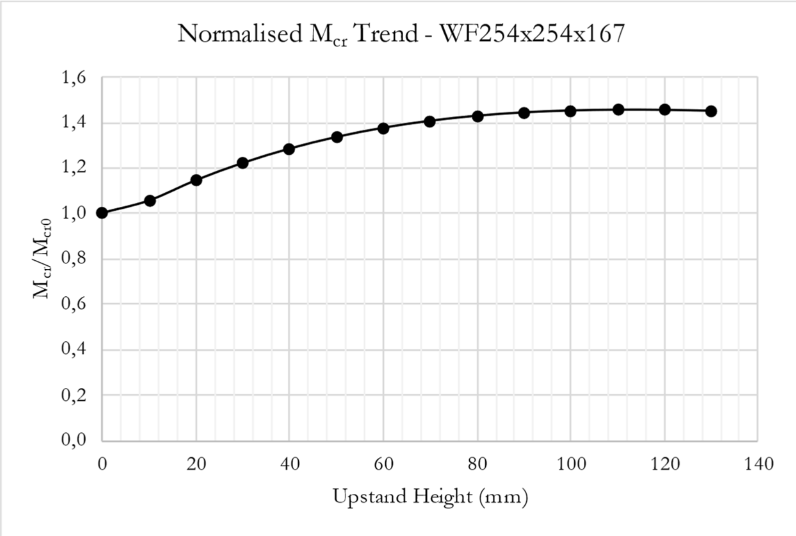

Fig.5-11 Normalised critical moment vs upstand height - B_{11}

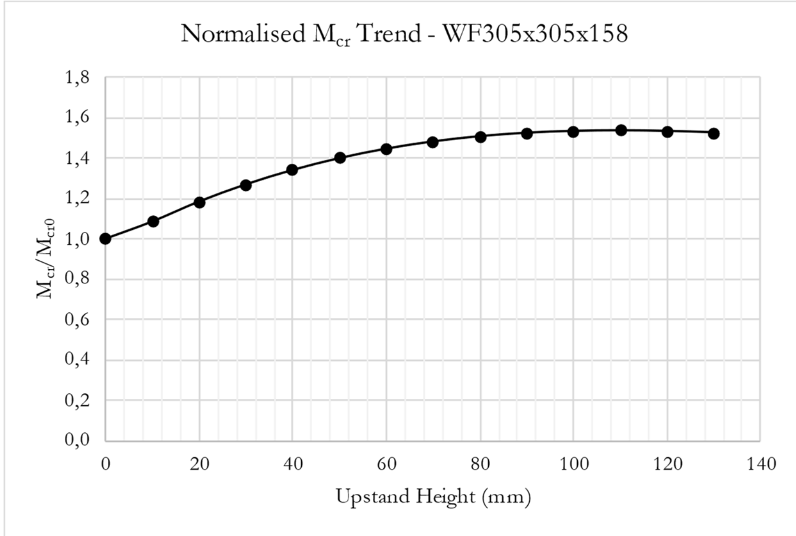

Fig.5-12 Normalised critical moment vs upstand height - B_{12}

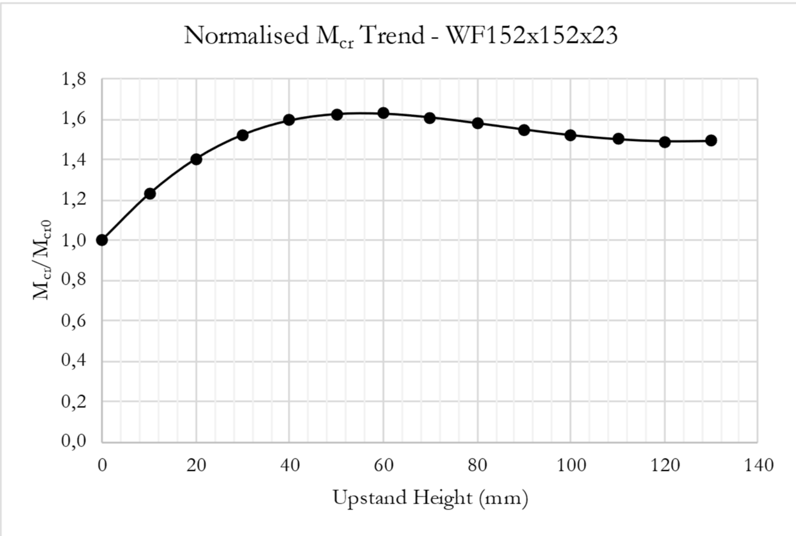

Fig.5-13 Normalised critical moment vs upstand height - B_{13}

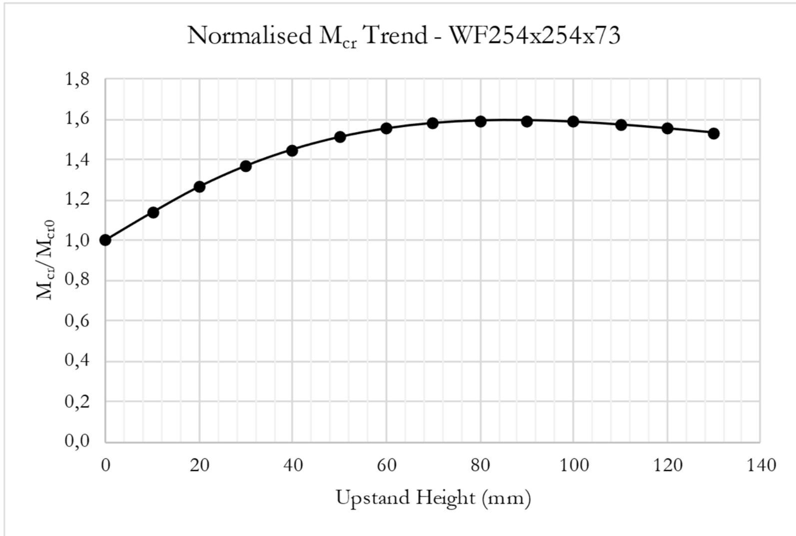

Fig.5-14 Normalised critical moment vs upstand height - B_{14}

5.3.2 Trends for the UDL case

The next load case to be considered is that of a uniformly distributed load (UDL) acting on the top flange. As with the point load case, summaries for all 14 beams are presented in the Figures and Tables that follow based on the (b/H) value of the beams. The trends for all the spans considered are presented in tabular form. A graphical summary for all spans is then presented to demonstrate the trend across the different spans. The critical load variation with upstand height is then presented in graphical form for a 2m span beam, the shortest span considered, with the critical moment normalised by expressing as a ratio of new critical moment to value at no upstand.

The narrow flange sections are presented first (b/H values 0.3, 0.4, 0.5, 0.6 & 0.7) followed by the wide flange sections (b/H values 0.9 & 1.0).

5.3.2.1 Trends for Beams with (b/H) = 0.3 & 0.4 UDL case

The sets of results are presented in the sequence indicated in Table 5.34 for the four members considered.

Table 5.34 First group of four 'NF' members under UDL load

Member	***Beam***	***b/H***	***Set 1***	***Set 2***	***Set 3***
NF 305x102x25	BU_1	0.3	Tabulated results for all spans	Plots of M_{cr} for all spans	Graph of normalised M_{cr} against upstand height for 2m span
NF 305x102x28	BU_2	0.3			
NF 406x140x39	BU_3	0.4			
NF 533x210x122	BU_4	0.4			

Table 5.35 Results for NF-305x102x25 with (b/H = 0.3) for all spans considered – UDL Load case

Beam: B305x102x25 — Load: *UDL*

2m

		Upstand Height (mm)													
	Load Position:	0	10	20	30	40	50	60	70	80	90	100	110	120	130
		Critical Elastic Moment (kNm)													
B305x102x25	ABOVE FLANGE	76,0	104,3	129,6	150,9	168,4	182,3	192,9	200,4	205,1	207,5	207,8	206,6	204,17	200,96
	% Increase:		37,2%	24,3%	16,5%	11,6%	8,3%	5,8%	3,9%	2,4%	1,1%	0,2%	-0,6%	-1,2%	-1,6%
	Cumulative % Inc.		37,2%	70,5%	98,6%	121,6%	139,9%	153,8%	163,6%	169,9%	173,0%	173,4%	171,8%	168,6%	164,4%

4m

		Upstand Height (mm)													
	Load Position:	0	10	20	30	40	50	60	70	80	90	100	110	120	130
		Critical Elastic Moment (kNm)													
B305x102x25	ABOVE FLANGE	26,0	34,2	41,6	48,0	53,4	58,0	61,8	64,8	67,0	68,7	69,8	70,5	70,71	70,65
	% Increase:		31,2%	21,6%	15,4%	11,4%	8,6%	6,5%	4,8%	3,5%	2,5%	1,6%	0,9%	0,4%	-0,1%
	Cumulative % Inc.		31,2%	59,6%	84,2%	105,2%	122,8%	137,2%	148,6%	157,4%	163,8%	168,0%	170,5%	171,5%	171,2%

6m

		Upstand Height (mm)													
	Load Position:	0	10	20	30	40	50	60	70	80	90	100	110	120	130
		Critical Elastic Moment (kNm)													
B305x102x25	ABOVE FLANGE	15,8	20,0	24,0	27,4	30,5	33,1	35,4	37,4	39,0	40,3	41,4	42,3	42,89	43,34
	% Increase:		26,9%	19,5%	14,5%	11,1%	8,7%	6,9%	5,5%	4,4%	3,4%	2,7%	2,0%	1,5%	1,0%
	Cumulative % Inc.		26,9%	51,7%	73,6%	92,9%	109,8%	124,3%	136,6%	146,9%	155,4%	162,2%	167,5%	171,5%	174,3%

8m

		Upstand Height (mm)													
	Load Position:	0	10	20	30	40	50	60	70	80	90	100	110	120	130
		Critical Elastic Moment (kNm)													
B305x102x25	ABOVE FLANGE	11,6	14,4	17,0	19,3	21,4	23,3	25,0	26,4	27,7	28,8	29,8	30,6	31,31	31,88
	% Increase:		24,1%	18,1%	13,8%	10,9%	8,8%	7,2%	5,9%	4,9%	4,0%	3,3%	2,7%	2,2%	1,8%
	Cumulative % Inc.		24,1%	46,5%	66,8%	84,9%	101,1%	115,6%	128,3%	139,4%	149,1%	157,4%	164,5%	170,4%	175,3%

10m

		Upstand Height (mm)													
	Load Position:	0	10	20	30	40	50	60	70	80	90	100	110	120	130
		Critical Elastic Moment (kNm)													
B305x102x25	ABOVE FLANGE	9,2	11,3	13,2	15,0	16,6	18,1	19,4	20,6	21,6	22,6	23,5	24,2	24,88	25,46
	% Increase:		22,3%	17,1%	13,3%	10,7%	8,8%	7,3%	6,2%	5,2%	4,4%	3,8%	3,2%	2,7%	2,3%
	Cumulative % Inc.		22,3%	43,2%	62,2%	79,6%	95,3%	109,6%	122,5%	134,1%	144,5%	153,8%	161,9%	169,1%	175,4%

Table 5.36 Results for NF-305x102x28 with (b/H = 0.3) for all spans considered – UDL Load case

Beam: B305x102x28 2m Load: *UDL*

		Upstand Height (mm)													
	Load Position:	0	10	20	30	40	50	60	70	80	90	100	110	120	130
		Critical Elastic Moment (kNm)													
B305x102x28	ABOVE FLANGE	100,1	134,1	165,6	192,3	214,4	232,3	246,1	256,2	263,1	267,1	268,6	268,1	266,12	263,05
	% Increase:		34,0%	23,5%	16,1%	11,5%	8,3%	6,0%	4,1%	2,7%	1,5%	0,6%	-0,2%	-0,7%	-1,2%
	Cumulative % Inc.		34,0%	65,4%	92,1%	114,2%	132,1%	145,9%	156,0%	162,9%	166,8%	168,3%	167,9%	165,9%	162,8%

4m

		Upstand Height (mm)													
	Load Position:	0	10	20	30	40	50	60	70	80	90	100	110	120	130
		Critical Elastic Moment (kNm)													
B305x102x28	ABOVE FLANGE	35,8	46,0	55,6	64,0	71,3	77,6	82,9	87,2	90,8	93,6	95,6	97,1	98,14	98,72
	% Increase:		28,5%	20,9%	15,2%	11,4%	8,8%	6,8%	5,3%	4,1%	3,1%	2,2%	1,6%	1,0%	0,6%
	Cumulative % Inc.		28,5%	55,4%	78,9%	99,4%	116,9%	131,7%	144,0%	153,9%	161,6%	167,5%	171,7%	174,4%	176,1%

6m

		Upstand Height (mm)													
	Load Position:	0	10	20	30	40	50	60	70	80	90	100	110	120	130
		Critical Elastic Moment (kNm)													
B305x102x28	ABOVE FLANGE	22,2	27,7	32,9	37,6	41,9	45,7	49,0	51,9	54,5	56,6	58,5	60,1	61,37	62,44
	% Increase:		24,9%	18,9%	14,3%	11,2%	9,0%	7,3%	6,0%	4,9%	4,0%	3,3%	2,7%	2,2%	1,7%
	Cumulative % Inc.		24,9%	48,5%	69,8%	88,9%	105,9%	121,0%	134,2%	145,7%	155,5%	163,9%	171,0%	176,9%	181,7%

8m

		Upstand Height (mm)													
	Load Position:	0	10	20	30	40	50	60	70	80	90	100	110	120	130
		Critical Elastic Moment (kNm)													
B305x102x28	ABOVE FLANGE	16,4	20,1	23,7	26,9	29,9	32,6	35,1	37,3	39,3	41,1	42,7	44,2	45,43	46,54
	% Increase:		22,6%	17,7%	13,7%	11,0%	9,1%	7,6%	6,4%	5,4%	4,6%	3,9%	3,3%	2,9%	2,4%
	Cumulative % Inc.		22,6%	44,3%	64,1%	82,2%	98,7%	113,7%	127,3%	139,6%	150,6%	160,4%	169,1%	176,8%	183,6%

10m

		Upstand Height (mm)													
	Load Position:	0	10	20	30	40	50	60	70	80	90	100	110	120	130
		Critical Elastic Moment (kNm)													
B305x102x28	ABOVE FLANGE	13,2	15,9	18,6	21,1	23,4	25,5	27,5	29,3	31,0	32,5	33,9	35,2	36,34	37,40
	% Increase:		21,2%	16,8%	13,3%	10,9%	9,1%	7,7%	6,6%	5,7%	4,9%	4,3%	3,8%	3,3%	2,9%
	Cumulative % Inc.		21,2%	41,5%	60,3%	77,7%	93,9%	108,8%	122,6%	135,2%	146,9%	157,5%	167,3%	176,1%	184,2%

Table 5.37 Results for NF-406x140x39 with (b/H = 0.4) for all spans considered – UDL Load case

Beam:	B406x140x39	2m										Load:	*UDL*		
		Upstand Height (mm)													
	Load Position:	0	10	20	30	40	50	60	70	80	90	100	110	120	130
		Critical Elastic Moment (kNm)													
B406x140x39	ABOVE FLANGE	302,9	391,6	474,4	547,3	610,6	664,7	709,8	746,5	775,3	796,6	811,1	819,4	822,36	820,67
	% Increase:		29,3%	21,1%	15,4%	11,6%	8,9%	6,8%	5,2%	3,8%	2,7%	1,8%	1,0%	0,4%	-0,2%
	Cumulative % Inc.		29,3%	56,6%	80,7%	101,6%	119,4%	134,3%	146,4%	155,9%	162,9%	167,7%	170,5%	171,5%	170,9%
		4m													
		Upstand Height (mm)													
	Load Position:	0	10	20	30	40	50	60	70	80	90	100	110	120	130
		Critical Elastic Moment (kNm)													
B406x140x39	ABOVE FLANGE	88,8	112,5	134,8	154,6	172,0	187,2	200,1	211,0	219,9	227,0	232,3	236,1	238,55	239,73
	% Increase:		26,7%	19,8%	14,7%	11,3%	8,8%	6,9%	5,4%	4,2%	3,2%	2,4%	1,6%	1,0%	0,5%
	Cumulative % Inc.		26,7%	51,7%	74,0%	93,6%	110,7%	125,3%	137,5%	147,6%	155,5%	161,5%	165,8%	168,5%	169,9%
		6m													
		Upstand Height (mm)													
	Load Position:	0	10	20	30	40	50	60	70	80	90	100	110	120	130
		Critical Elastic Moment (kNm)													
B406x140x39	ABOVE FLANGE	48,2	59,7	70,6	80,4	89,2	97,0	103,8	109,7	114,7	119,0	122,4	125,2	127,28	128,81
	% Increase:		23,9%	18,3%	13,9%	10,9%	8,7%	7,0%	5,7%	4,6%	3,7%	2,9%	2,2%	1,7%	1,2%
	Cumulative % Inc.		23,9%	46,6%	67,0%	85,2%	101,4%	115,5%	127,8%	138,3%	147,1%	154,2%	160,0%	164,3%	167,5%
		8m													
		Upstand Height (mm)													
	Load Position:	0	10	20	30	40	50	60	70	80	90	100	110	120	130
		Critical Elastic Moment (kNm)													
B406x140x39	ABOVE FLANGE	33,1	40,2	47,1	53,3	58,9	64,0	68,5	72,5	76,1	79,2	81,8	84,1	85,92	87,45
	% Increase:		21,7%	17,0%	13,2%	10,6%	8,6%	7,1%	5,9%	4,9%	4,1%	3,3%	2,7%	2,2%	1,8%
	Cumulative % Inc.		21,7%	42,3%	61,1%	78,2%	93,5%	107,2%	119,4%	130,1%	139,5%	147,5%	154,2%	159,9%	164,5%
		10m													
		Upstand Height (mm)													
	Load Position:	0	10	20	30	40	50	60	70	80	90	100	110	120	130
		Critical Elastic Moment (kNm)													
B406x140x39	ABOVE FLANGE	25,5	30,5	35,4	39,9	43,9	47,7	51,1	54,1	56,9	59,4	61,5	63,4	65,11	66,55
	% Increase:		20,0%	15,9%	12,6%	10,3%	8,5%	7,1%	6,0%	5,1%	4,3%	3,7%	3,1%	2,6%	2,2%
	Cumulative % Inc.		20,0%	39,1%	56,6%	72,7%	87,3%	100,7%	112,7%	123,5%	133,2%	141,8%	149,3%	155,8%	161,5%

Table 5.38 Results for NF-533x210x122 with (b/H = 0.4) for all spans considered – UDL Load case

Beam: B533x210x122 2m Load: *UDL*

		Upstand Height (mm)													
	Load Position:	0	10	20	30	40	50	60	70	80	90	100	110	120	130
		Critical Elastic Moment (kNm)													
B533x210x122	ABOVE FLANGE	3 394,8	3 890,3	4 464,7	4 990,4	5 468,5	5 900,1	6 286,5	6 629,0	6 929,0	7 188,1	7 408,0	7 590,6	7 737,88	7 852,14
	% Increase:		14,6%	14,8%	11,8%	9,6%	7,9%	6,5%	5,4%	4,5%	3,7%	3,1%	2,5%	1,9%	1,5%
	Cumulative % Inc.		14,6%	31,5%	47,0%	61,1%	73,8%	85,2%	95,3%	104,1%	111,7%	118,2%	123,6%	127,9%	131,3%

4m

		Upstand Height (mm)													
	Load Position:	0	10	20	30	40	50	60	70	80	90	100	110	120	130
		Critical Elastic Moment (kNm)													
B533x210x122	ABOVE FLANGE	1 026,8	1 164,6	1 323,0	1 469,4	1 604,1	1 727,4	1 839,7	1 941,2	2 032,3	2 113,3	2 184,7	2 246,8	2 300,16	2 345,19
	% Increase:		13,4%	13,6%	11,1%	9,2%	7,7%	6,5%	5,5%	4,7%	4,0%	3,4%	2,8%	2,4%	2,0%
	Cumulative % Inc.		13,4%	28,8%	43,1%	56,2%	68,2%	79,2%	89,0%	97,9%	105,8%	112,8%	118,8%	124,0%	128,4%

6m

		Upstand Height (mm)													
	Load Position:	0	10	20	30	40	50	60	70	80	90	100	110	120	130
		Critical Elastic Moment (kNm)													
B533x210x122	ABOVE FLANGE	572,0	642,2	721,9	796,4	865,8	930,1	989,7	1 044,6	1 094,9	1 140,8	1 182,5	1 220,0	1 253,70	1 283,63
	% Increase:		12,3%	12,4%	10,3%	8,7%	7,4%	6,4%	5,5%	4,8%	4,2%	3,7%	3,2%	2,8%	2,4%
	Cumulative % Inc.		12,3%	26,2%	39,2%	51,4%	62,6%	73,0%	82,6%	91,4%	99,4%	106,7%	113,3%	119,2%	124,4%

8m

		Upstand Height (mm)													
	Load Position:	0	10	20	30	40	50	60	70	80	90	100	110	120	130
		Critical Elastic Moment (kNm)													
B533x210x122	ABOVE FLANGE	400,1	445,6	496,7	544,8	590,0	632,5	672,2	709,4	744,0	776,2	806,0	833,5	858,78	881,93
	% Increase:		11,4%	11,5%	9,7%	8,3%	7,2%	6,3%	5,5%	4,9%	4,3%	3,8%	3,4%	3,0%	2,7%
	Cumulative % Inc.		11,4%	24,1%	36,2%	47,5%	58,1%	68,0%	77,3%	86,0%	94,0%	101,5%	108,3%	114,6%	120,4%

10m

		Upstand Height (mm)													
	Load Position:	0	10	20	30	40	50	60	70	80	90	100	110	120	130
		Critical Elastic Moment (kNm)													
B533x210x122	ABOVE FLANGE	311,6	345,0	382,0	417,1	450,3	481,8	511,6	539,7	566,2	591,1	614,5	636,4	656,90	675,99
	% Increase:		10,7%	10,7%	9,2%	8,0%	7,0%	6,2%	5,5%	4,9%	4,4%	4,0%	3,6%	3,2%	2,9%
	Cumulative % Inc.		10,7%	22,6%	33,8%	44,5%	54,6%	64,2%	73,2%	81,7%	89,7%	97,2%	104,2%	110,8%	116,9%

Table 5.39 Results for NF-305x102x25 (b/H = 0.3) – All spans consolidated trend (M_{cr}) - UDL

Span (m)	Upstand Height (mm)													
	0	10	20	30	40	50	60	70	80	90	100	110	120	130
	Mcr (kNm)													
2	76,0	104,3	129,6	150,9	168,4	182,3	192,9	200,4	205,1	207,5	207,8	206,6	204,2	201,0
4	26,0	34,2	41,6	48,0	53,4	58,0	61,8	64,8	67,0	68,7	69,8	70,5	70,7	70,6
6	15,8	20,0	24,0	27,4	30,5	33,1	35,4	37,4	39,0	40,3	41,4	42,3	42,9	43,3
8	11,6	14,4	17,0	19,3	21,4	23,3	25,0	26,4	27,7	28,8	29,8	30,6	31,3	31,9
10	9,2	11,3	13,2	15,0	16,6	18,1	19,4	20,6	21,6	22,6	23,5	24,2	24,9	25,5

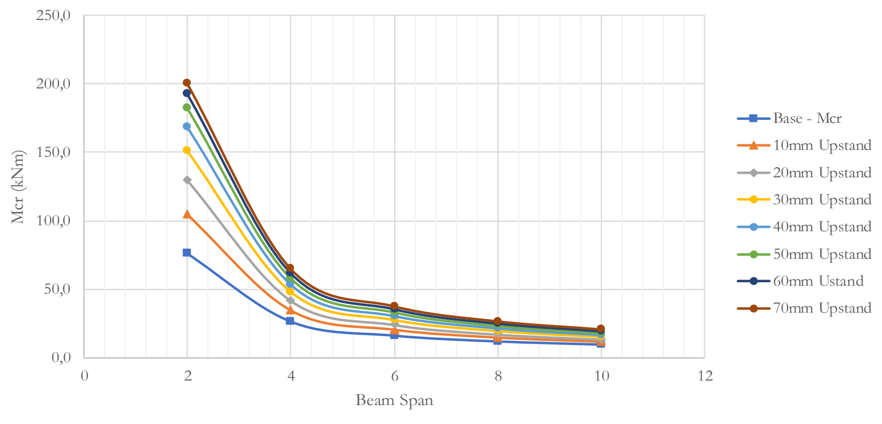

Table 5.40 Results for NF-305x102x28 (b/H = 0.3) – All spans consolidated trend (M_{cr}) - UDL

Span (m)	Upstand Height (mm)													
	0	10	20	30	40	50	60	70	80	90	100	110	120	130
	Mcr (kNm)													
2	100,1	134,1	165,6	192,3	214,4	232,3	246,1	256,2	263,1	267,1	268,6	268,1	266,1	263,1
4	35,8	46,0	55,6	64,0	71,3	77,6	82,9	87,2	90,8	93,6	95,6	97,1	98,1	98,7
6	22,2	27,7	32,9	37,6	41,9	45,7	49,0	51,9	54,5	56,6	58,5	60,1	61,4	62,4
8	16,4	20,1	23,7	26,9	29,9	32,6	35,1	37,3	39,3	41,1	42,7	44,2	45,4	46,5
10	13,2	15,9	18,6	21,1	23,4	25,5	27,5	29,3	31,0	32,5	33,9	35,2	36,3	37,4

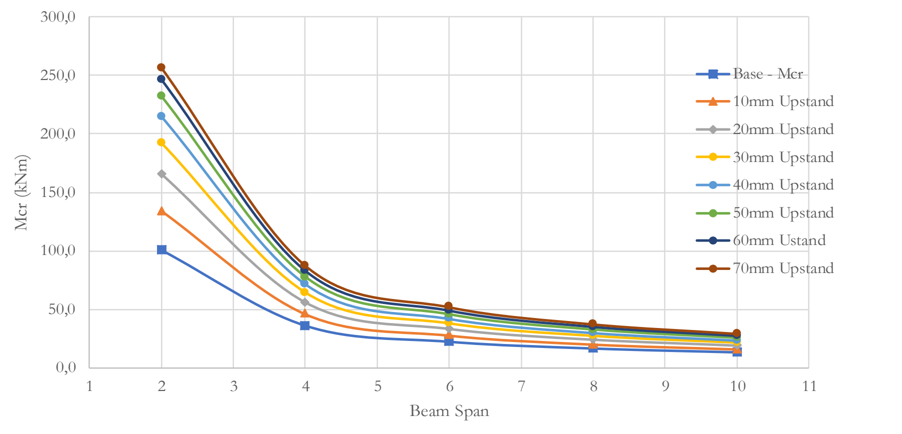

Table 5.41 Results for NF-406x140x39 (b/H = 0.4) – All spans consolidated trend (M_{cr}) - UDL

Span	Upstand Height (mm)													
	0	10	20	30	40	50	60	70	80	90	100	110	120	130
	Mcr (kNm)													
2	302,9	391,6	474,4	547,3	610,6	664,7	709,8	746,5	775,3	796,6	811,1	819,4	822,4	820,7
4	88,8	112,5	134,8	154,6	172,0	187,2	200,1	211,0	219,9	227,0	232,3	236,1	238,5	239,7
6	48,2	59,7	70,6	80,4	89,2	97,0	103,8	109,7	114,7	119,0	122,4	125,2	127,3	128,8
8	33,1	40,2	47,1	53,3	58,9	64,0	68,5	72,5	76,1	79,2	81,8	84,1	85,9	87,4
10	25,5	30,5	35,4	39,9	43,9	47,7	51,1	54,1	56,9	59,4	61,5	63,4	65,1	66,5

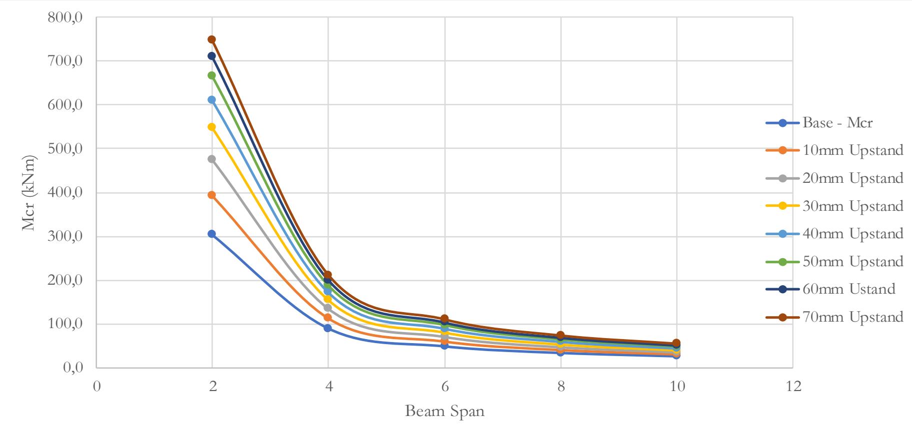

Table 5.42 Results for NF-533x210x122 (b/H = 0.4) – All spans consolidated trend (M_{cr}) – UDL

Span	Upstand Height (mm)													
	0	10	20	30	40	50	60	70	80	90	100	110	120	130
	Mcr (kNm)													
2	3 394,8	3 890,3	4 464,7	4 990,4	5 468,5	5 900,1	6 286,5	6 629,0	6 929,0	7 188,1	7 408,0	7 590,6	7 737,9	7 852,1
4	1 026,8	1 164,6	1 323,0	1 469,4	1 604,1	1 727,4	1 839,7	1 941,2	2 032,3	2 113,3	2 184,7	2 246,8	2 300,2	2 345,2
6	572,0	642,2	721,9	796,4	865,8	930,1	989,7	1 044,6	1 094,9	1 140,8	1 182,5	1 220,0	1 253,7	1 283,6
8	400,1	445,6	496,7	544,8	590,0	632,5	672,2	709,4	744,0	776,2	806,0	833,5	858,8	881,9
10	311,6	345,0	382,0	417,1	450,3	481,8	511,6	539,7	566,2	591,1	614,5	636,4	656,9	676,0

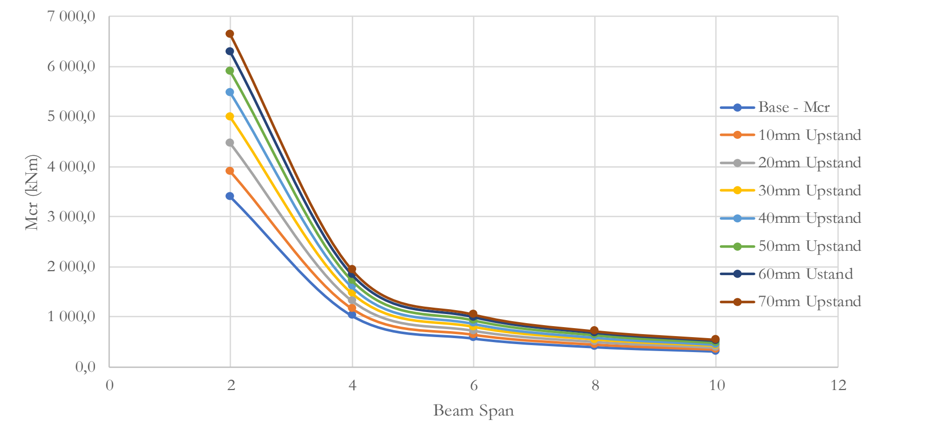

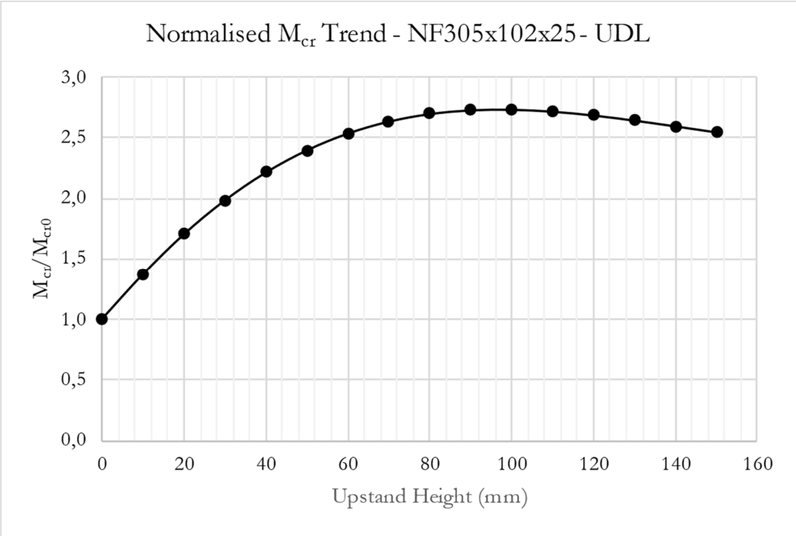

Fig.5-15 Normalised critical moment vs upstand height - BU_1

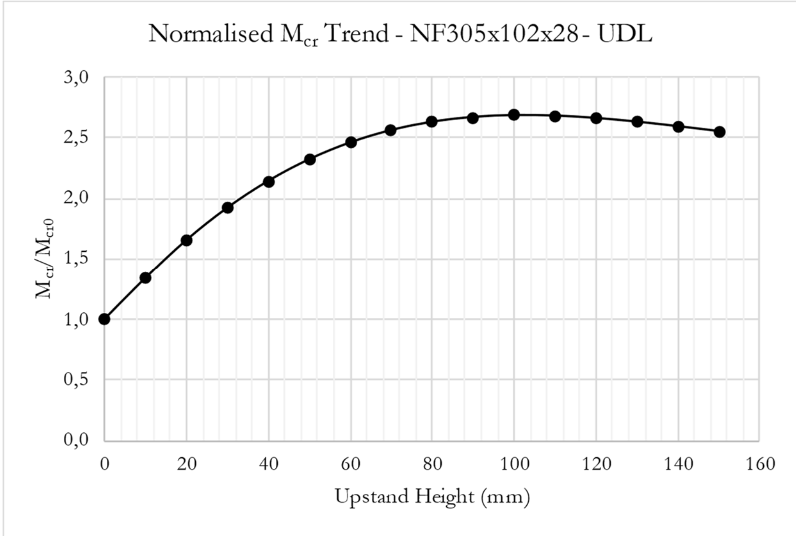

Fig.5-16 Normalised critical moment vs upstand height - BU_2

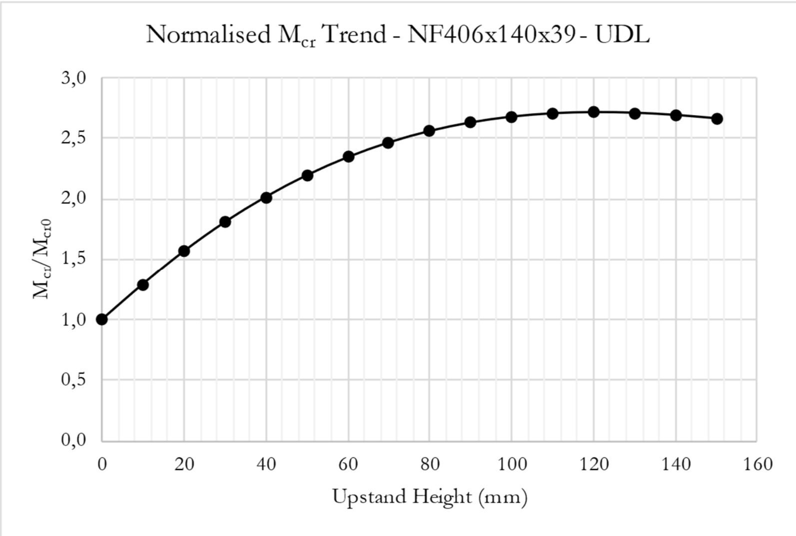

Fig.5-17 Normalised critical moment vs upstand height – BU_3

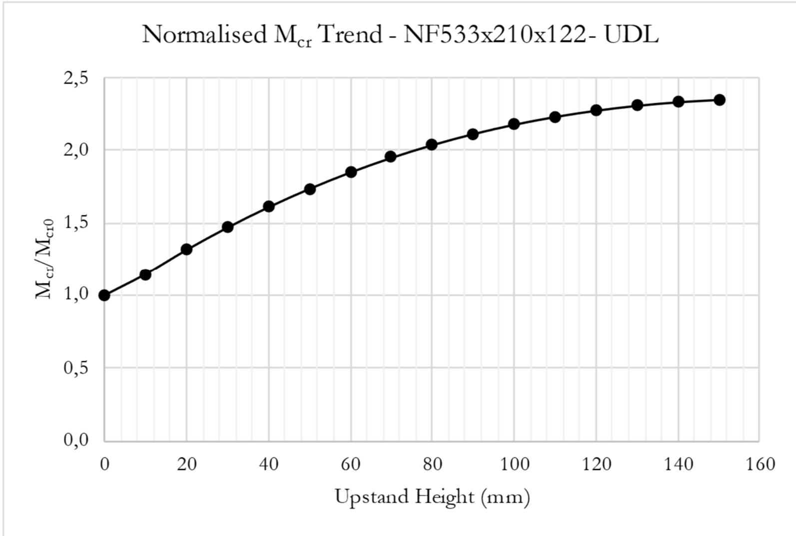

Fig.5-18 Normalised critical moment vs upstand height - BU_4

Tabulated results from Tables 5.35 to 5.38 show similar trends to what was observed with the point load case. The trend with percentage change is also similar with the first three members having higher initial percentage changes than the fourth member (BU_4). All other trends are similar to what was observed and reported for the point load case. The next set of four members are now considered.

5.3.2.2 Trends for Beams with (b/H) = 0.5 & 0.6 UDL case

The sets of results are presented in the sequence indicated in Table 5.43 for the four members considered.

Table 5.43 Second group of four 'NF' members under UDL

Member	***Beam***	***b/H***	***Set 1***	***Set 2***	***Set 3***
NF IPE 160	BU_5	0.5	Tabulated results for all spans	Plots of M_{cr} for all spans	Graph of normalised M_{cr} against upstand height for 2m span
NF 305x165x40	BU_6	0.5			
NF IPE 100	BU_7	0.6			
NF 254x146x31	BU_8	0.6			

Table 5.44 Results for NF-IPE 160 with (b/H = 0.5) for all spans considered – UDL Load case

Beam: IPE 160 2m Load: *UDL*

		Upstand Height (mm)													
	Load Position:	0	10	20	30	40	50	60	70	80	90	100	110	120	130
		Critical Elastic Moment (kNm)													
IPE 160	ABOVE FLANGE	30,9	41,2	49,9	56,4	61,1	64,1	65,7	66,4	66,3	65,9	65,2	64,7	64,22	64,02
	% Increase:		33,5%	21,1%	13,1%	8,2%	4,9%	2,6%	1,0%	-0,1%	-0,7%	-0,9%	-0,9%	-0,7%	-0,3%
	Cumulative % Inc.		33,5%	61,7%	82,9%	97,9%	107,6%	113,0%	115,0%	114,9%	113,4%	111,4%	109,5%	108,1%	107,5%

4m

		Upstand Height (mm)													
	Load Position:	0	10	20	30	40	50	60	70	80	90	100	110	120	130
		Critical Elastic Moment (kNm)													
IPE 160	ABOVE FLANGE	14,0	17,9	21,3	24,3	26,7	28,7	30,2	31,5	32,4	33,1	33,6	34,0	34,29	34,50
	% Increase:		27,5%	19,3%	13,6%	10,0%	7,4%	5,5%	4,1%	3,0%	2,2%	1,6%	1,1%	0,8%	0,6%
	Cumulative % Inc.		27,5%	52,1%	72,9%	90,1%	104,2%	115,5%	124,2%	131,0%	136,0%	139,7%	142,4%	144,4%	145,9%

6m

		Upstand Height (mm)													
	Load Position:	0	10	20	30	40	50	60	70	80	90	100	110	120	130
		Critical Elastic Moment (kNm)													
IPE 160	ABOVE FLANGE	9,4	11,8	13,9	15,8	17,5	19,0	20,3	21,4	22,3	23,1	23,8	24,4	24,88	25,30
	% Increase:		24,9%	18,3%	13,7%	10,6%	8,4%	6,7%	5,4%	4,4%	3,6%	3,0%	2,4%	2,0%	1,7%
	Cumulative % Inc.		24,9%	47,8%	68,0%	85,8%	101,4%	114,9%	126,6%	136,6%	145,2%	152,5%	158,6%	163,9%	168,3%

8m

		Upstand Height (mm)													
	Load Position:	0	10	20	30	40	50	60	70	80	90	100	110	120	130
		Critical Elastic Moment (kNm)													
IPE 160	ABOVE FLANGE	7,2	8,9	10,4	11,9	13,1	14,3	15,4	16,3	17,2	17,9	18,6	19,2	19,75	20,23
	% Increase:		23,5%	17,7%	13,7%	10,9%	8,9%	7,4%	6,2%	5,2%	4,4%	3,8%	3,3%	2,8%	2,4%
	Cumulative % Inc.		23,5%	45,4%	65,3%	83,3%	99,5%	114,2%	127,4%	139,3%	149,8%	159,3%	167,7%	175,2%	182,0%

10m

		Upstand Height (mm)													
	Load Position:	0	10	20	30	40	50	60	70	80	90	100	110	120	130
		Critical Elastic Moment (kNm)													
IPE 160	ABOVE FLANGE	5,8	7,1	8,4	9,5	10,6	11,5	12,4	13,2	14,0	14,7	15,3	15,9	16,41	16,90
	% Increase:		22,7%	17,3%	13,6%	11,0%	9,2%	7,7%	6,6%	5,7%	4,9%	4,3%	3,8%	3,3%	3,0%
	Cumulative % Inc.		22,7%	44,0%	63,6%	81,7%	98,3%	113,6%	127,7%	140,7%	152,6%	163,5%	173,4%	182,6%	190,9%

Table 5.45 Results for NF-305x165x40 with (b/H = 0.5) for all spans considered – UDL Load case

Beam: B305x165x40 — 2m — Load: *UDL*

		Upstand Height (mm)													
	Load Position:	0	10	20	30	40	50	60	70	80	90	100	110	120	130
		Critical Elastic Moment (kNm)													
B305x165x40	ABOVE FLANGE	436,9	540,2	635,5	716,6	783,9	838,0	879,6	909,8	929,6	940,2	942,8	939,0	929,97	917,25
	% Increase:		23,6%	17,7%	12,8%	9,4%	6,9%	5,0%	3,4%	2,2%	1,1%	0,3%	-0,4%	-1,0%	-1,4%
	Cumulative % Inc.		23,6%	45,4%	64,0%	79,4%	91,8%	101,3%	108,2%	112,8%	115,2%	115,8%	114,9%	112,8%	109,9%

4m

		Upstand Height (mm)													
	Load Position:	0	10	20	30	40	50	60	70	80	90	100	110	120	130
		Critical Elastic Moment (kNm)													
B305x165x40	ABOVE FLANGE	134,5	163,1	189,8	213,0	232,9	249,5	263,1	273,8	281,8	287,5	291,1	292,9	293,16	292,23
	% Increase:		21,3%	16,4%	12,2%	9,3%	7,1%	5,4%	4,1%	2,9%	2,0%	1,2%	0,6%	0,1%	-0,3%
	Cumulative % Inc.		21,3%	41,2%	58,4%	73,2%	85,6%	95,6%	103,6%	109,6%	113,8%	116,5%	117,8%	118,0%	117,3%

6m

		Upstand Height (mm)													
	Load Position:	0	10	20	30	40	50	60	70	80	90	100	110	120	130
		Critical Elastic Moment (kNm)													
B305x165x40	ABOVE FLANGE	75,9	90,4	104,1	116,3	126,9	136,2	144,1	150,8	156,2	160,6	163,9	166,4	168,14	169,19
	% Increase:		19,1%	15,1%	11,7%	9,2%	7,3%	5,8%	4,6%	3,6%	2,8%	2,1%	1,5%	1,0%	0,6%
	Cumulative % Inc.		19,1%	37,1%	53,1%	67,2%	79,4%	89,8%	98,5%	105,7%	111,4%	115,9%	119,2%	121,4%	122,8%

8m

		Upstand Height (mm)													
	Load Position:	0	10	20	30	40	50	60	70	80	90	100	110	120	130
		Critical Elastic Moment (kNm)													
B305x165x40	ABOVE FLANGE	53,6	62,9	71,8	79,8	87,0	93,4	99,1	104,0	108,2	111,9	114,9	117,4	119,42	121,01
	% Increase:		17,4%	14,1%	11,2%	9,0%	7,4%	6,0%	5,0%	4,1%	3,3%	2,7%	2,2%	1,7%	1,3%
	Cumulative % Inc.		17,4%	34,0%	49,0%	62,4%	74,4%	84,9%	94,1%	102,1%	108,8%	114,5%	119,2%	122,9%	125,9%

10m

		Upstand Height (mm)													
	Load Position:	0	10	20	30	40	50	60	70	80	90	100	110	120	130
		Critical Elastic Moment (kNm)													
B305x165x40	ABOVE FLANGE	41,9	48,7	55,2	61,2	66,6	71,5	75,9	79,9	83,4	86,5	89,3	91,6	93,65	95,38
	% Increase:		16,2%	13,3%	10,8%	8,9%	7,4%	6,2%	5,2%	4,4%	3,7%	3,1%	2,6%	2,2%	1,8%
	Cumulative % Inc.		16,2%	31,7%	45,9%	58,8%	70,6%	81,1%	90,6%	99,0%	106,4%	112,9%	118,5%	123,4%	127,5%

Table 5.46 Results for NF-IPE 100 with (b/H = 0.6) for all spans considered – UDL Load case

Beam:	IPE 100	2m								Load:	UDL				
		Upstand Height (mm)													
	Load Position:	0	10	20	30	40	50	60	70	80	90	100	110	120	130
		Critical Elastic Moment (kNm)													
IPE 100	ABOVE FLANGE	15,1	20,9	25,5	28,9	31,1	32,5	33,4	33,8	34,1	34,3	34,5	34,8	35,21	35,77
	% Increase:		38,3%	21,9%	13,0%	7,8%	4,6%	2,6%	1,4%	0,8%	0,6%	0,6%	0,9%	1,2%	1,6%
	Cumulative % Inc.		38,3%	68,6%	90,5%	105,3%	114,8%	120,3%	123,3%	125,0%	126,2%	127,6%	129,6%	132,4%	136,1%
		4m													
		Upstand Height (mm)													
	Load Position:	0	10	20	30	40	50	60	70	80	90	100	110	120	130
		Critical Elastic Moment (kNm)													
IPE 100	ABOVE FLANGE	3,9	5,1	6,3	7,2	8,0	8,7	9,2	9,6	10,0	10,3	10,5	10,8	10,94	11,11
	% Increase:		33,3%	21,8%	15,1%	11,0%	8,2%	6,2%	4,8%	3,8%	3,0%	2,4%	2,0%	1,7%	1,5%
	Cumulative % Inc.		33,3%	62,3%	86,8%	107,3%	124,3%	138,3%	149,8%	159,2%	166,9%	173,3%	178,7%	183,5%	187,8%
		6m													
		Upstand Height (mm)													
	Load Position:	0	10	20	30	40	50	60	70	80	90	100	110	120	130
		Critical Elastic Moment (kNm)													
IPE 100	ABOVE FLANGE	2,6	3,5	4,2	4,9	5,5	6,0	6,4	6,8	7,2	7,5	7,8	8,1	8,28	8,48
	% Increase:		31,5%	21,6%	15,8%	12,1%	9,6%	7,7%	6,3%	5,3%	4,4%	3,7%	3,2%	2,8%	2,4%
	Cumulative % Inc.		31,5%	59,9%	85,1%	107,4%	127,3%	144,8%	160,3%	173,9%	186,0%	196,7%	206,3%	214,8%	222,4%
		8m													
		Upstand Height (mm)													
	Load Position:	0	10	20	30	40	50	60	70	80	90	100	110	120	130
		Critical Elastic Moment (kNm)													
IPE 100	ABOVE FLANGE	2,0	2,6	3,2	3,7	4,2	4,6	5,0	5,3	5,6	5,9	6,2	6,5	6,69	6,89
	% Increase:		30,6%	21,4%	16,1%	12,6%	10,2%	8,5%	7,1%	6,1%	5,2%	4,6%	4,0%	3,5%	3,1%
	Cumulative % Inc.		30,6%	58,6%	84,1%	107,4%	128,6%	148,0%	165,8%	181,9%	196,7%	210,3%	222,7%	234,1%	244,5%
		10m													
		Upstand Height (mm)													
	Load Position:	0	10	20	30	40	50	60	70	80	90	100	110	120	130
		Critical Elastic Moment (kNm)													
IPE 100	ABOVE FLANGE	1,6	2,1	2,6	3,0	3,4	3,7	4,0	4,3	4,6	4,9	5,2	5,4	5,61	5,81
	% Increase:		30,1%	21,4%	16,3%	13,0%	10,7%	9,0%	7,7%	6,6%	5,8%	5,1%	4,5%	4,0%	3,6%
	Cumulative % Inc.		30,1%	57,9%	83,5%	107,3%	129,4%	150,0%	169,1%	186,9%	203,5%	219,0%	233,4%	246,9%	259,5%

Table 5.47 Results for NF-254x146x31 with (b/H = 0.6) for all spans considered – UDL Load case

Beam: B254x146x31 Load: *UDL*

2m

		Upstand Height (mm)													
	Load Position:	0	10	20	30	40	50	60	70	80	90	100	110	120	130
		Critical Elastic Moment (kNm)													
B254x146x31	ABOVE FLANGE	218,5	275,8	326,5	368,0	400,6	424,9	441,6	451,7	455,9	455,4	451,3	444,5	436,24	427,28
	% Increase:		26,2%	18,4%	12,7%	8,9%	6,1%	3,9%	2,3%	0,9%	-0,1%	-0,9%	-1,5%	-1,9%	-2,1%
	Cumulative % Inc.		26,2%	49,4%	68,4%	83,3%	94,5%	102,1%	106,7%	108,7%	108,4%	106,5%	103,5%	99,7%	95,6%

4m

		Upstand Height (mm)													
	Load Position:	0	10	20	30	40	50	60	70	80	90	100	110	120	130
		Critical Elastic Moment (kNm)													
B254x146x31	ABOVE FLANGE	71,3	87,7	102,5	115,0	125,3	133,6	140,0	144,7	147,8	149,6	150,4	150,3	149,49	148,28
	% Increase:		22,9%	16,9%	12,2%	9,0%	6,6%	4,8%	3,3%	2,2%	1,2%	0,5%	-0,1%	-0,5%	-0,8%
	Cumulative % Inc.		22,9%	43,7%	61,2%	75,7%	87,3%	96,3%	102,8%	107,2%	109,8%	110,8%	110,7%	109,6%	107,9%

6m

		Upstand Height (mm)													
	Load Position:	0	10	20	30	40	50	60	70	80	90	100	110	120	130
		Critical Elastic Moment (kNm)													
B254x146x31	ABOVE FLANGE	42,0	50,5	58,4	65,2	71,1	76,0	80,1	83,5	86,1	88,1	89,5	90,4	90,97	91,21
	% Increase:		20,3%	15,5%	11,7%	9,0%	7,0%	5,4%	4,2%	3,1%	2,3%	1,6%	1,1%	0,6%	0,3%
	Cumulative % Inc.		20,3%	38,9%	55,1%	69,1%	80,9%	90,7%	98,6%	104,8%	109,5%	112,9%	115,2%	116,5%	117,0%

8m

		Upstand Height (mm)													
	Load Position:	0	10	20	30	40	50	60	70	80	90	100	110	120	130
		Critical Elastic Moment (kNm)													
B254x146x31	ABOVE FLANGE	30,4	36,0	41,2	45,8	49,9	53,5	56,6	59,2	61,5	63,3	64,8	66,0	66,95	67,65
	% Increase:		18,4%	14,5%	11,3%	9,0%	7,2%	5,8%	4,7%	3,8%	3,0%	2,4%	1,8%	1,4%	1,0%
	Cumulative % Inc.		18,4%	35,5%	50,8%	64,3%	76,1%	86,3%	95,1%	102,4%	108,5%	113,5%	117,4%	120,5%	122,8%

10m

		Upstand Height (mm)													
	Load Position:	0	10	20	30	40	50	60	70	80	90	100	110	120	130
		Critical Elastic Moment (kNm)													
B254x146x31	ABOVE FLANGE	24,1	28,2	32,1	35,6	38,7	41,6	44,1	46,3	48,2	49,9	51,4	52,6	53,66	54,52
	% Increase:		17,1%	13,7%	10,9%	8,9%	7,3%	6,1%	5,0%	4,2%	3,5%	2,9%	2,4%	2,0%	1,6%
	Cumulative % Inc.		17,1%	33,2%	47,8%	60,9%	72,7%	83,1%	92,3%	100,4%	107,4%	113,4%	118,6%	122,9%	126,5%

Table 5.48 Results for NF-IPE 160 (b/H = 0.5) – All spans consolidated trend (M_{cr}) – UDL

	Upstand Height (mm)													
Span	0	10	20	30	40	50	60	70	80	90	100	110	120	130
	Mcr (kNm)													
2	30,9	41,2	49,9	56,4	61,1	64,1	65,7	66,4	66,3	65,9	65,2	64,7	64,2	64,0
4	14,0	17,9	21,3	24,3	26,7	28,7	30,2	31,5	32,4	33,1	33,6	34,0	34,3	34,5
6	9,4	11,8	13,9	15,8	17,5	19,0	20,3	21,4	22,3	23,1	23,8	24,4	24,9	25,3
8	7,2	8,9	10,4	11,9	13,1	14,3	15,4	16,3	17,2	17,9	18,6	19,2	19,7	20,2
10	5,8	7,1	8,4	9,5	10,6	11,5	12,4	13,2	14,0	14,7	15,3	15,9	16,4	16,9

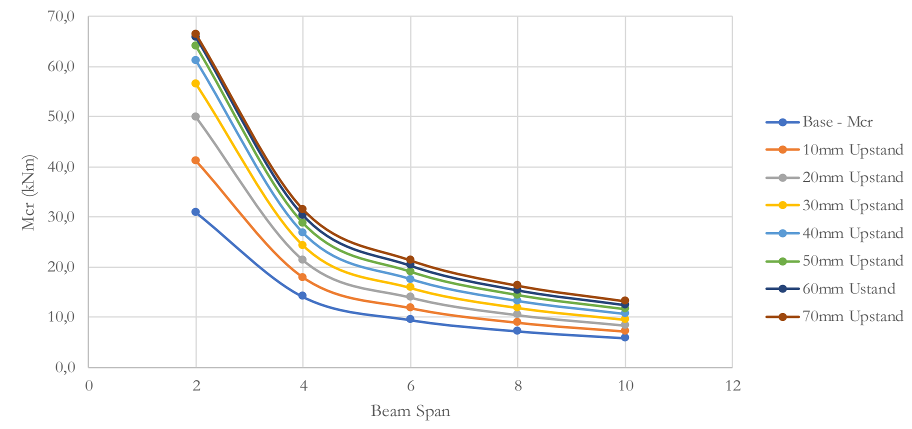

Table 5.49 Results for NF-254x146x31 (b/H = 0.5) – All spans consolidated trend (M_{cr}) - UDL

Span	0	10	20	30	40	50	60	70	80	90	100	110	120	130
	Mcr (kNm)													
2	436,9	540,2	635,5	716,6	783,9	838,0	879,6	909,8	929,6	940,2	942,8	939,0	930,0	917,3
4	134,5	163,1	189,8	213,0	232,9	249,5	263,1	273,8	281,8	287,5	291,1	292,9	293,2	292,2
6	75,9	90,4	104,1	116,3	126,9	136,2	144,1	150,8	156,2	160,6	163,9	166,4	168,1	169,2
8	53,6	62,9	71,8	79,8	87,0	93,4	99,1	104,0	108,2	111,9	114,9	117,4	119,4	121,0
10	41,9	48,7	55,2	61,2	66,6	71,5	75,9	79,9	83,4	86,5	89,3	91,6	93,7	95,4

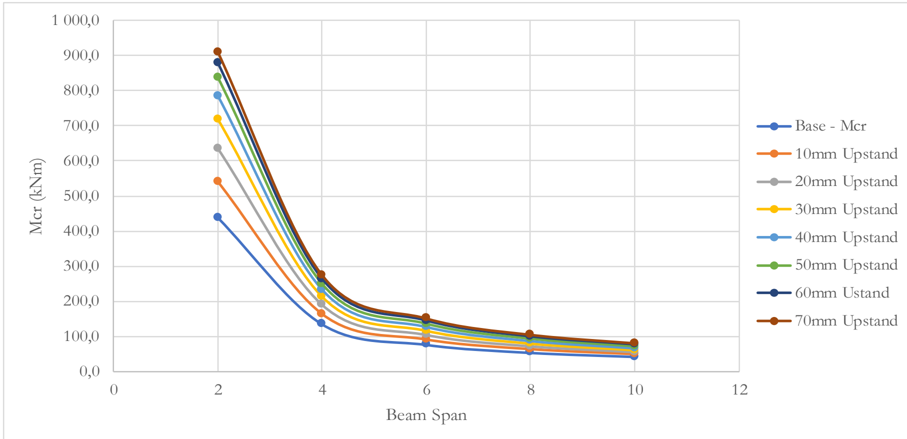

Table 5.50 Results for NF-IPE 100 (b/H = 0.6) – All spans consolidated trend (M_{cr}) – UDL

	Upstand Height (mm)													
Span (m)	0	10	20	30	40	50	60	70	80	90	100	110	120	130
	Mcr (kNm)													
2	15,1	20,9	25,5	28,9	31,1	32,5	33,4	33,8	34,1	34,3	34,5	34,8	35,2	35,8
4	3,9	5,1	6,3	7,2	8,0	8,7	9,2	9,6	10,0	10,3	10,5	10,8	10,9	11,1
6	2,6	3,5	4,2	4,9	5,5	6,0	6,4	6,8	7,2	7,5	7,8	8,1	8,3	8,5
8	2,0	2,6	3,2	3,7	4,2	4,6	5,0	5,3	5,6	5,9	6,2	6,5	6,7	6,9
10	1,6	2,1	2,6	3,0	3,4	3,7	4,0	4,3	4,6	4,9	5,2	5,4	5,6	5,8

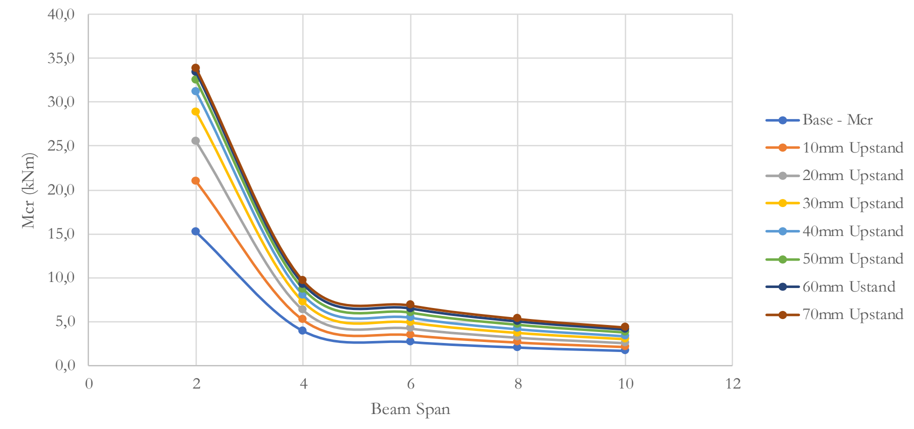

Table 5.51 Results for NF-254x146x31 (b/H = 0.6) – All spans consolidated trend (M_{cr}) – UDL

	Upstand Height (mm)													
Span (m)	0	10	20	30	40	50	60	70	80	90	100	110	120	130
	Mcr (kNm)													
2	218,5	275,8	326,5	368,0	400,6	424,9	441,6	451,7	455,9	455,4	451,3	444,5	436,2	427,3
4	71,3	87,7	102,5	115,0	125,3	133,6	140,0	144,7	147,8	149,6	150,4	150,3	149,5	148,3
6	42,0	50,5	58,4	65,2	71,1	76,0	80,1	83,5	86,1	88,1	89,5	90,4	91,0	91,2
8	30,4	36,0	41,2	45,8	49,9	53,5	56,6	59,2	61,5	63,3	64,8	66,0	67,0	67,7
10	24,1	28,2	32,1	35,6	38,7	41,6	44,1	46,3	48,2	49,9	51,4	52,6	53,7	54,5

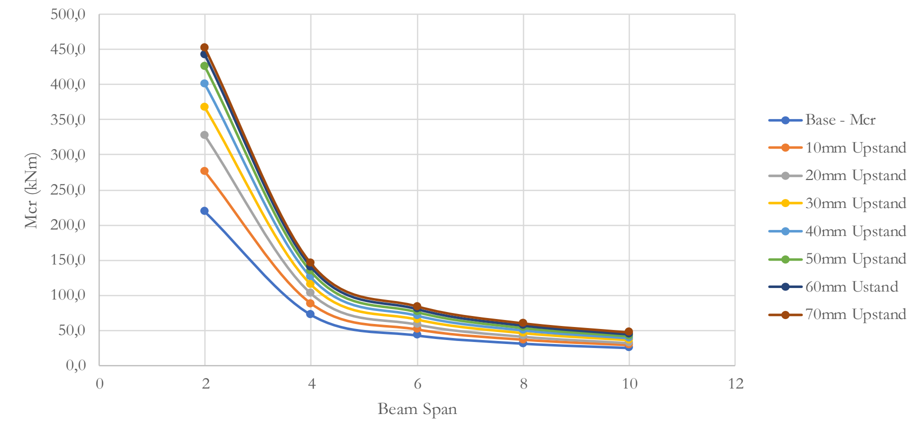

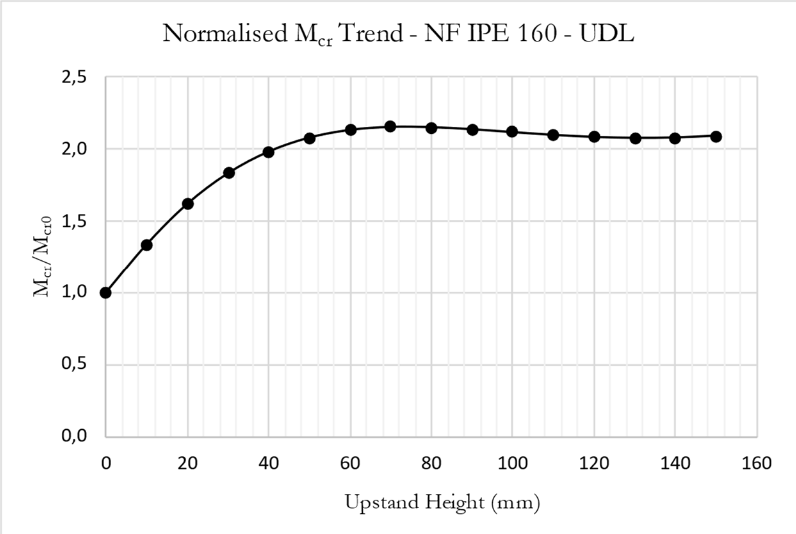

Fig.5-19 Normalised critical moment vs upstand height – BU_5

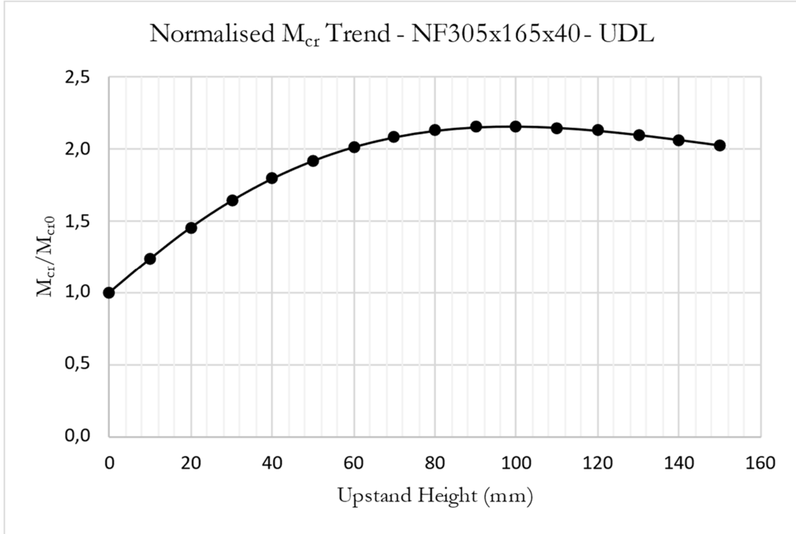

Fig.5-20 Normalised critical moment vs upstand height - BU_6

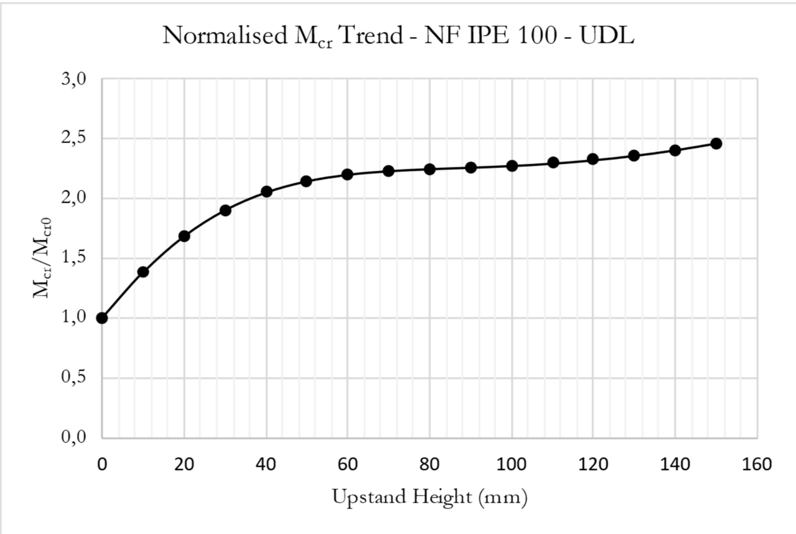

Fig.5-21 Normalised critical moment vs upstand height – BU_7

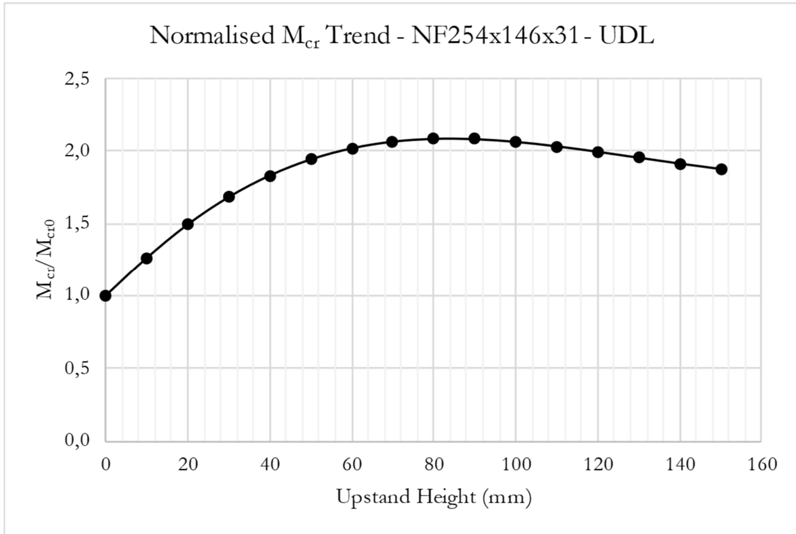

Fig.5-22 Normalised critical moment vs upstand height - BU_8

Tabulated results for the four members from Table 5.44 to 5.47 show similar trends to the last group of four members and also to what was observed with the point load case. The percentages of change in critical elastic moment also lie within the same range for both load cases. The trend can therefore be said to be consistent for the loading conditions and members considered.

5.3.2.3 Trends for Beams with (b/H) = 0.7 for UDL case

The sets of results are presented in the sequence indicated in Table 5.52 for the two members considered.

Table 5.52 Last group of two 'NF' members under UDL

Member	***Beam***	***b/H***	***Set 1***	***Set 2***	***Set 3***
NF 203x133x25	BU_9	0.7	Tabulated results for all spans	Plots of M_{cr} for all spans	Graph of normalised M_{cr} against upstand height for 2m span
NF 203x133x30	BU_{10}	0.7			

Table 5.53 Results for NF-203x133x25 with (b/H = 0.7) for all spans considered – UDL Load case

Beam: B203x133x25 2m Load: *UDL*

		Upstand Height (mm)													
	Load Position:	0	10	20	30	40	50	60	70	80	90	100	110	120	130
		Critical Elastic Moment (kNm)													
B203x133x25	ABOVE FLANGE	128,1	163,0	192,6	215,5	232,0	243,0	248,9	250,9	249,6	246,1	241,4	236,1	230,85	226,24
	% Increase:		27,2%	18,1%	11,9%	7,7%	4,7%	2,5%	0,8%	-0,5%	-1,4%	-1,9%	-2,2%	-2,2%	-2,0%
	Cumulative % Inc.		27,2%	50,3%	68,1%	81,1%	89,6%	94,3%	95,7%	94,8%	92,1%	88,3%	84,2%	80,1%	76,5%

4m

		Upstand Height (mm)													
	Load Position:	0	10	20	30	40	50	60	70	80	90	100	110	120	130
		Critical Elastic Moment (kNm)													
B203x133x25	ABOVE FLANGE	45,3	55,8	65,0	72,6	78,6	83,2	86,5	88,6	89,9	90,4	90,3	89,8	89,09	88,28
	% Increase:		23,2%	16,5%	11,6%	8,3%	5,8%	4,0%	2,5%	1,4%	0,5%	-0,1%	-0,5%	-0,8%	-0,9%
	Cumulative % Inc.		23,2%	43,5%	60,1%	73,4%	83,5%	90,8%	95,6%	98,3%	99,4%	99,2%	98,2%	96,6%	94,8%

6m

		Upstand Height (mm)													
	Load Position:	0	10	20	30	40	50	60	70	80	90	100	110	120	130
		Critical Elastic Moment (kNm)													
B203x133x25	ABOVE FLANGE	28,0	33,6	38,8	43,2	46,8	49,9	52,4	54,3	55,7	56,8	57,5	57,9	58,16	58,23
	% Increase:		20,3%	15,2%	11,3%	8,6%	6,5%	4,9%	3,7%	2,7%	1,9%	1,2%	0,8%	0,4%	0,1%
	Cumulative % Inc.		20,3%	38,7%	54,4%	67,6%	78,5%	87,3%	94,2%	99,4%	103,2%	105,7%	107,3%	108,1%	108,3%

8m

		Upstand Height (mm)													
	Load Position:	0	10	20	30	40	50	60	70	80	90	100	110	120	130
		Critical Elastic Moment (kNm)													
B203x133x25	ABOVE FLANGE	20,7	24,5	28,0	31,1	33,8	36,1	38,1	39,8	41,2	42,3	43,2	43,9	44,47	44,88
	% Increase:		18,6%	14,3%	11,1%	8,7%	6,9%	5,5%	4,4%	3,5%	2,7%	2,1%	1,6%	1,2%	0,9%
	Cumulative % Inc.		18,6%	35,6%	50,6%	63,7%	75,0%	84,6%	92,7%	99,5%	104,9%	109,3%	112,7%	115,3%	117,3%

10m

		Upstand Height (mm)													
	Load Position:	0	10	20	30	40	50	60	70	80	90	100	110	120	130
		Critical Elastic Moment (kNm)													
B203x133x25	ABOVE FLANGE	16,5	19,4	22,1	24,5	26,6	28,6	30,2	31,7	33,0	34,1	35,0	35,8	36,43	36,97
	% Increase:		17,4%	13,7%	10,9%	8,8%	7,1%	5,9%	4,8%	4,0%	3,3%	2,7%	2,2%	1,8%	1,5%
	Cumulative % Inc.		17,4%	33,6%	48,1%	61,0%	72,5%	82,6%	91,5%	99,2%	105,8%	111,4%	116,1%	120,1%	123,4%

Table 5.54 Results for NF-203x133x30 with (b/H = 0.7) for all spans considered – UDL Load case

Beam: B203x133x30 2m Load: *UDL*

		Upstand Height (mm)													
	Load Position:	0	10	20	30	40	50	60	70	80	90	100	110	120	130
		Critical Elastic Moment (kNm)													
B203x133x30	ABOVE FLANGE	169,9	211,9	248,7	277,6	299,0	313,7	322,6	326,4	326,4	323,5	318,8	313,2	307,47	302,15
	% Increase:		24,7%	17,4%	11,6%	7,7%	4,9%	2,8%	1,2%	0,0%	-0,9%	-1,5%	-1,8%	-1,8%	-1,7%
	Cumulative % Inc.		24,7%	46,4%	63,4%	76,0%	84,7%	89,9%	92,1%	92,1%	90,4%	87,7%	84,4%	81,0%	77,9%

4m

		Upstand Height (mm)													
	Load Position:	0	10	20	30	40	50	60	70	80	90	100	110	120	130
		Critical Elastic Moment (kNm)													
B203x133x30	ABOVE FLANGE	64,3	77,7	89,9	100,1	108,5	115,1	120,2	124,0	126,6	128,1	128,9	129,1	128,93	128,45
	% Increase:		20,8%	15,7%	11,4%	8,4%	6,2%	4,4%	3,1%	2,1%	1,3%	0,6%	0,2%	-0,2%	-0,4%
	Cumulative % Inc.		20,8%	39,8%	55,7%	68,7%	79,1%	87,0%	92,9%	96,9%	99,3%	100,6%	100,9%	100,5%	99,8%

6m

		Upstand Height (mm)													
	Load Position:	0	10	20	30	40	50	60	70	80	90	100	110	120	130
		Critical Elastic Moment (kNm)													
B203x133x30	ABOVE FLANGE	40,9	48,5	55,5	61,6	66,9	71,5	75,3	78,5	81,0	83,1	84,7	85,9	86,80	87,43
	% Increase:		18,5%	14,5%	11,1%	8,6%	6,8%	5,4%	4,2%	3,3%	2,5%	1,9%	1,4%	1,0%	0,7%
	Cumulative % Inc.		18,5%	35,6%	50,6%	63,6%	74,7%	84,1%	91,8%	98,1%	103,2%	107,1%	110,0%	112,2%	113,7%

8m

		Upstand Height (mm)													
	Load Position:	0	10	20	30	40	50	60	70	80	90	100	110	120	130
		Critical Elastic Moment (kNm)													
B203x133x30	ABOVE FLANGE	30,6	35,8	40,7	45,1	49,1	52,6	55,7	58,3	60,7	62,7	64,4	65,8	67,02	68,02
	% Increase:		17,1%	13,7%	10,8%	8,7%	7,1%	5,9%	4,8%	4,0%	3,3%	2,7%	2,2%	1,8%	1,5%
	Cumulative % Inc.		17,1%	33,1%	47,5%	60,4%	71,8%	81,9%	90,6%	98,3%	104,8%	110,3%	115,0%	119,0%	122,3%

10m

		Upstand Height (mm)													
	Load Position:	0	10	20	30	40	50	60	70	80	90	100	110	120	130
		Critical Elastic Moment (kNm)													
B203x133x30	ABOVE FLANGE	24,7	28,6	32,4	35,9	39,0	41,9	44,4	46,8	48,8	50,7	52,3	53,8	55,05	56,17
	% Increase:		16,2%	13,2%	10,6%	8,8%	7,3%	6,2%	5,2%	4,4%	3,8%	3,2%	2,8%	2,4%	2,0%
	Cumulative % Inc.		16,2%	31,5%	45,5%	58,2%	69,8%	80,2%	89,6%	98,1%	105,6%	112,2%	118,1%	123,3%	127,8%

Table 5.55 Results for NF-203x133x25 (b/H = 0.7) – All spans consolidated trend (M_{cr}) – UDL

	Upstand Height (mm)													
Span	0	10	20	30	40	50	60	70	80	90	100	110	120	130
(m)	Mcr (kNm)													
2	128,1	163,0	192,6	215,5	232,0	243,0	248,9	250,9	249,6	246,1	241,4	236,1	230,9	226,2
4	45,3	55,8	65,0	72,6	78,6	83,2	86,5	88,6	89,9	90,4	90,3	89,8	89,1	88,3
6	28,0	33,6	38,8	43,2	46,8	49,9	52,4	54,3	55,7	56,8	57,5	57,9	58,2	58,2
8	20,7	24,5	28,0	31,1	33,8	36,1	38,1	39,8	41,2	42,3	43,2	43,9	44,5	44,9
10	16,5	19,4	22,1	24,5	26,6	28,6	30,2	31,7	33,0	34,1	35,0	35,8	36,4	37,0

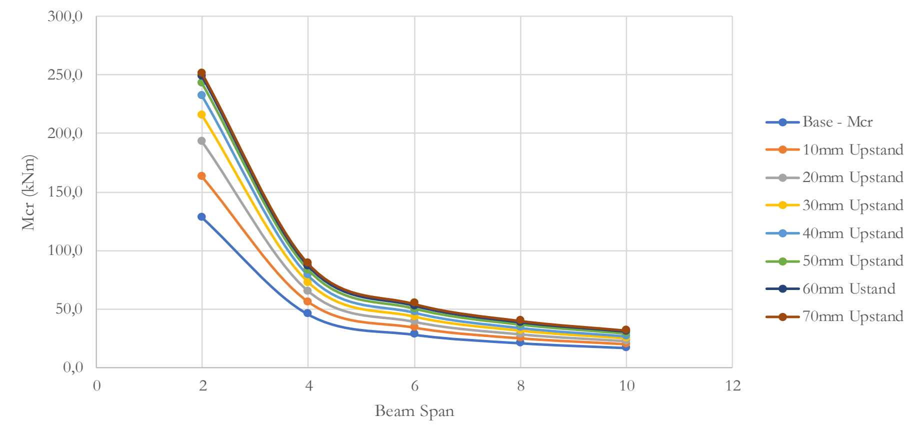

Table 5.56 Results for NF-203x133x30 (b/H = 0.7) – All spans consolidated trend (M_{cr}) – UDL

	Upstand Height (mm)													
Span	0	10	20	30	40	50	60	70	80	90	100	110	120	130
(m)	Mcr (kNm)													
2	169,9	211,9	248,7	277,6	299,0	313,7	322,6	326,4	326,4	323,5	318,8	313,2	307,5	302,2
4	64,3	77,7	89,9	100,1	108,5	115,1	120,2	124,0	126,6	128,1	128,9	129,1	128,9	128,5
6	40,9	48,5	55,5	61,6	66,9	71,5	75,3	78,5	81,0	83,1	84,7	85,9	86,8	87,4
8	30,6	35,8	40,7	45,1	49,1	52,6	55,7	58,3	60,7	62,7	64,4	65,8	67,0	68,0
10	24,7	28,6	32,4	35,9	39,0	41,9	44,4	46,8	48,8	50,7	52,3	53,8	55,1	56,2

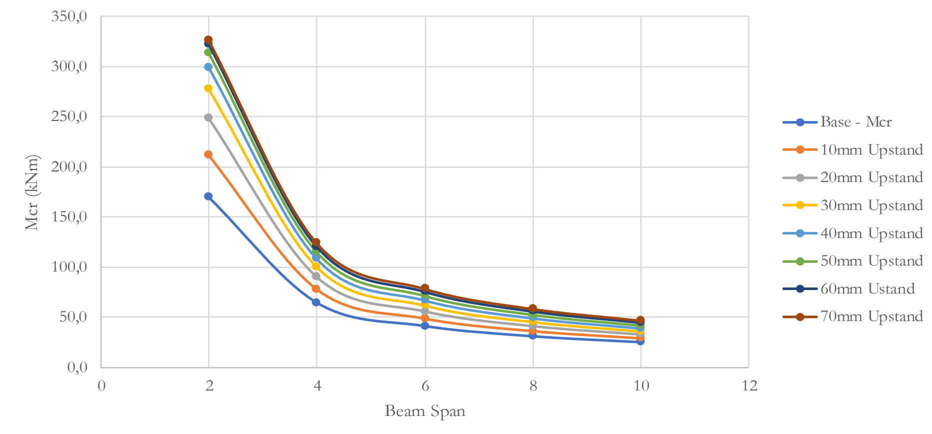

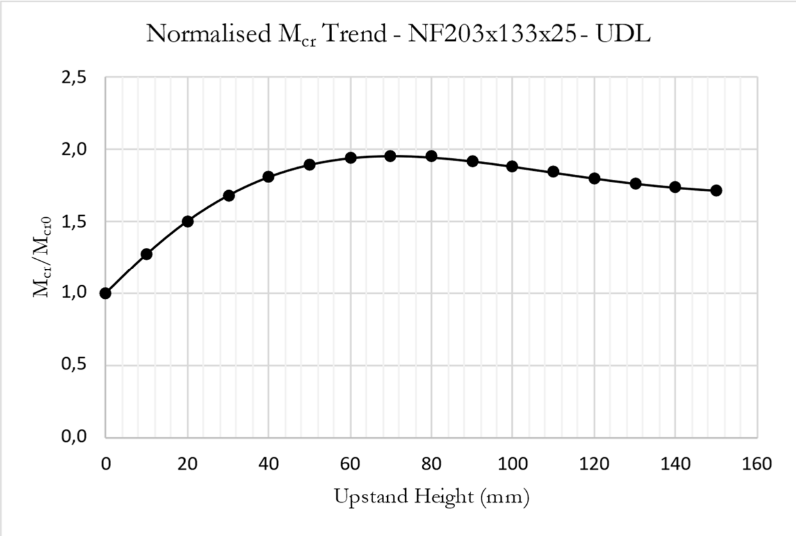

Fig.5-23 Normalised critical moment vs upstand height – BU_9

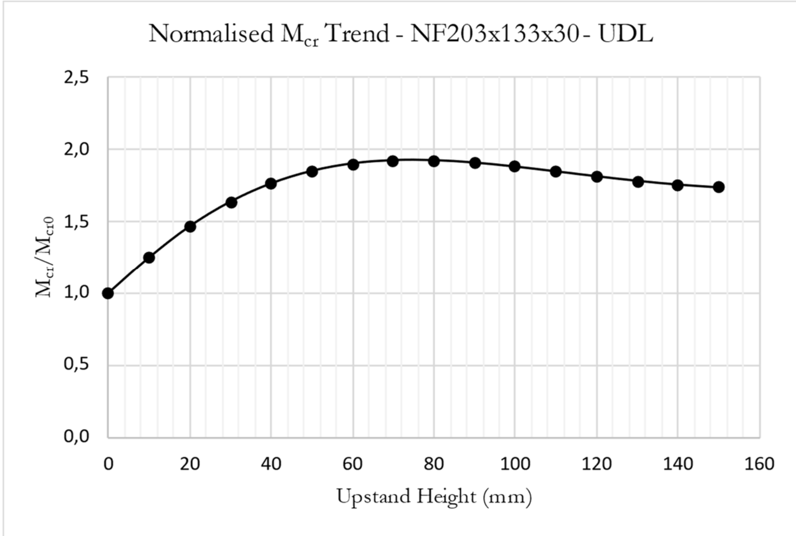

Fig.5-24 Normalised critical moment vs upstand height - BU_{10}

As for the previous members considered for the UDL case it is observed from the tabulated results in Tables 5.53 and 5.54 that the trend is consistent with what was observed for the point load case. The range of percentages of change in the critical elastic moment is also in a similar range for both the UDL case and the point load case.

5.3.2.4 Trends for Beams with (b/H) = 0.9 & 1.0 for UDL load case

Four beams are considered under the category of wide flange (WF) members as was done for the point load case. The sets of results are presented in the sequence indicated in Table 5.57 for the four members considered. This covers beams BU_{11} to BU_{14}.

Table 5.57 Group of four 'WF' members for the UDL load case

Member	***Beam***	***b/H***	***Set 1***	***Set 2***	***Set 3***
WF 254x254x167	BU_{11}	0.9	Tabulated results for all spans	Plots of M_{cr} for all spans	Graph of normalised M_{cr} against upstand height for 2m span
WF 305x305x158	BU_{12}	0.9			
WF 152x152x23	BU_{13}	1.0			
WF 254x254x73	BU_{14}	1.0			

Table 5.58 Results for WF-254x254x167 with (b/H = 0.9) for all spans considered – UDL Load case

Beam: H254x254x167 2m Load: *UDL*

		Upstand Height (mm)													
	Load Position:	0	10	20	30	40	50	60	70	80	90	100	110	120	130
		Critical Elastic Moment (kNm)													
H254x254x167	ABOVE FLANGE	6 034,2	6 370,0	6 919,9	7 385,3	7 770,5	8 080,4	8 320,7	8 497,6	8 617,9	8 688,7	8 717,4	8 711,4	8 677,97	8 623,89
	% Increase:		5,6%	8,6%	6,7%	5,2%	4,0%	3,0%	2,1%	1,4%	0,8%	0,3%	-0,1%	-0,4%	-0,6%
	Cumulative % Inc.		5,6%	14,7%	22,4%	28,8%	33,9%	37,9%	40,8%	42,8%	44,0%	44,5%	44,4%	43,8%	42,9%

4m

		Upstand Height (mm)													
	Load Position:	0	10	20	30	40	50	60	70	80	90	100	110	120	130
		Critical Elastic Moment (kNm)													
H254x254x167	ABOVE FLANGE	2 486,8	2 632,0	2 834,0	3 015,0	3 175,7	3 317,1	3 440,0	3 545,7	3 635,4	3 710,2	3 771,5	3 820,6	3 858,95	3 887,84
	% Increase:		5,8%	7,7%	6,4%	5,3%	4,5%	3,7%	3,1%	2,5%	2,1%	1,7%	1,3%	1,0%	0,7%
	Cumulative % Inc.		5,8%	14,0%	21,2%	27,7%	33,4%	38,3%	42,6%	46,2%	49,2%	51,7%	53,6%	55,2%	56,3%

6m

		Upstand Height (mm)													
	Load Position:	0	10	20	30	40	50	60	70	80	90	100	110	120	130
		Critical Elastic Moment (kNm)													
H254x254x167	ABOVE FLANGE	1 634,4	1 731,7	1 854,9	1 968,7	2 073,3	2 169,1	2 256,3	2 335,3	2 406,6	2 470,6	2 527,7	2 578,4	2 623,14	2 662,39
	% Increase:		6,0%	7,1%	6,1%	5,3%	4,6%	4,0%	3,5%	3,1%	2,7%	2,3%	2,0%	1,7%	1,5%
	Cumulative % Inc.		6,0%	13,5%	20,5%	26,9%	32,7%	38,0%	42,9%	47,2%	51,2%	54,7%	57,8%	60,5%	62,9%

8m

		Upstand Height (mm)													
	Load Position:	0	10	20	30	40	50	60	70	80	90	100	110	120	130
		Critical Elastic Moment (kNm)													
H254x254x167	ABOVE FLANGE	1 238,3	1 312,6	1 401,7	1 485,3	1 563,7	1 636,9	1 705,2	1 768,7	1 827,6	1 882,1	1 932,3	1 978,6	2 021,13	2 060,08
	% Increase:		6,0%	6,8%	6,0%	5,3%	4,7%	4,2%	3,7%	3,3%	3,0%	2,7%	2,4%	2,1%	1,9%
	Cumulative % Inc.		6,0%	13,2%	20,0%	26,3%	32,2%	37,7%	42,8%	47,6%	52,0%	56,0%	59,8%	63,2%	66,4%

10m

		Upstand Height (mm)													
	Load Position:	0	10	20	30	40	50	60	70	80	90	100	110	120	130
		Critical Elastic Moment (kNm)													
H254x254x167	ABOVE FLANGE	1 003,0	1 063,4	1 133,4	1 199,8	1 262,7	1 322,2	1 378,4	1 431,5	1 481,5	1 528,6	1 572,8	1 614,2	1 653,12	1 689,51
	% Increase:		6,0%	6,6%	5,9%	5,2%	4,7%	4,3%	3,9%	3,5%	3,2%	2,9%	2,6%	2,4%	2,2%
	Cumulative % Inc.		6,0%	13,0%	19,6%	25,9%	31,8%	37,4%	42,7%	47,7%	52,4%	56,8%	60,9%	64,8%	68,4%

Table 5.59 Results for WF-305x305x158 with (b/H = 0.9) for all spans considered – UDL Load case

Beam: H305x305x158 2m Load: *UDL*

		Upstand Height (mm)													
	Load Position:	0	10	20	30	40	50	60	70	80	90	100	110	120	130
		Critical Elastic Moment (kNm)													
H305x305x158	ABOVE FLANGE	7 501,2	8 148,3	8 901,0	9 546,5	10 088,8	10 532,7	10 883,6	11 148,1	11 333,1	11 446,7	11 496,9	11 492,7	11 442,80	11 356,11
	% Increase:		8,6%	9,2%	7,3%	5,7%	4,4%	3,3%	2,4%	1,7%	1,0%	0,4%	0,0%	-0,4%	-0,8%
	Cumulative % Inc.		8,6%	18,7%	27,3%	34,5%	40,4%	45,1%	48,6%	51,1%	52,6%	53,3%	53,2%	52,5%	51,4%

4m

		Upstand Height (mm)													
	Load Position:	0	10	20	30	40	50	60	70	80	90	100	110	120	130
		Critical Elastic Moment (kNm)													
H305x305x158	ABOVE FLANGE	2 479,8	2 676,8	2 901,7	3 100,2	3 273,1	3 421,6	3 546,7	3 649,7	3 732,3	3 795,8	3 842,2	3 873,1	3 890,42	3 896,03
	% Increase:		7,9%	8,4%	6,8%	5,6%	4,5%	3,7%	2,9%	2,3%	1,7%	1,2%	0,8%	0,4%	0,1%
	Cumulative % Inc.		7,9%	17,0%	25,0%	32,0%	38,0%	43,0%	47,2%	50,5%	53,1%	54,9%	56,2%	56,9%	57,1%

6m

		Upstand Height (mm)													
	Load Position:	0	10	20	30	40	50	60	70	80	90	100	110	120	130
		Critical Elastic Moment (kNm)													
H305x305x158	ABOVE FLANGE	1 474,1	1 582,9	1 704,7	1 814,8	1 913,7	2 001,6	2 079,1	2 146,6	2 204,6	2 253,7	2 294,6	2 327,8	2 354,08	2 374,10
	% Increase:		7,4%	7,7%	6,5%	5,4%	4,6%	3,9%	3,2%	2,7%	2,2%	1,8%	1,4%	1,1%	0,9%
	Cumulative % Inc.		7,4%	15,6%	23,1%	29,8%	35,8%	41,0%	45,6%	49,6%	52,9%	55,7%	57,9%	59,7%	61,1%

8m

		Upstand Height (mm)													
	Load Position:	0	10	20	30	40	50	60	70	80	90	100	110	120	130
		Critical Elastic Moment (kNm)													
H305x305x158	ABOVE FLANGE	1 070,8	1 145,7	1 228,0	1 303,8	1 373,3	1 436,5	1 493,8	1 545,4	1 591,4	1 632,3	1 668,2	1 699,5	1 726,43	1 749,41
	% Increase:		7,0%	7,2%	6,2%	5,3%	4,6%	4,0%	3,5%	3,0%	2,6%	2,2%	1,9%	1,6%	1,3%
	Cumulative % Inc.		7,0%	14,7%	21,8%	28,2%	34,2%	39,5%	44,3%	48,6%	52,4%	55,8%	58,7%	61,2%	63,4%

10m

		Upstand Height (mm)													
	Load Position:	0	10	20	30	40	50	60	70	80	90	100	110	120	130
		Critical Elastic Moment (kNm)													
H305x305x158	ABOVE FLANGE	851,8	909,0	971,1	1 029,0	1 082,7	1 132,5	1 178,4	1 220,6	1 259,1	1 294,2	1 326,0	1 354,6	1 380,34	1 403,25
	% Increase:		6,7%	6,8%	6,0%	5,2%	4,6%	4,1%	3,6%	3,2%	2,8%	2,5%	2,2%	1,9%	1,7%
	Cumulative % Inc.		6,7%	14,0%	20,8%	27,1%	33,0%	38,4%	43,3%	47,8%	51,9%	55,7%	59,0%	62,1%	64,7%

Table 5.60 Results for WF-152x152x23 with (b/H = 1.0) for all spans considered – UDL Load case

Beam:	H152x152x23	2m									Load:	*UDL*			
		Upstand Height (mm)													
	Load Position:	0	10	20	30	40	50	60	70	80	90	100	110	120	130
H152x152x23	ABOVE FLANGE	125,7	154,8	177,2	192,3	201,0	204,4	203,7	200,1	195,1	189,5	184,4	180,3	177,46	176,16
	% Increase:		23,2%	14,5%	8,5%	4,5%	1,7%	-0,4%	-1,7%	-2,5%	-2,8%	-2,7%	-2,2%	-1,6%	-0,7%
	Cumulative % Inc.		23,2%	41,0%	53,0%	60,0%	62,6%	62,1%	59,2%	55,2%	50,8%	46,7%	43,4%	41,2%	40,2%

		4m													
		Upstand Height (mm)													
	Load Position:	0	10	20	30	40	50	60	70	80	90	100	110	120	130
H152x152x23	ABOVE FLANGE	45,3	54,2	61,4	66,9	70,7	73,0	74,2	74,5	74,0	73,2	72,2	71,2	70,26	69,56
	% Increase:		19,6%	13,4%	8,9%	5,7%	3,3%	1,6%	0,3%	-0,5%	-1,1%	-1,4%	-1,4%	-1,3%	-1,0%
	Cumulative % Inc.		19,6%	35,6%	47,6%	56,0%	61,2%	63,8%	64,4%	63,5%	61,7%	59,4%	57,2%	55,1%	53,6%

		6m													
		Upstand Height (mm)													
	Load Position:	0	10	20	30	40	50	60	70	80	90	100	110	120	130
H152x152x23	ABOVE FLANGE	28,2	33,1	37,2	40,6	43,2	45,1	46,4	47,2	47,7	47,8	47,7	47,5	47,25	46,97
	% Increase:		17,3%	12,5%	9,0%	6,4%	4,4%	2,9%	1,8%	0,9%	0,3%	-0,2%	-0,4%	-0,6%	-0,6%
	Cumulative % Inc.		17,3%	32,0%	43,8%	53,0%	59,8%	64,5%	67,5%	69,1%	69,5%	69,3%	68,5%	67,6%	66,6%

		8m													
		Upstand Height (mm)													
	Load Position:	0	10	20	30	40	50	60	70	80	90	100	110	120	130
H152x152x23	ABOVE FLANGE	20,9	24,2	27,1	29,6	31,6	33,2	34,5	35,4	36,1	36,5	36,8	37,0	37,03	37,03
	% Increase:		15,9%	12,0%	9,0%	6,8%	5,1%	3,8%	2,7%	1,9%	1,3%	0,8%	0,4%	0,2%	0,0%
	Cumulative % Inc.		15,9%	29,8%	41,4%	51,0%	58,7%	64,8%	69,3%	72,5%	74,7%	76,1%	76,8%	77,1%	77,0%

		10m													
		Upstand Height (mm)													
	Load Position:	0	10	20	30	40	50	60	70	80	90	100	110	120	130
H152x152x23	ABOVE FLANGE	16,8	19,3	21,5	23,5	25,1	26,5	27,7	28,6	29,3	29,9	30,4	30,7	30,92	31,08
	% Increase:		15,0%	11,6%	9,0%	7,0%	5,5%	4,3%	3,4%	2,6%	2,0%	1,5%	1,1%	0,8%	0,5%
	Cumulative % Inc.		15,0%	28,3%	39,8%	49,7%	57,9%	64,8%	70,3%	74,8%	78,2%	80,8%	82,8%	84,1%	85,1%

Table 5.61 Results for WF-254x254x73 with (b/H = 1.0) for all spans considered – UDL Load case

Beam: H254x254x73 2m Load: *UDL*

		Upstand Height (mm)													
	Load Position:	0	10	20	30	40	50	60	70	80	90	100	110	120	130
		Critical Elastic Moment (kNm)													
H254x254x73	ABOVE FLANGE	1 813,8	2 065,7	2 299,8	2 490,6	2 640,5	2 751,9	2 828,1	2 872,9	2 890,4	2 885,0	2 861,5	2 824,4	2 778,20	2 726,96
	% Increase:		13,9%	11,3%	8,3%	6,0%	4,2%	2,8%	1,6%	0,6%	-0,2%	-0,8%	-1,3%	-1,6%	-1,8%
	Cumulative % Inc.		13,9%	26,8%	37,3%	45,6%	51,7%	55,9%	58,4%	59,4%	59,1%	57,8%	55,7%	53,2%	50,3%

4m

		Upstand Height (mm)													
	Load Position:	0	10	20	30	40	50	60	70	80	90	100	110	120	130
		Critical Elastic Moment (kNm)													
H254x254x73	ABOVE FLANGE	570,3	642,0	709,6	766,5	813,2	850,4	878,6	898,7	911,6	918,2	919,6	916,7	910,51	902,00
	% Increase:		12,6%	10,5%	8,0%	6,1%	4,6%	3,3%	2,3%	1,4%	0,7%	0,1%	-0,3%	-0,7%	-0,9%
	Cumulative % Inc.		12,6%	24,4%	34,4%	42,6%	49,1%	54,1%	57,6%	59,8%	61,0%	61,2%	60,7%	59,6%	58,2%

6m

		Upstand Height (mm)													
	Load Position:	0	10	20	30	40	50	60	70	80	90	100	110	120	130
		Critical Elastic Moment (kNm)													
H254x254x73	ABOVE FLANGE	327,5	364,8	400,4	431,3	457,7	479,8	497,9	512,3	523,3	531,2	536,5	539,4	540,49	540,00
	% Increase:		11,4%	9,8%	7,7%	6,1%	4,8%	3,8%	2,9%	2,1%	1,5%	1,0%	0,6%	0,2%	-0,1%
	Cumulative % Inc.		11,4%	22,3%	31,7%	39,8%	46,5%	52,0%	56,4%	59,8%	62,2%	63,8%	64,7%	65,0%	64,9%

8m

		Upstand Height (mm)													
	Load Position:	0	10	20	30	40	50	60	70	80	90	100	110	120	130
		Critical Elastic Moment (kNm)													
H254x254x73	ABOVE FLANGE	233,4	258,0	281,6	302,6	321,1	337,1	350,8	362,4	372,0	379,7	385,8	390,4	393,73	395,93
	% Increase:		10,5%	9,2%	7,5%	6,1%	5,0%	4,1%	3,3%	2,6%	2,1%	1,6%	1,2%	0,8%	0,6%
	Cumulative % Inc.		10,5%	20,6%	29,6%	37,5%	44,4%	50,3%	55,3%	59,4%	62,7%	65,3%	67,3%	68,7%	69,6%

10m

		Upstand Height (mm)													
	Load Position:	0	10	20	30	40	50	60	70	80	90	100	110	120	130
		Critical Elastic Moment (kNm)													
H254x254x73	ABOVE FLANGE	183,8	202,0	219,6	235,5	249,7	262,5	273,7	283,5	292,0	299,2	305,3	310,3	314,44	317,71
	% Increase:		9,9%	8,7%	7,2%	6,1%	5,1%	4,3%	3,6%	3,0%	2,5%	2,0%	1,7%	1,3%	1,0%
	Cumulative % Inc.		9,9%	19,5%	28,1%	35,9%	42,8%	48,9%	54,3%	58,9%	62,8%	66,1%	68,9%	71,1%	72,9%

Table 5.62 Results for WF-254x254x167 (b/H = 0.9) – All spans consolidated trend (M_{cr}) – UDL

Span (m)	Upstand Height (mm)													
	0	10	20	30	40	50	60	70	80	90	100	110	120	130
	Mcr (kNm)													
2	6 034,2	6 370,0	6 919,9	7 385,3	7 770,5	8 080,4	8 320,7	8 497,6	8 617,9	8 688,7	8 717,4	8 711,4	8 678,0	8 623,9
4	2 486,8	2 632,0	2 834,0	3 015,0	3 175,7	3 317,1	3 440,0	3 545,7	3 635,4	3 710,2	3 771,5	3 820,6	3 858,9	3 887,8
6	1 634,4	1 731,7	1 854,9	1 968,7	2 073,3	2 169,1	2 256,3	2 335,3	2 406,6	2 470,6	2 527,7	2 578,4	2 623,1	2 662,4
8	1 238,3	1 312,6	1 401,7	1 485,3	1 563,7	1 636,9	1 705,2	1 768,7	1 827,6	1 882,1	1 932,3	1 978,6	2 021,1	2 060,1
10	1 003,0	1 063,4	1 133,4	1 199,8	1 262,7	1 322,2	1 378,4	1 431,5	1 481,5	1 528,6	1 572,8	1 614,2	1 653,1	1 689,5

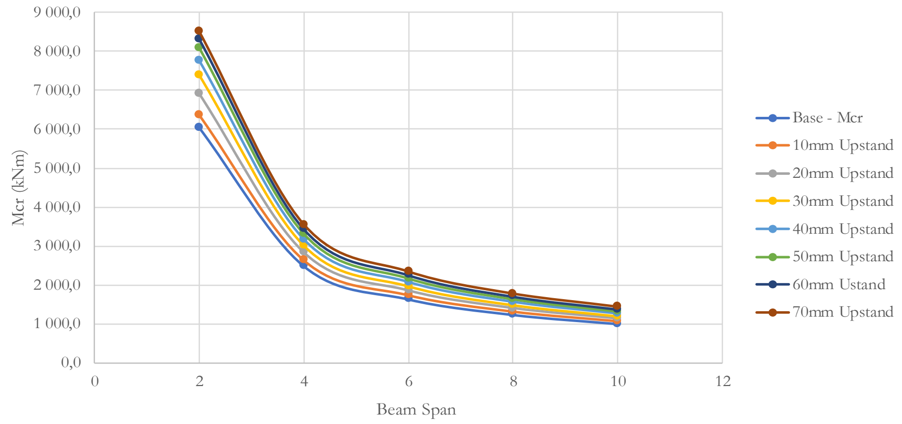

Table 5.63 Results for WF-305x305x158 (b/H = 0.9) – All spans consolidated trend (M_{cr}) – UDL

Span (m)	Upstand Height (mm)													
	0	10	20	30	40	50	60	70	80	90	100	110	120	130
	Mcr (kNm)													
2	7 501,2	8 148,3	8 901,0	9 546,5	10 088,8	10 532,7	10 883,6	11 148,1	11 333,1	11 446,7	11 496,9	11 492,7	11 442,8	11 356,1
4	2 479,8	2 676,8	2 901,7	3 100,2	3 273,1	3 421,6	3 546,7	3 649,7	3 732,3	3 795,8	3 842,2	3 873,1	3 890,4	3 896,0
6	1 474,1	1 582,9	1 704,7	1 814,8	1 913,7	2 001,6	2 079,1	2 146,6	2 204,6	2 253,7	2 294,6	2 327,8	2 354,1	2 374,1
8	1 070,8	1 145,7	1 228,0	1 303,8	1 373,3	1 436,5	1 493,8	1 545,4	1 591,4	1 632,3	1 668,2	1 699,5	1 726,4	1 749,4
10	851,8	909,0	971,1	1 029,0	1 082,7	1 132,5	1 178,4	1 220,6	1 259,1	1 294,2	1 326,0	1 354,6	1 380,3	1 403,2

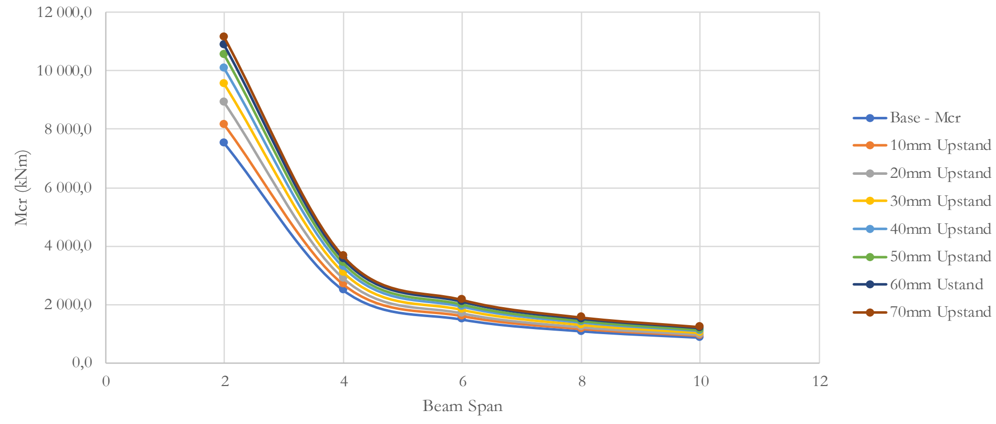

Table 5.64 Results for WF-152x152x23 with (b/H = 1.0) – All spans consolidated trend (M_{cr}) – UDL

	Upstand Height (mm)													
Span (m)	0	10	20	30	40	50	60	70	80	90	100	110	120	130
	Mcr (kNm)													
2	125,7	154,8	177,2	192,3	201,0	204,4	203,7	200,1	195,1	189,5	184,4	180,3	177,5	176,2
4	45,3	54,2	61,4	66,9	70,7	73,0	74,2	74,5	74,0	73,2	72,2	71,2	70,3	69,6
6	28,2	33,1	37,2	40,6	43,2	45,1	46,4	47,2	47,7	47,8	47,7	47,5	47,3	47,0
8	20,9	24,2	27,1	29,6	31,6	33,2	34,5	35,4	36,1	36,5	36,8	37,0	37,0	37,0
10	16,8	19,3	21,5	23,5	25,1	26,5	27,7	28,6	29,3	29,9	30,4	30,7	30,9	31,1

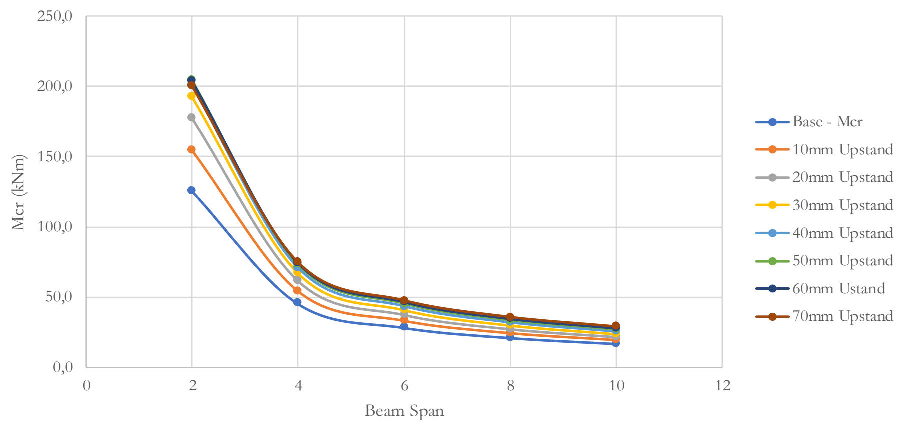

Table 5.65 Results for WF-254x254x73 with (b/H = 1.0) – All spans consolidated trend (M_{cr}) – UDL

	Upstand Height (mm)													
Span	0	10	20	30	40	50	60	70	80	90	100	110	120	130
	Mcr (kNm)													
2	1 813,8	2 065,7	2 299,8	2 490,6	2 640,5	2 751,9	2 828,1	2 872,9	2 890,4	2 885,0	2 861,5	2 824,4	2 778,2	2 727,0
4	570,3	642,0	709,6	766,5	813,2	850,4	878,6	898,7	911,6	918,2	919,6	916,7	910,5	902,0
6	327,5	364,8	400,4	431,3	457,7	479,8	497,9	512,3	523,3	531,2	536,5	539,4	540,5	540,0
8	233,4	258,0	281,6	302,6	321,1	337,1	350,8	362,4	372,0	379,7	385,8	390,4	393,7	395,9
10	183,8	202,0	219,6	235,5	249,7	262,5	273,7	283,5	292,0	299,2	305,3	310,3	314,4	317,7

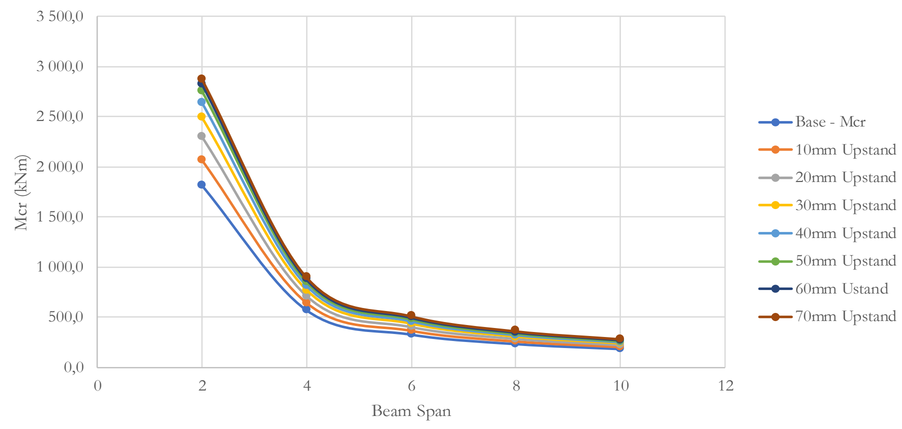

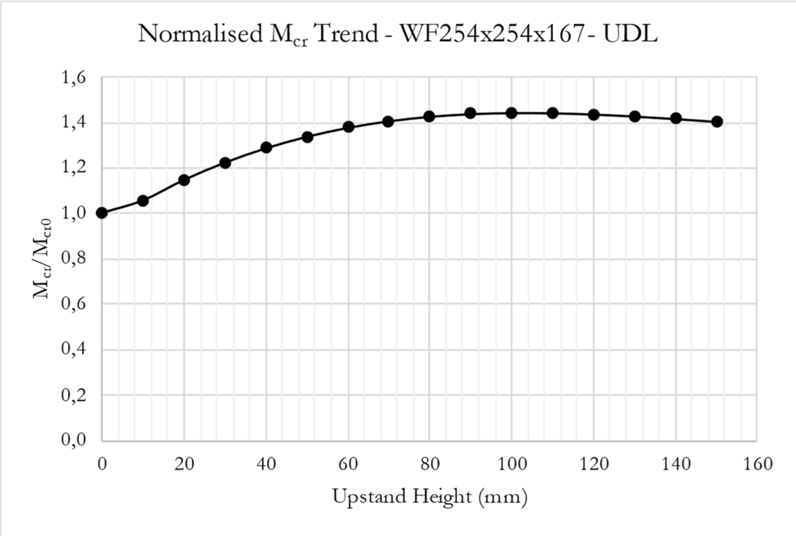

Fig.5-25 Normalised critical moment vs upstand height – BU_{11}

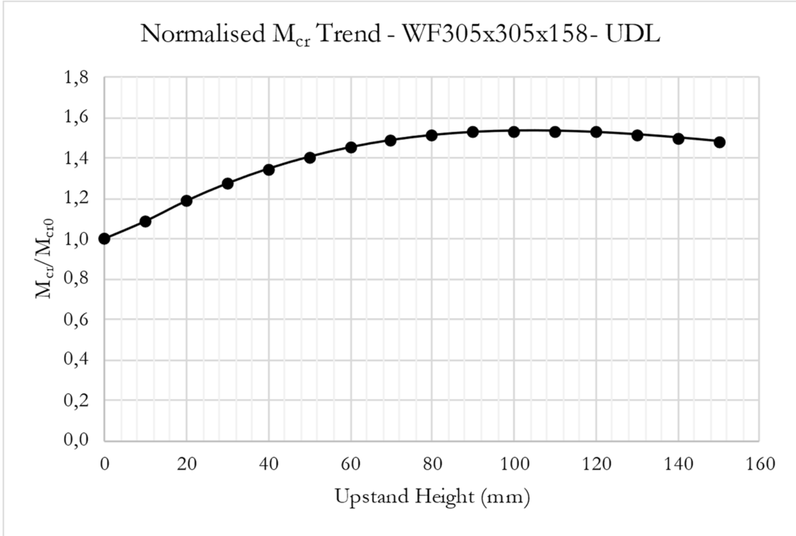

Fig.5-26 Normalised critical moment vs upstand height - BU_{12}

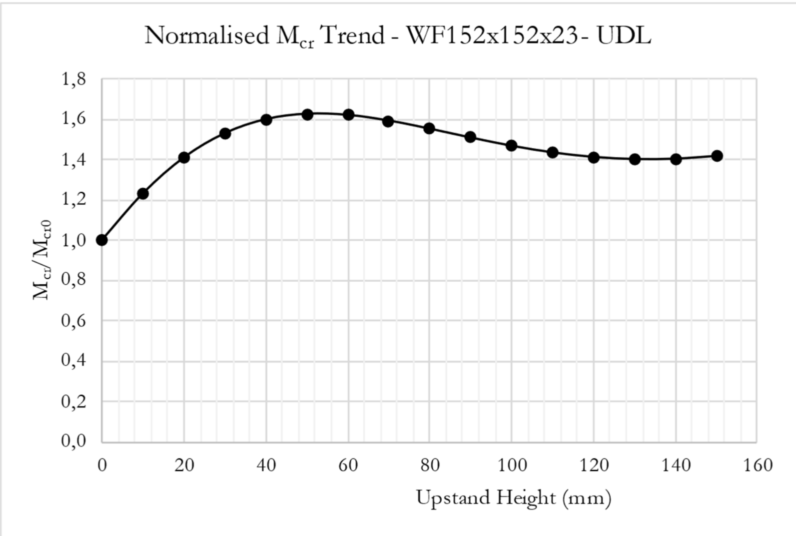

Fig.5-27 Normalised critical moment vs upstand height – BU_{13}

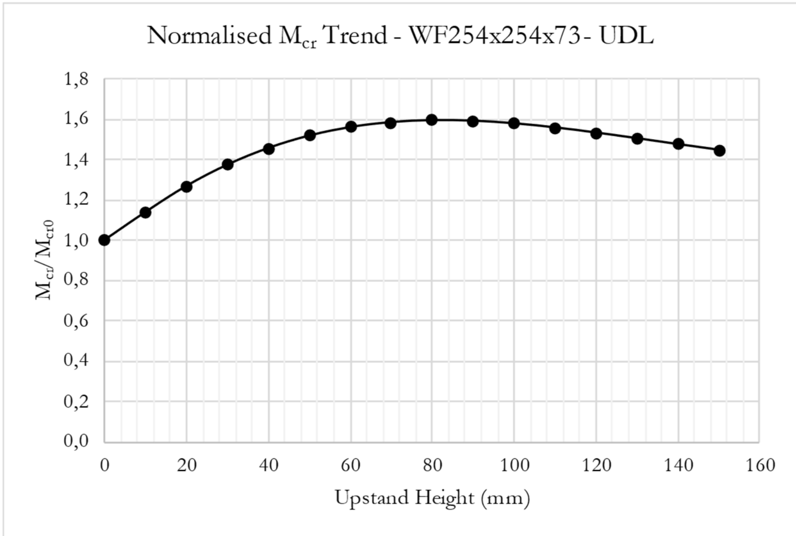

Fig.5-28 Normalised critical moment vs upstand height - BU_{14}

As with the point load case the trends from the UDL case for the wide flange members matches the trend observed for the narrow flange sections. However, the percentage changes are again lower than those observed for the narrow flange sections. The members with b/H = 0.9 have the lowest values of percentage change for peak values at low upstand height. Given these observations it can be concluded that the UDL case as well as the point load case give similar trends across upstand height and member span.

5.3.3 Discussion of results in 5.3.1 & 5.3.2

The results presented for the point load and the UDL case have shown similar trends. This is observed from the tabulated results, the summarised plots over multiple spans as well as the graphs for the 2m span case. The critical elastic moment is observed to have a greater percentage change in the critical elastic moment for the narrow-flange sections than for the wide-flange sections. This is not particularly surprising given that the narrow flange sections have a higher ratio of major axis second moment of area to minor axis second moment of area.

For all members, initially there is a significant change in the critical elastic moment as the upstand height increases but this diminishes with increase in upstand height. In some cases, it is observed that a peak value is reached followed by a decline in value as upstand height increases. This trend is similar to that exhibited by the shear centre position movement as the upstand height increases. This indicates a correlation between the shear centre movement and the critical elastic moment value. This means that simply increasing the upstand height for these monosymmetric section beams with the monosymmetry introduced by the stiffeners will not necessarily continually increase the critical elastic moment of the member. There is a danger that the return, in flexural capacity, starts to diminish despite greater stiffener height. The stiffening of a beam where stiffeners introduce monosymmetry such as in the case studied leads to an optimisation problem where the point at which an increase in stiffener height no longer leads to increased returns in terms of flexural capacity needs to be identified. This will thus help to save on material and workmanship, and ensure that stiffeners are used optimally.

In the case of doubly symmetric members an increase in section properties of second moment of area (minor axis), torsional constant and warping constant will always lead to an increase in the critical elastic moment of a member. This generally translates into increased flexural strength. Monosymmetric sections on the other hand, particularly the ones considered here, are thus unique in the sense that the monosymmetry can influence the critical elastic moment, and subsequently the flexural strength, negatively despite an increase in these section properties. Although it has previously been known that the distance between the applied load and the shear centre position has an effect on critical buckling moment (Anderson and Trahair, 1972) and that the value of the monosymmetry constant has an effect on the critical buckling moment (Goodier, 1942) it has not been previously shown that the effect of strengthening a member can have an effect of monosymmetry where this starts out as a positive effect and with increase efforts to strengthen then induces a negative effect. In many cases the introduction of monosymmetry only goes in one direction either an increase or a decrease in critical elastic moment. An example is an I-shaped section simply supported beam with different flange properties such as same thickness but different widths. If the wider flange is in compression this produces an increase in critical elastic moment, whereas when the wider flange is in tension the critical elastic moment is reduced. This is illustrated in Fig.5-29 (a) with the shear centre and centroid movement shown as well. Without carefully analysing trends for a monosymmetric section such as the one considered in this study this phenomenon where the geometry of the section is essentially the same but yielding different outcomes may be missed altogether. As has been indicated previously monosymmetric sections tend to present surprising results when compared to doubly symmetric members. The members considered in this study are not different.

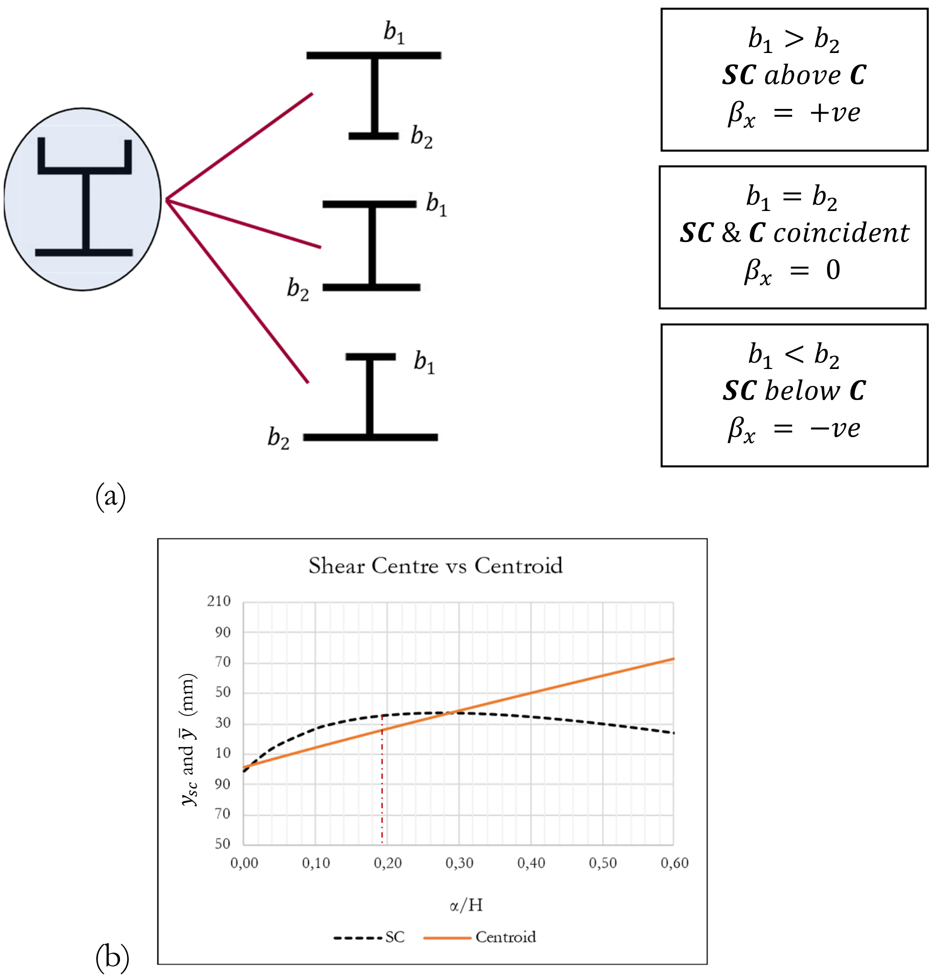

Fig.5-29 Illustration of I-shaped section properties with equal thickness flanges (a) compared to unique properties of section considered in the current study (b)

In the chapter that follows the outcomes observed her are extended to investigate practical application. The increase in critical elastic moment is plotted against the 'η' parameter which is $'{}^{\alpha}/_{H}'$ so that a trend comparison with the plots for shear centre position movement as well as centroid position movement relative to the 'η' parameter can be made. In this way the point with the uniquely observed phenomenon of coincidence of shear centre and centroid position can be investigated for correlation with the changes in the critical elastic moment that have been observed.

5.4 CONCLUSION

The trends of the elastic critical moment relative to the change in upstand height have been studied by way of a parametric study in this section. It has been shown that the upstands have a profound influence on the nature of the critical elastic moment. Initially at low upstand heights there is a high increase in elastic critical moment. This increase is at a diminishing rate for increase in upstand height. This means that for a same unit increase in upstand height the corresponding increase in the elastic critical moment is declining. At higher upstand heights the increase diminishes to such an extent that in some sections it peaks and starts to reduce with increase in upstand height. This leads to a situation where further increase beyond a certain point result in a declining critical elastic moment value despite increasing the upstand height.

It is also noted that although this observed behaviour is consistent across short and long spans alike, the percentage increase in the critical elastic moment for corresponding upstand heights decreases with an increase in span. This means that the effect of monosymmetry is felt greater with shorter spans than it is with longer spans. Despite this the gains observed for all spans are still significant making the use of upstands as stiffeners a viable consideration.

The trends are also consistent for both narrow flange and wide flange members. However, the percentage increase is seemingly less for wide flange members compared to that for narrow flange members for corresponding upstand heights. However, the numerical moment values for wide flange members are noteworthy given that these members already have high values of critical elastic moment for the unstiffened member due to their high second moment of area values about the minor axis. This value has an influence on the critical elastic moment. It may be the case therefore that low increase values are still mitigated by high numerical values for these wide flange sections in practical use.

CHAPTER 6 PRACTICAL APPLICATIONS

Advantage can be taken of the behaviour observed in Chapter 3 and that observed in the previous chapter for the case of strengthening existing members or indeed for optimised cross sections used at first application. For greenfield projects the use of smaller stiffened members in lieu of larger members could align with principles of 'lean design' where material use is optimised. The opportunities presented by the current study present a designer with an alternative cross-section to consider. Although the approach and principles can be used for members fabricated with upstands prior to use, the focus of the study will now be on the case of strengthening existing members to demonstrate the beneficial application of these upstands. The need to strengthen existing steel beam members can arise for various reasons including change in the use of the structure with a resulting increase in applied load i.e., re-purposing use. Other reasons may involve maintenance requirements such as addressing effects of degradation over time. If the removal and replacement of the existing beam needs to be avoided due to cost or feasibility factors, or indeed to reduce carbon footprint then strengthening an existing member presents a viable option. The carbon offset of re-use rather than replacement aligns well with the principles of sustainability.

6.1 PRACTICAL APPLICATION FOR STRENGTHENING CASE

Several authors have presented studies on strengthening existing steel members. A study by Hanson (1977) reported a shift that was taking place at the time from removal and replacement of buildings towards rehabilitation and re-use. A change in economic balance was attributed to at this stage. Since then, the sustainability aspect has also become an important consideration for re-use of existing structures or parts of structures as focus has now been intensified on carbon footprint of structures and associated activities in the value chain. The replacement of a beam would now include the carbon footprint from manufacture of both members including the installation, de-mounting and disposal of the first member as well as the mounting of the second or replacement member. Rehabilitation, on the other hand, would substitute the replacement member with only the parts and activities needed to carry out the strengthening of the existing member.

Several authors have presented methods for strengthening or stiffening existing steel beams. In the case of increasing the critical elastic buckling moment these have either involved altering the cross-section geometric properties or increasing the torsional or warping stiffness of the member. Steel plates or even pieces of other types of steel members are typically used for this. Two approaches were highlighted by Tsavdaridis (2015) for reinforcing existing flexural systems as adding new framing to supplement the existing system or reinforcing existing beams, girders and their connections. Reinforcing the existing members was stated as normally being the easier option. The author presenting possible options for welding strengthening elements to flanges. Some practical approaches for strengthening existing steel beams have been discussed by Koshmidder-Hatch (2014). These include the use of bolted-on members, weld-on plates and concrete encasement. Practical limitations to welding on site were highlighted.

6.1.1 Determination of Required Upstand Height

The trends observed, particularly when considering the consolidated results across spans, indicate that for some spans the choice of upstand height required for a particular application becomes an optimisation problem. This is particularly true where the trend is such that the critical elastic moment increases with upstand height, reaches a peak or stationery point and then decreases. This implies that upstand heights beyond the 'peak point' become uneconomical for lateral-stability considerations. In these regions the negative effect of monosymmetry suppresses the effects of increase in section properties. This is illustrated in Fig.5-28 which is extracted from Table 5.32 for a NF-305x102x25 section.

	Upstand Height (mm)													
Span	0	10	20	30	40	50	60	70	80	90	100	110	120	130
(m)	Mcr (kNm)													
2	76,0	104,3	129,6	150,9	168,4	182,3	192,9	200,4	205,1	207,5	207,8	206,6	204,2	201,0
4	26,0	34,2	41,6	48,0	53,4	58,0	61,8	64,8	67,0	68,7	69,8	70,5	70,7	70,6
6	15,8	20,0	24,0	27,4	30,5	33,1	35,4	37,4	39,0	40,3	41,4	42,3	42,9	43,3
8	11,6	14,4	17,0	19,3	21,4	23,3	25,0	26,4	27,7	28,8	29,8	30,6	31,3	31,9
10	9,2	11,3	13,2	15,0	16,6	18,1	19,4	20,6	21,6	22,6	23,5	24,2	24,9	25,5

Fig.5-28 Results for NF-305x102x25 with (b/H = 0.3) showing optimisation considerations

It can be seen that the critical elastic moment for an upstand height of 130mm matches closely that for an upstand height of 70mm for a 2m member span. Although the upstand height of 130mm would give higher cross-section properties, it would not present any real advantage if the failure mode were governed by an instability failure. It means that based on instability alone the 70mm upstand would present a better option than the 130mm for a similar level of performance. It is acknowledged that real behaviour may lead to slightly different resistance moments due to nonlinear behaviour as well as nature of imperfections, however, considerations based on elastic behaviour are a proxy indicator of what the choice will look like. It is noticed from the trend in Fig.5-28 that the longer the span the higher the upstand height where the 'peak value' is attained.

6.1.2 Selection for Strengthening Existing Sections - Examples

In this section we will now consider specific examples where the trends observed in the previous sections can be applied for initial selection of upstand height as a strengthening mechanism for the beam. The first two examples consider a narrow flange beam where a larger alternative size member based on the steel handbook sections is compared to the alternative option of using a stiffened member. For the larger size member its' location in the handbook in terms of size hierarchy relative to the stiffened member original size is noted. Only the elastic critical load and the stiffness are used in this section of the study. The next two examples will then consider similar cases for wide flange sections.

6.1.2.1 Example 1(a): NF-IPE 120 at 4m span – Point Load case

For the NF-IPE 120 the summary of the critical elastic moment and second moment of area data for the base member and stiffened sections is presented in Table 6.1 for the point load case. The upstand height at which the shear centre and centroid are coincident is given by the critical upstand height value, α_c.

Table 6.1 Properties of NF-IPE 120 for comparison – Point Load

	Upstand height (mm)										
	0	10	20	30	40	50	60	70	80	90	100
M_{cr} (kNm)	7.5	9.8	11.8	13.5	14.9	16.2	17.2	18.0	18.7	19.3	19.7
I_x ($x10^6 mm^4$)	3.06	3.55	4.10	4.73	5.44	6.24	7.14	8.13	9.24	10.46	11.79

$\alpha_c = 37mm$

Table 6.2 Higher size sections – no upstands

	NF-IPE 140	NF-IPE 160
M_{cr} (kNm)	11.5	16.5
I_x ($x10^6 mm^4$)	5.25	8.35

The next higher doubly symmetric size sections in the steel handbook are the IPE 140 and IPE 160 (If IPE_{AA} sizes are ignored) and the critical elastic moment values as well as second moment of area are presented in Table 6.2. The values for the IPE 120 with upstands are compared to these values. It can be seen from Tables 6.1 and 6.2 that an IPE 120 member with an upstand height of 20mm exceeds the critical load of an IPE 140 and an upstand height of 40mm gives a second moment area value which exceeds that for the IPE 140. Similarly, an IPE 120 with an upstand height of 60mm has a critical load which exceeds that of the IPE 160. An upstand height of 80mm gives a section with a higher second moment of area. This shows that the ultimate limit state is met or exceeded at a lower upstand heigh than is the service limit state which is dependent on major axis flexural stiffness and by proxy the second moment of area. If the ultimate limit state is the governing factor in the design, then an IPE 120 section with 20mm upstands and one with 60mm upstands can be used instead of replacing the existing member with an IPE 140 or IPE 160 respectively. If the governing factor is a service limit state, then upstand heights of 40mm and 80mm respectively would be required in lieu of replacing with an IPE 140 or IPE 160 respectively.

Strength gain from monosymmetry effects is experienced up to an upstand height of 37mm denoted by the symbol α_c for critical upstand in accordance with findings reported in section 3.9 and 5.3.4. Beyond that upstand height, monosymmetry no longer has a positive contribution and thus upstand heights beyond say 40mm (rounding off to nearest 5mm) may no longer be advantageous. A more comprehensive optimisation is outside the scope of the current study.

6.1.2.2 Example 1(b): NF-IPE 120 at 4m span – UDL case

For the NF-IPE 120 the summary of the critical elastic moment and second moment of area data for the base member and stiffened sections is presented in Table 6.3 for the UDL load case.

Table 6.3 Properties of NF-IPE 120 for comparison - UDL

	Upstand height (mm)										
	0	10	20	30	40	50	60	70	80	90	100
M_{cr} (kNm)	6.3	8.2	9.9	11.3	12.5	13.5	14.3	14.9	15.4	15.9	16.2
I_x ($x10^6mm^4$)	3.06	3.55	4.10	4.73	5.44	6.24	7.14	8.13	9.24	10.46	11.79

Table 6.4 Higher size sections – no upstands

$\alpha_c = 37mm$

	NF-IPE 140	NF-IPE 160
M_{cr} (kNm)	9.7	14
I_x ($x10^6mm^4$)	5.25	8.35

The outcome for the UDL case is similar to observations for the point load case in 6.1.2.1. For an ultimate limit state governing the design upstand heights on the IPE 120 of 20mm and 60mm with be sufficient to mat the corresponding values for an IPE 140 and IPE 160 respectively. Since section properties are unchanged in comparison to the previous case upstand height values of 40mm and 80mm respectively will match or exceed corresponding values for the IPE 140 and IPE 160 respectively for the member stiffness. Another example for a narrow flange member follows. Based on a direct comparison, the α_c value this would favour consideration for substitution of the IPE 140 over the IPE 160 based on the critical upstand value of about 40mm.

6.1.2.3 Example 2 (a): NF-254x146x37 - Point Load

For the NF-254x146x37 the summary of the critical elastic moment and second moment of area data for the base member and stiffened sections is presented in Table 6.5.

Table 6.5 Properties of NF-254x146x37 for comparison – Point Load

	Upstand height (mm)										
	0	10	20	30	40	50	60	70	80	90	100
M_{cr} (kNm)	117.4	141.0	163.1	182.1	198.1	211.5	222.4	231.1	237.7	242.6	246.1
I_x ($x10^6mm^4$)	54.7	58.4	62.3	66.5	70.9	75.6	82.6	85.9	91.5	97.4	103.6

Table 6.6 Higher size sections – no upstands $\alpha_c = 77mm$

	NF-305x165x40	NF-356x175x45
M_{cr} (kNm)	152.8	174.9
I_x ($x10^6mm^4$)	84.2	118.4

In this example the beam is compared to unstiffened beams that are positioned five and eight times higher in the handbook. However, if compared by weight they are one and three times higher respectively in position. Upstand heights of 20mm and 30mm give sufficient values to match or exceed the critical moment values respectively for the 305x165x40 and 365x175x45 respectively. Although the critical moment values of the two sections as given in Table 6.6 are higher than that of the unstiffened 254x146x37 it is noted that even with small upstand height values the critical moment gain is significant on the stiffened member. The case for a governing condition of the service limit state (stiffness) does not yield such encouraging results though as much higher upstand heights are required to match or exceed those of the members in Table 6.6 against which the stiffened member is compared. An upstand height of 70mm would be required to match the second moment of area of the 305x165x40. An upstand height higher than the limiting value of 100mm considered here would be required to match the second moment of area of the 356x175x45.

It means that a service limit state of deflection may negate the consideration of many higher size members in this case.

6.1.2.4 Example 2 (b): NF-254x146x37 - UDL

For the NF-254x146x37 the summary of the critical elastic moment and second moment of area data for the base member and stiffened sections is presented in Table 5.64 for the UDL load case.

Table 6.7 Properties of NF-254x146x37 for comparison - UDL

	Upstand height (mm)										
	0	10	20	30	40	50	60	70	80	90	100
M_{cr} (kNm)	102.3	123.2	142.9	159.8	174.2	186.0	195.6	203.0	208.6	212.5	215
I_x ($\times 10^6 mm^4$)	54.7	58.4	62.3	66.5	70.9	75.6	80.6	85.9	91.5	97.4	103.6

Table 6.8 Higher size sections – no upstands $\alpha_c = 77mm$

	NF-305x165x40	NF-356x175x45
M_{cr} (kNm)	134.5	154.4
I_x ($\times 10^6 mm^4$)	84.2	118.4

As in the previous example, the outcome for the UDL case is similar to observations for the point load case. For an ultimate limit state governing the design upstand heights on the 254x146x37 of 20mm and 30mm with be sufficient to match the corresponding values for the 305x165x40 and 356x175x45 respectively. Since section properties are unchanged in comparison to the previous case (6.1.2.3) the observations for the service limit state of deflection are similar.

Wide flange sections are considered in the examples that follow.

6.1.2.5 Example 3 (a): WF-152x152x30 – Point Load

For the WF-152x152x30 the summary of the critical elastic moment and second moment of area data for the base member and stiffened sections is presented in Table 5.--.

Table 6.9 Properties of WF-152x152x30 for comparison – Point Load

	Upstand height (mm)										
	0	10	20	30	40	50	60	70	80	90	100
M_{cr} (kNm)	89.3	104.5	117.7	128.3	136.5	142.5	146.8	149.6	151.3	152.1	152.4
I_x ($x10^6mm^4$)	17.25	18.50	19.96	21.61	23.47	25.55	27.87	30.43	33.24	36.31	39.65

Table 6.10 Higher size sections – no upstands $\alpha_c = 41mm$

	WF-152x152x37	WF-203x203x46
M_{cr} (kNm)	134.2	233
I_x ($x10^6mm^4$)	21.90	44.95

The section is compared to members one and two sizes higher in the handbook. The member two sizes higher has critical moment and second moment of area values that are higher than what is obtained from the member with upstands considered. The member one size higher is matched for critical moment at an upstand height of 40mm and for second moment of area similarly at an upstand height of 40mm. This means that strengthening the existing beam with 40mm upstands can be considered in lieu of replacing with the next higher sized beam. This upstand height is also within the range of the critical upstand height, α_c, and therefore within the range where monosymmetry acts beneficially to enhance the critical elastic moment.

6.1.2.6 Example 3 (b): WF-152x152x30 - UDL

Table 6.11 Properties of WF-152x152x30 for comparison - UDL

	Upstand height (mm)										
	0	10	20	30	40	50	60	70	80	90	100
M_{cr} (kNm)	77.0	90.3	101.7	110.8	117.8	122.7	126.0	128.0	128.8	128.9	128.4
I_x ($x10^6mm^4$)	17.25	18.50	19.96	21.61	23.47	25.55	27.87	30.43	33.24	36.31	39.65

Table 6.12 Higher size sections – no upstands $\alpha_c = 41mm$

	WF-152x152x37	WF-203x203x46
M_{cr} (kNm)	115.0	203.8
I_x ($x10^6mm^4$)	21.90	44.95

Observations for the UDL case are similar to those presented for the point load case in 6.1.2.5. Another wide flanged section is considered in the example that follows.

6.1.2.7 Example 4 (a): WF-254x254x107 – Point Load

For the WF-254x254x107 the summary of the critical elastic moment and second moment of area data for the base member and stiffened sections is presented in Table 5.70.

Table 6.13 Properties of WF-254x254x107 for comparison – Point Load

	Upstand height (mm)										
	0	10	20	30	40	50	60	70	80	90	100
M_{cr} (kNm)	1238.5	1355.0	1478.5	1585.4	1676.8	1753.5	1816.7	1867.6	1907.0	1937.0	1958.2
I_x ($x10^6mm^4$)	173.3	180.9	189.2	198.2	207.9	218.4	229.6	241.6	254.4	268.0	282.5

Table 6.14 Higher size sections – no upstands $\alpha_c = 69mm$

	WF-254x254x132	WF-305x305x118
M_{cr} (kNm)	1816.7	1747.4
I_x ($x10^6mm^4$)	222.6	272.4

The sections selected for comparison are one size higher and four sizes higher in the handbook. The member four sizes higher is a deeper section. For the WF-254x254x132, which is one size higher, an upstand height on the stiffened member of 60mm matches both the critical moment as well as the second moment of area and thus would be sufficient for both ultimate and service limit state criteria for critical moment and deflection. For the WF-305x305x118 an upstand height on the stiffened member of 50mm is sufficient to match the critical moment whereas an upstand height of 100mm would be required to match the stiffness. This means that if ultimate limit state is the governing limit state then an upstand height of 60mm, which is below the critical upstand height of 69mm, would suffice as a stiffener to be used on the existing beam in lieu of replacing with a section one or four sizes higher in the handbook.

6.1.2.8 Example 4 (b): WF-254x254x107 - UDL

Table 6.15 Properties of WF254x254x107 for comparison – UDL

	Upstand height (mm)										
	0	10	20	30	40	50	60	70	80	90	100
M_{cr} (kNm)	1080.1	1183.3	1292.0	1386.1	1466.1	1532.7	1586.8	1629.3	1661.4	1684.0	1698.5
I_x ($x10^6 mm^4$)	173.3	180.9	189.2	198.2	207.9	218.4	229.6	241.6	254.4	268.0	282.5

Table 6.16 Higher size sections – no upstands $\alpha_c = 69mm$

	WF-254x254x132	WF-305x305x118
M_{cr} (kNm)	1576.0	1542.6
I_x ($x10^6 mm^4$)	222.6	272.4

An upstand height of 60mm on the stiffened member gives a critical load that matches or just exceeds that of both members of higher size. For the 305x305x118 member the stiffness is only matched when the stiffened member has an upstand height of 100mm. This means that the governing criteria would determine the required upstand height in lieu of replacing with the doubly symmetric member.

The four examples presented have highlighted how a member strengthened with upstand stiffeners can be selected in place of replacing with sections that have higher size or place higher in the steel sections handbook. This presents an opportunity to exploit strengthening of existing members instead of replacing them with other doubly symmetric members of higher size. Once the comparison has been made on the basis of the critical elastic moment and the stiffness, the decision process can be progressed one step further by considering actual real-life behaviour. This is done by incorporating material constitutive laws, geometrical and material imperfections and then carrying out a second-order analysis. This would present a more economical alternative to physical testing of models. The comparison on this basis is presented in Chapter 6. The approach presented in the current chapter therefore serves as a preliminary check with the final check based on the nonlinear model (second order) analysis results. In addition to this any other criteria that is critical to the designer can be applied such as weight of member or cost comparison of strengthening existing member rather than replacing with a new doubly symmetric member. Sustainability considerations will also be important. Replacing with a new member, for instance, adds not only the carbon footprint of the manufacture, transportation and installation of the new member but also removal and disposal of the existing member. A four-meter (4m) span has been considered in the study presented. This study can be extended to other spans to check for consistency.

For the preliminary check the upstand stiffener thickness can also be varied to observe the change in outputs particularly where the stiffened case either provides properties just greater or less than the member to which it is being compared. There may be cases whereby by simply adjusting the stiffener thickness a desired outcome is obtained. Examples for narrow flange and wide flange members are presented in the section that follows.

6.1.3 Plate thickness sensitivity check

From the examples presented in 6.1.2 four cases are used to study the change in stiffener thickness and assess how this changes the section properties of interest i.e., the critical elastic moment and the second moment of area. The cases selected are the ones where the critical elastic moment and the second moment of area criteria were not met at the same upstand height. The lower upstand height requirement between the two criteria is selected to investigate the magnitude of stiffener thickness that may be required to meet the criteria that would have demanded a greater stiffener height. Four cases for a point load are presented based on Examples 1 to 4 in the previous section.

6.1.3.1 Section NF-IPE 120 compared with NF-IPE 160

In this first case the results from Example 1(a) in 6.1.2.1 with Table 6.1 and Table 6.2 are used. Upstand heights of 60mm and 80mm were found to be required on the IPE 120 to meet critical load and second moment area requirements respectively of the IPE 160. The upstand height of 60mm which is the lesser of two is selected as a starting point. This is shown in the cells shaded grey in Fig.6-1. The convention of shaded cells for the 'base case' is maintained for all the subsequent examples. The stiffener thickness is then varied to observe changes in the desired properties; the critical elastic moment and the second moment of area. Stiffener thicknesses greater than the base case are of particular importance, however, thicknesses below the base case are also included in order to observe the trends either side of the base case. The results obtained are presented in the figures that follow.

Example 1(a)

*Point Load Case

	Member	IPE 120					Upstand Height (mm)	60

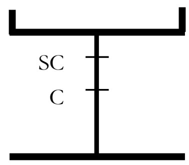

		t_α (mm)						
		5	5,5	6	6,3	7,5	10	12,5	15
M_{cr} (kNm)		14,2	15,2	16,4	17,2	20,7	30,3	42,8	57,7
I_x (x10^6 mm^4)		6,55	6,79	7,01	7,14	7,61	8,44	9,10	9,66
% Change in t_α		-20,6%	-12,7%	-4,8%	0,0%	19,0%	58,7%	98,4%	138,1%
% Change in M_{cr}		-17,4%	-11,6%	-4,7%	0,0%	20,3%	76,2%	148,8%	235,5%
% Change in I_x		-8,3%	-4,9%	-1,8%	0,0%	6,6%	18,2%	27,5%	35,3%

	Member	IPE 160

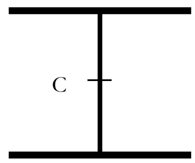

M_{cr} (kNm)	16,5
I_x (x10^6 mm^4)	8,35

Fig.6-1 Results for NF-IPE 120 upstand thickness parametric vs NF-IPE 160 properties

It can be seen from the results that the 60mm upstand height can be maintained with the thickness increased to 10mm (approximately 59% increase) from the 'base' thickness of 6.3mm. This gives a critical moment as well as a second moment of area that matches that for the IPE 160. The 80mm upstand height at base thickness had given a second moment of area of 9.24 x 10^6 mm^4. Increasing the thickness to 10mm for a 60mm upstand height gives a second moment of area of 8.44 x 10^6 mm^4 which is greater than that for the IPE 160. If the upstands were incremented at 5mm intervals, an upstand height of 75mm would have revealed a second moment of area of 8.67 x 10^6 mm^4 that meets the requirement. A check of the cross-section area shows:

$A_{up\ 60}$ = 60 x 10 (600 mm^2)

$A_{up\ 75}$ = 75 x 6.3 (472.5 mm^2)

Where 'up 60' and 'up 75' refer to the area associated with the considered upstand height.

A check of the area values reveals that the option of a higher upstand height would be optimal compared to a thicker upstand. However, it does reveal that cases do exist where a given criteria such as stiffness can be achieved by varying the stiffener thickness. It is noted that the sensitivity of the critical elastic moment is greater than that of the second moment of area in response to a change in thickness.

6.1.3.2 Section NF-254x146x37 compared with NF-356x175x45

In this second case the results from Example 2(a) in 6.1.2.3 as well as Tables 6xx and 6xx are referred to. An upstand height of 30mm was sufficient to meet the critical moment requirements. At the maximum considered height of 100mm the second moment of area criteria was not yet met. The stiffener thickness is now varied, and results observed.

Example 2(a) *Point Load Case									
	Member		254x146x37					Upstand Height (mm)	100
	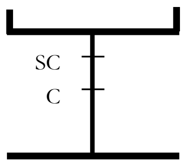								
	t_α (mm)								
		5,0	7,5	10,0	10,9	12,5	15,0	17,5	20,0
M_{cr} (kNm)		174,4	200,8	232,6	246,1	273,3	324,9	388,3	463,8
I_x ($x10^6$ mm^4)		81,60	91,90	100,70	103,60	108,40	115,10	121,00	126,30
% Change in t_α		-54,1%	-31,2%	-8,3%	0,0%	14,7%	37,6%	60,6%	83,5%
% Change in M_{cr}		-29,1%	-18,4%	-5,5%	0,0%	11,1%	32,0%	57,8%	88,5%
% Change in I_x		-21,2%	-11,3%	-2,8%	0,0%	4,6%	11,1%	16,8%	21,9%
	Member		356x175x45						
	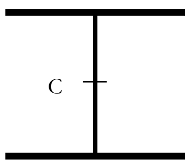								
M_{cr} (kNm)	174,9								
I_x ($x10^6$ mm^4)	118,40								

Fig.6-2 Results for NF-254x146x37 upstand thickness parametric vs NF-356x175x45

In this case if the 100mm high upstand has its thickness increased from 10.9mm to 17.5mm the second moment of area criteria (stiffness) is now also met. The increase in thickness is approximately 60%.

6.1.3.3 Section WF-152x152x30 compared with WF-203x203x46

In this third case the results from Example 3(a) in 6.1.2.5 as well as Tables 6xx and 6xx are referred to. None of the upstand heights, up to the maximum considered of 100mm met either critical elastic moment criteria or second moment of area criteria. Results from the stiffener thickness parametric study are given in Fig.6-3.

Example 3(a)

*Point Load Case

	Member		152x152x30					Upstand Height (mm)	100
	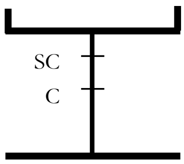								
	t_α (mm)								
		5,0	7,5	9,0	9,4	10,0	12,5	15,0	17,5
M_{cr} (kNm)		114,4	132,5	147,7	152,4	160,0	199,5	252,4	318,7
I_x ($x10^6$ mm^4)		31,20	36,32	38,90	39,65	40,62	44,30	47,51	50,33
% Change in t_α		-46,8%	-20,2%	-4,3%	0,0%	6,4%	33,0%	59,6%	86,2%
% Change in M_{cr}		-24,9%	-13,1%	-3,1%	0,0%	5,0%	30,9%	65,6%	109,1%
% Change in I_x		-21,3%	-8,4%	-1,9%	0,0%	2,4%	11,7%	19,8%	26,9%

	Member	203x203x46
	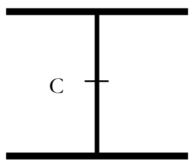	
M_{cr} (kNm)	233	
I_x ($x10^6$ mm^4)	44,95	

Fig.6-3 Results for WF-152x152x30 upstand thickness parametric vs WF-203x203x46

It can be seen from the results that increasing the stiffener thickness from 9.4mm to 15mm (approximately 60% increase) results in the stiffened section meeting the critical elastic moment and second moment of area requirement. The area associated with this case or that for the upstand height that is required at base thickness can be compared to determine the case with lower cross section area should this form an additional basis for comparison.

6.1.3.4 Section WF-254x254x107 compared with WF-305x305x118

In this third case the results from Example 4(a) in 5.4.2.7 as well as Tables 5.70 and 5.71 are referred to. An upstand height of 50mm met the critical elastic moment criteria while an upstand height of 100mm was required to meet the . Results from the stiffener thickness parametric study are given in Fig.5-32.

Example 4(a)
*Point Load Case

	Member		254x254x107					Upstand Height (mm)	50
	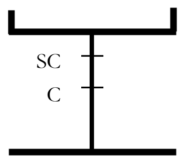								
	t_{α} (mm)								
	10,0	12,5	15,0	17,5	20,5	30,0	32,5	35,0	37,5
M_{cr} (kNm)	1 484,5	1 542,9	1 603,6	1 668,4	1 753,5	2 101,4	2 217,3	2 344,6	2 483,4
I_x ($x10^6$ mm^4)	196,90	202,30	207,50	212,50	218,40	235,50	239,70	243,00	247,70
% Change in t_{α}		-39,0%	-26,8%	-14,6%	0,0%	46,3%	58,5%	70,7%	82,9%
% Change in M_{cr}		-12,0%	-8,5%	-4,9%	0,0%	19,8%	26,4%	33,7%	41,6%
% Change in I_x		-7,4%	-5,0%	-2,7%	0,0%	7,8%	9,8%	11,3%	13,4%

	Member	305x305x118
	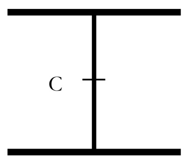	
M_{cr} (kNm)	1747,4	
I_x ($x10^6$ mm^4)	272,40	

Fig.6-4 Results for WF-254x254x107 upstand thickness parametric vs WF-305x305x118

In this case despite an increase in the upstand thickness of up to 82% the second moment of area criteria is not reached. The option of a greater upstand height may turn out to be a more viable alternative. The thickness would have to be increased further until the criteria is fulfilled, this can then be compared to the option of increasing the upstand height further.

6.1.4 Summary

Examples based on varying the plate thickness have been briefly explored in section *6.1.3* to demonstrate that desired outcomes can be obtained not only by varying the upstand height, α, but also by varying the plate thickness, t_α.This may become an option to consider if a limit upstand height is established but the required outcome is not met. The plate thickness can then be adjusted, based on the sensitivity, to obtain the required outcome.

6.2 CHOICE OF UPSTAND HEIGHT

6.2.1 General Approach

Although several other strengthening approaches have been presented for steel members the uniqueness of the current approach lies in the way the behaviour of monosymmetric sections is exploited. In this particular case a doubly symmetric section is converted into a monosymmetric section and the effect of monosymmetry, in addition to other cross-section properties, is exploited in those regions where beneficial outcomes are obtained. Because monosymmetry can also work against the designer, the opportune region where benefits can be exploited has to be identified. The '*Wagner effect*' has been presented in chapter 3 and this explains why the behaviour of monosymmetric sections can be peculiar in this regard. One of the key factors that influences the behaviour of monosymmetric sections is the position of the shear centre relative to the point of load application. The other is the position of the shear centre relative to the centroid which has an effect on the monosymmetry constant. Because both of these are shifting as the upstand height is varied this leads to the kind of situation described above where there is unique behaviour and a particular region of upstand heights giving outcomes that are desirable. It can be shown using an 'equivalent doubly symmetric section' approach that the monosymmetry does play a significant part in the member behaviour. The approach is demonstrated by using the illustrations shown in Fig.6-5 and those that follow.

(a) Monosymmetric section (b) Equivalent doubly symmetric section

Fig.6-5 Monosymmetric section and corresponding equivalent doubly symmetric section

The monosymmetric section obtained from introducing upstands is shown in Fig.6-5 (a). The equivalent doubly symmetric section is generated by taking the cross-section properties of the monosymmetric section and setting only the monosymmetry constant, β_x, to zero. In the equation for the critical elastic moment the distance from the load application point to the shear centre is required. For the equivalent doubly symmetric section this is taken as 'x' the distance to the centroid of the monosymmetric section since for a doubly symmetric section the shear centre would lie at the same point as the centroid of the cross-section. The critical elastic moment is then determined for the monosymmetric section for different upstand heights as previously done. At each upstand height the critical elastic moment for the corresponding equivalent doubly symmetric section is also determined and recorded. The results for the two are then plotted so that a direct comparison can be made. An example of values for a monosymmetric section and its equivalent doubly symmetric section at different upstand heights is presented in Mudenda and Zingoni (2018) and an extract shown in Fig.6-6 for a WF-152x152x30 section.

Section properties and results for beams with α varying from 50 to 100.

Section	α = 50	α = 62.5	α = 75	α = 100
ρ	0.73	0.76	0.78	0.82
I_y	10.45×10^6	11.66×10^6	12.87×10^6	15.30×10^6
J	126.05×10^3	132.81×10^3	139.94×10^3	154.03×10^3
C_w	37.01×10^9	36.76×10^9	37.29×10^9	40.35×10^9
M_{cr} for monosymmetric section (kNm)				
6 m	84.6	87.5	89.1	88.8
9 m	53.1	55.8	57.8	60.1
M_{cr} for equivalent doubly symmetric section (kNm)				
6 m	82	88.5	95.1	108.6
9 m	52	56.2	60.5	69.2

Fig.6-6 Properties of a monosymmetric section as well as its 'equivalent doubly symmetric' section for selected upstand heights (Mudenda and Zingoni, 2018)

The outcome is generally of the form shown in Fig.6-7 indicating that there is a region where the monosymmetric section has a higher critical elastic moment value than the equivalent doubly symmetric section. In this region the increase in critical elastic moment can be attributed to the effect of monosymmetry and not necessarily on the cross-section properties alone.

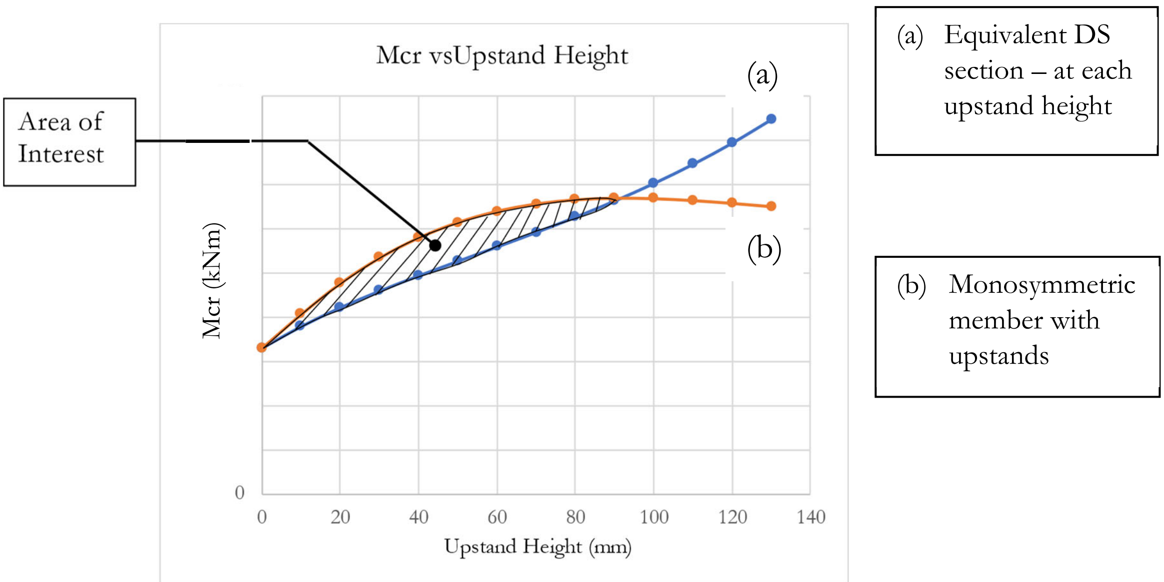

Fig.6-7 Comparison of critical elastic moment from monosymmetric section and equivalent doubly symmetric section

This is because similar cross-section properties are used in the doubly symmetric section. Once the shear centre position in the monosymmetric section coincides with the centroid and moves below it the '*Wagner effect*' now creates a situation where the critical elastic moment starts to diminish despite the section properties attaining greater values. The increasing section properties are demonstrated by the equivalent doubly symmetric section critical moment continuously increasing. The shaded area in Fig.6-7 becomes the area of interest where the effect of monosymmetry can be exploited.

The trend described above is studied for different members particularly those presented in section 6.1. This is to investigate whether the area of interest is consistent in narrow flange as well as wide flange sections. The four sections under point load as well as the four under a UDL as presented in 6.1 are considered. Observed trends are compared to the 'critical upstand value' for the section at which the shear centre is found to be coincident with the centroid. An example determination is provided in Appendix B.

6.2.2 Area of interest study – Point Load Case

The results of the 'area of interest' are presented in the section that follows for the cross-sections listed in Table 6.17 and evaluated for four different spans.

Table 6.17 Sections evaluated for 'Area of interest' study

Member	Load Type	Spans (m)	Figure No.
NF-IPE 120	Point Load	2, 4, 6, 8	6-8 to 6-11
NF-254x146x37	Point Load	2, 4, 6, 8	6-12 to 6-15
WF-152x152x30	Point Load	2, 4, 6, 8	6-16 to 6-19
WF-254x254x107	Point Load	2, 4, 6, 8	6-20 to 6-23

The results are discussed in the sections that follow.

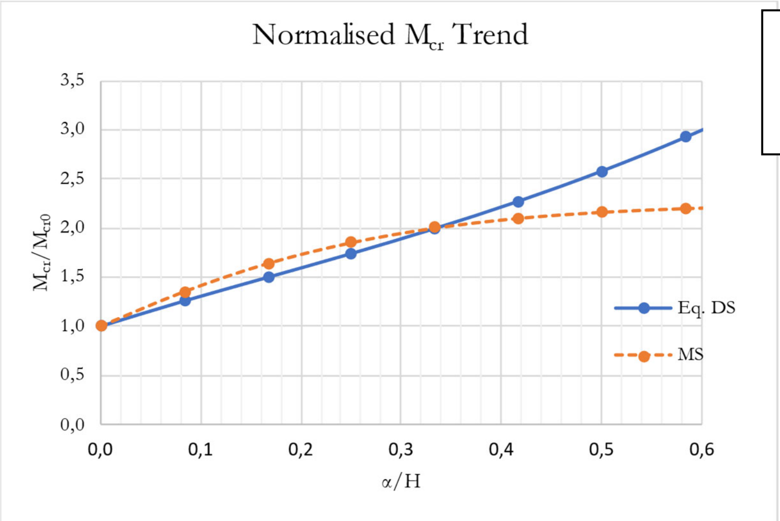

(b)

Fig.6-8 NF-IPE 120 normalised plot for (2m span)

SC = C

$^{\alpha}/_{H} = 0.29$

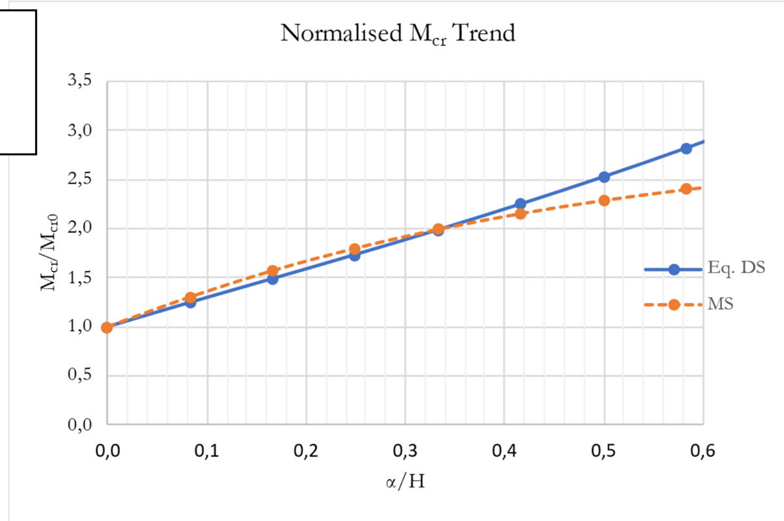

(b)

Fig.6-9 NF-IPE 120 normalised plot for (4m span)

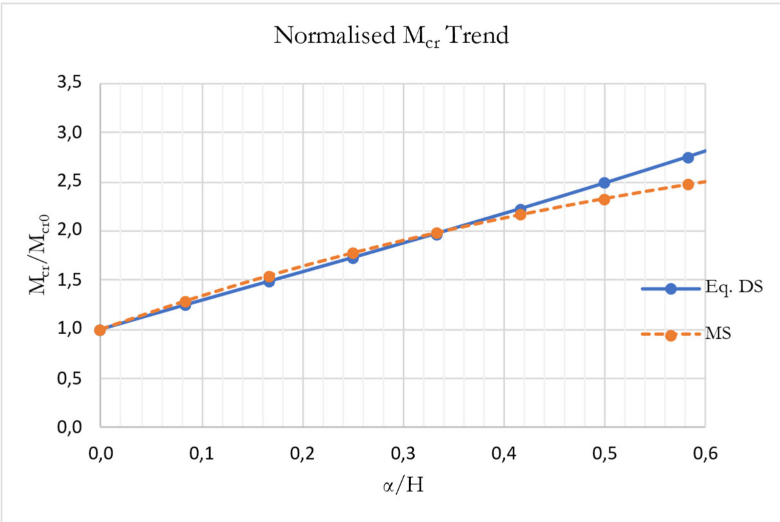

(a)

Fig.6-10 NF-IPE 120 normalised plot for (6m span)

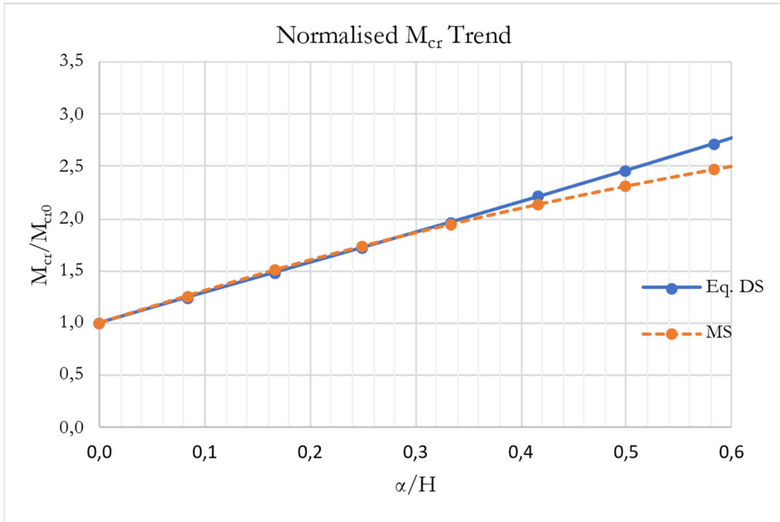

(b)

Fig.6-11 NF-IPE 120 normalised plot for (8m span)

An average value for the $\alpha/_H$ value at coincidence of 0.305 was obtained for narrow-flange sections in chapter 3. For the NF-IPE 120 considered in Fig.'s 6-8 to 6-11 an actual value of 0.29 is obtained. This applies to all spans. For all the graphs, and spans, it can be observed that the trend line for the monosymmetric section critical elastic moment crosses that for the corresponding 'equivalent doubly symmetric' section between the $\alpha/_H$ values of 0.2 and 0.4. This point roughly coincides with that associated with the coincidence point just mentioned. This, therefore, means that the point of coincidence of the shear center and the centroid is a good proxy or indicator of the cut-off point of our 'area of interest' highlighted in Fig.6-7. The key point of shear center and centroid coincidence thus is not simply a peculiar observation of a cross section property but also gives an indication of the upstand height at which the benefits of monosymmetry in these members terminates.

It is also worth noting the for shorter spans the monosymmetry effect appears to be greater than that experienced in longer spans. This is consistent with the percentage gains trends observed in Chapter 5. Another narrow-flange section is considered in the next set of figures.

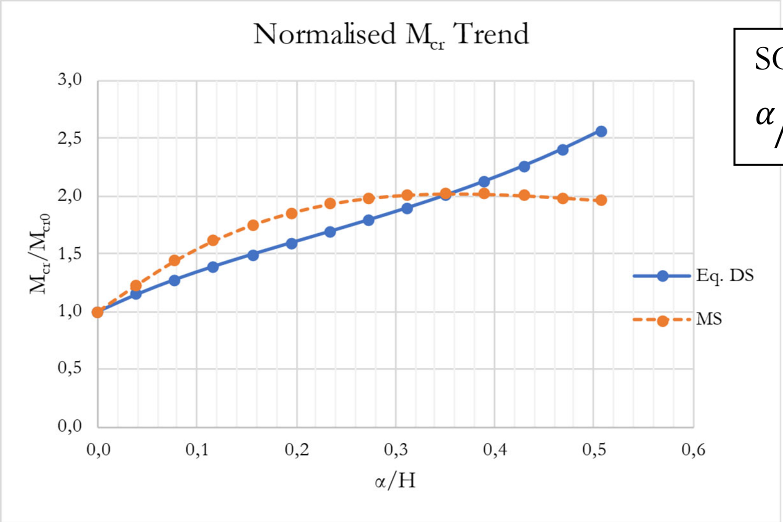

(a)

SC = C

$^{\alpha}/_{H} = 0.30$

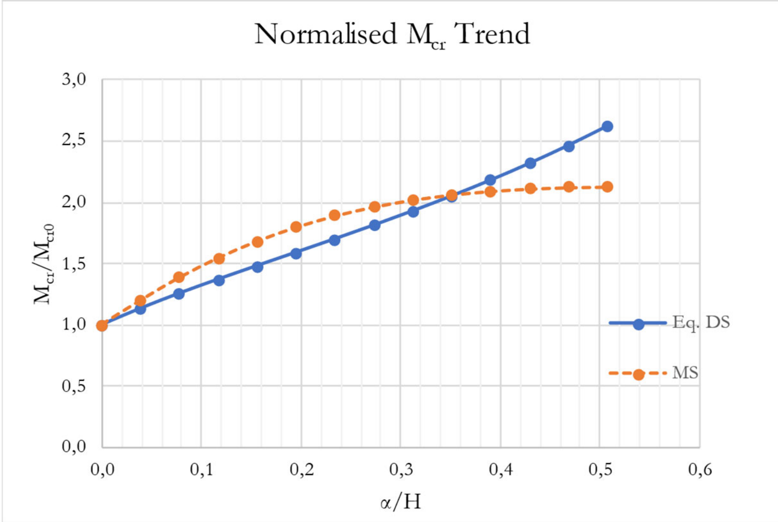

(b)

Fig.6-12 NF-254x146x37 normalised plot for (2m span)

Fig.6-13 NF-254x146x37 normalised plot for (4m span)

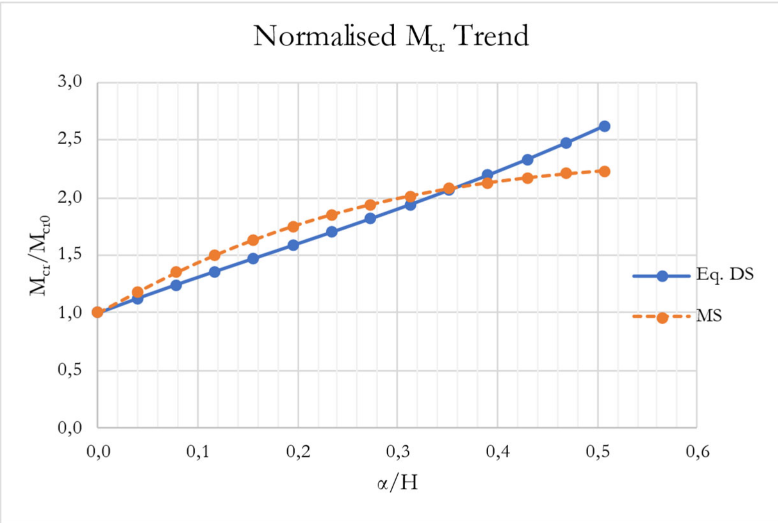

(a)

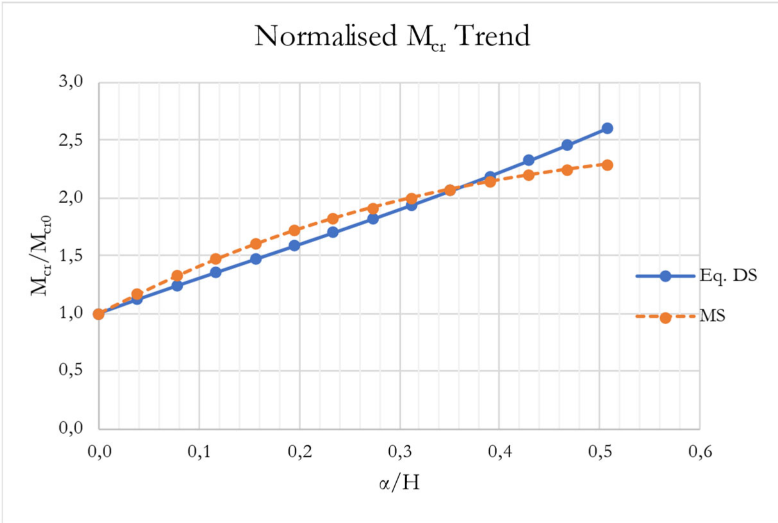

(b)

Fig.6-14 NF-254x146x37 normalised plot for (6m span)

Fig.6-15 NF-254x146x37 normalised plot for (8m span)

For the second narrow-flange section which is a NF-254x146x37 a value of $\alpha/_H$ of 0.30 is obtained for the coincidence point of the shear center and centroid. The graphs show that the trendline for the monosymmetric section critical elastic moment crosses that for the corresponding ‘equivalent doubly symmetric’ section between the $\alpha/_H$ values of 0.3 and 0.4. Although in this case the point where the trendlines cross is at an $\alpha/_H$ value slightly greater than that of the coincidence point, it is still a good proxy or indicator of the cut-off point of our ‘area of interest’ highlighted in Fig.6-7. The trend with a declining effect of the monosymmetry for longer spans is also observed here.

Observations for wide-flange sections are explored in the two cases that follow.

SC = C

$\alpha/_{H} = 0.31$

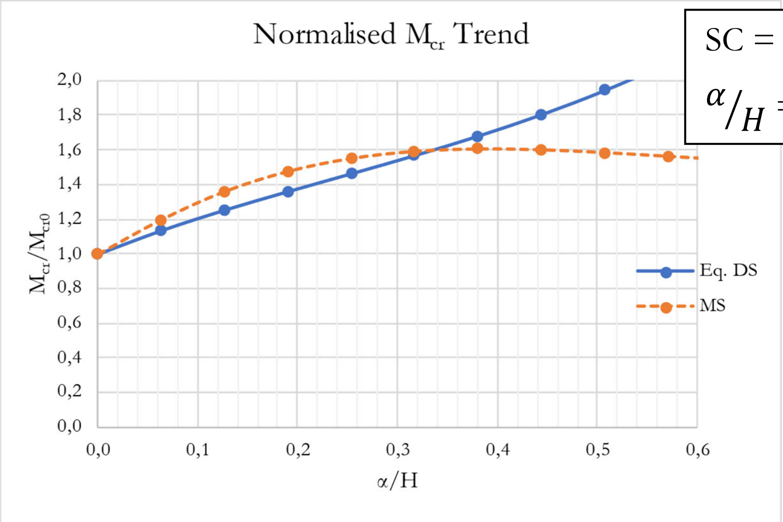

(a)

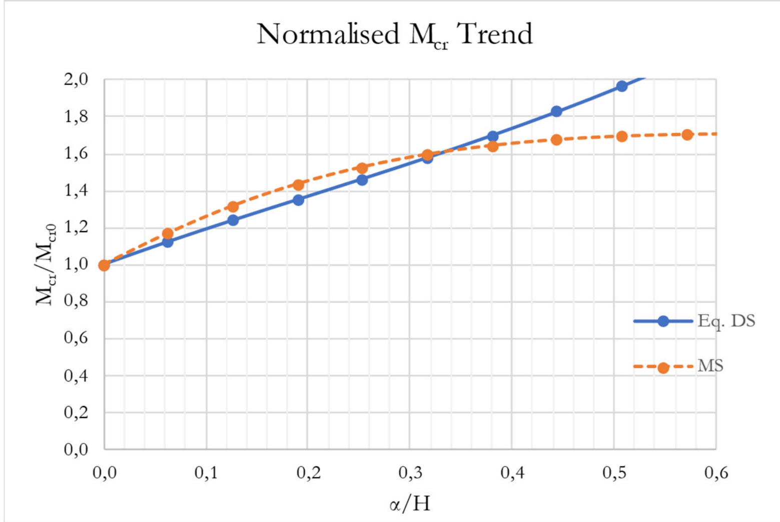

(b)

Fig.6-16 WF-152x152x30 normalised plot for (2m span)

Fig.6-17 WF-152x152x30 normalised plot for (4m span)

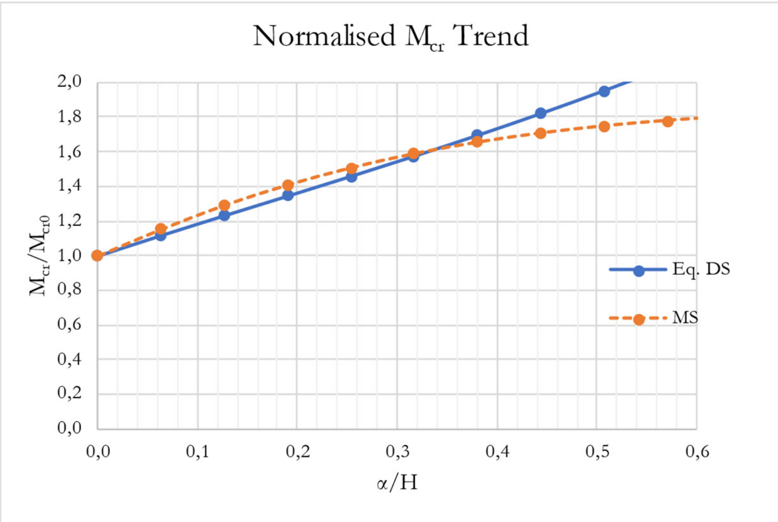

(a)

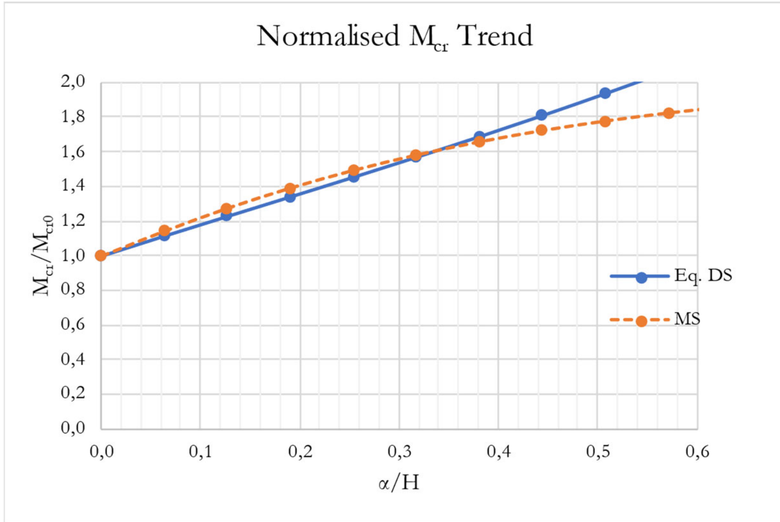

(b)

Fig.6-18 WF-152x152x30 normalised plot for (6m span)

Fig.6-19 WF-152x152x30 normalised plot for (8m span)

For the WF-152x152x30 a value of $\alpha/_{H}$ of 0.31 is obtained for the coincidence point of the shear center and centroid. The graphs show that the trendline for the monosymmetric section critical elastic moment crosses that for the corresponding 'equivalent doubly symmetric' section between the $\alpha/_{H}$ values of 0.3 and 0.4 but closer to 0.3. This indicates that for wide flange sections, as was the case for narrow flange sections, the coincidence point is a good indicator of the point where the area of interest terminates. This as indicated earlier marks the limit of the upstand heights where the greatest advantage can be obtained from effects of monosymmetry.

SC = C

$\alpha/_H = 0.27$

(b)

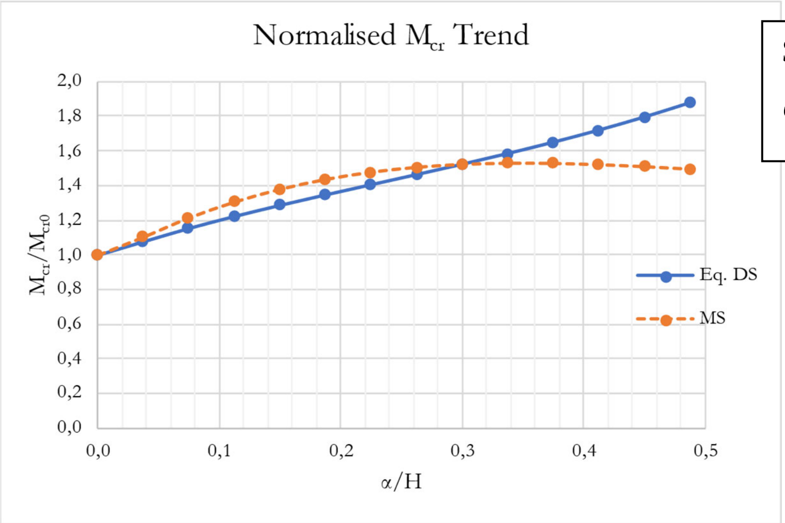

Fig.6-20 WF-254x254x107 normalised plot for (2m span)

(b)

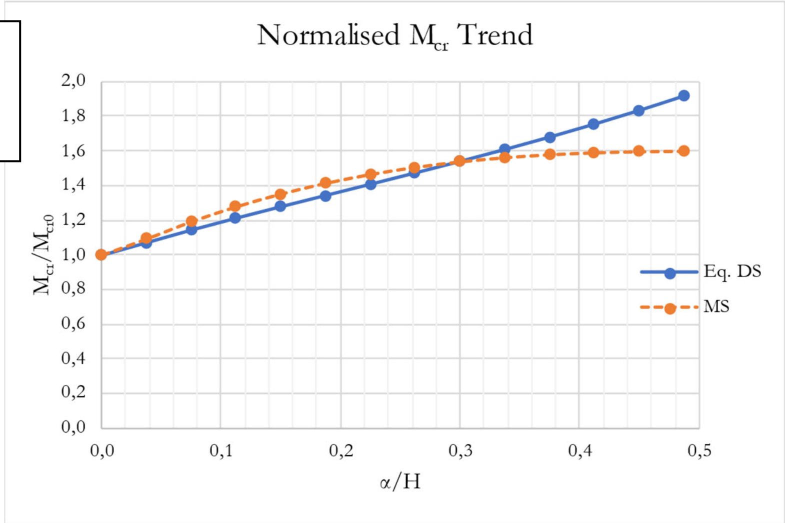

Fig.6-21 WF-254x254x107 normalised plot for (4m span)

(b)

Fig.6-22 WF-254x254x107 normalised plot for (6m span)

(b)

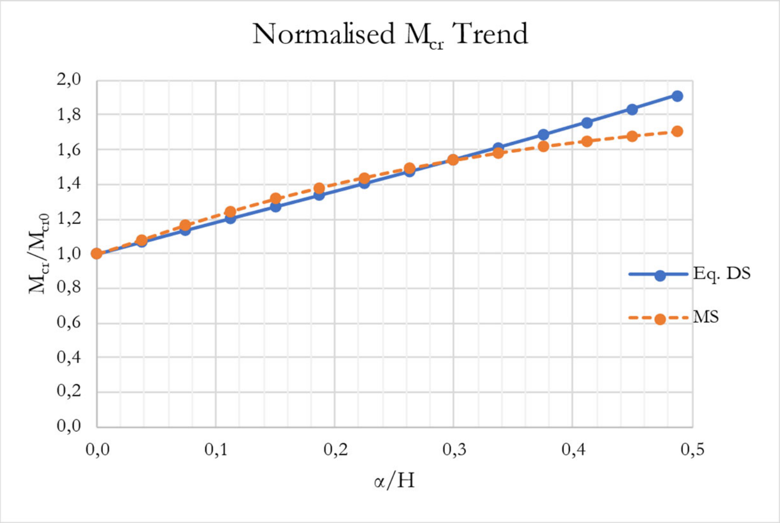

Fig.6-23 WF-254x254x107 normalised plot for (8m span)

For the WF-254x254x107 a value of ${}^{\alpha}/_{H}$ of 0.27 is obtained for the coincidence point of the shear center and centroid. The graphs show that the trendline for the monosymmetric section critical elastic moment crosses that for the corresponding 'equivalent doubly symmetric' at a value of ${}^{\alpha}/_{H}$ of about 0.3 which is just slightly higher than the value obtained for the coincidence point. This indicates that for this wide flange section, as was the case for previous examples considered, the coincidence point is a good indicator of the point where the area of interest terminates. This shows that the coincidence point is consistently a good indicator of the point where the area of interest terminates and thus has a significance for design.

In summary results show that for the narrow flange (NF) beams:

- The two plots coincide at an α/H value of between 0.3 and 0.4.

For the wide flange (WF) beams:

- The two graphs coincide at an α/H value close to 0.3

This trend is observed to be consistent for the sections considered here. The relationship between the critical elastic moment and α/H for the monosymmetric section and for the 'equivalent doubly symmetric' section is observed to correlate with the observation of the shear centre and centroid coincidence point presented in Chapter 3. It was observed there that the coincidence of the shear center and the centroid occurs for all cross sections studied between α/H (presented as 'η') values of 0.25 and 0.35. The average values obtained in section 3.9 also fall within this range. This indicates that identifying the upstand height for which the shear center and centroid coincide gives an indication where the benefits of monosymmetry to the stiffened section decline or begin to reverse. The coincidence point is therefore a good indicator of the maximum stiffener height that should be considered for significant benefit from the effect of monosymmetry. Beyond this point any benefit is driven only by the cross-section properties and in fact the monosymmetry then begins to work against any gains obtained by further increase in section properties (from increasing the upstand height).

Based on the elastic critical moment a decision process can be established as shown in Fig.6-24.

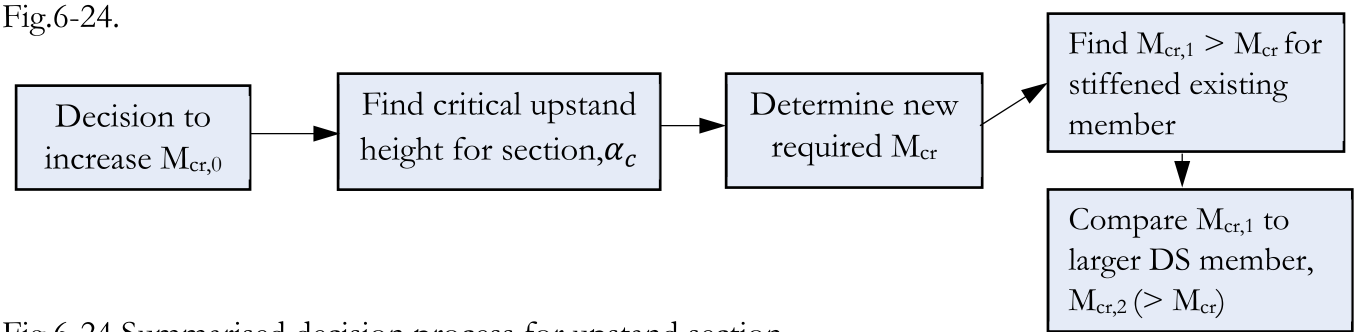

Fig.6-24 Summarised decision process for upstand section

6.2.3 Area of interest study – UDL Case

The results for the UDL case are generated for a NF-254x146x37 for a 2m and a 4m span and presented in Fig.'s 6-25 and 6-26. In both cases the curves for the monosymmetric beam with upstands and that for the equivalent doubly symmetric member meet at a 'η' value that lies between 0.3 and 0.4 as was observed for the point load case. This shows that the observation is consistent.

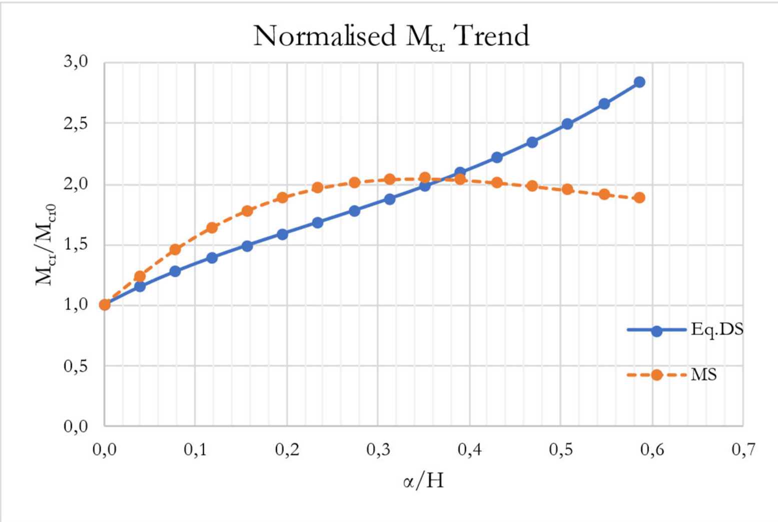

Fig.6-25 NF-254x146x37-UDL normalised plot for (2m span)

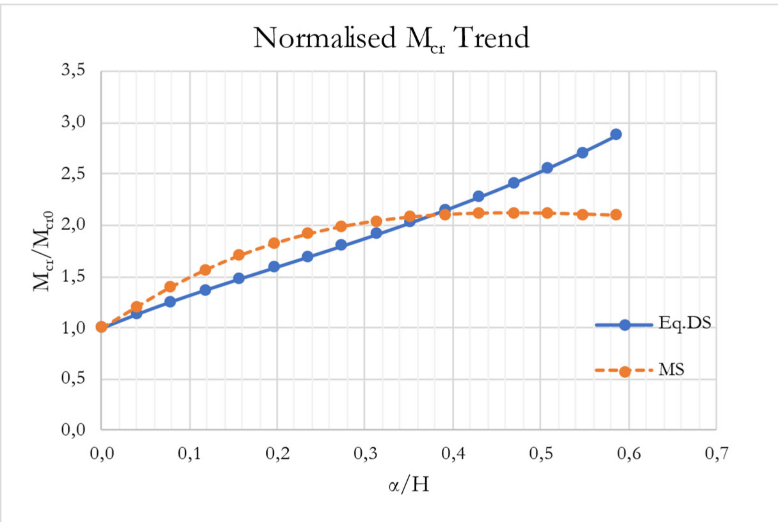

Fig.6-26 NF-254x146x37-UDL normalised plot for (4m span)

These two cases are compared with the graphs for the point load case as presented in Fig.'s 6-12 and 6-13. The comparison can be seen in Fig.'s 6-27 and 6-28.

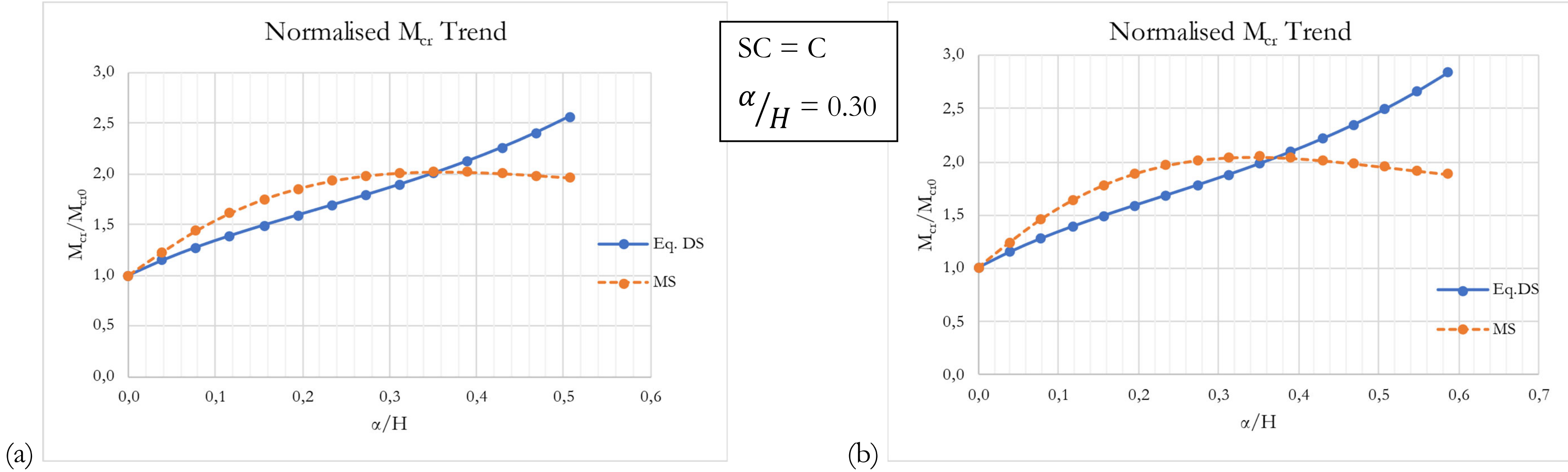

Fig.6-27 Comparison of NF-254x146x37 normalised plot for Point load (a) and UDL (b) for a 2m span

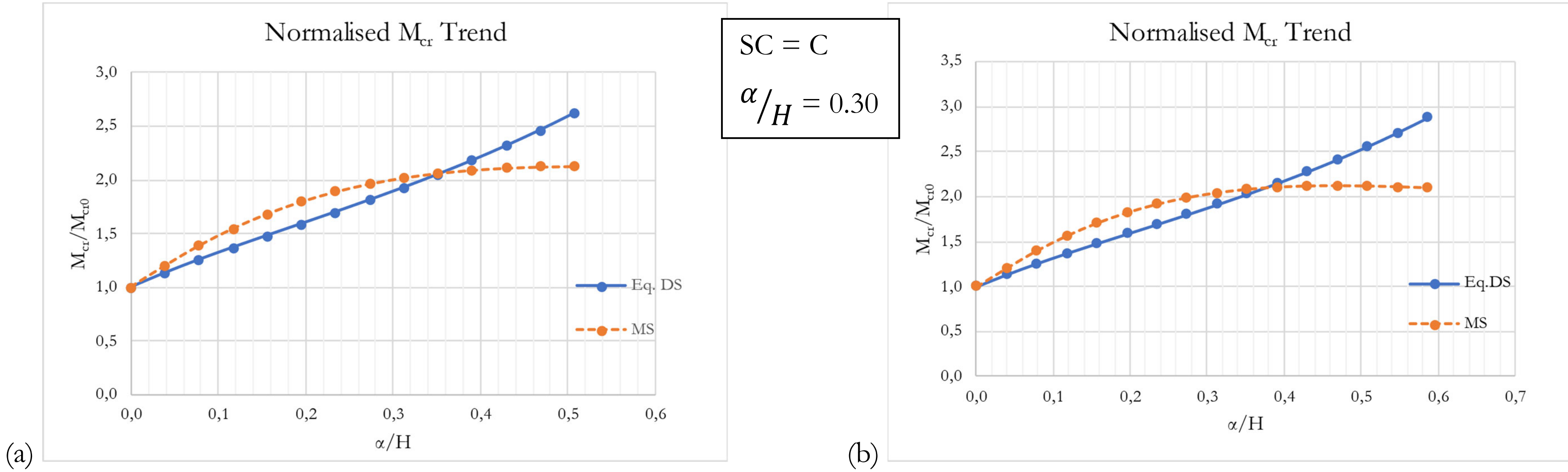

Fig.6-28 Comparison of NF-254x146x37 normalised plot for Point load (a) and UDL (b) for a 4m span

The behaviour for the point load case and that for the UDL can thus be observed to be similar.

6.3 SUMMARY AND CONCLUSION

In this chapter the relationship between the upstand height and the critical elastic moment has been studied. The trend with regard the critical moment as the upstand height approaches and passes the upstand height at which the values for the monosymmetric section and that for the 'equivalent doubly symmetric' section are the same has been investigated and this has led to the identification of a region where the effect of monosymmetry can be exploited. This region can be correlated to the point of coincidence that was highlighted in Chapter 3. This means that the coincident shear centre and centroid point acts as a useful proxy that can determine a limiting critical upstand height of a strengthened section where the beneficial effect of monosymmetry can best be exploited.

Whereas a study based on the elastic critical moment allows us to study many different cases relatively easily for determination of behaviour trends this type of failure is theoretical and does not allow us to observe the strength trends of a member in real life. A real-life member will possess imperfections and will have a material that obeys a specific constitutive law and thus a nonlinear analysis needs to be carried out to determine the real member strength. This will be the subject of the chapter that follows. The aim is to extend the study from this chapter to real life cases. Finite element analysis is employed for the nonlinear analysis study. This would complete the process necessary to make a design decision when confronted with the potential to exploit the gains from monosymmetry.

CHAPTER 7 NONLINEAR ANALYSIS OF MEMBERS

7.1 INTRODUCTION

Although the linear buckling analysis carried out in Chapters 5 and 6 provides many useful insights on the behaviour and trends of upstand stiffened steel beams undergoing lateral-torsional buckling, the critical moment values do not necessarily give a true indication of the strength of a beam in real life. The critical elastic moment is in effect only applicable to slender beams. For short and intermediate span beams failure is initiated by material yield before the elastic critical moment can be attained. This leads to the need for inelastic buckling to be considered due to the material yielding in parts of the member. Inelastic buckling leads to failure moments that lie below that predicted by the elastic critical moment equation. In addition to inelastic buckling real beams have initial geometric imperfections. These imperfections lead to secondary effects such as nonlinear behaviour and can further reduce the ultimate load that the member can carry. Consideration of both inelastic material behaviour and geometrical imperfections helps in predicting the actual strength of real beams.

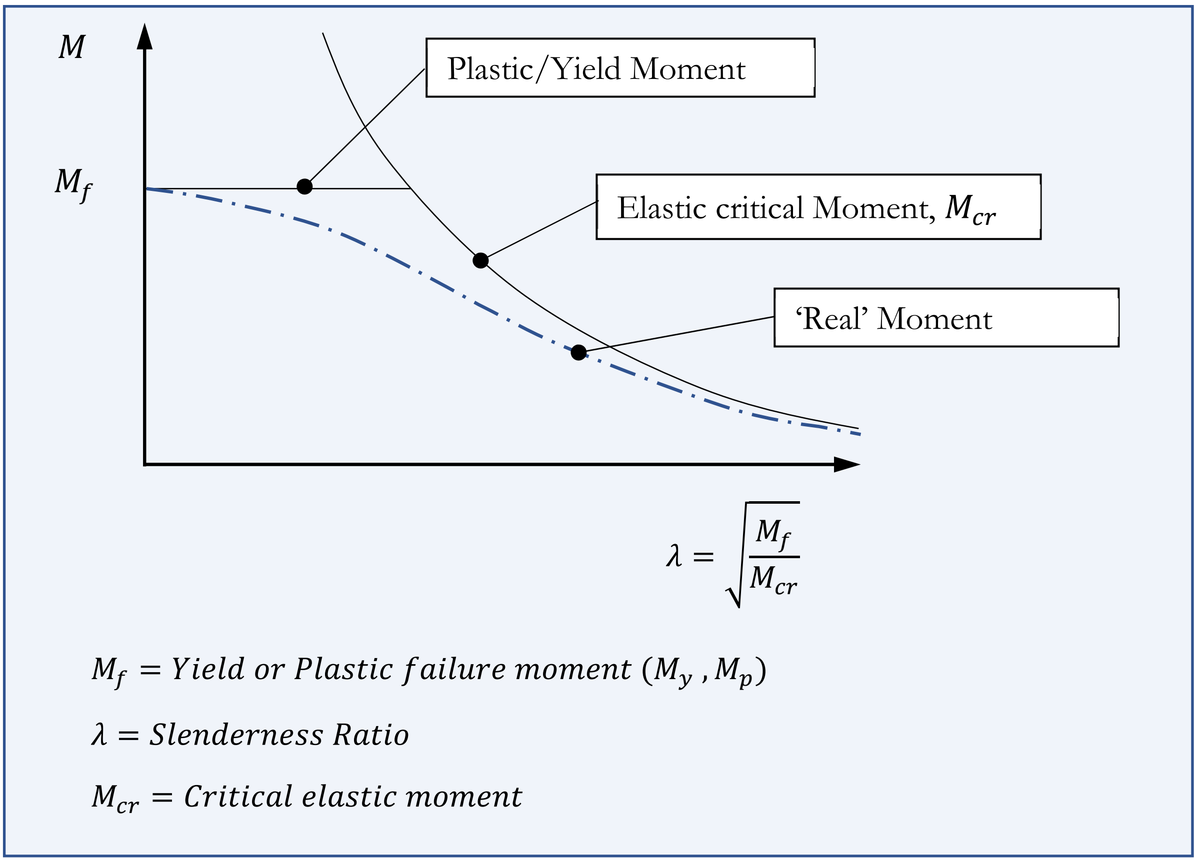

Fig.7-1 Real beam behaviour relative to two 'ideal' upper bounds

In Fig.7-1 the two upper bounds of theoretical beam capacity; the critical elastic moment and the material failure moment (M_y for class 3 sections and M_p for class 1 & 2 sections) are shown on a typical normalised plot of moment capacity (M) against beam slenderness (λ). At a slenderness value of '1' the critical elastic moment has the same value as the failure moment. The real behaviour of the member is also shown with the effect of inelastic buckling and geometrical imperfection most markedly affecting intermediate slenderness beams which are the most prevalent practical cases. Beams with low slenderness tend towards a material failure whereas highly slender members tend towards a buckling failure. Design equations, which are based on and meant to predict the actual strength of real members, would typically follow the trend shown for the 'real' moment behaviour.

Though many studies have been carried out on the behaviour of monosymmetric steel beams there remains a noticeable lack of design guidance. This can be attributed to not many studies extending considerations from the elastic behaviour to the elastic-plastic behaviour with consideration of imperfections. Such a consideration is a first step towards establishing design guides. It was observed by Trahair (2012) that three design codes; the Eurocode 3, AS4100 and AISC did not have design guidance on monosymmetric sections that correctly accounted for the member behaviour. Although Hsu et al (2012) and MacCrimmon (2004) have used provisions in the AISC standard to design compound monosymmetric sections made from I-section beams with channel caps it is not clear whether this approach and the sections of the standard used would apply to other monosymmetric sections generally. Moreover, the simplified equations for the monosymmetry constant are based on the work of Kitipornchai and Trahair (1980) which was given with a validity range. The work presented by MacCrimmon (2004) converts the compound section into an 'equivalent' I-shaped section just to be able to use the simplified equation. It is therefore essential that work such as presented in the current study is extended into the elastic-plastic range so that real member behaviour can be predicted, and this information translated to practical design applications. An approach suggested by Knobloch et al. (2020) who have reported on the revision of the Eurocode 3 provisions has been considered here. That is, the use of geometric and material nonlinear with imperfection analysis (GMNIA). Another version considered which does not include residual stress effects is the geometric and material nonlinear analysis (GMNA) approach. The approach used in the current study is presented in section 7.2.3.

7.2 ULTIMATE MEMBER STRENGTH

Although the linear buckling analysis carried out in Chapter 5 provides many useful insights on the member behaviour once upstand stiffeners are introduced the application for strengthening examples are based on a theoretical load capacity (the critical elastic moment). To translate these observations to 'real life' scenarios the models used must be adapted to consider material behaviour as well as geometrical out-of-straightness which are inherent in real members. This section looks at these important considerations and how they are accounted for in the current study.

7.2.1 Inelastic Behaviour

It has been reported by Kitipornchai and Wong-Chung (1987) that beams of practical slenderness fail in the inelastic range. Consideration of inelastic behaviour is thus essential for the determination of member strength. Inelastic behaviour is unique to members undergoing flexure owing to the nature of stress distribution. Because the longitudinal stress varies with distance from the bending axis (neutral axis) extreme parts of the member can start to yield so that some parts of the beam may be in a plastic state when buckling happens. If parts of the member start to yield with load increase the effective elastic portion of the beam which is available to provide rigidity against buckling starts to diminish. This then causes buckling to happen at a load level which will be lower than the elastic buckling load based on the unyielded cross section. In studying the inelastic buckling of beams Nethercot (1973) used a procedure where the elastic portion of the beam was successively reduced depending on the load level and the buckling load then determined based on the elastic portion of the beam. This approach works for the case of uniform moment loading where stress is uniform along the member but becomes more complex for other loading cases. These effects where parts of the member have yielded with loss of strength and rigidity are what inelastic behaviour is associated with. The yielding of material also means the loss of linear elastic behaviour of the cross section and hence the response becomes inelastic. Inelasticity therefore stems from the material behaviour or response across the section. A material stress-strain (constitutive relationship) needs to be employed in the analysis so that portions subject to yielding during the analysis are appropriately accounted for.

In the current study a quad-linear model presented by Yun and Gardner (2017) has been adopted. This model is based on a statistical analysis of material stress-strain data for several tests on various hot-rolled mild steel grades including S355JR which is the predominantly used structural steel grade in South Africa. The model is shown in Fig.7-2. With the values for the key parameters on the graph given in equations (7.1) to (7.5).

$$f(\varepsilon) = \begin{cases} E\varepsilon & for\ \varepsilon \leq \varepsilon_y \\ f_y & for\ \varepsilon_y < \varepsilon < \varepsilon_{sh} \\ f_y + E_{sh}(\varepsilon - \varepsilon_{sh}) & for\ \varepsilon_{sh} < \varepsilon < C_1\varepsilon_u \\ f_{C_1\varepsilon_u + \frac{f_u - f_{C_1\varepsilon_u}}{\varepsilon_u - \varepsilon_{sh}}(\varepsilon - C_1\varepsilon_u)} & for\ C_1\varepsilon_u < \varepsilon < \varepsilon_u \end{cases} \tag{7.1}$$

$$\varepsilon_u = 0.6\left(1 - \frac{f_y}{f_u}\right) \qquad but\ \varepsilon_u \geq 0.06\ for\ hot-rolled\ steels \tag{7.2}$$

$$\varepsilon_{sh} = 0.1\,\frac{f_y}{f_u} - 0.055 \qquad but\ 0.015 \le \varepsilon_{sh} \le 0.03 \tag{7.3}$$

$$C_1 = \frac{\varepsilon_{sh} + 0.25(\varepsilon_u - \varepsilon_{sh})}{\varepsilon_u} \tag{7.4}$$

$$E_{sh} = \frac{f_u - f_y}{0.4(\varepsilon_u - \varepsilon_{sh})} \tag{7.5}$$

The new model was reported as an improvement on models developed based on lower grade steels that were prevalent a few decades ago. These models are less suitable for the wide range of modern steel grades now in common use. Some key advantages of the quad-linear model are reported as the more accurate predictions of ε_{sh} and E_{sh} as well as the more accurate representation of the stiffness loss in the strain hardening region.

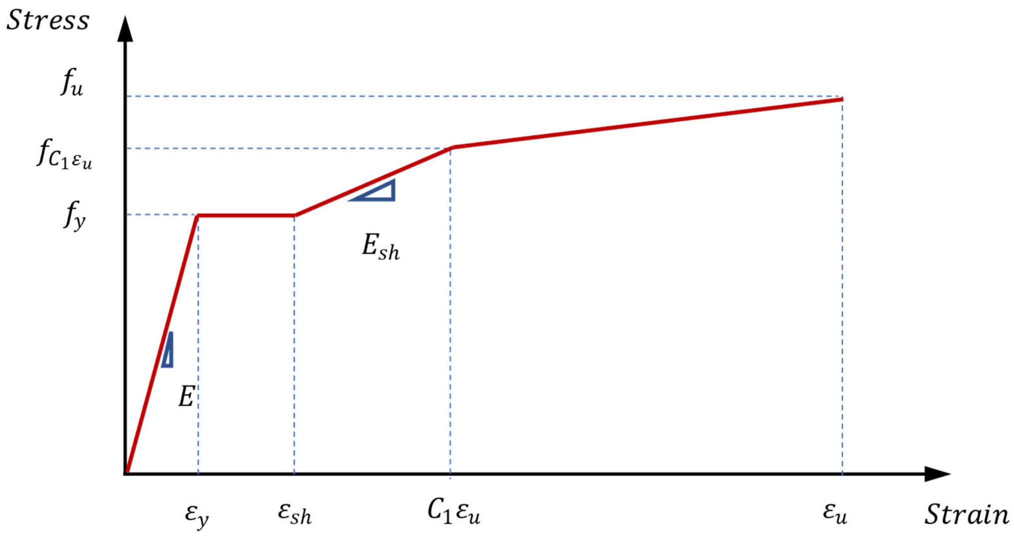

Fig.7-2 Quad-linear stress-strain curve adapted from Yun and Gardner (2017)

This model was thus also deemed by the authors to be more accurate than the bi-linear and tri-linear models that were up to that point commonly used. The strain values are converted to plastic strain values for use in the analysis software for the current study.

7.2.2 Geometric out of straightness

The geometry of the member when considering applied loads can have considerable effects on the outcome of an analysis. This is best illustrated by using a cantilever column shown in Fig.6.2. One of the differences between first (1st) order and second (2nd) order analysis is that in first order analysis the approach to geometry is that the loads are applied to, and load effects considered on, an undeformed configuration of the member. This is shown on Fig.7-3 (a). For the second order analysis load effects must be considered on the deformed configuration of the member. These effects normally require the use of a stepwise incremental approach to correctly determine. The load effects on the example cantilever column are shown in Fig.7-3 (b) and the reaction now has an additional term due to the applied load causing a secondary effect known as a 'second-order effect' and hence necessitating the use of a second order analysis to determine.

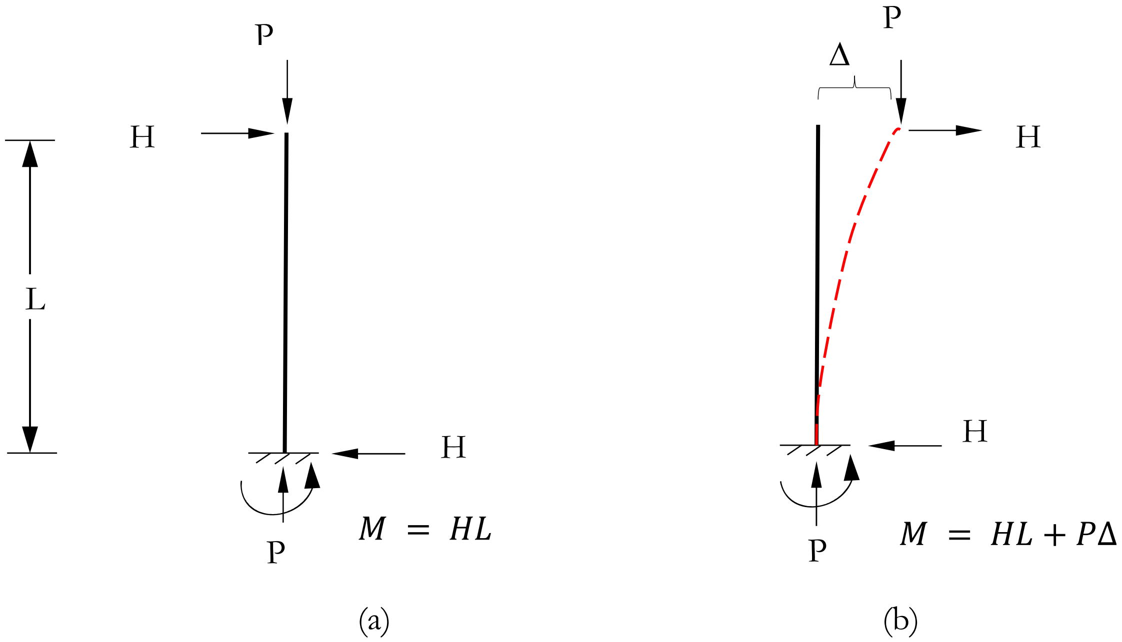

Fig.7.3 Load effects on undeformed (a) and deformed (b) configuration of a cantilever column

For the lateral-torsional buckling of beams an initial geometric out-of-straightness of the member must be considered in the analysis. The effects of the loads initially acting on this undeformed configuration is then accounted for in the analysis. The initial deformation can either be purely translational or a combination of a translation and a rotation. The out-of-straightness is defined by the out of plane distance 'u' shown in Fig.7-4.

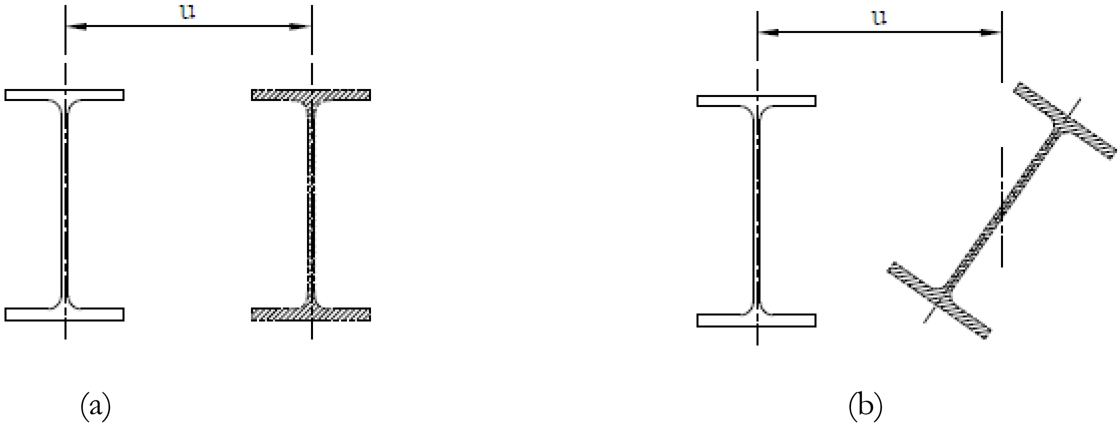

Fig.7-4 Geometric out-of-straightness for an I beam with translation only (a) and translation with rotation (b)

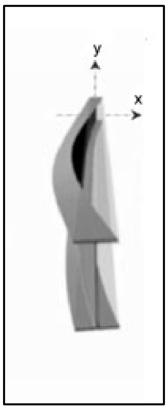

Fig.7-5 3D Illustration of out-of-straightness (Source: MS PowerPoint, online pictures)

The orientation on plan is shown in Fig.7-6.

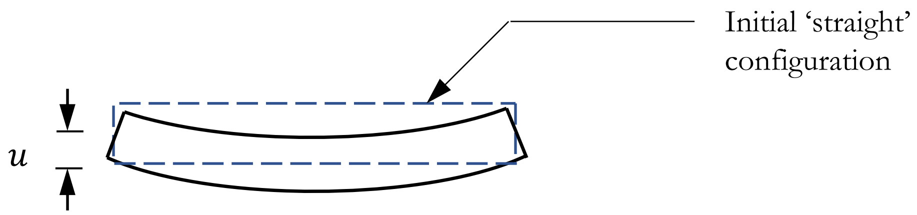

Fig.7-6 Geometric out-of-straightness for an I beam shown in plan

The geometric out-of-straightness used in the current study takes the form of a half-Sine wave and the value of the lateral displacement at midspan is obtained from the South African standard SANS2001-CS1 (2012). This standard gives allowable tolerances between restraints for steel beams in Table 3 - (4). Allowable deviations for plate girders are also given in Table 5 - (14) of this standard. The value of the deviation for beams is given as:

$$u = \frac{L}{1000} \; or \; 3mm, \text{ whichever is greater} \qquad (7.6)$$

$$u = \frac{L}{500} \; or \; 25mm, \text{ whichever is lesser} \qquad (7.7)$$

Based on equations (7.6) and (7.7) the greater of the two limits is then used as the lateral displacement for the out-of-straightness. This value has been worked out for different spans as an illustration and is presented in Table 7-1.

Table 7-1 Maximum values of out-of-straightness (in 'mm') for different spans

Span *(m)*	**Equation (6.6)**	**Equation (6.7)**	**Used in Model**
2	3	4	4
4	4	8	8
6	6	12	12
8	8	16	16
10	10	20	20

The appropriate deformation values from Table 7-1 are used in the analysis models for the nonlinear analysis.

7.2.3 Nonlinear Analysis for member strength

As indicated in the introduction a form of second-order nonlinear analysis that gives a good estimate of member strength is the GMNA type. This analysis only differs from GMNIA in that imperfections in the form of residual-stresses are not included in the model. The effect of leaving out the residual stresses can vary depending on the nature and distribution of the residual stresses and also on the slenderness of the beam. Members of intermediate slenderness are the most affected by residual stresses in the beam. In this case since both the doubly symmetric as well as monosymmetric members are modelled using GMNA the loss in accuracy is predicted to be consistent and thus still justifying this as an acceptable first step in comparison based on realistic estimate of member strength. The combination of out-of-straightness, material stress-strain behaviour and a second order analysis already goes a long way in predicting member strength. For slender members the loss of accuracy from omitting residual stresses is typically minimal as slender members behave in a manner that can be predicted well even with an elastic analysis. Furthermore, the present results (where residual stresses are omitted) would actually be near-exact in those cases where the fabrication process of the section is such that the accumulation of residual stresses is prevented, or any accumulated such stresses are subsequently removed.

7.3 ANALYSIS APPROACH IN SOFTWARE

7.3.1 The Newton-Raphson Method

The Newton-Raphson method is a mathematical approach for solving nonlinear problems. Sources of nonlinearity are either material, geometrical or contact. From a mathematical perspective the effect of nonlinearity is to affect the stiffness matrix. In linear analysis there is no need to update the stiffness matrix. With nonlinear analysis the stiffness matrix has to be updated with respect to the new geometrical configuration at the end of each analysis step. Some of the differences between linear and nonlinear systems are highlighted in Table 7-2. The Newton-Raphson method considers the nonlinear aspects of the mathematical problem. The mathematical implementation of the method involves the use of a Taylor's series expansion with higher order terms neglected. The derivative of the nonlinear function gives the desired tangent stiffness.

Table 7-2 Comparison of Linear and Nonlinear systems

Linear System	Nonlinear System
1. Formulated as a small-displacement problem 2. Geometric nonlinearity is ignored 3. Kinematic relationships are linearized 4. Elements are formulated in the original configuration (use original nodal coordinates)	1. Formulated as a large-displacement problem 2. Geometric non-linearity cannot be ignored 3. Kinematic relationships are nonlinear 4. Elements distort from their original shapes as deformation increases

In the case of material nonlinearity, the analysis model considers material behaviour post yield as per the indicated behaviour on the stress-strain curve.

When the load displacement relationship is plotted on a graph some important points can be located on such a graph. These are highlighted in Fig.7-7. This depicts the case of 'limit-load' buckling. In this case the limit point is of particular importance as it represents a peak value in load carrying capacity if followed by a softening of the material. Because this point is critical in determining member strength for beams made from ductile materials the nonlinear analysis method employed must be able to correctly identify this point.

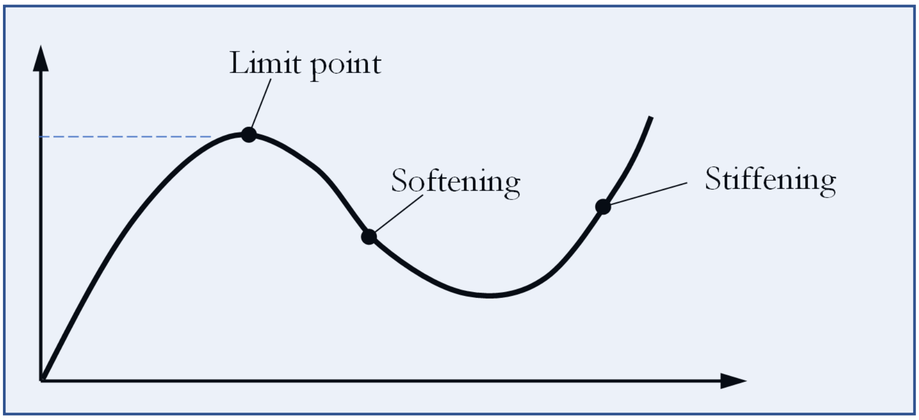

Fig.7-7 Limit load buckling showing point and regions of interest

One limitation of the Newton-Raphson method is that it is not able to correctly capture softening behaviour. It is thus unable to capture the unstable part of the load-displacement curve. A method proposed by Riks (1979) provides a solution to this limitation in the Newton-Raphson method. This method is based on an approach that aims to determine a parameter, λ, at the limit point, which is a proportion of a reference load used at the start of the nonlinear analysis. This parameter is referred to in the software analysis as the 'load proportionality factor' (LPF). The method proposed by Riks (1979) has come to be widely known as the Arc-Length method. In the arc-length method the software conducts the nonlinear analysis by applying the load incrementally and computing the stiffness matrix at each time-step to determine the load at which the member becomes unstable or experiences softening.

7.3.2 Arc-Length Method

The software Abaqus implements the Arc-Length method through the 'step' option of the 'RIKS analysis'. As indicated earlier this method allows for the capture of softening behaviour while applying load control. With reference to the load-displacement graph illustrated in Fig.7-8 the method is based on an initial point (f_0, u_0) and a reference load (f_{ref}).

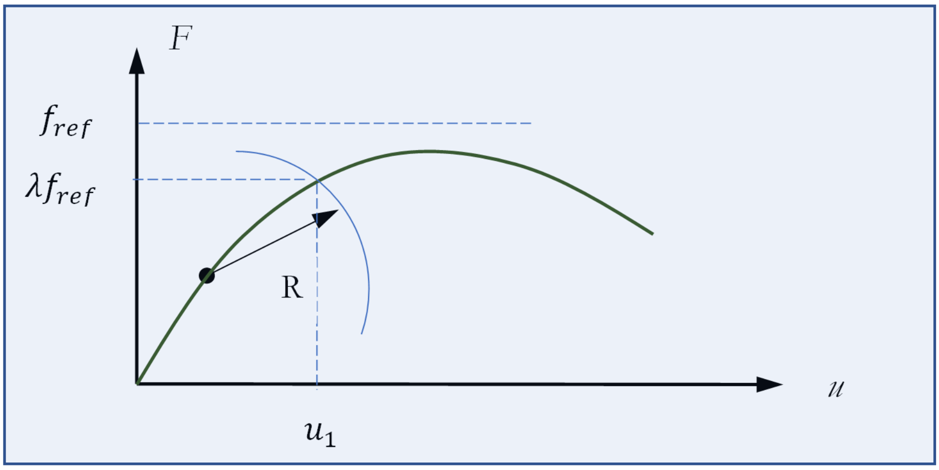

Fig.7-8 Arc-Length method

From the initial point an arc is drawn around the point to determine the next equilibrium point. The load at this point is expressed as a factor, λ, multiple of the reference load (λf_{ref}). The factor, λ, is called the load proportionality factor and is an unknown in the calculations. This new equilibrium point becomes the new initial point for the next iteration. The radius of the arc presents an additional equation for solving the equilibrium problem so that the number of equations now matches the number of unknowns. This additional equation is given as:

$$R = \sqrt{\frac{(\lambda - \lambda_0)}{\lambda_{max}^2} + \frac{(u_1 - u_0)^2}{u_{max}^2}} \tag{7.8}$$

where,

λ_{max}, u_{max} are scaling factors

$u_0, \lambda_0 = {f_0}/{f_{ref}}$ come from the initial point

λ and u_1 are load and displacement that are solved for.

The Newton-Raphson method is employed to solve for the unknown displacements and load proportionality factor.

The software Abaqus has a 'stopping criteria' which allows the user to define the conditions under which the iteration will terminate. If this is not specified, the process can proceed without ending. In the current study the maximum number of iterations is restricted to one hundred (100) and the initial increment is set to a value of 0.01. Some solvers can adjust the step increment depending on convergence characteristics. The load proportionality factor (LPF) from the analysis is used to determine the member strength. The reference load is the lowest buckling eigenvalue obtained from the linear eigenvalue buckling analysis. This is one of the reasons why the linear eigenvalue buckling analysis is first performed. It generates the reference load that can be scaled to give the maximum load that can be carried by the member when a nonlinear analysis is carried out.

7.3.3 Software Models (Abaqus)

The models considered in the nonlinear analysis study were based on the four cases for the point load at midspan presented in sections 6.1.2.1, 6.1.2.3, 6.1.2.5 and 6.1.2.7 whose results were generated from the equations developed in Chapter 4. These four cases represent two narrow-flange and two wide-flange sections respectively and the span considered was 4m as presented in the sections mentioned. The software Abaqus has been used for the nonlinear analysis. A shell model was employed for the finite element analysis. This was employed due to its minimal demand on computational time. Models made with solid elements require more elements to obtain acceptable results and are costly on computational time. A global seed of 8mm was used with a constant aspect ratio for the elements. The justification of this seed is presented in Fig.7-9 which is a mesh convergence study based on the NF-IPE120 from 6.1.2.1. The element used is the general-purpose shell element S4R which is a four-node shell element with reduced integration and having displacement and rotational degrees of freedom at each node.

Seed	**50**		**25**			**12.5**			**8**		**6.25**
Nodes	581		1 630			7 150			15 717		25 311
Time	15ms		12ms			17ms			23ms		26
Mcr (kNr	6.232		6.204			6.902			6.920		6.929

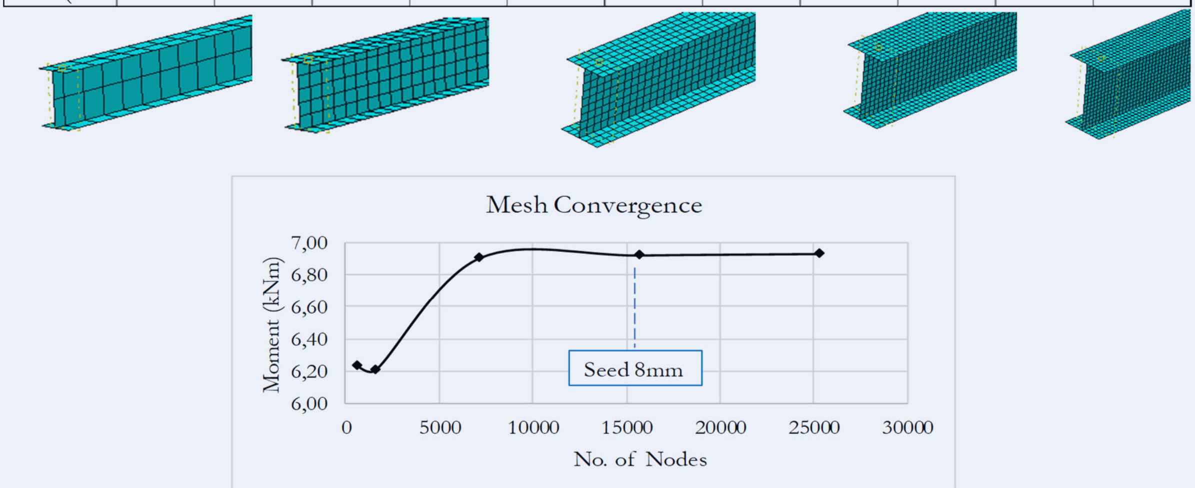

Fig.7-9 Beam Mesh convergence study

The boundary conditions are based on the 'fork type' supports described in previous chapters. This boundary condition allows for the flanges to warp freely while preventing rotation of the member at the supports. The displacement constraints placed at the supports in the coordinate 'x', 'y' and 'z' directions are indicated as U_x, U_y and U_z in Fig.7-10. The coordinate axes are shown. To simulate a roller supported beam lateral movement of the axis is allowed at one end and prevented at the other (U_z).

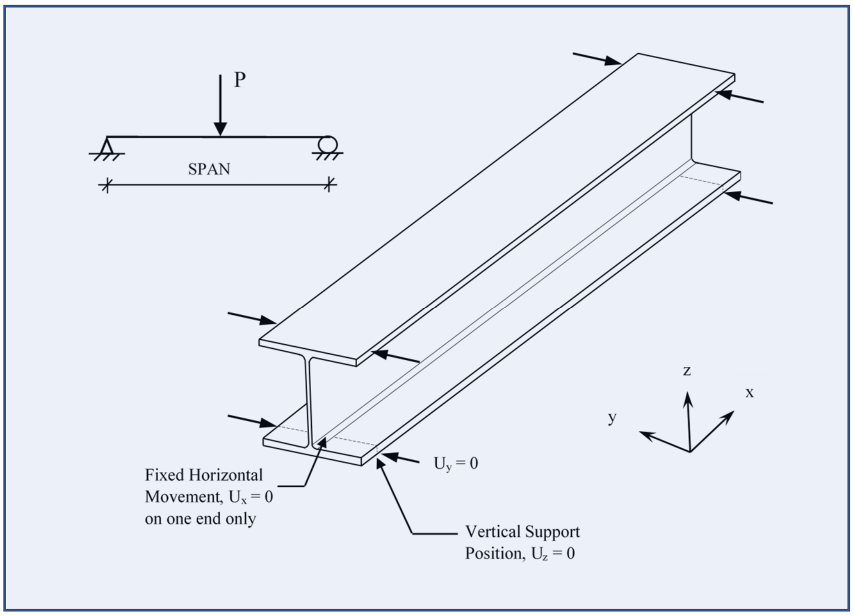

Fig.7-10 Beam boundary conditions (Mudenda & Zingoni, 2018)

The shell model was first based on the element to be strengthened so that this result could be compared to the results from Chapter 6 (section 6.1.2). The strengthened beam is then modelled for the eigenvalue buckling analysis and then for the member strength based on the nonlinear analysis (GMNA). The modelling process employed is summarised in Fig.7-11.

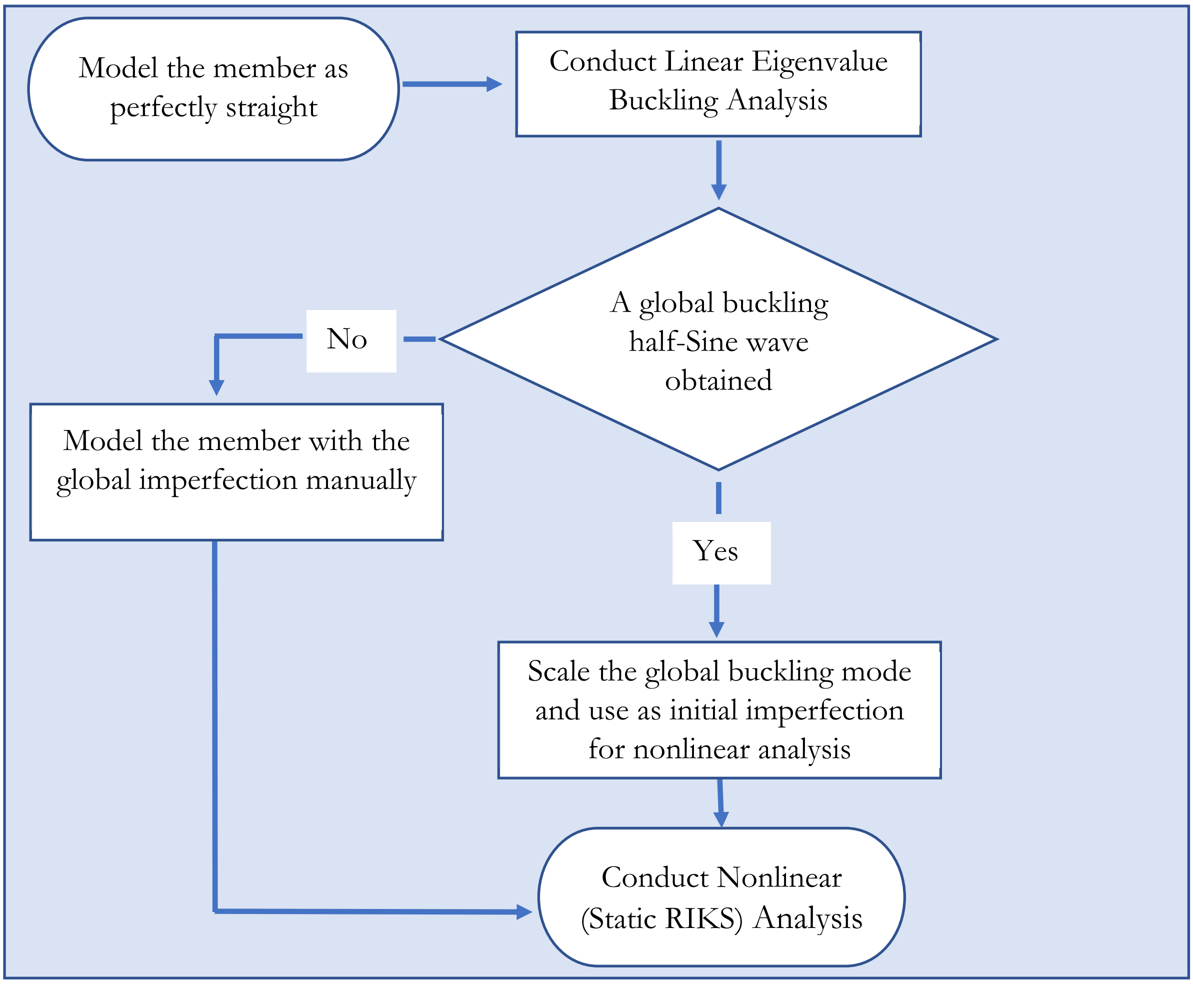

Fig.7-11 Modelling process for the nonlinear analysis

The Abaqus software implements the nonlinear analysis by way of the 'static RIKS' approach. This is based on the Arc-Length method discussed in 7.3.2. The total number of increments as well as an increment step size are input to allow for a termination point and an initial increment step size. The software has an in-built algorithm that varies the increment step should the need arise due to solution difficulties. A termination point needs to be specified otherwise the analysis will continue running without ending. There is an option to manually terminate the analysis by way of a 'kill' analysis command.

An approach where the software extracts the deformed geometry configuration from a linear Eigenvalue buckling analysis for use in a nonlinear analysis is employed in the current study. This is a functionality that the software has. This works for as long as there exists an eigenmode with the desired geometrical profile, a half Sine wave, in this case. In cases where a half Sine wave is not obtained in the Eigenvalue buckling analysis the out-of-straightness can be modelled manually in the software prior to commencing the nonlinear analysis. In this scenario it is easier to generate a model that only has a translational out-of-straightness. A study by Boissonnade and Somja (2012) showed that although the translation and rotation case is more accurate, there is no significant loss of accuracy when the translational is used on its own in lieu of a combination of translation and rotation. The option for use of either approach was therefore kept open depending on the nature of Eigenmodes obtained from the linear buckling analysis. An example of a linear buckling analysis output is shown in Fig. 7-12 for a NF-IPE120 beam.

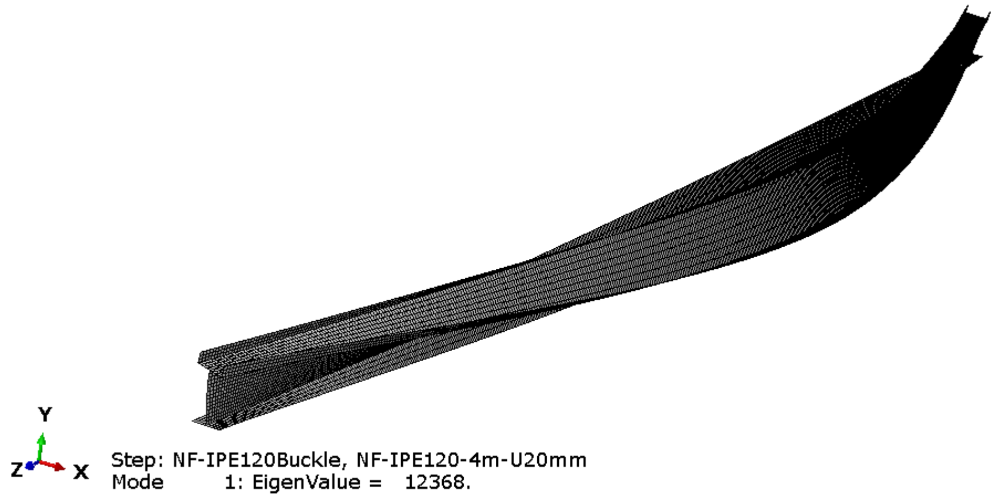

Fig.7-12 A beam buckling mode from an eigenvalue analysis showing translation and twist

Stiffeners were not used at the load application points. The buckling modes are observed to be global modes indicating no local effects from the point load application. An output from the nonlinear analysis of a NF-IPE140 beam is shown in Fig.7-13 at the point of analysis termination. The large displacements at failure in the model are evident.

Fig.7-13 A beam failure configuration at a given timestep under nonlinear analysis

A plot of the load proportionality factor (LPF) against the arc length is generated as part of the history output in the software. A typical plot is shown in Fig.7-14. The software also allows for displacement data for any point in the model to be extracted. This can be done by specifying the point of interest prior to starting the analysis. Points of interest may include the midspan of the beam or the point of load application.

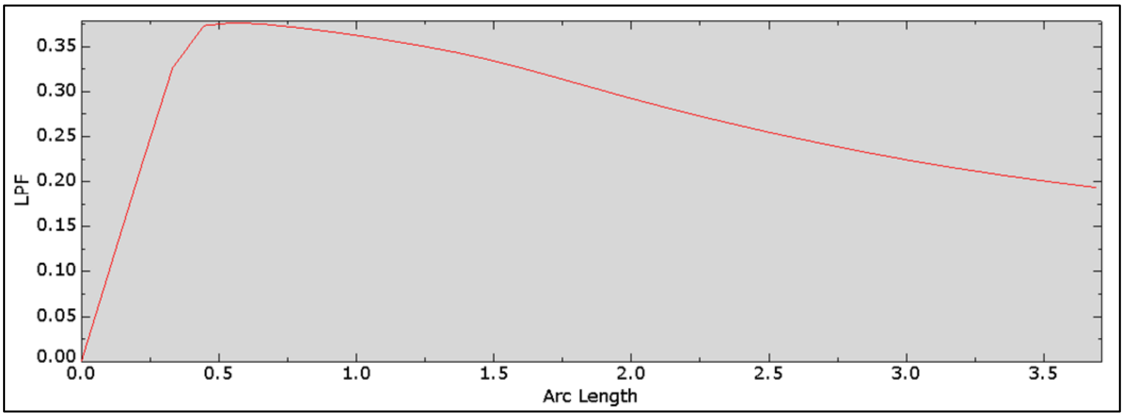

Fig.7-14 A plot of the LPF for a 254x254x107 – 4m span Beam (nonlinear analysis)

The results obtained from the analysis are presented in the section that follows.

7.4 RESULTS

As indicated the nonlinear analysis was performed on the four examples from Chapter 6 that had point load at midspan loading. The results for the nonlinear analysis are presented here in Tables 7-3 to 7-6.

Table 7-3

Beam Under consideration:			**Next Larger DS beams considered**	
NF-IPE 120 Span: 4m M_{cr0} = 7.5 (kNm)			**Beam:** NF-IPE 140	**Beam:** NF-IPE 160
Upstand: 20mm	**Upstand: 60mm**			
$\boldsymbol{\alpha/H = 0.17}$	$\boldsymbol{\alpha/H = 0.5}$			
M_{cr} = 12.37	M_{cr} = 17.45		M_{cr} = 10.63	M_{cr} = 15.34
M_r = 11.92	M_r = 18.5		M_r = 10.06	M_r = 14.17
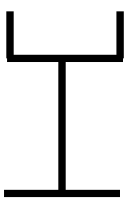	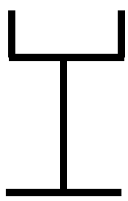		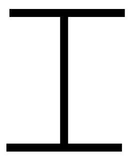	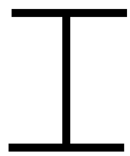

*M_{cr0} *is the critical elastic moment for the beam under consideration before upstands are introduced*

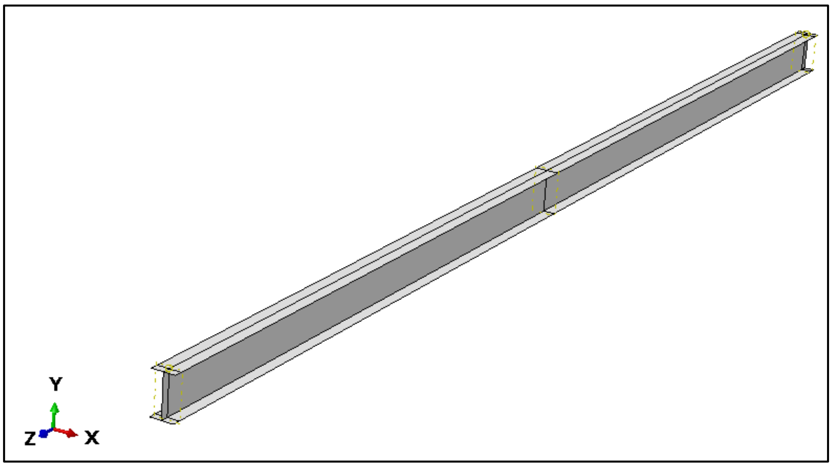

(a) Beam model

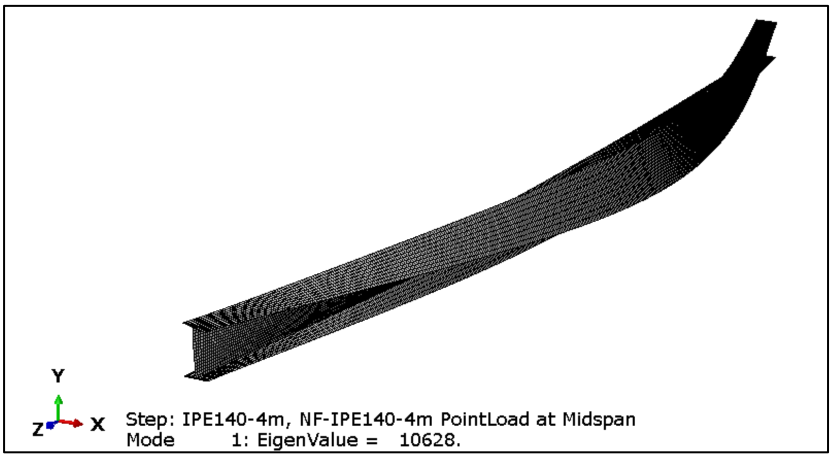

(b) First eigenvalue and buckling mode

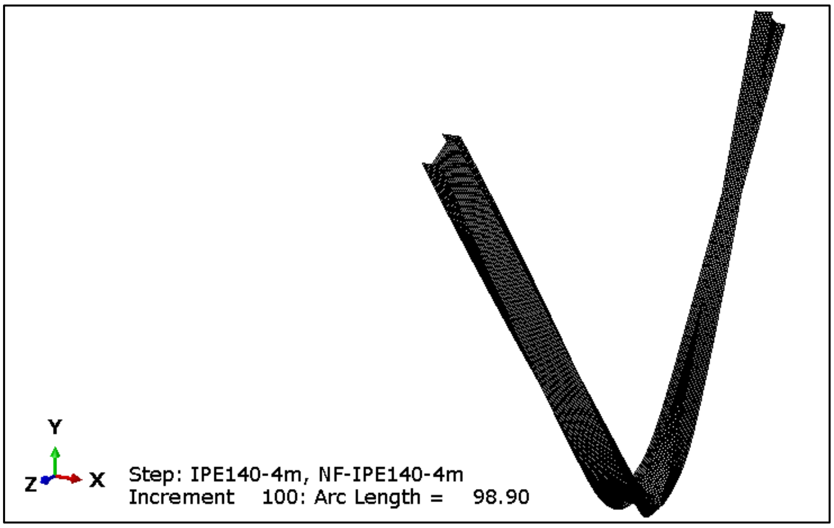

(c) deformation at nonlinear analysis termination

Fig.7-15 NF-IPE140 Abaqus model (a) first eigenvalue and buckling mode for M_{cr} (b) and deformation at termination of nonlinear analysis (c)

It was shown in Chapter 6 that for upstand heights of 20mm and 60mm to the NF-IPE120 beam under consideration would give critical elastic moments greater than those of the next two higher sizes NF-IPE140 and NF-IPE 160 respectively. This is revealed to be true for the moment capacities obtained from the nonlinear analysis as well. This means that a real beam is therefore likely to exhibit performance that is like what has been observed from the elastic buckling value considerations. This therefore justifies the viability of strengthening the existing section as an option for consideration. An upstand height of only 20mm in this case giving a favourable outcome.

It should, however, be noted that even though the upstand height of 60mm gives greater strength than the next higher section the value of $\alpha/_H$ is greater than the critical value of one third of height and thus the benefit of monosymmetry for this section will not be realised. This is therefore not an optimum section. Other factors, such as weight or cost, would have to weight in its favour for consideration. The results for the other narrow flange member, the NF-254x146x37 are presented in Table 7-4.

Table 7-4

Beam Under consideration:			**Next Larger DS beams considered**	
NF-254x146x37 Span: 4m M_{cr0} = 117.4 (kNm)			**Beam:** NF-305x165x40	**Beam:** NF-356x171x45
Upstand: 20mm	**Upstand: 30mm**			
$\boldsymbol{\alpha/_H}$ **= 0.08**	$\boldsymbol{\alpha/_H}$ **= 0.12**			
M_{cr} = 169.7	M_{cr} = 188.3		M_{cr} = 138.9	M_{cr} = 161.3
M_r = 124.2	M_r = 137.6		M_r = 104.9	M_r = 120.8
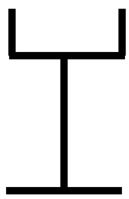	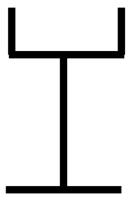		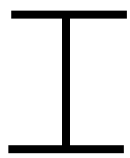	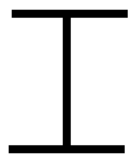

*M_{cr0} *is the critical elastic moment for the beam under consideration before upstands are introduced*

It was shown in Chapter 6 that upstand heights of 20mm and 30mm give greater critical moment than two selected higher strength beams. The nonlinear analysis is also consistent with this observation. Greater strength is achieved in both cases respectively. These upstand heights both give an $\alpha/_H$ value that is lower than the critical value and thus indicates that the strengthened members remain in the desired region for exploiting the benefits of monosymmetry. This is a desirable outcome. The choice of using these upstand heights still also depends on other factors such as weight and associated costs, and therefore this comparison constitutes only one of several criteria that design engineers will use to make such choices. The results for the wide flange sections are presented in the tables that follow.

Table 7-5

Beam Under consideration:		**Next Larger DS beams considered**
WF-152x152x30 Span: 4m M_{cr0} = 89.3 (kNm)		**Beam:** WF-152x152x37
Upstand: 40mm		
$\boldsymbol{\alpha/H}$ **= 0.25**		
M_{cr} = 139.6		M_{cr} = 124.8
M_r = 97.0		M_r = 85.3
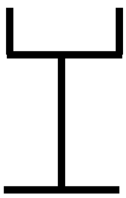		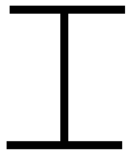

*M_{cr0} *is the critical elastic moment for the beam under consideration before upstands are introduced*

It was shown in Chapter 6 that an upstand height of 40mm gives a greater critical moment than that for a member one size higher. The comparison is now extended to strength after nonlinear analysis. The outcome, as with the narrow-flange case, is consistent. The α/H value is just at the limiting point and thus still conforms to the desired optimum region.

Table 7-6

Beam Under consideration:		**Next Larger DS beams considered**	
WF-254x254x107 Span: 4m M_{cr0} = 1238.5 (kNm)		**Beam:** WF-254x254x132	**Beam:** WF-305x305x118
Upstand: 60mm			
$\boldsymbol{\alpha/H}$ **= 0.22**			
M_{cr} = 1835.8		M_{cr} = 1616.9	M_{cr} = 1552.3
M_r = 612.9		M_r = 609.4	M_r = 562.2
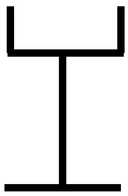		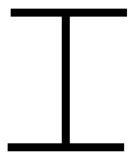	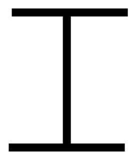

*M_{cr0} *is the critical elastic moment for the beam under consideration before upstands are introduced*

It was shown in Chapter 6 that an upstand height of 60mm matches or exceeds the critical moment for two members of higher size in the handbook. The outcome for the nonlinear analysis, as before, is consistent. The α/H value is below the limiting point and thus still within the desired optimum region.

It can be seen from the results obtained that the conclusions reached based on the elastic critical moment comparison in Chapter 6 example sections are consistent for the nonlinear analysis case as well. This means that the viability of the approach is demonstrated as the nonlinear analysis carried out gives a better indication of what the strength will be in real members. Although residual stresses have not been considered in this analysis the consideration of geometric out-of-straightness and inelasticity mean that the strength value determined are close to the actual values. A study by Vales and Stan (2017) revealed that for the beam sections they considered the difference between results obtained from models with and without residual stress was not significant. Also, the study by Kitipornchai and Trahair (1975b) reported that for the I-beams tested, which included ordinary beams with residual stress and annealed beams with no residual stress, the effect from geometrical imperfection was reported to be greater than that from residual stress. However, the effect of residual stress should not be simply dismissed. The effects of residual stress have been reported to vary depending on the beam parameters and are still essential to consider for member strength. A study by Kitipornchai and Wong-Chung (1987) found that degree of monosymmetry and residual stress pattern influenced the inelastic strength of welded monosymmetric beams. Therefore, consideration of residual stress will need to be an approach for further studies on this topic. A comparison of member strength from GMNA and GMNIA would serve to highlight the sensitivity to residual stresses as shown in Fig.7-16. The difference between these two is not anticipated to be as significant as the difference between linear elastic critical buckling values to GMNA values.

It must be clarified that the use of GMNA in the current study is based on obtaining a reasonable estimate of real member behaviour with the imperfection of residual stress omitted only because the information is not yet available. Hence it is a GMNIA approach but with the 'I' dropped due to not including residual stress effects. This should not be confused with an approach as envisaged in Eurocode 3 (CEN, 2005) where a second order analysis can be carried out in conjunction with an 'equivalent geometrical imperfection' which accounts for all imperfections including the residual stress. This imperfection is typically much larger than the out-of-straightness from member manufacturing tolerances as it has to account for all imperfections.

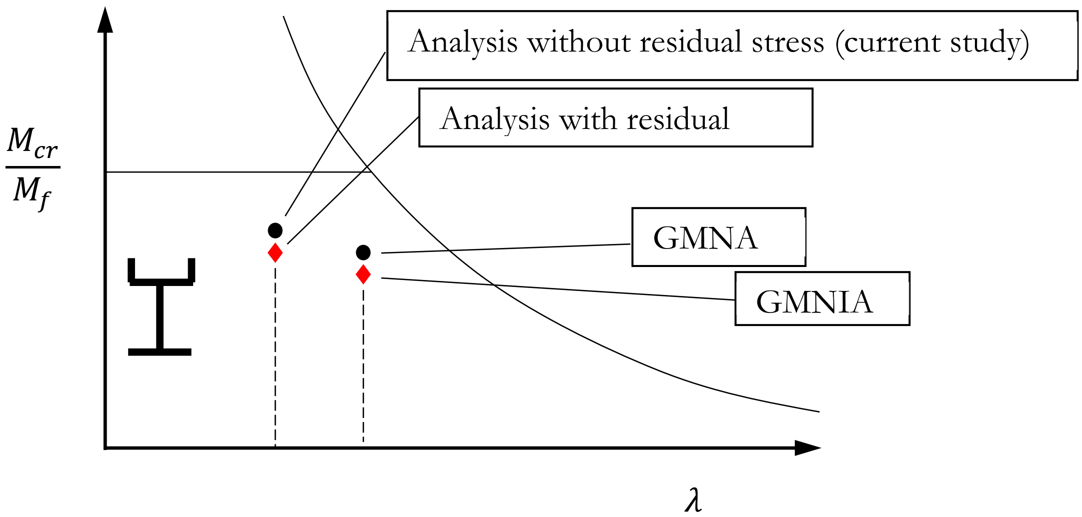

Fig.7-16 Illustration of possible residual stress effect on member strength obtained from nonlinear analysis that did not consider this imperfection

It is also observed that by considering upstand heights within the optimisation or 'area of interest' region, based on the critical $^{\alpha}/_{H}$ values, there exists viable options for strengthening of existing members with desirable returns. The use of stiffened members in lieu of replacing with doubly symmetric members of larger size should therefore be given consideration as it is a viable option. In the one case for the NF-IPE120 example where the critical $^{\alpha}/_{H}$ value would be exceeded when considering a section two sizes higher the option of strengthening with upstands would need to be given careful consideration as in this region the monosymmetry is no longer in the beneficial or desirable region.

7.5 CONCLUSION

In this chapter the concepts of using monosymmetry as an aid to strengthen existing beams has been extended from considering the elastic behaviour to considering behaviour in the elastic-plastic range. This has been done by employing nonlinear analysis incorporating geometric out-of-straightness and material constitutive law so that an understanding of real member behaviour is obtained. It was observed that the use of monosymmetry for beneficial effect of strengthening existing members is viable and has been demonstrated for simply supported beams loaded by a central point load. This had been verified from the results of both the linear elastic and the nonlinear analysis. This presents an approach that engineers can use when considering the strengthening of existing members or replacing with doubly symmetric steel members that possess greater strength and stiffness than the existing member. This presents an option that may be economical and conform to sustainability principles such as that of lean design. The benefits of re-use of an existing member by strengthening in lieu of having to replace with another member can lead to significant carbon offset. This is because disposal costs, monetary and carbon, of the existing member as well as purchase and assembly costs for the new member are dispensed with.

Engineers also need to be aware that strengthening members with upstands is an optimisation exercise when considering the behaviour in bending for laterally unrestrained beams. Increasing the upstand height eventually leads to a diminishing return in bending strength. The upstand height corresponding to the coincident shear centre and centroid is an indicator that designers can use for the point where the benefit for flexure from monosymmetry effects terminates.

CHAPTER 8 SUMMARY, CONCLUSIONS AND FUTURE WORK

8.1 SUMMARY

8.1.1 Geometrical Properties & Uniqueness

The study has clearly shown the uniqueness of having monosymmetric sections that possess properties typically associated with doubly symmetric sections. The property that has particularly been the focus of this study is the point where the shear centre and the centroid are coincident for a monosymmetric section. It has been shown that this point occurs at an upstand height of about a third of member height for narrow flange sections and about a quarter of the height for wide flange sections. This applies for the case where the upstand height plate thickness matches that of the section flange. It has further been shown that the point of coincidence is a proxy for the region where monosymmetry can be exploited as a strengthening and stiffening aid. Beyond this point there is diminishing return of the flexural capacity despite an increase in upstand height and in typical section properties.

Equations for determining the shear centre and centroid position for the cross section considered in the current study have been derived and presented in polynomial form. Equating these general equations gives the upstand height corresponding to the coincidence point. Other section properties required to obtain the critical elastic moment are also presented. One of these critical properties is the monosymmetry constant. There has been widespread use of the simplified approximate equations developed by Kitipornchai and Trahair (1980). These are found in many publications and steel design handbooks. It must be noted that at the time the authors specified a 'validity range' for this approximate equation. It is desirable to have a way to obtain this parameter without the restriction of a validity range. The method proposed by Hsu et al (2012) for I-section beams with channel caps and extended to the section considered in the current study presents a proven, accurate, easy to use and generalised approach for determining the monosymmetry constant for any section that can be idealised as an assembly of plate elements.

The approaches that have been employing in generating equations for key geometrical parameters in the current study can be extended to other cross section types particularly those that can be simplified as an assembly of plates. This is particularly true for the monosymmetry constant. The methods largely yield equations in polynomial form making application straightforward and convenient.

8.1.2 Critical elastic moment behaviour with change in upstand height

The critical elastic moment behaviour with change in upstand height has been investigated in chapters 5 and 6. In chapter 5 it was shown that the behaviour with increase in upstand height is consistent for both narrow flange as well as wide flange flexural members. The behaviour is characterised by an increase in elastic critical moment which is high at low upstand heights but increasing at a diminishing rate as the upstand height increases. In some cases, this behaviour leads to a peak followed by a decreasing elastic moment as upstand height increases. This creates two regions, one were the monosymmetry effect works to increase the critical elastic moment and another where the monosymmetry effects works to counteract the increasing section properties and decreases the value of the critical elastic moment. The upstand height corresponding to a coincident shear centre and centroid is a good indicator of where this transition happens. Therefore, in considering the optimal maximum upstand height that can be considered for strengthening this unique point defines the upstand limit to consider for the opportune returns. Having established this point, the study was then progressed to show how this unique behaviour can be exploited for the purpose of strengthening existing sections. The concept can also be utilised if initial member selection is being carried out with smaller sections being optimised with upstands in lieu of larger doubly symmetric sections.

8.1.3 Strengthening Approach

It has previously been recognised that monosymmetric I-sections are generally more efficient in resisting loads, provided the compressive bending stresses are taken by the larger flange (Wang & Kitipornchai, 1986b). Thus, the benefits that can be obtained by exploiting the effects of monosymmetry are recognised. However, it has also been pointed out that the effects of monosymmetry introduce some complications in the elastic buckling analysis that must be considered carefully. Building on this, the current study presents an opportunity to strengthen existing sections by exploiting the beneficial effects of monosymmetry.

The uniqueness discussed in 8.1.1 can be used to optimise the use of flange upstand stiffeners for increasing the flexural capacity of a section. Increase in the member stiffness is also a secondary benefit. This means that the use of flange upstands as stiffeners needs to be carefully approached as the gain in strength is characterised by a decreasing return in strength increase as the stiffener height increases. The trend is such that for low stiffener heights a significant gain in flexural capacity is observed. This tapers off with increase in the upstand height. As has been shown in section 6.2.1 there exists an upstand height range, from zero height to the height at which the critical moment for the monosymmetric section matches that of a fictitious 'equivalent doubly symmetric' section (closely related to the upstand height where shear centre and geometric centroid are coincident) where the benefit of monosymmetry leads to, in many cases, significant strength gain. It is this range that must be exploited for an optimised performance. Beyond this point the monosymmetry works counter to the increasing geometrical properties and thus is no longer performing optimally.

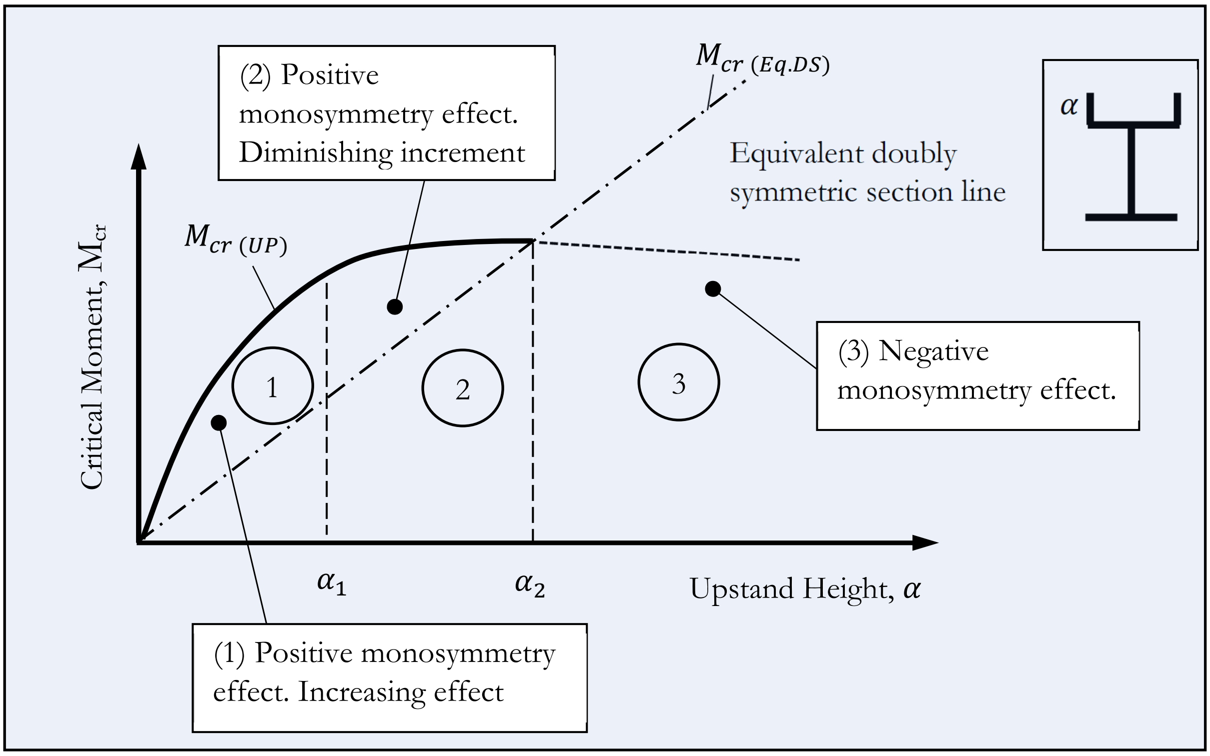

Fig.8-1 Three typical phase areas of the critical moment vs upstand height relationship

Phase 1: $M_{cr\ (UP)}$	$-\ M_{cr\ (Eq.DS)}$	(+ve) increasing with increase in upstand height
Phase 2: $M_{cr\ (UP)}$	$-\ M_{cr\ (Eq.DS)}$	(+ve) decreasing with increase in upstand height
Phase 3: $M_{cr\ (UP)}$	$-\ M_{cr\ (Eq.DS)}$	(-ve) decreasing with increase in upstand height

$M_{cr\ (UP)}$ = *Critical elastic moment for cross section with upstands*
$M_{cr\ (Eq.DS)}$ = *Critical elastic moment for 'equivalent doubly symmetric section'*

The phases of returns from monosymmetry effect are shown in Fig.8-1. Designers must thus aim for region 1 and 2 to maximise the returns on monosymmetry effect for the section considered in the current study. These observations hold true for the single curvature load cases considered. Effects under double curvature can be quite complex as highlighted by Xie and Mohareb (2022) as the monosymmetry effect is acting differently in the two parts of the member with different curvature. The complexity arises from the fact that in double curvature situations the *Wagner effect* interacts with the moment gradient as it passes from negative to positive. This behaviour does not form part of the current study. Future studies considering practical reversal of stiffener placement in the negative moment regions can be explored.

8.1.4 Member Strength and Design Codes of Practice

There is currently no guidance given by the South African standard for steel design (SANS10162-1) on the design on unrestrained monosymmetric steel beams. This standard is largely based on the Canadian standard (CAN/CSA-S16). However, even though the Canadian standards have been updated over the years to include some guidance on monosymmetric beams the South African standard has not matched these changes. Updates to the Canadian standard have been reported on by Xie and Mohareb (2022). It was reported that provisions in the 2014 version of the Canadian standard (CSA, 2014) which were further updated in 2019 (CSA, 2019) provided equations for determining the critical elastic moment for monosymmetric beams subjected to general loading and/or end moments. Some inconsistencies and ambiguities were identified by the authors to still exist even with these provisions. For instance, the simplified equation for the monosymmetry constant is linked to the second moment of area of the 'flange in compression'. However, in the case of double curvature bending both flanges will experience compression. No guidance is given on what to do in such a case. It was also found that when compared to finite element model results the equations provided in some cases overestimate or underestimate the critical elastic moment. The authors developed equations to remedy some of the observed shortcomings. However, whereas the authors offer solutions for the elastic critical moment equation no mention is made as to whether the code addresses the next, and equally critical, issue of how the member strength is determined. Consideration of inelastic behaviour and inherent imperfections would be needed for this next step.

A study by Nethercot (1973) into inelastic buckling of monosymmetric beams had already shown that inelastic buckling behaviour of monosymmetric I-beams showed a marked difference to that observed with their doubly symmetric counterparts. This was further confirmed by Lindner (1976). Although Nethercot (1973) did not include residual stress in the analysis Lindner (1976) included these and obtained similar results. This author also compared the obtained results to provisions in the European standard at the time, ECCS, and highlighted the deficiencies should the standard be used to design monosymmetric I-sections. Attempts to compare inelastic buckling design provisions for monosymmetric sections in codes of practice to observed behaviour and offer solutions have been presented by Kitipornchai and Wong-Chung (1987) and Trahair (2012). The first set of authors considered the inelastic buckling of welded monosymmetric beams and looked at provisions in Australian, North American, European and British standards (AS1250, AISC specification, ECCS and BS5950 respectively). It was concluded that design rules in these codes of practice did not appear to accurately reflect the inelastic buckling behaviour of welded monosymmetric I-beams. In some cases, design rules tended to err on the unconservative side. It was noted by Trahair (2012) that design methods presented for monosymmetric I-beams against LTB were not well supported by research. In this study welded as well as hot-rolled I-beams were considered. Simple but accurate approaches for hot-rolled beams in uniform bending were presented with less accurate but conservative equations for moment gradient proposed. The design rules of the North American, Australian and European standards (AISC, AS4100 and Eurocode 3 respectively) were evaluated and found not to correctly capture the observed behaviour trends.

Design guides such as the SASCH (2016) appear to indicate approaches similar to those used for doubly symmetric beams such as use of similar moment gradient factors. Using approaches typically implemented for doubly symmetric beams can lead to inaccurate results as monosymmetric sections have their peculiarities. An approach by MacCrimmon (2009) employs an equation for the design of monosymmetric section crane girders based on AISC procedures but does not explicitly indicate whether these procedures were developed exclusively for monosymmetric sections or are borrowed from the design of doubly symmetric sections. The rest of the design procedures presented by the author are based on the Canadian standards.

In the latest updates to Eurocode 3 (EC3) guidance for monosymmetric section design has been incorporated but is only provided for members under single curvature. For more general case the use of GMNIA is recommended (Knobloch et al, 2020). There remains therefore a gap in obtaining a simplified set of design guidelines for the design of monosymmetric sections susceptible to LTB. It is fair to say the lack of such design guidance is a manifestation of the complexities associated with the behaviour of monosymmetric sections.

Given this backdrop the use of nonlinear analysis, and particularly GMNIA, becomes a convenient option for determining the member strength of monosymmetric sections for a given loading. The approach applied in chapter 7 would be an appropriate one to use. Imperfections can be appropriately randomised based on a stochastic approach so that a statistical characteristic strength is obtained. From this a design strength can then be determined. Deterministic approaches based on the extreme imperfection values may also yield realistic design strengths. This approach would address the limitation with regards lack of design guidance for all possible loading and support conditions. However, there is a time penalty for development and calibration of an appropriate model. Also, some knowledge of the magnitude and distribution of residual stress in the member will need to be obtained.

8.1.5 Decision model from study findings

Based on the current study a decision model in the form of a flow diagram is presented in Fig.8-2 for the case where the upstands are considered as an option to strengthen an existing doubly symmetric beam. The diagram illustrates where the relevant equations are applied to arrive at the final decision point. For slender beams the critical elastic moment serves as a good enough decision point as well.

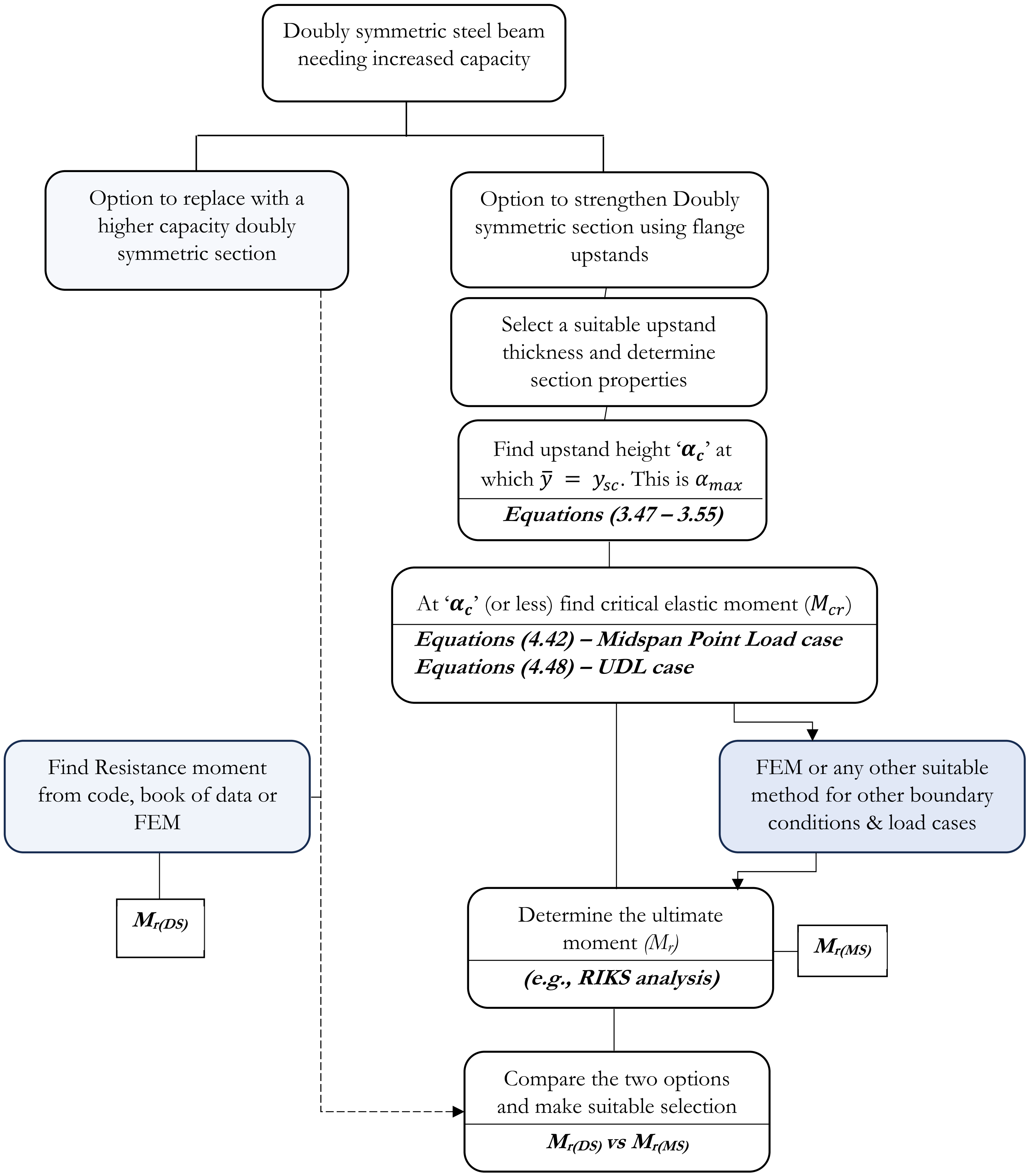

Fig.8-2 Decision model flow diagram for application of upstands as a strengthening option

8.2 CONCLUSIONS

The observed behaviour of monosymmetric sections created by introducing flange upstands as stiffeners to doubly symmetric beams has been discussed. The uniqueness of the shear centre and centroid being coincident for a given upstand height has been shown to be an important phenomenon and a proxy for member behaviour. This provides an important basis for determining a desirable target range of upstand heights for strengthening existing doubly symmetric sections. Other aspects such as the monosymmetry constant taking on a value of zero at a different upstand height from that pertaining to the coincident point remain to be explored.

The study of using upstand heights on doubly symmetric I-sections to form a monosymmetric section has revealed some curious outcomes. Top of these is the fact that monosymmetric sections can, at unique points, take on properties typically associated with doubly symmetric sections i.e., a coincident shear centre and centroid and a monosymmetry constant of zero. It has also been shown that the use of upstands on the compression flange of simply supported beams presents a viable approach to strengthening doubly symmetric sections by making use of the beneficial effects of monosymmetry in a defined range. The culmination of this range is approximated by the point of coincidence of the shear centre and centroid. Beyond this point the monosymmetry effect is such that it now counters strength gain. There is therefore a defined region that can be optimally exploited to obtain the greatest benefits from the monosymmetry effect. This is shown to be the case, in the current study, for beams carrying a uniformly distributed load or a central point load. The desirable strengthening has been demonstrated using both elastic and inelastic moment to demonstrate its viability.

Existing numerical methods can be used to predict the elastic buckling loads of the monosymmetric section considered in the current study. The Rayleigh-Ritz energy approach was utilized to obtain the polynomial equation that was used to obtain the critical elastic moments for two load cases. Codes of practice and standards currently still lack a complete set of design rules that would cater for what can be considered as the possible standard load or support cases that monosymmetric sections would be subjected to in practice. This gap means that for many cases, designers will have to resort to the use of software for both linear elastic analysis as well as nonlinear inelastic buckling analysis to determine member strength. This is due to the complexity that is encountered with monosymmetric sections.

The approach presented in the current study conforms to principles of lean design and zero waste by eliminating the need to replace existing members or by making possible the use of smaller members and thus conserving materials. These imperatives also have the potential to reduce detrimental carbon emissions. The availability of computer programmes that facilitate inelastic buckling analysis with consideration of imperfections makes it possible to accurately predict real member strength and overcomes the limitation of lack of design guidance generally observed with design codes of practice and design standards.

8.3 CONTRIBUTION TO KNOWLEDGE

This study has made a significant contribution to knowledge in the following areas:

(a) It is stated in mainstream publications and texts such as Ziemian (2010) that in monosymmetric sections the shear centre and geometric centroid are not at the same position. Something typically associated with doubly symmetric sections. It has been shown in this study that monosymmetric sections can possess properties typically associated with doubly symmetric sections. These include a coincident shear centre and centroid, as well as a monosymmetry constant of 'zero'. This has been demonstrated for I-shaped sections transformed into monosymmetric sections by addition of flange upstands as stiffeners.

(b) The study has also shown that when flange upstands are used as a strengthening approach for existing doubly symmetric steel beams the upstand height corresponding to the coincident shear centre and centroid (as in [(a)] above) acts as a proxy to indicate critical upstand heights for optimal returns on the strengthening approach.

(c) For doubly symmetric sections strengthened by flange upstands there exists a viable range of upstand heights that would give sufficient gain in strength to negate the need to replace with a larger sized similar doubly symmetric member.

(d) The study has confirmed that the resort to approximate equations for the monosymmetry constant, largely with validity ranges, can be dispensed with for members that can be idealised as an assembly of plates. There is therefore a viable and accurate approach that is easy to implement and does not suffer the restriction of a validity range.

(e) The study has contributed to addressing the need for reduction in carbon footprint. The world at large is grappling with an unfolding climate emergency. It has been indicated that release of greenhouses gases (referred to as carbon or carbon dioxide equivalent) over the period of large-scale industrialisation in the past century is now leading to global warming. The impacts of this are wide ranging and have potential to deliver devastating effects to humans (Arnold, 2020). A rise in global temperature of 1.5^0 C beyond pre-industrialisation levels is indicated as the tipping point beyond which the impact of global warming will become severe and the effects difficult to control. Controlling the amount of carbon we release into the atmosphere has become an imperative to prevent this impending catastrophe. The Institution of Structural Engineers (IStructE) through its climate emergency task group has been leading a concerted effort in rallying structural engineers to be agents of change on climate change. Action points for structural engineers identified include:

1. **Get Informed**: Understand what is happening and how your decisions impact the climate
2. **Low Carbon:** Controlling carbon is as important as controlling cost and safety
3. **Lean design**: Reduce material use safely through efficient, precise design
4. **Zero waste**: Design structures that are easily reused and recycled
5. **Influence the brief**: Convince clients to pursue low-carbon designs
6. **Get involved**: Exchange information through the institution and lobby for change

Based on these action points the current work has been identified to conform to the imperatives of 2, 3 and 4. Should the use of a beam or the loading to be applied change there is an alternative to dismounting the existing beam, disposing of it and replacing with a larger capacity member. The alternative is to strengthen the existing beam. The concept can also be employed at preliminary design stage when carrying out member selection. Smaller sections with upstands can be considered in the place of larger doubly symmetric sections should their use prove economical.

8.4 FUTURE WORK

Given the promising outcomes of the use of upstands as a strengthening technique, the study should be progressed to experimental models to validate the findings. Determination of residual stress profile in these strengthened sections also needs to be included as part of the experimental work.

In the current study the focus has been largely on the relationship between the shear centre position relative to the centroid and the corresponding critical elastic moment. Although uniqueness was observed for the monosymmetry constant, the study did not focus on this because this parameter also depends on the relative position of the shear centre and centroid. Future studies can be extended to the relationship between the shear centre and the monosymmetry constant as well as investigate the relationship between the monosymmetry constant and the critical elastic moment in case there are unique elements there as well.

Since only single curvature load cases are considered in this study, behaviour of beams subjected to double curvature should be investigated so that guidance for both single and double curvature cases are developed. The versatility of stiffener placement may require stiffener position to be altered to match, in some practical way, the moment profile of the member.

The study can also be extended to high strength steel members due to their increasingly prevalent use. Some properties that are unique to these types of steel may influence member behaviour particularly for the nonlinear analysis case.

REFERENCES

AISC 2010. Specification for structural steel buildings. *ANSI/AISC 360.* Chicago, Ill.: ANSI/AISC.

ALWIS, W. & WANG, C. 1996. Wagner term in flexural-torsional buckling of thin-walled open profile columns. *Engineering Structures,* 18**,** 125-132.

ANDERSON, J. M. & TRAHAIR, N. S. 1972. Stability of monosymmetric beams and cantilevers. *Journal of the Structural Division,* 98**,** 269-286.

ANDRADE, A., CAMOTIM, D. & E COSTA, P. 2007. On the evaluation of elastic critical moments in doubly and singly symmetric I-section cantilevers. *Journal of Constructional Steel Research,* 63**,** 894-908.

ARONOLD, W. 2020. The structural engineer's responsibility in this climate emergency. *The Structural Engineer***,** 10-11.

ASSOCIATION, C. S. 2009. Limit states design of steel structures. *CAN/CSA-S16-14.* Mississauga Ontario: CSA.

ASSOCIATION, C. S. 2014. Limit states design of steel structures. *CAN/CSA-S16-14.* Mississagua, Ontario: CSA.

ASSOCIATION, C. S. 2019. Limit states design of steel structures. *CAN/CSA-S16-19.* Mississagua, Ontario: CSA.

ATTARD, M. 1986. Lateral buckling analysis of beams by the fem. *Computers & Structures,* 23**,** 217-231.

AUSTRALIA, S. 1998. AS4100. *Steel Structures.* Sydney, Australia.

AYDIN, R., GUNAYDIN, A., KIRAC, N. & OZBASARAN, H. 2013. On the evaluation of critical lateral buckling loads of prismatic steel beams. *In:* TOPPING, B. & IVANYI, P. (eds.) *Proceedings of the Fourteenth International Conference on Civil, Structural and Environmental Engineering Computing.* Stirlingshire, Scotland: Civil-Comp press.

BAJER, M., BARNAT, J. & PIJAK, J. 2017. Lateral Torsional Buckling of Selected Cross-Section Types. *Procedia Engineering,* 190**,** 106-110.

BALAZ, I. & KOLEKOVA, Y. Stability of monosymmetric beams. *In:* DUBINA, D. & IVANYI, M., eds. Stability and Ductility of Steel Structures (SDSS'99), 1999. Elsevier Sciences Ltd.

BENTLEY. n.d. *STAAD.Pro Help. D4.E.6.2 Members subject to Bending* [Online]. Available Online: Bentley. Available: https://docs.bentley.com/LiveContent/web/STAAD.Pro%20Help-v18/en/GUID-55A3F593-27E6-4D50-AA11-BF22BD6B90E7.html [Accessed 29 July 2023].

BARSOUM, G. & GALLAGHER, R. 1970. Finite element analysis of torsional and torsional-flexural stability problems. *International Journal for Numerical Methods in Engineering,* 2**,** 335-352.

BIJAK, R. 2019. Lateral-torsional buckling moment of simply supported unrestrained monosymmetric beams. *IOP Conference series: Materials Science and Engineering, WMCAUS 2018*.

BIJAK, R., KOLODZIEJ, G. & SIEDLECKA, M. 2019. Lateral-Torsional Buckling Resistance of Crane Runway Girders. *MS&E,* 471**,** 052076.

BILD, S., CHEN, G. & TRAHAIR, N. S. 1992. Out-of-plane strengths of steel beams. *Journal of Structural Engineering,* 118**,** 1987-2003.

BLEICH, F. 1952. *Buckling strength of metal structures*, Mc Graw-Hill Book Company, Inc.

BRADFORD, M., WOOLCOCK, S. & KITIPORNCHAI, S. Lateral buckling design of crane runway beams. *In:* WANG, C. M., LIU, G. & ANG, K. K., eds. Proceedings of the Second International Conference on Structural Stability, ICSSD 2002, 16-18 December 2002 Singapore.

BRADFORD, M. A. 1992. Lateral-Distortional buckling of steel I—Section members. *Journal of Constructional Steel Research,* 23**,** 97-116.

BRADFORD, M. A. & LIU, X. 2016. Flexural-torsional buckling of high-strength steel beams. *Journal of Constructional Steel Research,* 124**,** 122-131.

BRADFORD, M. A. & TRAHAIR, N. S. 1983. Lateral stability of beams on seats. *Journal of Structural Engineering,* 109**,** 2212-2215.

BROWN, P. & TRAHAIR, N. S. 1968. Finite integral solution of differential equations. *Civil Engineering Transactions,* 10**,** 193-196.

CAMOTIM, D., ANDRADE, A. & BASAGLIA, C. 2012. Some thoughts on a surprising result concerning the lateral-torsional buckling of monosymmetric I-section beams. *Thin-Walled Structures,* 60**,** 216-221.

CEN 2002. EN 1990:2002. *Basis of structural design.* Brussels: European Committee for Standardization.

CEN 2005. EN 1993-1-1:2005. *Eurocode 3: Design of steel structures - Part 1-1: General rules and rules for buildings.* Brussels (Belgium): European Committee for Standardization.

CSA 2009. Limit states design of steel structures. *CAN/CSA-S16-14*. Mississauga, Ontario: CAN/CSA.

CSA 2014. Limit states design of steel structures. *CAN/CSA-S16-14*. Mississagua, Ontarion: CAN/CSA.

CSA 2019. Limit states design of steel structures. *CAN/CSA-S16-19*. Mississagua, Ontario: CAN/CSA.

CHAJES, A. 1974. *Principles of structural stability theory,* Englewood Cliffs, N.J., Prentice Hall, Inc.

COUTO, C. & REAL, P. 2019. A proposal based on the effective section factor for the lateral-torsional buckling of beams with slender I-shaped welded sections. *Thin-Walled Structures,* 145**,** 106389.

DAHMANI, L. 2015. Lateral torsional buckling of an eccentrically loaded channel section beam. *ICCBE 2015: XIII International Conference on Civil and Building Engineering.* Paris.

DE JONG, H. 1990. An approach to more complicated lateral-buckling problems. *Journal of Constructional Steel Research,* 16**,** 231-246.

DEMIRHAN, A., EROGLU, H., MUTLU, E., YILMAZ, T. & ANIL, O. 2020. Experimental and numerical evaluation of inelastic lateral-torsional buckling of I-section cantilevers. *Journal of Constructional Steel Research,* 168**,** 105991.

DIMAGGIO, F., GOMZA, A., THOMAS, W. & SALVADORI, M. G. 1952. Lateral Buckling of Beams in Bending and Compression. *Journal of the Aeronautical Sciences.*

DJUBEK, J. & MRAZIK, A. 1958. Stability of thin-walled member structures. Bratislava: USTARCH-Slovak Academy of Sciences.

DJURIC-MIJOVIC, D. & TRAJKOVIC, M. 2007. Influence of the cross-section shape on the lateral torsional buckling capacity. *WIT Transactions on Modelling and Simulation,* 46**,** 117-126.

DUX, P. & KITIPORNCHAI, S. 1983. Inelastic beam buckling experiments. *Journal of Constructional Steel Research,* 3**,** 3-9.

ECCS 1976. ECCS Manual on stability *Chapter 5 Lateral Supported and Unsupported Beams* Paris.

EKSTROM, C.-M. & WESLEY, D. 2017. *Lateral-torsional Buckling of Steel Channel Beams. A parametric study through FE-analysis.* Masters, Chalmers University of Technology.

ENV 1993-1-1:(1992). *Design of steel structures.* European Prestandard.

ENV 1999-1-1: (1998). *Design of Aluminium structres.* European prestandard.

ERKMEN, R. E. & ATTARD, M. M. 2011. Lateral-torsional buckling analysis of thin-walled beams including shear and pre-buckling deformation effects. *International Journal of Mechanical Sciences,* 53**,** 918-925.

ELLIFRITT, D. S. & LUE, D. M. 1998. Design of crane runway beam with channel. *Engineering Journal,* 35**,** 41-49.

FALGOUST, M. 2004. *On the validity of the Wagner hypothesis for thin-walled open profile members.* University of Pittsburgh.

FISH, J. & BELYTSCHKO, T. 2007. *A first course in finite elements,* The Atrium, Southern Gate, Chichester, West Sussex, PO19 8SQ, England, John Wiley & Sons Ltd.

FLINT, A. 1948. *On the lateral stability of beams.* PhD PhD thesis, University of Bristol.

FUKUMOTO, Y., ITOH, Y. & KUBO, M. 1980. Strength variation of laterally unsupported beams. *Journal of the Structural Division,* 106**,** 165-181.

GALAMBOS, T. V. 1960. Inelastic Lateral Buckling of Beams. Fritz Engineering Laboratory.

GALAMBOS, T. V. 1963. The Influence of the Adjacent Spans on the Rotation Capacity of Beams. Fritz Engineering Laboratory.

GALAMBOS, T. V. 1968. *Structural Members and Frames,* Englewood Cliffs, N.J., Prentice-Hall Inc.

GALAMBOS, T. V. 1998. *Guide to Stability Design Criteria for Metal structures,* New York, John Wiley & Sons.

GALAMBOS, T. V. & SUROVEK, A. E. 2008. *Structural stability of steel : concepts and applications for structural engineers,* Hoboken, N.J., John Wiley & Sons.

GELERA, K. & PARK, J. S. 2012. Elastic lateral torsional buckling strength of monosymmeric stepped I-beams *KSCE Journal of Civil Engineering,* 16**,** 785-793.

GELLIN, S. & LEE, G. 1988. Finite elements available for the analysis of noncurved thin-walled structures. *In:* BULL, J. (ed.) *Finite element analysis of thin-waled structures.* London, U.K., 1-45: Elsevier Applied Science.

GENGSHU, T. & SHAOFAN, C. 1989. The elastic buckling of interbraced girders. *Journal of Constructional Steel Research,* 14**,** 87-105.

GOODIER, J. 1942. *Flexural-Torsional Buckling of Bars of Open Section,* Ithaca N.Y., Cornell University Engineering Experiment Station. Bulleting No. 28.

GOTO, Y. & CHEN, W. 1989. On the validity of Wagner hypothesis. *International Journal of Solids and Structures,* 25**,** 621-634.

GUPTA, P., WANG, S. & BLANDFORD, G. 1996. Lateral-torsional buckling of nonprismatic I-beams. *Journal of Structural Engineering,* 122.

HANCOCK, G. J. 1978. Loacl, Distortional and Lateral Buckling of I-Beams. *Journal of the Structural Division,* 104**,** 1787-1798.

HANSON, R. D. 1977. Repair, Strengthening and Rehabilitation of Buildings: recommendations for needed research. Ann Arbor, Michigan 48109.

HELWIG, T., FRANK, K. & YURA, J. 1997. Lateral-torsional buckling of singly symmeric I-beams. *Journal of Structural Engineering,* 123**,** 1172-1179.

HILL, H. 1942. The lateral instability of unsymmetrical I beams. *Tenth Annual Meeting I.Ae.S*. New York.

HOFF, N. 1944. A strain energy derivation of the torsional-flexural buckling loads of straight columns of thin-walled open sections. *Quarterly of Applied Mathematics,* 1**,** 341-345.

HSU, W., LUE, D. & CHEN, Y. 2012. Deasing aid for moment strength of built-up crane runway girders. *International Journal of Steel Structures,* 12**,** 403-417.

HUGHES, A., ILES, D. & MALIK, A. 2011. *Design of steel beams in torsion - SCI Publication P385,* Silwood Park, Ascot, Berkshire, United Kingdom, SCI.

HUSSAIN, A., LIU, Y. & CHAN, S. 2018. Finite element modeling and design of single angle member under bi-axial bending. *Structures,* 16**,** 373-389.

IOANNIDIS, G. & KOUNADIS, A. 1994. Lateral post-buckling analysis of monosymmetric I-beams under uniform bending. *Journal of Constructional Steel Research,* 30**,** 1-12.

JOHNSON, C. & WILL, K. 1974. Beam buckling by finite element procedure. *Journal of the Structural Division,* 100**,** 669-685.

JOHNSTON, B. 1941. Lateral Buckling of I-Section Columns with Eccenric End Loads in the Plane of the Web. *Transactions of the American Society of Mechanical Engineers,* 63**,** A-176.

KALA, Z. 2013. Elastic lateral-torsional buckling of simply supported hot-rolled steel i-beams with random imperfections. *11th International Conference on Modern Building Materials, structures and techniques, MBMST 2013*. Procedia Engineering.

KALA, Z. & VALES, J. 2017a. Global sensitivity analysis of lateral-torsional buckling resistance based on finite element simulations. *Engineering Structures,* 134**,** 37-47.

KALA, Z. & VALES, J. 2017b. Sensitivity assessment and lateral-torsional buckling design of I-beams using solid finite elements. *Journal of Constructional Steel Research,* 139**,** 110-122.

KANG, Y., LEE, S. & YOO, C. 1992. On the dispute concerning the validity of the Wagner hypothesis. *Computers & Structures,* 43**,** 853-861.

KIRKE, B. & AL-JAMEL, I. H. 2004. *Steel Structures Design Manual to AS4100.*

KITIPORNCHAI, S. & TRAHAIR, N. S. 1975a. Buckling of Inelastic I-Beams under moment gradient. *Journal of the Structural Division,* 101**,** 991-1004.

KITIPORNCHAI, S. & TRAHAIR, N. S. 1975b. Inelastic buckling of simply supported steel I-beams. *Journal of the Structural Division,* 101**,** 1333-1347.

KITIPORNCHAI, S. & TRAHAIR, N. S. 1980. Buckling properties of monosymmetric I-Beams. *Journal of the Structural Division,* 106**,** 941-957.

KITIPORNCHAI, S. & WANG, C. 1986. Lateral buckling of tee beams under moment gradient. *Computers & Structures,* 23**,** 69-76.

KITIPORNCHAI, S., WANG, C. & TRAHAIR, N. 1986. Buckling of monosymmetric I-beams under moment gradient. *Journal of Structural Engineering,* 112**,** 781-799.

KITIPORNCHAI, S., WANG, C. & TRAHAIR, N. 1987. Closure to "Buckling of monosymmetric I-Beams under moment gradient" by Kitipornchai, S. , Wang, C.M. and Trahair, N.S. (April, 1986, Vol.112, No.4). *Journal of Structural Engineering,* 113**,** 1391-1395.

KITIPORNCHAI, S. & WONG-CHUNG, A. D. 1987. Inelastic buckling of welded monosymmetric I-beams. *Journal of Structural Engineering,* 113**,** 740-756.

KNOBLOCH, M., BUREAU, A., KUHLMANN, U., DA SILVA, L. S., SNIJDER, H., TARAS, A., BOURS, A., -L & JORG, F. 2020. Structural member stability verification in the new Part 1-1 of the second generation of Eurocode 3. Part 2: Member buckling design rules and further innovations. *Steel Construction.* 13 (3):208 - 222.

KOSHMIDDER-HATCH, D. 2014. *Strengthening existing steelwork* [Online]. Available: newsteelconstruction.com/wp/strengthening-existing-steelwork [Accessed 31.01 2022]

KOVAC, M. 2012. Lateral-torsional buckling of web-tapered I-beams. 1D and 3D FEM approach. *Procedia Engineering,* 40**,** 217-222.

KUBO, M. & FUKUMOTO, Y. 1988. Lateral-torsional buckling of thin-walled I-Beams. *Journal of Structural Engineering,* 114**,** 841-855.

KUCUKLER, M., GARDNER, L. & MACORINI, L. 2014. A stiffness reduction method for the in-plane design of structural steel elements. *Engineering Structures,* 73**,** 72-84.

LA POUTRE, D. 2000. Lateral torsional buckling of channel shaped sections. *T9 Report: Experimental Research.* Eindhoven University of Technology.

LAMB, A. & EAMON, C. 2015. Load height and moment factors for doubly symmetric wide flange beams. *Journal of Structural Engineering,* 141**,** 04015069.

LEE, G. 1960. A survey on the lateral instability of beams. *Welding Research Council.*

LEE, G. & GALAMBOS, T. 1962. Post-Buckling Strength of Wide-Flange Beams. *Journal of the Engineering Mechanics Division,* 88**,** 59-75.

LINDNER, J. 1976. The ultimate load of monosymmetric sections due to lateral-torsional buckling. *Final Report, IABSE***,** 353-357.

LOPEZ, A., YONG, D. J. & SERNA, M. A. 2006. Lateral-Torsional Buckling of Steel beams: A General Expression for The Moment Gradient Factor. *In:* CAMOTIM, D. *E. A.* (ed.) *Stability and Ductility of Steel Structures.* Lisbon, Portugal, September 6-8.

LU, L., SHEN, S., SHEN, Z. & HU, X. 1983. *Stability of Steel Structural Members (in Chinese),* Beijing, Publishing House of Chinese Construction Industry.

LUE, D., LIU, J. & LIN, C. 2007. Numerical evaluation on warping constants of general cold-formed steel open sections. *Steel Structures,* 7**,** 297-309.

MACCRIMMON, R. A. 2004. *Guide for the design of crane-supporting steel structures,* 3760 14th Avenue, Suite 200. Markham, Ontario L3R 3T7, Canadian Institute of Steel Construction.

MANARIN, M., DRIVER, R. G. & LI, Y. Moment gradient factor for lateral-torsional buckling of T-shaped beams. Proceedings of the Annual Stability Conference, April 2-5 2019 St. Louis, Missouri. Structural Stability Research Council.

MANDAL, P. & CALLADINE, C. 2002. Lateral-Torsional buckling of beams and the Southwell plot. *International Journal of Mechanical Sciences,* 44**,** 2557-2571.

MICHELL, A. 1899. XXXII. Elastic stability of long beams under transverse forces. *The London, Edinburgh, and Dublin Philosophical Magazine and Journal of Science,* 48**,** 298-309.

MOHAMMADI, E., HOSSEINI, S. & ROHANIMANESH, M. 2016. Elastic lateral-torsional buckling strength and torsional bracing stiffness requirements for monosymmetric I-beams. *Thin-Walled Structures,* 104**,** 116-125.

MOHRI, F., BROUKI, A. & ROTH, J. 2003. Theoretical and numerical stability analyses of unrestrained, mono-symmetric thin-walled beams. *Journal of Constructional Steel Research,* 59**,** 63-90.

MOHRI, F., DAMIL, N. & POTIER-FERRY, M. 2010. Theoretical and numerical models for lateral buckling stability of monosymmetric I section beams. *Thin-Walled Structures,* 48**,** 299-315.

MOHRI, F., DAMIL, N. & POTIER-FERRY, M. 2012. Pre-buckling deflection effects on stability of thin-walled beams with open sections. *Steel and Composite Structures,* 13**,** 71-89

MORKHADE, S. & GUPTA, L. 2013. Effect of load height on buckling resistance of steel beams. *Procedia Engineering,* 51**,** 151-158.

MOVAGHATI, S. Strengthening beam sections of industrial buildings against lateral torsional buckling. Proceedings of the Annual Stability Conference. Structural Stability Research Council., 2019 St. Louis, Missouri. April 2-5.

MUDENDA, K. & ZINGONI, A. 2018. Lateral-torsional buckling behavior of hot-rolled steel beams with flange upstands. *Journal of Constructional Steel Research,* 144**,** 53-64.

NEMIR, M. T. M. 1985. *Finite element stability analysis of thin-walled steel structures.* PhD Thesis, University of Salford.

NETHERCOT, D. A. 1973. Inelastic Buckling of Monosymmetric I-Beams. *Journal of the Structural Division,* 99**,** 1696-1701.

NETHERCOT, D. 1974. Buckling of welded beams and girders. *IABSE Publications,* 34.

NISHINO, F. 1965. Error in finite difference solutions of local buckling strength. *23rd Annual meeting of Japan National Congress for Applied Mechanics.* University of Tokyo.

O'CONNOR, C. 1964. The buckling of a monosymmetric beam loaded in the plane of symmetry. *Australian Journal of Applied Science,* 15**,** 191-203.

O'HEACHTEIRN, P. & NETHERCOT, D. 1988a. Lateral Buckling Behaviour of Monosymmetric Plate Girders. *Journal of Constructional Steel Research,* 11**,** 261-282.

O'HEACHTEIRN, P. & NETHERCOT, D. 1988b. Lateral Buckling Tests on Monosymmetric Plate Girders. *Journal of Constructional Steel Research,* 11**,** 241-259.

OJALVO, M. 1981. Wagner hypothesis in beam and column theory. *Journal of the Engineering Mechanics Division,* 107**,** 669-677.

OZBASARAN, H. 2013. Finite differences approach for calculating elastic lateral torsional buckling moment of cantilever I sections. *Journal of Science and Technology - A - Applied Sciences and Technology,* 14**,** 143-152.

PANDEY, M. D. & SHERBOURNE, A. N. 1990. Elastic, Lateral-Torsional Stability of Beams: General Considerations. *Journal of Structural Engineering,* 116**,** 317-335.

PAPANGELIS, J., TRAHAIR, N. S. & HANCOCK, G. J. 1998. Elastic flexural-torsional buckling of structures by computer. *Computers & Structures,* 68**,** 125-137.

PARK, J. & STALLINGS, J. 2003. Lateral-torsional buckling of stepped beams. *Journal of Structural Engineering,* 129**,** 1457-1465.

PEKOZ, T. 1992. lateral buckling of singly symmetric beams. *Eleventh International Specialty Conference on Cold-Formed Steel structures.* St. Louis, Missouri, U.S.A.

PI, Y. & TRAHAIR, N. 2000. Distortion and Warping at Beam Supports. *Journal of Structural Engineering,* 126**,** 1279-1287.

PI, Y., TRAHAIR, N. & RAJASEKARAN, S. 1992. Energy Equation for Beam Lateral Buckling. *Journal of Structural Engineering,* 118**,** 1462-1479.

PI, Y. & TRAHAIR, N. S. 1997. Lateral-distortional buckling of hollow flange beams. *Journal of Structural Engineering,* 123**,** 695-702.

PIOTROWSKI, R. & SZYCHOWSKI, A. 2019. Lateral Torsional Buckling of Steel Beams Elastically Restrained at the Support Nodes. *Applied Sciences,* 9.

POWELL, G. & KLINGNER, R. 1970. Elastic lateral buckling of steel beams. *Journal of the Structural Division,* 96**,** 1919-1932.

PRANDTL, L. 1903. Zur torsion von prismatischen staben. *Physikalische Zeitschrift,* 4**,** 758-770.

PRANDTL, L. 1907. *Zeitschrift des Vereins Deutschner Ingenieure.*

PRASAD, J. & GALAMBOS, T. 1963. The influence of the adjacent span on the rotation capacity of beams. Bethlehem, Pennsylvania: Fritz Engineering Laboratory, Lehigh University.

PROKON ver.3.1. (2019). Prokon software consultants (pty) Ltd.

RAFTOYIANNIS, I. & ADAMANKOS, T. 2010. Critical lateral-torsional buckling moments of steel web-tapered I-beams. *The Open Construction and Building Technology Journal,* 4**,** 105-112.

RAJASEKARAN, S. & MURRAY, D. 1973. Finite element solution of inelastic beam equations. *Journal of the Structural Division,* 99**,** 1025-1041.

REBELO, C., LOPES, N., DA SILVA, L. S., NETHERCOT, D. & REAL, P. 2009. Statistical evaluation of the lateral-torsional buckling resistance of steel I-beams-Part 1: variability of the Eurocode 3 resistance model. *Journal of Constructional Steel Research,* 64**,** 818-831.

RIKS, E. 1979. An incremental approach to the solution of snapping and buckling problems. *International Journal of Solids and Structures,* 15**,** 529-551.

ROBERTS, T. & AZIZIAN, Z. 1983. Instability of thin walled bars. *Journal of Engineering Mechanics,* 109.

ROBERTS, T. & AZIZIAN, Z. 1984. Instability of monosymmetric I-Beams. *Journal of Structural Engineering,* 110**,** 1415-1419.

ROBERTS, T. & BURT, C. 1985. Instability of Monosymmetric I-Beams and Cantilevers. *International Journal of Mechanical Sciences,* 27**,** 313-324.

ROCKEY, K. & NETHERCOT, D. 1971. Stabilisation of beams against lateral buckling. *International Speciality Conference on Cold-Formed Steel Structures*, Paper 4.

SABS 2011. The structural use of stee. Part 1: Limit-states design of hot-rolled steelwork. *SANS 10162-1 : 2011*. 1 Dr Lategan Road, Groenkloof, Pretoria: South African Bureau of Standards.

SABS 2012. Construction Works - Part CS1: Structural Steelwork. *SANS 2001-CS1*. 1 Dr Lategan Road, Groenkloof, Pretoria: South African Bureau of Standards.

SAISC 2016. *Southern African Steel Construction Handbook (SASCH).*

SALVADORI, M. G. 1955. Lateral Buckling of I-Beams. *Transactions of the American Society of Civil Engineers,* 120**,** 1165-1177.

SAUCHA, J. & RADOS, J. 2001. A critical review of Vlasov's General Theory of Stability of In-Plane Bending of Thin-Walled Elastic Beams. *Meccanica,* 36**,** 177-190.

SAYED-AHMED, E. Moment-gradient factor for lateral torsion-flexure buckling of steel I-beams. 2nd International Conference on Structural Engineering, Mechanics and Computation (SEMC 04): Progress in Structural Engineering, Mechanics and Computation, 2004 Cape Town, South Africa.

SEAH, L. & KHONG, P. 1990. Lateral-torsional buckling of channel beams. *Journal of Constructional Steel Research,* 17**,** 265-282.

SHOKOUHIAN, M. & SHI, Y. 2015. Flexural strength of hybrid steel I-beams based on slenderness. *Engineering Structures,* 93**,** 114-128.

SNIJDER, H., BIJLAARD, F. & STEENBERGEN, H. FEM simulations of lateral torsional buckling experiments on channel sections loaded in bending. Proceedings of the 3rd european conference on Steel Structures, 2002.

SOLTANI, M. & ASGARIAN, B. 2018. Determination of lateral-torsional buckling load of simply supported prismatic thin-walled beams with mono-symmetric cross-sections using the finite difference method. *Amirkabir Journal of Civil Engineering,* 50**,** 23-26.

SUBRAMANIAN, L. & WHITE, D. W. 2017. Resolving the disconnects between lateral torsional buckling experimental tests, test simulations and design strength equations. *Journal of Constructional Steel Research,* 128**,** 321-334.

SURLA, A., KANG, Y. S. & PARK, J. S. 2015. Inelastic buckling assessment of monosymmetric I-beams having stepped and non-compact flange sections. *Journal of Constructional Steel Research,* 114**,** 325-337.

SYSTEMES, D. n.d. SIMULIA User Assistance 2017. Dassault Systemes.

SZALAI, J. & PAPP, F. 2005. A new residual stress distribution for hot-rolled I-shaped sections. *Journal of Constructional Steel Research,* 61**,** 845-861.

SZEWCZAK, R. M., SMITH, E. A. & DEWOLF, J. T. 1983. Beams with torsional stiffeners. *Journal of Structural Engineering,* 109**,** 1635-1647.

TANKOVA, T., DA SILVA, L. S., BALAKRISHNAM, M., RODRIGUES, D., LAUNERT, B., PASTERNAK, H. & TUN, T. Y. 2019. Residual stress in welded I section steel members. *Engineering Structures,* 197**,** 109398.

TARAS, A., PUIG, M. G. & UNTERWEGER, H. 2013. Behaviour and design of members with monosymmetric cross-section. *Structures and Buidlings,* 166**,** 413-423.

TEBEDGE, N. & TALL, L. 1973. Residual stresses in structural steel shapes - a summary of measured values. Lehigh Preserve Institutional Repository.

THEVENDRAN, V. & SHANMUGAM, N. 1991. Lateral buckling of doubly symmetric beams containing openings. *Journal of Engineering Mechanics,* 117**,** 1427-1441.

TIMOSHENKO, S. 1936. *Theory of Elastic Stability,* New York, McGraw-Hill Book Co. Inc.

TIMOSHENKO, S. & GERE, J. M. 1961. *Theory of elasticity stability,* New York, McGraw-Hill.

TIMOSHENKO, S. & GOODIER, J. 1951. *Theory of Elasticity,* New Youk, McGraw-Hill Book Company, Inc.

TONG, G. & ZHANG, L. 2003. An analysis of current stability theories for thin-walled members. *Advances in Structural Engineering,* 6**,** 283-292.

TRAHAIR, N. S. 1993. *Flexural-torsional buckling of structures*, CRC press.

TRAHAIR, N. S. 1996. Laterally unsupported beams. *Engineering Structures,* 18**,** 759-768.

TRAHAIR, N. S. 2002. Moment capacities of steel angle sections. *Journal of Structural Engineering,* 128**,** 1387-1393.

TRAHAIR, N. S. 2003. Lateral buckling strengths of steel angle section beams. *Journal of Structural Engineering,* 129**,** 784-791.

TRAHAIR, N. S. 2008. Lateral buckling of monorail beams. *Engineering Structures,* 30**,** 3213-3218.

TRAHAIR, N. S., BRADFORD, M. A., NETHERCOT, D. A. & GARDNER, L. 2008. *The Behaviour and Design of Steel Structures to EC3,* 2 Park Square, Milton Park, Abingdon, Oxon OX14 4RN, Taylor & Francis.

TRAHAIR, N. S. 2010. Steel cantilever strength by inelastic lateral buckling. *Journal of Constructional Steel Research,* 66**,** 993-999.

TRAHAIR, N. S. 2011. *Wagner's beam cycle,* Sydney, The University of Sydney.

TRAHAIR, N. S. 2012. Inelastic buckling design of monosymmetric I-beams. *Engineering Structures,* 34**,** 564-571.

TRAHAIR, N. S. 2016. Torsional equations for lateral buckling. *Research Report R964*. Sydney NSW 2006 Australia: School of Civil Engineering, The University of Sydney.

TRAHAIR, N. S. 2019. Inelastic lateral buckling of continuous steel beams. *Engineering Structures,* 190**,** 238-245.

TRAHAIR, N. S. & HANCOCK, G. J. 2004. Steel member strength by inelastic lateral buckling. *Journal of Structural Engineering,* 130**,** 64-69.

TRAHAIR, N. S. & KITIPORNCHAI, S. 1972. Buckling of Inelastic I-Beams under uniform moment. *Journal of the Structural Division,* 98**,** 2551-2566.

TRAYER, G. W. & MARCH, H. W. 1930. The torsion of members having sections common in aircraft construction. *Report No. 334*. National Advisory Committee for Aeronautics (NACA).

TSAVDARIDIS, K. D. 2015. Strengthening Techniques: Code-Deficient Steel Buildings. *In:* BEER, M., KOUGIOUMTZOGLOU, I. A., PATELLI, E. & AU, S.-K. (eds.) *Encyclopedia of Earthquake Engineering.* Berlin, Heidelberg: Springer Berlin Heidelberg.

VALENTINO, J. & TRAHAIR, N. S. 1998. Torsional Restraint Against Elastic Lateral Buckling. *Journal of Structural Engineering,* 124**,** 1217-1225.

VALES, J. & STAN, T.-C. 2017. FEM modelling of lateral-torsional buckling using shell and solid elements. *Procedia Engineering,* 190**,** 464-471.

VENTER, S., SKORPEN, S. & VAN RENSBURG, B. 2019. A refined approach to lateral-torsional buckling of overhang beams. *Journal of the South African Institution of Civil Engineering,* 61**,** 2-18.

VLASOV, V. 1961. *Thin-walled elastic beams,* Jerusalem, Israel, Israel Program for Scientific Translation.

WAGNER, H. 1936. Torsion and buckling of open sections. *Technical Memorandum No.807. NACA.*

WAGNER, H. & PRETSCHNER, W. 1934. Torsion and buckling of open sections. *Luftfahrtforschung,* XI.

WANG, C. & KITIPORNCHAI, S. 1986a. Buckling Capacities of Monosymmetric I-Beams. *Journal of Structural Engineering,* 112**,** 2373-2391.

WANG, C. & KITIPORNCHAI, S. 1986b. On stability of monosymmetric cantilevers. *Engineering Structures,* 8**,** 169-180.

WANG, C., KITIPORNCHAI, S. & THEVENDRAN, V. 1987. Buckling of braced monosymmetric cantilevers. *International Journal of Mechanical Sciences,* 29**,** 321-337.

WANG, C., KITIPORNCHAI, S. & THEVENDRAN, V. 1990. Optimal Design of I-Beams Against Lateral Buckling. *Journal of Engineering Mechanics,* 116**,** 1902-1923.

WANG, C. & KITIPORNCHAI, S. 1991. Integrated view of methods in buckling analysis. *International Journal of Applied Engineering Education,* 7**,** 381-387.

WANG, C., WANG, L. & ANG, K. K. 1994. Beam-Buckling Analysis via Automated Rayleigh-Ritz Method. *Journal of Structural Engineering,* 120**,** 200-211.

WANG, Z.-Q., ZHAO, J.-C. & GONG, J.-H. 2012. Restrained torsion of open thin-walled beams including shear deformation effects. *Journal of Zhejiang University - SCIENCE A (Applied Physics & Engineering),* 13**,** 260-273.

WHITE, D. W. & JUNG, S.-K. 2003. Simplified Lateral Torsional Buckling Equations for I- and Channel-Section Members. *Structural Engineering, Mechanics and Materials.* Atlanta, GA: School of Civil and Environmental Enginering, Georgia Institute of Technology.

WINKLER, R., KINDMANN, R. & KNOBLOCH, M. 2017. Lateral Torsional Buckling Behaviour of Steel Beams - On the Influence of the Structural System. *Structures,* 11**,** 178-188.

WONG, E., DRIVER, R. G. & HEAL, T. W. 2015. Simplified approach to estimating the elastic lateral-torsional buckling capacity of steel beams with top-flange loading. *Canadian Journal of Civil Engineering,* 42.

XIE, W. & MOHAREB, M. 2022. Elastc critical moment for monosymmetric beams under linear moment gradients. *Canadian Journal of Civil Engineering,* 49**,** 731-745.

XU, Y., SHI, Y., WU, Y. & BAN, H. 2018. Experimental and Numerical Study on Lateral-Torsional Buckling of High Performance Steel Beams. *International Journal of Structural Stability and Dynamics,* 18**,** 1850090.1 - 1850090.29.

YANG, B., XIONG, G., DING, K., NIE, S., ZHANG, W., HU, Y. & DAI, G. 2016. Experimental and Numerical Studies on Lateral-Torsional Buckling of GJ Structural Steel Beams Under a Concentrated Loading Condition. *International Journal of Structural Stability and Dynamics,* 16**,** 1640004.1 - 1640004.23.

YILMAZ, T. & KIRAC, N. 2016. On the evaluation of critical lateral-torsional buckling loads of monosymmetric beam-columns. *International Journal of Civil and Environmental Engineering,* 10.

YILMAZ, T., KIRAC, N. & TURAB, K. Lateral-Torsional Buckling of European Wide Flange I-Section Beams. 2nd World Congress on Civil, Structural and Environmental Engineering (CSEE 17), 2017 Barcelona, Spain - April 2-4.

YOSHIDA, H. & MAEGAWA, K. 1984. Lateral Instability of I-Beams with Imperfections. *Journal of Structural Engineering,* 110**,** 1875-1892.

YOSHIDA, H., NETHERCOT, D. & TRAHAIR, N. S. 1977. Analysis of inelastic buckling of continuous beams. *Proceedings IABSE***,** 1-14.

YOUNG, B. 1975. Residual stress in hot rolled members. *IABSE Reports of the working commissions,* 23.

YUAN, W.-B., KIM, B. & CHEN, C.-Y. 2013. Lateral-torsional buckling of steel web tapered tee-section cantilevers. *Journal of Constructional Steel Research,* 87**,** 31-37.

YUN, X. & GARDNER, L. 2017. Stress-strain curves for hot-rolled steels. *Journal of Constructional Steel Research,* 133**,** 36-46.

YURA, J. 2001. Fundamentals of Beam Bracing. *Engineering Journal,* First Quarter**,** 11-26.

YURA, J. & PHILLIPS, B. 1992. Bracing requirements for elastic steel beams. *Research Project 3-5-90/1-1239 "Bracing Effects of Bridge Decks".* Austin, Texas: Center for Transportation Research, Bureau of Engineering Research, The University of Texas at Austin.

ZHANG, L. & GENGSHU, T. 2008. Elastic flexural-torsional buckling of thin-walled cantilevers. *Thin-Walled Structures,* 46**,** 27-37.

ZHANG, W.-F., LIU, Y.-C., CHEN, K.-S. & DENG, Y. 2017a. Dimensionless analytical solution and new design formula for lateral-torsional buckling of I-beams under linear distributed moment via linear stability theory. *Mathematical Problems in Engineering,* 2017.

ZHANG, W., LIU, F. & XI, F. 2018. Lateral torsional buckling of steel beams under transverse impact loading. *Shock and Vibration,* 2018.

ZHANG, Y., YANG, B., XIONG, G., ELCHALAKANI, M. & NIE, S. Lateral torsional buckling investigation on welded Q460GJ structural steel unrestrained singly-symmetric beams under a point load. Proceedings of Eurosteel 2017, 2017b. 1245-1254.

ZIEMIAN, R. D. 2010. *Guide to stability design criteria for metal structures,* Hoboken, New Jersey, John Wiley & Sons. Inc.

ZIRAKIAN, T. & BOYAJIAN, D. 2018. Research on Distortional Buckling of Steel I-Section Beams. *Journal of Steel Structures & Construction,* 4.

APPENDIX A - SECOND MOMENT OF AREA TRENDS

(1) Table A1: I-section

Check on (k_1) factor stiffness Ratio

Beam **NF305x102x25** B/H: 0,3

E: *200 000* MPa

Upstand: (mm)	0	10	20	30	40	50	60	70	80	90	100	110	120	130	140	150	160
I_x (mm^4)	43 427 979	46 748 157	50 211 851	53 828 313	57 606 455	61 554 904	65 682 059	69 996 126	74 505 152	79 217 050	84 139 618	89 280 560	94 647 497	100 247 978	106 089 494	112 179 480	118 525 329
Change:		*7,65%*	*7,41%*	*7,20%*	*7,02%*	*6,85%*	*6,70%*	*6,57%*	*6,44%*	*6,32%*	*6,21%*	*6,11%*	*6,01%*	*5,92%*	*5,83%*	*5,74%*	*5,66%*
I_y (mm^4)	1 228 296	1 542 088	1 855 880	2 169 672	2 483 465	2 797 257	3 111 049	3 424 842	3 738 634	4 052 426	4 366 218	4 680 011	4 993 803	5 307 595	5 621 387	5 935 180	6 248 972
Change:		*25,55%*	*20,35%*	*16,91%*	*14,46%*	*12,64%*	*11,22%*	*10,09%*	*9,16%*	*8,39%*	*7,74%*	*7,19%*	*6,70%*	*6,28%*	*5,91%*	*5,58%*	*5,29%*
EI_y/EI_x	**0,028**	**0,033**	**0,037**	**0,040**	**0,043**	**0,045**	**0,047**	**0,049**	**0,050**	**0,051**	**0,052**	**0,052**	**0,053**	**0,053**	**0,053**	**0,053**	**0,053**
														0,0529	0,0530	0,0529	0,0527

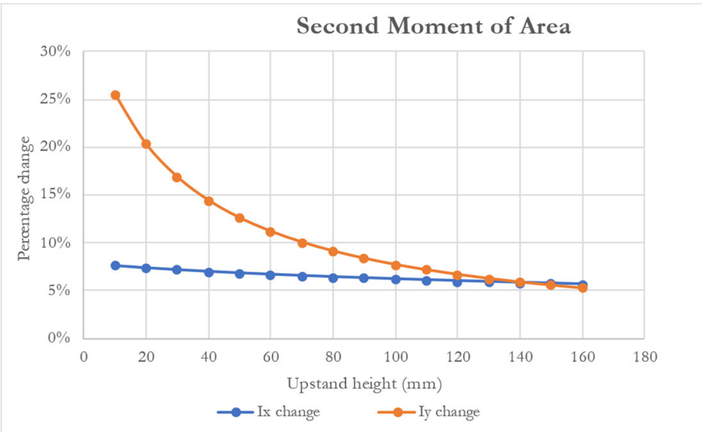

Figure. A1

(2) Table A2: I-section

Check on (k_1) factor stiffness Ratio

Beam	**NF406x140x39**	B/H:	0,4
E:	*200 000*	MPa	

Upstand: (mm)	0	10	20	30	40	50	60	70	80	90	100	110	120	130	140	150	160
I_x *(mm⁴)*	120 969 789	127 859 519	134 962 228	142 290 115	149 854 930	157 668 040	165 740 490	174 083 047	182 706 235	191 620 372	200 835 597	210 361 889	220 209 092	230 386 927	240 905 009	251 772 859	262 999 915
Change:		*5,70%*	*5,56%*	*5,43%*	*5,32%*	*5,21%*	*5,12%*	*5,03%*	*4,95%*	*4,88%*	*4,81%*	*4,74%*	*4,68%*	*4,62%*	*4,57%*	*4,51%*	*4,46%*
I_y *(mm⁴)*	4 094 650	4 858 626	5 622 603	6 386 579	7 150 555	7 914 532	8 678 508	9 442 485	10 206 461	10 970 437	11 734 414	12 498 390	13 262 367	14 026 343	14 790 320	15 554 296	16 318 272
Change:		*18,66%*	*15,72%*	*13,59%*	*11,96%*	*10,68%*	*9,65%*	*8,80%*	*8,09%*	*7,49%*	*6,96%*	*6,51%*	*6,11%*	*5,76%*	*5,45%*	*5,17%*	*4,91%*
EI_y/EI_x	**0,034**	**0,038**	**0,042**	**0,045**	**0,048**	**0,050**	**0,052**	**0,054**	**0,056**	**0,057**	**0,058**	**0,059**	**0,060**	**0,061**	**0,061**	**0,062**	**0,062**

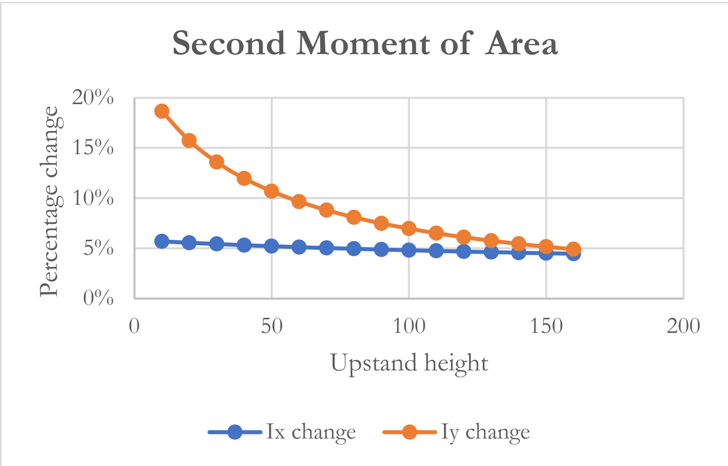

Figure. A2

(3) Table A3: I-section

Check on (k_1) factor stiffness Ratio

Beam	**NF IPE 160**	B/H:	0,5
E:	*200 000*	MPa	

Upstand: (mm)	0	10	20	30	40	50	60	70	80	90	100	110	120	130
I_x *(mm^4)*	8 346 265	9 340 990	10 436 282	11 640 251	12 960 841	14 405 875	15 983 090	17 700 154	19 564 684	21 584 259	23 766 426	26 118 708	28 648 608	31 363 615
Change:		*11,92%*	*11,73%*	*11,54%*	*11,35%*	*11,15%*	*10,95%*	*10,74%*	*10,53%*	*10,32%*	*10,11%*	*9,90%*	*9,69%*	*9,48%*
I_y *(mm^4)*	681 533	888 119	1 094 706	1 301 292	1 507 878	1 714 465	1 921 051	2 127 637	2 334 223	2 540 810	2 747 396	2 953 982	3 160 569	3 367 155
Change:		*30,31%*	*23,26%*	*18,87%*	*15,88%*	*13,70%*	*12,05%*	*10,75%*	*9,71%*	*8,85%*	*8,13%*	*7,52%*	*6,99%*	*6,54%*
EI_y/EI_x	**0,082**	**0,095**	**0,105**	**0,112**	**0,116**	**0,119**	**0,120**	**0,120**	**0,119**	**0,118**	**0,116**	**0,113**	**0,110**	**0,107**

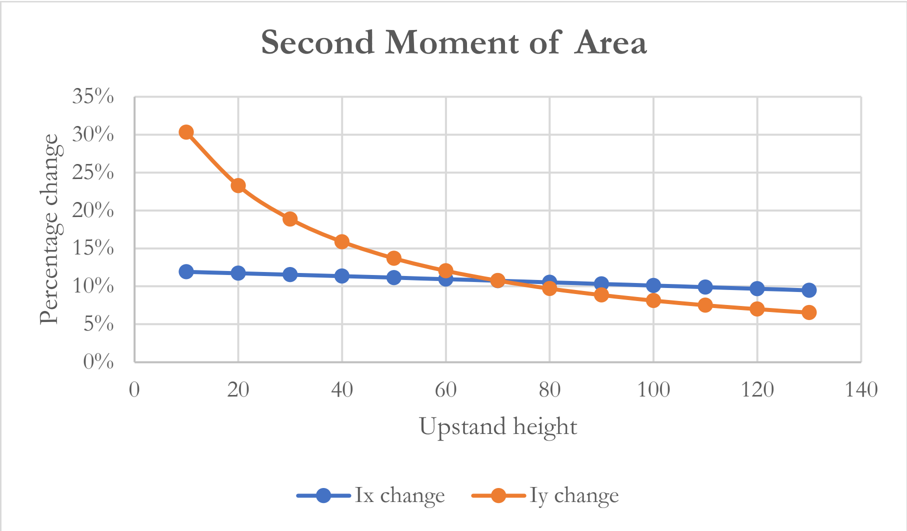

Figure. A3

(4) Table A4: H-section

Check on (k_1) factor stiffness Ratio

Beam **WF254x254x167** B/H: 0,9

E: *200 000* MPa

Upstand: (mm)	0	10	20	30	40	50	60	70	80	90	100	110	120	130
I_x (mm^4)	297 561 392	311 332 636	326 174 022	342 118 631	359 199 394	377 449 115	396 900 486	417 586 099	439 538 459	462 789 998	487 373 078	513 320 001	540 663 016	569 434 327
Change:		*4,63%*	*4,77%*	*4,89%*	*4,99%*	*5,08%*	*5,15%*	*5,21%*	*5,26%*	*5,29%*	*5,31%*	*5,32%*	*5,33%*	*5,32%*
I_y (mm^4)	97 898 492	106 541 624	115 184 756	123 827 889	132 471 021	141 114 153	149 757 286	158 400 418	167 043 550	175 686 683	184 329 815	192 972 947	201 616 080	210 259 212
Change:		*8,83%*	*8,11%*	*7,50%*	*6,98%*	*6,52%*	*6,12%*	*5,77%*	*5,46%*	*5,17%*	*4,92%*	*4,69%*	*4,48%*	*4,29%*
EI_y/EI_x	**0,329**	**0,342**	**0,353**	**0,362**	**0,369**	**0,374**	**0,377**	**0,379**	**0,380**	**0,380**	**0,378**	**0,376**	**0,373**	**0,369**

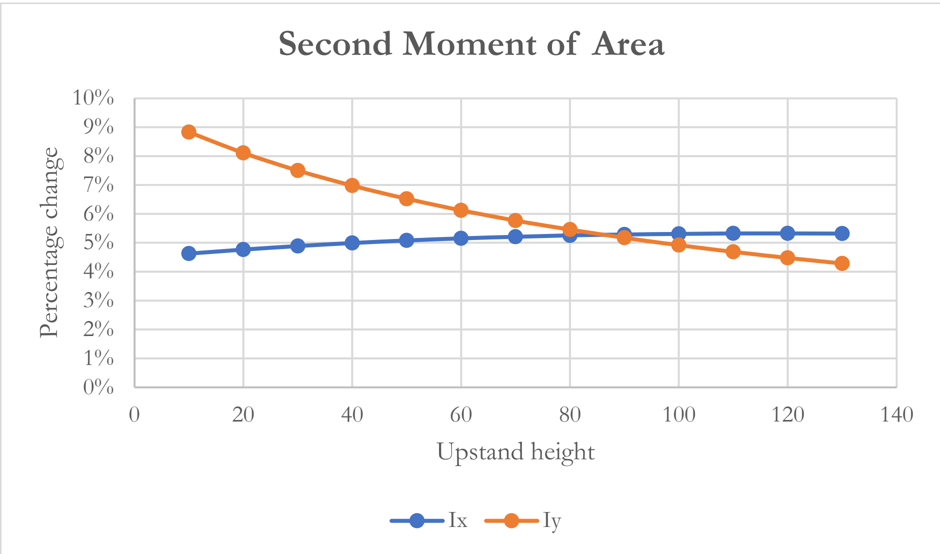

Figure. A4

(5) Table A5: H-section

Check on (k_1) factor stiffness Ratio

Beam **WF152x152x23** B/H: 1,0

E: *200 000* MPa

Upstand: (mm)	0	10	20	30	40	50	60	70	80	90	100	110	120	130
I_x *(mm^4)*	12 351 952	13 209 879	14 209 839	15 359 951	16 668 122	18 142 093	19 789 471	21 617 745	23 634 315	25 846 497	28 261 547	30 886 660	33 728 987	36 795 637
Change:		*6,95%*	*7,57%*	*8,09%*	*8,52%*	*8,84%*	*9,08%*	*9,24%*	*9,33%*	*9,36%*	*9,34%*	*9,29%*	*9,20%*	*9,09%*
I_y *(mm^4)*	4 014 179	4 735 481	5 456 783	6 178 086	6 899 388	7 620 690	8 341 992	9 063 295	9 784 597	10 505 899	11 227 202	11 948 504	12 669 806	13 391 108
Change:		*17,97%*	*15,23%*	*13,22%*	*11,68%*	*10,45%*	*9,47%*	*8,65%*	*7,96%*	*7,37%*	*6,87%*	*6,42%*	*6,04%*	*5,69%*
EI_y/EI_x	**0,325**	**0,358**	**0,384**	**0,402**	**0,414**	**0,420**	**0,422**	**0,419**	**0,414**	**0,406**	**0,397**	**0,387**	**0,376**	**0,364**

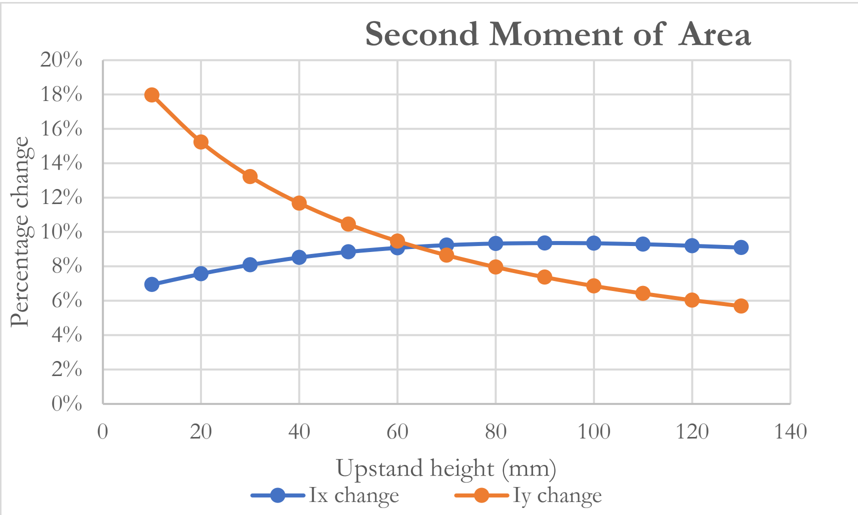

Figure. A5

APPENDIX B – EQUIVALENT DOUBLY SYMMETRIC SECTION CRITICAL MOMENT DETERMINATION

The concept of the 'equivalent doubly symmetric' section involves using the geometrical properties of the corresponding monosymmetric section with a given upstand height and setting the monosymmetry constant to zero. The height from centroid to application point of the load is then also applied in the critical elastic moment equation. This gives an indication of what the critical elastic moment would be without the influence of monosymmetry.

For the Equivalent doubly symmetric section, as indicated in Section 6.2.1 and illustrated in Fig.6-5, the following procedure is followed to generate the critical elastic moment values for the different upstand heights:

1. Start with the critical elastic moment equation for the monosymmetric section and for the considered loading. The hight at which the load is applied must be accounted for in the equation. For point load:

$$0.715429366\,P^2 - \frac{EI_y\pi^4}{2L^3}\left(\frac{GJB\,\pi^2}{2L} + \frac{EC_wB\,\pi^2}{2L^3}\right) - \frac{EI_y\pi^4 P}{2L^3}(0.366850274\,\beta_x + a) = 0 \qquad (B1.a)$$

2. Determine the centroid position of the section. Designate the distance from the centroid to the load application point as 'x'. For top flange loading: $x = H - \bar{y}$.

3. Determine the geometrical properties of the section.

4. Use the information in (3) and (4) with a monosymmetry constant ($\beta_x = 0$) in the equation in (1).

$$0.715429366\,P^2 - \frac{EI_y\pi^4}{2L^3}\left(\frac{GJ\pi^2}{2L} + \frac{EC_w\pi^2}{2L^3}\right) - \frac{EI_y\pi^4 P}{2L^3}(x) = 0 \qquad (B1.b)$$

5. The resulting critical elastic moment is $M_{cr-Eq.DS}$.

6. For the monosymmetric section critical elastic moment, M_{cr}, the distance at which the load is applied is taken relative to the shear centre and is designated 'a_{top}' for loading above the shear centre, and 'a_{bot}' for loading below the shear centre.

7. Plot the M_{cr} and is $M_{cr-Eq.DS}$ values at the different upstand heights.

<u>Example:</u>

Beam: **NF254x146x37**

Span: 2m $t_\alpha = t_f$

Loading: Point Load on top flange

*Use Equation (4.61) for M_{cr}

Using equations (3.47) to (3.55), α_c = 77mm.

Table B1: Moment values for monosymmetric section and equivalent doubly symmetric section

Upstand (α) in mm	α/H	Monosymmetric section		Eq. Doubly symmetric section	
		a_{top} (mm)	M_{cr}	$x = H - \bar{y}$ (mm)	$M_{cr-Eq.DS}$
0	0			128.00	**331**
25	0.10	*97.82*	***507.5***	113.31	**442**
50	0.20	*86.36*	***615.1***	99.00	**527.4**
77	0.30	*84.02*	***664.0***	83.96	**616**
90	0.35	*84.97*	***669.6***	76.80	**664**

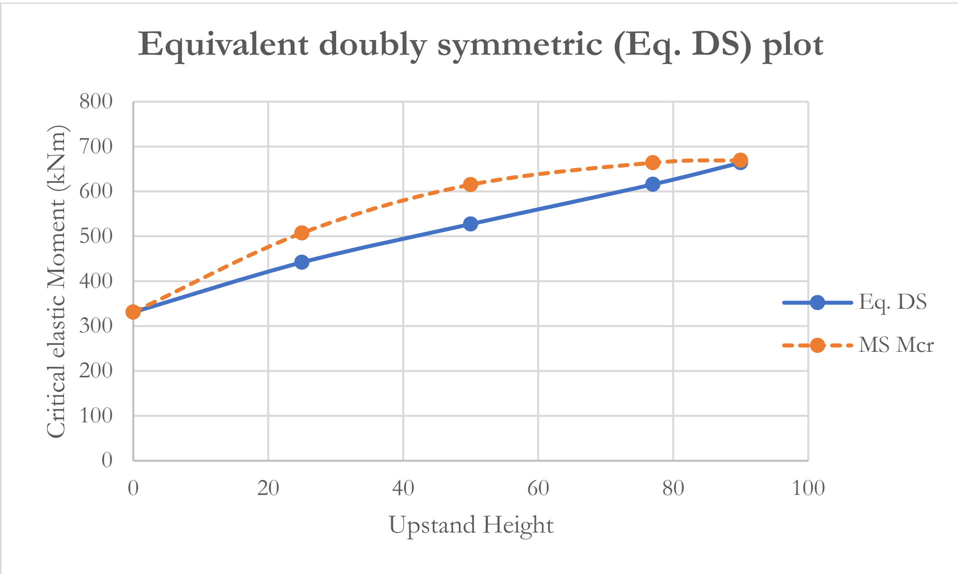

Fig.B1 Plot of critical elastic moment of a monosymmetric section (MS M_{cr}) for 2m span and corresponding 'equivalent doubly symmetric' section critical moment values (Eq. DS) for a NF254x146x37.